The Dissertation Committee for Robin Garrett Tuchscherer Certifies that this is the approved version of the following dissertation:

Strut-and-Tie Modeling of Reinforced Concrete Deep Beams: Experiments and Design Provisions

Committee:

Oguzhan Bayrak, Supervisor

Sharon L. Wood

James O. Jirsa

John E. Breen

Eric B. Becker

Strut-and-Tie Modeling of Reinforced Concrete Deep Beams: Experiments and Design Provisions

by

Robin Garrett Tuchscherer, B. S., M. S.

Dissertation

Presented to the Faculty of the Graduate School of

The University of Texas at Austin

in Partial Fulfillment

of the Requirements

for the Degree of

Doctor of Philosophy

The University of Texas at Austin

December 2008

Acknowledgements

Spending the last three years working on this project has been immensely enjoyable and rewarding. I owe this to all participants, contributors, and even the innocent bystanders. Thank you very much for your patience, knowledge, support, elbow grease, and/or humor along the way.

First of all, thank you to our sponsor: the Texas Department of Transportation. Without their generous support, this project would not have been possible. Also, I would like to specifically thank Dean Van Landuyt (TxDOT Project Director) and John Vogel (TxDOT Project Advisor). Thank you for your input and involvement during important project phases.

Thank you Dr. Bayrak. I am grateful for the energy, pragmatism, and good-nature that you bring to each task at hand; whether it is a five hour meeting or trip to the coffee shop afterwards. Thanks to your tutelage, I am a better engineer and scientist. Also, thank you Committee Members: Dr. Wood, Dr. Jirsa, Dr. Breen, and Dr. Becker. Your contributions and sage advice during the PhD process and project meetings is greatly appreciated.

I owe a huge thanks to fellow grad student David Birrcher, my breakfast taco brother-in-arms. It is because of your comprehension of the project and dedication that we were able to accomplish as much as we did. I appreciate your efforts, perspective, and friendship. Thank you Matt Huizinga. Your efforts in getting the project started and working out the details, were extremely valuable and greatly appreciated. Speaking of getting the project started, thank you Mike Brown. This project is a continuation of what you started. Your input and friendship is always appreciated.

I also want to acknowledge the other hard-working students that have assisted with the project, scraping their knuckles for us on a daily basis, including: Mike McCarthy, Gary Lehman, Brian Schnittker, Erin O' Malley, Patrick Harkin, James Kleineck, James Plantes, David Wald, and Ryan Kalina. In addition, thanks to the staff at the Ferguson Lab, including: Dennis Fillip, Blake Stasney, Andrew Valentine, and Barbara Howard.

Finally, last but not least. Thank you to my Mom and Dad; and my wife, Nicole. It is your unconditional love, encouragement, and friendship that have shaped me into who I am. Thank you for your support. Thank you for this accomplishment.

Strut-and-Tie Modeling of Reinforced Concrete Deep Beams: Experiments and Design Provisions

Publication No._____

Robin Garrett Tuchscherer, Ph.D.

The University of Texas at Austin, 2008

Supervisor: Oguzhan Bayrak

Bridge bents (deep beams) in the State of Texas have experienced diagonal cracking problems with increasing frequency. These field related issues, taken in combination with discrepancies that exist between design provisions for strut and tie modeling (STM), were the impetus for the funding of the current project. The overall objective of the project was to develop safe and consistent design guidelines in regard to both the strength and serviceability of deep beams. In order to accomplish this research objective and related tasks, a database of 868 deep beam tests was assembled from previous research. Inadvertently, many of the beams in this database were considerably smaller, did not contain sufficient information, or contained very little shear reinforcement. As a result, filtering criteria were used to remove 724 tests from the database. The criteria were chosen to consider only beams that represent bent caps designed in the field. In addition to the 144 tests that remained in the database, 34 tests were conducted as part of the current experimental program resulting in 178 total tests available for evaluation purposes. Two additional tests were conducted on beams without shear reinforcement, thus they did not meet the filtering criteria. However, the results from these tests provided valuable information regarding deep beam behavior. Beams that were fabricated and tested as part of the current experimental program ranged in size from, 36”x48”, 21”x75”,

21”x42”, and 21”x23”. These tests represent some of the largest deep beam shear tests ever conducted. STM details that were investigated included: (i) the influence that triaxial confinement of the load or support plate has on strength and serviceability performance; and (ii) the influence that multiple stirrup legs distributed across the web has on strength and serviceability performance. Based on the findings of the experimental and analytical program, a new strut-and-tie modeling procedure was proposed for the design of deep beam regions. The procedure is based on an explicitly defined single-panel truss model with non-hydrostatic nodes. An important aspect of the new STM design methodology is that it was comprehensively derived based on all the stress checks that constitute an STM design. Thus, the new method considers every facet of a STM design. The newly proposed STM procedure is simple, more accurate, and more conservative in comparison with the ACI 318-08 and AASHTO LRFD (2008) STM design provisions. As such, the implementation of the new design provisions into ACI 318 and AASHTO LRFD is recommended.

Table of Contents

List of Tables

List of Figures

Notation

a = shear span; depth of equivalent rectangular stress block; height of the back face of the CCC node, in.

a/d = shear span-to-depth ratio measured center of span to center of support

$\mathbf{A_1}$ = loaded area, in^2

$\mathbf{A_2}$ = area of the lower base of the largest frustum of a pyramid, cone, or tapered wedge contained wholly within the support and having for its upper base the loaded area, and having side slopes of 1 vertical to 2 horizontal, in^2

$\mathbf{A_c}$ = minimum cross sectional area of the strut, in^2

$\mathbf{A_{nz}}$ = area of the face of a nodal zone, in^2

$\mathbf{A_s}$ = area of tension reinforcement, in^2

$\mathbf{A_s'}$ = area of compression reinforcement, in^2

$\mathbf{A_{si}}$ = total area of surface reinforcement at spacing s_i in the i-th layer crossing a strut, with reinforcement at an angle α_i to the axis of the strut, in^2

$\mathbf{A_v}$ = Area of shear reinforcement perpendicular to the flexural tension reinforcement, in^2

$\mathbf{A_{vh}}$ = area of shear reinforcement parallel to the flexural tension reinforcement, in^2

$\mathbf{b_l}$ = width of the bearing plate at the CCC node

$\mathbf{b_s}$ = width of the bearing plate at the CCT node

$\mathbf{b_w}$ = width of beam web, in.

d = distance from extreme compression fiber to centroid of longitudinal tension reinforcement

$\mathbf{f_c'}$ = specified compressive strength of concrete, psi

$\mathbf{f_{ce}}$ = effective compressive strength of concrete in nodal zone, psi

$\mathbf{F_n}$ = nominal strength of a node face, kip

$\mathbf{f_s}$ = stress in tension reinforcement, psi

$\mathbf{f_s'}$ = stress in compression reinforcement, psi

$\mathbf{F_u}$ = Force acting on the face of a nodal zone, kip

$\mathbf{f_y}$ = specified yield strength of tensile reinforcement, ksi.

$\mathbf{f_{yl}}$ = measured yield strength of longitudinal tensile reinforcement, ksi

$\mathbf{f_{yv}}$ = measured yield strength of vertical transverse reinforcement, ksi.

$\mathbf{f_{yvh}}$ = measured yield strength of horizontal transverse reinforcement, ksi.

$\mathbf{h}$ = beam height, in.

$\mathbf{l_b}$ = length of bearing plate, in.

$\mathbf{l_l}$ = length of the bearing plate at the CCC node

$\mathbf{l_s}$ = length of the bearing plate at the CCT node

$\mathbf{m}$ = bearing capacity/confinement modification factor, $\sqrt{\frac{A_2}{A_1}} \leq 2$

$\mathbf{M_u}$ = applied factored moment at the critical section, in.-lb

$\mathbf{P_L}$ = measured applied live load, kip

$\mathbf{P_D}$ = estimated self weight of beam, kip

$\mathbf{P_{TR}}$ = estimated weight of the transfer girders, kip

$\mathbf{R_A}$ = measured reaction at the support closest to the load, kip

$\mathbf{R_B}$ = measured reaction at the support furthest from the load, kip

$\mathbf{s_1}$ = center-to-center spacing of transverse reinforcement in the vertical direction, in.

$\mathbf{s_2}$ = Center-to-center spacing of transverse reinforcement in the horizontal direction, in.

$\mathbf{s_i}$ = center-to-center spacing of reinforcement of the i-th layer adjacent to the surface of the member, in.

$\mathbf{V_u}$ = applied factored shear at the critical section, lb

$\mathbf{V_{crack}}$ = measured shear carried at the time the first diagonal crack forms (determined as illustrated in Figure 4-3), kip

$\mathbf{V_{test}}$ = maximum shear carried in test region, including the estimated self weight of the specimen and transfer girders, kip

$\mathbf{w_s}$ = width of the node-to-strut interface, in.

$\mathbf{w_t}$ = distance from extreme tension fiber to centroid of longitudinal tension reinforcement

$\boldsymbol{\alpha}$ = proportion of applied load that flows to near support

$\boldsymbol{\alpha_i}$ = angle between the axis of a strut and the bars in the i-th layer of reinforcement crossing that strut

α_s = the smallest angle between the compression strut and adjoining tension tie, degrees

β_n = factor to account for the effect of the anchorage of ties on the effective compressive strength of a nodal zone

Δ_{BEAM} = displacement due to flexural and shear deformations

Δ_{FAR} = recorded displacement at far reaction point

Δ_{LOAD} = recorded displacement at load point

Δ_{NEAR} = recorded displacement at near reaction point

Δ_{RBM} = displacement due to rigid body motion

ε_s = the tensile strain in the concrete in the direction of the tensile tie

θ = angle of strut measured from the horizontal axis

ν = efficiency factor, concrete effectiveness factor

$\rho_{\perp}$ = ratio of reinforcement perpendicular to the axis of the strut

ρ_h = ratio of horizontal transverse reinforcement to effective area, $A_{vh}/b \cdot s_2$

ρ_l = ratio of longitudinal tensile reinforcement to effective area, $A_s/b \cdot d$

ρ_l' = ratio of longitudinal compression reinforcement to effective area, $A_s'/b \cdot d$

ρ_v = ratio of vertical transverse reinforcement to effective area, $A_v/b \cdot s_1$

ω_{DL} = estimated uniform self weight, kip/ft

CHAPTER 1

Introduction

1.1 OVERVIEW

A *deep beam* is a structural member whose behavior is dominated by shear deformations. In practice, engineers typically encounter deep beams when designing transfer girders, pile supported foundations, or bridge bents. Until recently, the design of deep beams per U.S. design standards was based on empirically derived expressions and *rules of thumb*. The structural design standards, AASHTO LRFD (2008) and ACI 318-08, adopted the use of strut-and-tie modeling (STM) for the design of deep beams or other regions of discontinuity in 1994 and 2002, respectively. Based on the theory of plasticity, STM is a design method that idealizes stress fields as axial members of a truss. The primary advantage of STM is its versatility. In other words, it is valid for any given loading or geometry. However, the primary weakness of STM is also its versatility. The freedom associated with the method results in a vague and inconsistently defined set of guidelines. Because of the lack of a well-ordered design process, many practitioners are reluctant to use STM. A goal of the current research program is overcome this ambiguity through the development of consistent and safe STM provisions.

For structural members exposed to public view or environmental elements, serviceability performance of the structure is arguably a more significant concern than its strength. Typically, the serviceability performance of deep members is quantified by the width and spacing of cracks that form under the application of service loads. In order to control this cracking behavior, a minimum amount of crack control reinforcement is provided. However, the various design provisions inconsistently define minimum reinforcement requirements and there is not much background available to resolve these differences. Hence, another goal of the current research program is to experimentally examine the minimum

reinforcement provisions and recommend a practical and justifiable minimum amount based on both strength and serviceability performance.

As part of the current research program, a database of 904 deep beam specimens has been compiled. Of these 904 tests, 36 have been fabricated and tested as part of the current project; therefore, data from 868 specimens has been collected from previous research. Data from these 868 specimens was used to develop the current deep beam shear design provisions. However, the majority of these specimens were significantly smaller than actual beams designed in practice. A typical test specimen may have an area of 100-in^2 whereas a typical bridge bent or transfer girder can have an area that is ten to fifteen times larger. As such, it is not possible to address the current research objectives based on the data collected from past specimens alone. Therefore, in order to accomplish the goals of the current project, it was necessary to examine beams whose size and construction is more representative of those used in the field. As a result, 36 specimens were fabricated and tested as part of the current research program. These specimens represent some of the largest deep beam shear tests ever conducted.

1.2 PROJECT OBJECTIVE

The current research project was funded by the Texas Department of Transportation (TxDOT). Since the inclusion of STM provisions in the AASHTO LRFD specifications in 1994, TxDOT engineers have been examining the impact that the provisions have on the design of their bent caps. In general, the provisions are considered *confusing* as a result of the discrepancy that exists when transitioning between sectional shear and STM provisions. In addition, bents in the State of Texas are experiencing diagonal cracking problems with increasing frequency. These field related issues, taken in combination with discrepancies in the AASHTO LRFD provisions, were the impetus for TxDOT to fund the current project. As a result, the overall goal for the project is to develop appropriate

strength and serviceability design guidelines for bent caps and other deep beams. In order to properly address specific project tasks, findings from the current experimental program and those from previous research were used.

1.3 PROJECT SCOPE

An extensive amount of literature was reviewed and a database of 904 deep beam shear tests compiled. This database represents the current state of knowledge of deep beam shear. In addition, it provides a powerful tool for evaluating and comparing different design provisions to one another.

The beams that make up the database are relatively small in size and less applicable for the development of design provisions for very large elements like transfer girders and bridge bents. Therefore, as part of the current project, large-scale beams have been fabricated and tested. These beams represent some of the largest deep beam tests ever conducted. They are of a scale that is representative of deep beams used in practice.

The objectives of the current project were accomplished by performing the following tasks. These tasks specifically address the inconsistencies contained in current design provisions. A brief summary of the project tasks can be summarized as follows:

1. Determine the influence that the distribution of stirrups across the width of a beam web has on the strength and serviceability behavior of a deep beam.
2. Determine the influence that triaxially confined bearing plates has on the strength and serviceability behavior of a deep beam.
3. Determine the influence that the amount of transverse reinforcement has on the strength and serviceability behavior of a deep beams.
4. Determine the influence that the depth of a deep beam specimen has on the strength and serviceability performance.

5. Propose a simple STM design methodology for the design of deep beams.
6. Address the discrepancy that exists between sectional shear and STM estimations in the *transition region* (i.e. at a/d = 2). Make a recommendation as to the accuracy of a STM model.
7. Make a recommendation on a methodology for determining the service level stress that causes the first diagonal crack for a deep beam.
8. Make a recommendation on a methodology for relating the maximum diagonal crack width of a deep beam to its residual capacity.

In order to address the stated tasks, an experimental program was developed that is directly correlated to tasks 1 through 4. The findings for tasks 1 and 2 are presented in this document (Tuchscherer 2008) and the findings for task 3 and 4 are presented by Birrcher (2008). Based on an analysis of the results collected from the experimental portion of this project, recommendations were developed. These recommendations are presented in tasks 5 through 8. The task 5 design recommendation is presented in this document (Tuchscherer 2008) and the task 6 through 8 recommendations are presented by Birrcher (2008). Specifics on the organization of this document are presented in the following section.

1.4 ORGANIZATION

A background of deep beam behavior, including the past research that has been used to formulate current deep beam provisions is presented in Chapter 2. Additionally, research conducted in the past that has specifically studied an aspect of the current objectives (task 1 and 2) is summarized in Chapter 2. Chapter 3 presents an overview of the experimental program including the fabrication, instrumentation, and testing procedures for the experimental portion of the current project. A series of beams were fabricated and tested in order to determine the influence of distributing stirrups across a beam's web (task 1). The results of this testing series are discussed in Chapter 4. Also, a series of beams were fabricated

and tested in order to study the influence of bearing plate size and triaxial confinement (task 2). The results of this testing series are discussed in Chapter 5. After presenting the experimental portion of this project, a new strut-and-tie modeling design methodology is proposed and presented in Chapter 6 (task 4). All the findings and conclusions of this part of the research program are summarized in Chapter 7. Upon summarizing the findings, revisions to the AASHTO LRFD (2008 Interim) and ACI 318-08 provisions are proposed and presented in Appendix A and Appendix B respectively. Finally, an example problem is presented in Appendix C in order to illustrate the differences between the proposed provisions and the relevant parts of the AASHTO LRFD (2008) and ACI 318-08 specifications.

CHAPTER 2

Background on Strut-and-Tie Modeling of Deep Beams

2.1 DEEP BEAM VS. SECTIONAL BEHAVIOR

Typically, reinforced concrete members are designed to resist shear and flexural forces based on the assumption that strains vary linearly at a section. Referred to as the *Bernoulli hypothesis* or *beam theory*, the mechanical behavior of a beam is commonly defined by assuming that *plane sections remain plane*. The region of a structure where the Bernoulli hypothesis is valid is referred to as a *B-region* (B standing for *beam* or *Bernoulli*). In B-regions, the internal state of stress can be derived from the sectional forces before and after the concrete cracks. Therefore, the design of these regions is often referred to as a *sectional design*.

A *deep beam design* must be treated differently than a sectional design because the assumptions used to derive the sectional theory are no longer valid. A deep beam is a member whose shear span-to-depth, *a/d*, ratio is relatively small such that nonlinear shearing strains dominate the behavior. Typically, a region of a beam with an a/d ratio less than 2.0 to 2.5 is considered to behave as a deep beam; whereas, a region of a beam with a greater a/d ratio is assumed to behave according to sectional principles. For example, the beam shown in Figure 2-1 has an a/d ratio of approximately two to the right of the concentrated load and five to the left of the load. The left side of the beam (Section A-A) contains a B-region and stresses can be determined according to sectional methods. The right side of the beam (Section B-B) is considered a deep beam region. Shear strains dominate the behavior and beam theory cannot be used to determine the internal state of stress.

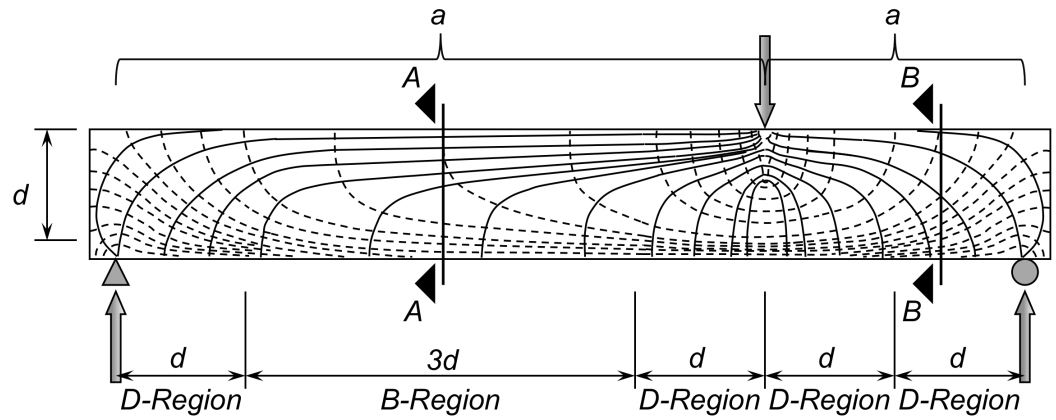

Figure 2-1. Stress trajectories in B-regions and near discontinuities (D-regions).

Nonlinear strain distributions are often caused either by abrupt changes in geometry or abrupt changes in loading. These regions of discontinuity are referred to as *D-regions* (D standing for *discontinuity* or *disturbance*). An elastic stress analysis suggests that the localized effect of a concentrated load or geometric discontinuity will attenuate about one member depth away from the discontinuity (St. Venant's Principle). For this reason, D-Regions are assumed to extend one member depth from the load or discontinuity. Figure 2-1 illustrates the location of B-regions and D-regions in a typical simply supported beam loaded at a single point.

Due to the nonlinearity of strains and inelasticity of concrete, a general theory of behavior is complicated to derive in a D-region. As a result, designers typically employ either empirically derived design methods or a hypothetical truss model such as a *strut-and-tie model* (STM).

The theoretical background of STM is presented in Section 2.2. Specific details related to the elements that form a truss model are presented in Section 2.3. Next, a summary of current code provisions is presented in Section 2.4. Finally, a historical background of the current design provisions is presented in Sections 2.5 and 2.6.

2.2 THEORETICAL BACKGROUND ON STRUT-AND-TIE MODELING

A strut-and-tie model idealizes the complex flow of stresses in a structural member as axial elements in a truss member. The compressive stress fields are resisted by concrete *struts* and the tensile stress fields are resisted by reinforcing steel *ties*. Struts and ties intersect at regions called *nodes*. Struts, ties, and nodes are the three elements that comprise a STM and they must be proportioned to resist the applied forces. According to the *lower bound theory of plasticity*, the capacity of a STM is always less than the structure's actual capacity provided the truss is in equilibrium and *safe*. A safe STM must have sufficient deformation capacity to redistribute forces into the assumed truss elements, and the stresses applied to the elements must not exceed their *yield* or *plastic flow* capacity. Failure of a STM can be attributed to crushing of the struts, crushing of concrete at the face of a node, yielding of the ties, or anchorage failure of the ties.

As an example, the loads supported by the beam shown in Figure 2-1 can be supported by the determinate truss shown in Figure 2-2. The same truss model is shown in Figure 2-3 with the concrete struts, nodes, and reinforcement drawn to scale. In Figure 2-3, the portions of the beam not considered in the truss model have been removed in order to illustrate the concept of a lower-bound solution. For this particular example, a fraction of the original beam is considered to resist the applied forces. If the laws of statics are satisfied and the materials do not exceed their yield capacity, then the estimated strength of the STM is less than or equal to the actual capacity of the beam.

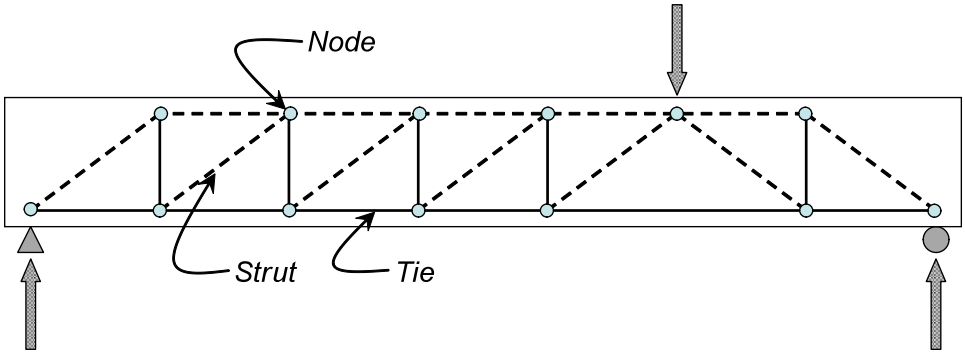

Figure 2-2. Strut-and-tie model: Simply supported beam supporting concentrated load.

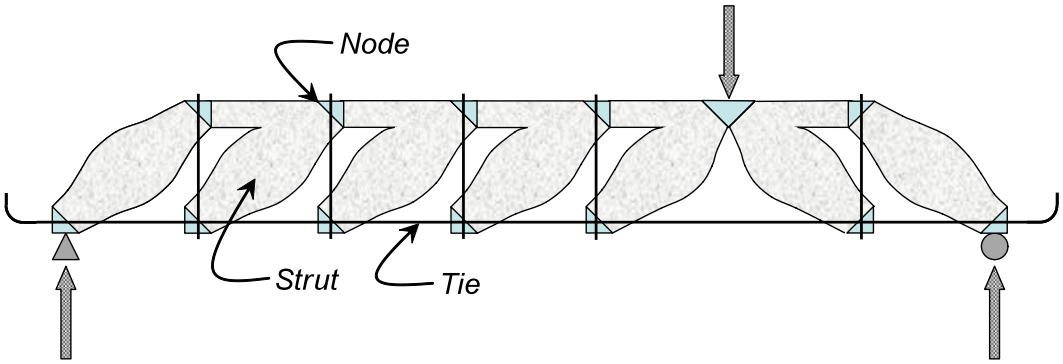

Figure 2-3. Strut-and-tie model with truss elements drawn to scale.

A STM is a powerful design tool as it is valid for any stable truss configuration a designer chooses. However, the downfall of an STM can also be attributed to its adaptability. There are no right or wrong solutions, but there are good and bad choices that can be made in developing a solution. For example, if the selected model varies substantially from the actual stress field, then the structure must undergo substantial deformation in order to develop the poorly assumed model. As a result, there is an increased chance that wide cracks could form. According to Schlaich et al. (1987):

> *Doubts could arise as to whether the correct model has been chosen out of several possible ones. In selecting the model, it is helpful to realize that loads try to use the path with the least forces and deformations. Since reinforced ties are much more deformable than concrete struts, the model*

with the least ties is the best. Of course, it should be understood that there are no unique or optimum solutions. Replacing a continuous set of smooth curves by individual polygonal lines is an approximation and leaves ample room for subjective decisions.

In developing a strut-and-tie model for a structure, the first step is to calculate the reactions supporting the applied loads. For example, consider the right side (deep beam portion) of the beam shown in Figure 2-1. Assume that the point load is 100-kips and ignore the self-weight of the beam. According to statics, 71-kips will flow to the right support and 29-kips to the left (i.e. $100 \cdot 5/7 = 71$). The right portion (i.e. deep beam portion) is illustrated in Figure 2-4.

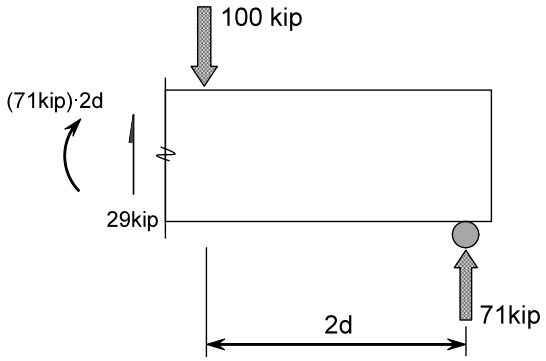

Figure 2-4. Step 1 for STM is calculation of support reactions.

For the next step, it is common to employ some type of linear elastic analysis in order to visualize the flow of forces within the member; and align the struts and ties according to the stress trajectories. Schlaich et al. (1987) recommend aligning struts within ±15° of the stress trajectories. In order to ensure adequate deformation capacity to develop the steel stresses, the orientation of the struts should not be excessively shallow. According to Ramirez and Breen (1991):

Large deviations from 45-degrees of the angle of inclination will demand excessive strains in the reinforcement together with extremely wide crack openings at failure. These diagonals must be [less than 65-degrees and greater than 30-degrees].

Also, if pictures of the cracking pattern in a similar structure are available, the location of the struts and ties can be arranged within the structure such that struts follow the known crack patterns (MacGregor 2002).

Based on the aforementioned guidelines for laying out a truss model and the stress trajectories shown in Figure 2-1, either a *one-panel* or *two-panel* truss is an appropriate solution. These two options are presented in Figure 2-5. Notice that the point load is divided into 71 and 29-kips for the sake of convenience. However, the equilibrium of the model has not been changed.

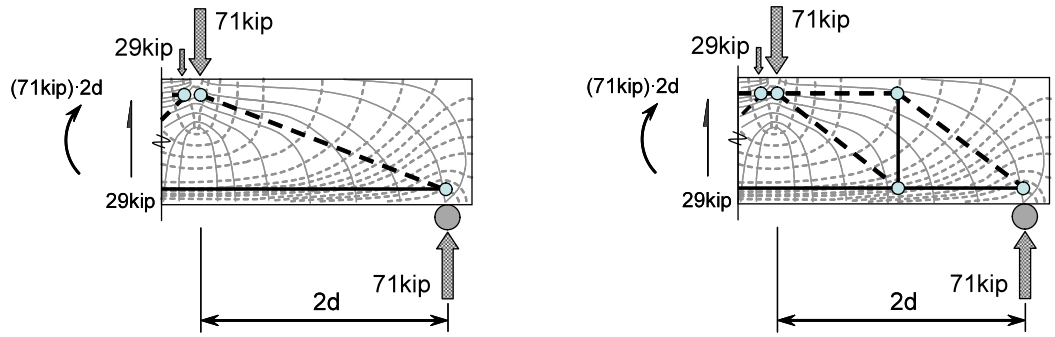

Figure 2-5. STM: (a) One-panel and (b) two-panel.

For an a/d ratio less than two, the transfer of shear predominantly results from compressive stresses flowing directly from the load to the support (i.e. one-panel truss model). For this type of behavior, the capacity of the beam is primarily dependent on the compressive strength of concrete in the direct strut. The transverse reinforcement (i.e. stirrups) has little influence on the shear strength. A one-panel shear failure is illustrated in Figure 2-6 for a deep beam with an a/d ratio equal to 1.2.

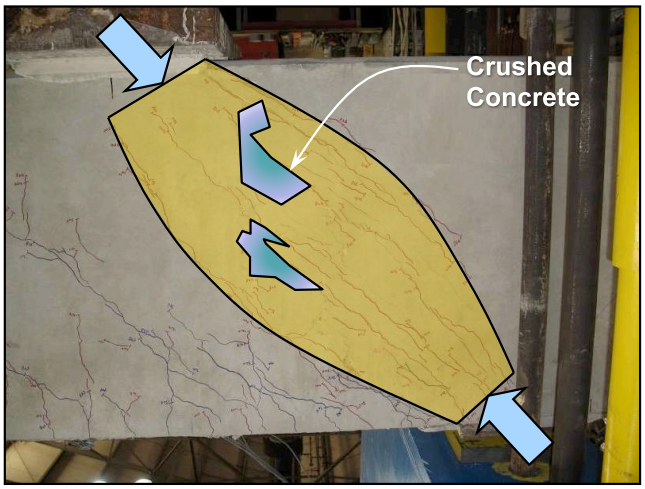

Figure 2-6. Direct strut or one-panel shear failure (a/d = 1.2).

If the a/d ratio exceeds a value of two, the mechanism of shear failure is better characterized as sectional shear rather than deep beam shear. The ability of a structure to resist sectional shear is due to many attributes of the cross-section including: the friction force along the inclined crack due to aggregate interlock; the increased shear capacity of the confined compression region; dowel-action of the horizontal reinforcement; and the tensile resistance of the vertical reinforcement. The vertical reinforcement is a primary component that provides the sectional shear resistance of a beam. After a diagonal crack has formed, the vertical reinforcement is the main mechanism with which the structure transfers shear stresses across the crack and to the support. Thus, the yielding of the stirrups typically precedes a sectional shear failure. A two-panel strut-and-tie model is akin to sectional shear behavior as the yielding of the vertical reinforcement largely influences both. A two-panel truss failure is illustrated in Figure 2-7 for a deep beam with an a/d ratio equal to 2.5.

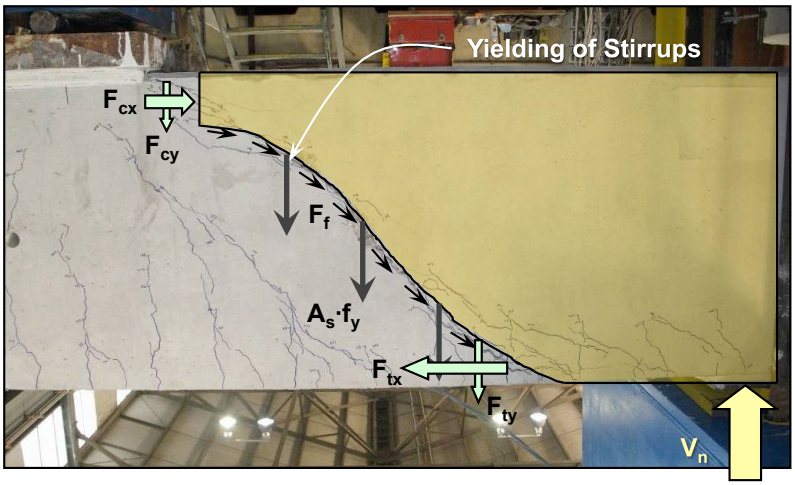

Figure 2-7. Sectional or two-panel shear failure (a/d = 2.5).

When the a/d ratio is near two, the shear mechanism may be attributed to a combination of both one and two-panel behavior. For example, consider the beam with an a/d ratio equal to 1.85 presented in Figure 2-8.

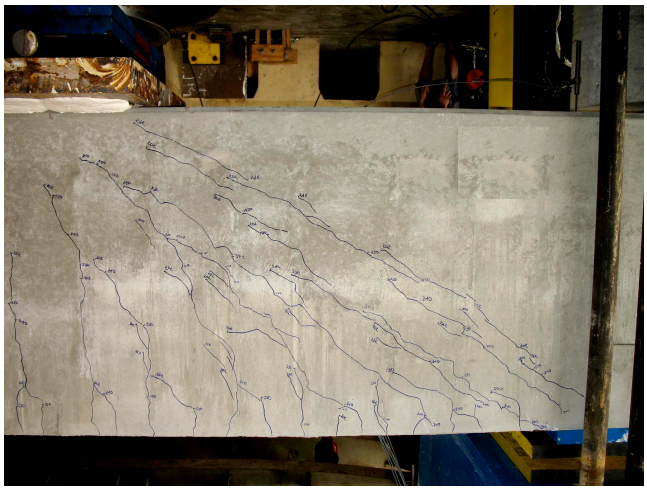

Figure 2-8. Combination of one and two-panel behavior (a/d = 1.85).

Upon examination of the cracking pattern, a combination of a one and two-panel model may be more appropriate. However, additional accuracy may not necessarily benefit the designer given the additional complication. Ultimately, the decision on which model to use is left to the discretion of the designer. According to the principles of STM, either model will result in a safe solution.

According to Kani et al. (1979), the transition in shear behavior between a direct strut (one-panel) and sectional shear (two-panel) occurs at an a/d ratio of 2.5:

> *The graphs of the [shear capacity versus a/d ratio] results seem to be made up of two different functions of which a/d = 2.5 is the point of intersection. There should be two totally different laws of failure governing each region.*

Therefore, a one-panel strut-and-tie model is used to evaluate all beams tested as part of current and past experimental programs where a/d ≤ 2.5. The implication of using a one-panel model for a/d ratios up to 2.5 is discussed in Chapter 6.

Once a truss model has been selected, the next step is to proportion its elements (struts, ties, and nodes) accordingly. Details on these elements are presented as follows.

2.2.1 Struts

Struts vary in shape depending on their location within a structure. Most struts in a two dimensional STM are *bottle-shaped*. That is, they spread laterally along their length. The lateral spreading of a bottle-shaped strut introduces tensile stresses transverse to the strut. These tensile stresses could potentially cause cracking along the length of the strut resulting in premature failure. Hence, transverse reinforcement should be provided in order to control the cracking. Often, bottle-shaped struts in an STM are idealized as *prismatic*. However, this simplification does not eliminate the fact that the strut is, in actuality, still bottle-shaped and at a risk of splitting longitudinally. Transverse reinforcement must be provided. Prismatic struts exist in the compression zone of a beam's flexural region. Figure 2-9 illustrates bottle-shaped, prismatic, and idealized prismatic struts found in a typical STM. Design guidelines for the proportioning of struts are discussed in Section 2.3.4.

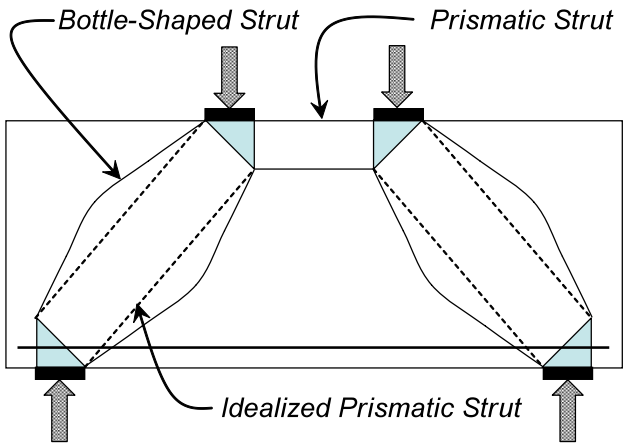

Figure 2-9. STM containing prismatic and bottle-shaped struts.

2.2.2 Ties

In general, reinforcing steel is placed at tie locations in an STM. The reinforcement should be distributed so that its centroid coincides with the tie location. Selection and placement of reinforcement for strength of a STM is straightforward. Details such as bar spacing, distribution, and anchorage are factors that deserve the most consideration when selecting and placing the reinforcement. Design guidelines for proportioning and placing tie reinforcement are presented in Section 2.3.5.

2.2.3 Nodal Zones

Nodes are named based on the nature of the elements that frame into them. For example, the nodal zone where two struts and a tie intersect is referred to as a *CCT* node (*C* stands for *compression* and *T* stands for *tension*). If more than three forces intersect at a node, it is often necessary to resolve some of the forces to end up with three resulting forces. The three types of nodes commonly used in a STM are shown in Figure 2-10.

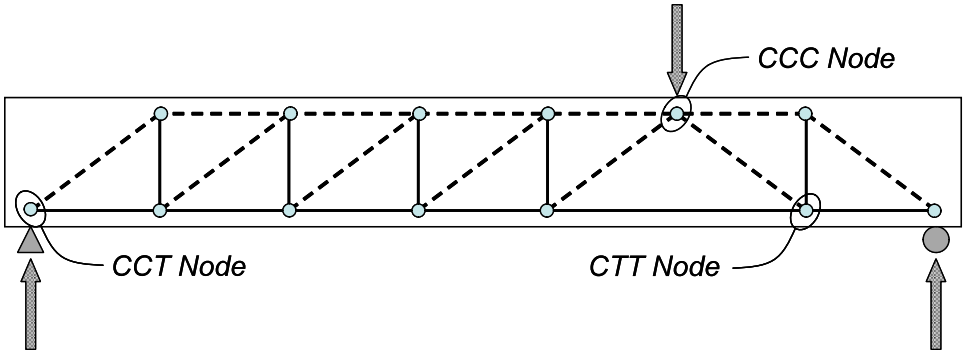

Figure 2-10. Nodal zones typically employed in STMs.

Ideally, nodes may be proportioned so that the stresses on all faces are equal. If the stresses are equal on all faces, the ratio of the area of the side face is proportional to the applied force. In this case, the node is called a *hydrostatic node*. Principal stresses are equal on all sides of a hydrostatic node; thus, shear stresses do not exist within the node. However, the requirement of equal stresses on all faces of a node is rarely realized in practice as the requirement is impractical or too cumbersome to accomplish. Therefore, most nodal regions are *non-hydrostatic*. Figure 2-11 illustrates the states of stress associated with hydrostatic and non-hydrostatic nodes.

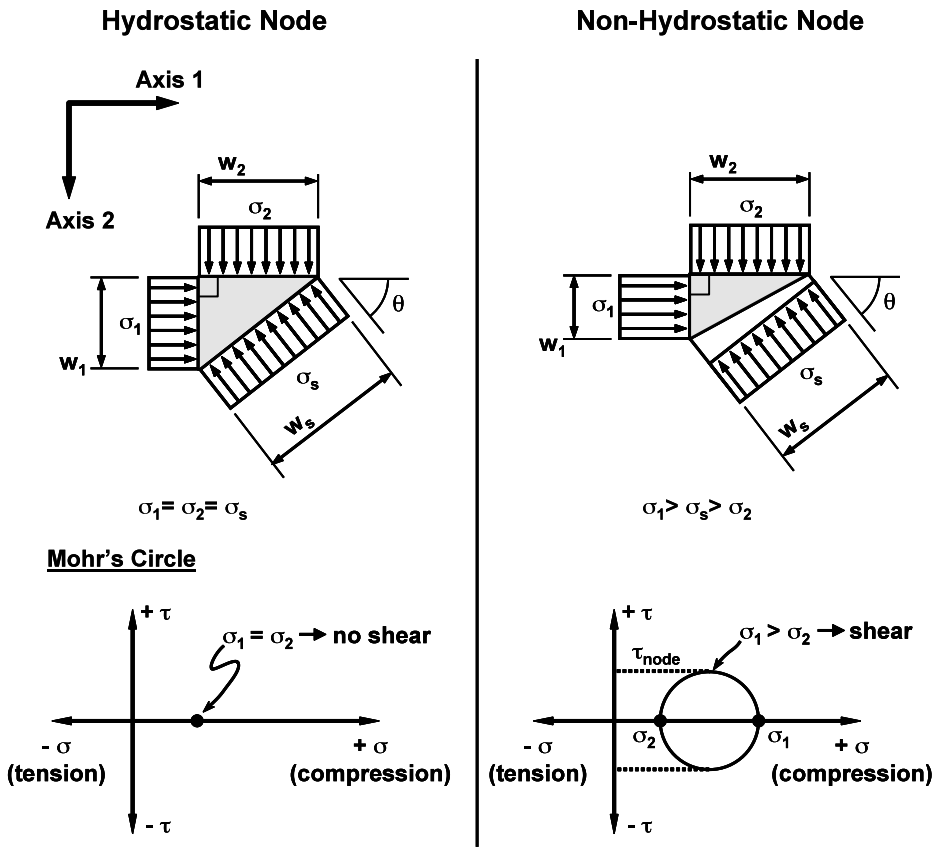

Figure 2-11. Stresses on hydrostatic and non-hydrostatic nodes (Brown et al. 2006).

It is important to note that both hydrostatic and non-hydrostatic nodes are idealizations of reality. That is, they are proportioning techniques that have been established for ease and consistency when creating a truss model. The influence that node type has on a strut-and-tie model is illustrated in Figure 2-12.

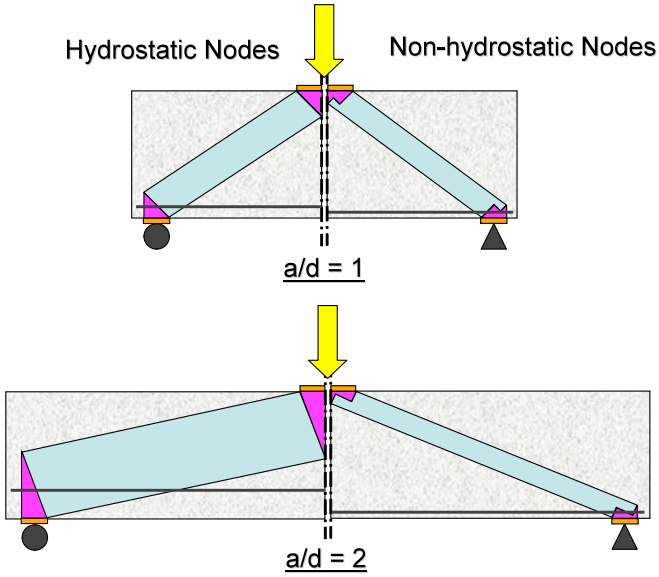

Figure 2-12. Difference between hydrostatic and non-hydrostatic nodes as the strut angle decreases.

Proportioning a hydrostatic node is a relatively straightforward procedure. The size of a strut framing into a hydrostatic node is based on the stress underneath the bearing plate. In other words, the stress at the back face and node-to-strut interface is equivalent to the bearing stress, σ_2 (Figure 2-11). As a result, the dimensions of all three nodal faces are based on the bearing stress. As shown in Figure 2-12, this procedure can result in an unrealistically large strut as the strut angle becomes shallower.

It is well documented that the shear capacity of a beam decreases as the a/d ratio increases. When hydrostatic nodes are used in a truss model, the strength of a strut must be proportionally reduced as the a/d ratio increases in order to counteract the struts increasing size. Contrarily, when non-hydrostatic nodes are used, the dimension of the strut-to-node interface decreases slightly as the a/d ratio increases, thereby accounting for the reduction in shear strength.

It is difficult to maintain hydrostatic nodal regions whose boundaries are consistent with other beam details such as location of the longitudinal reinforcement and flexural capacity. Non-hydrostatic nodes, on the other hand,

are proportioned based on an established set of guidelines that considers these additional beam details. As such, these conventional proportioning techniques are presented as follows.

2.3 PROPORTIONING ELEMENTS OF A STM

The capacity of a beam as determined from a STM is inherently connected to the proportions of the nodal regions. Procedures for proportioning nodes have been well established by past researchers. These established sets of guidelines are presented in Sections 2.3.1 through 2.3.3. For the sake of consistency, the following proportioning techniques are used to evaluate all of the beams contained in past and current experimental programs.

2.3.1 Proportioning a CCC Node

Refer to the CCC node shown in Figure 2-10. It has been magnified and is presented approximately to scale in Figure 2-13.

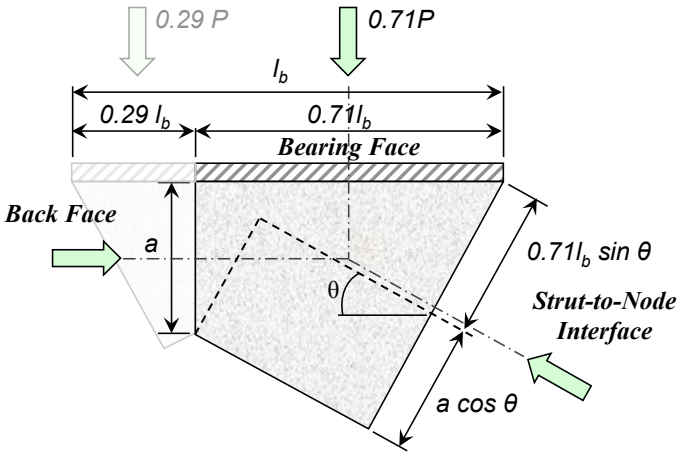

Figure 2-13. CCC Node.

For the beam shown in Figure 2-10, 71% of the applied load flows into the right support and the other 29% is transferred to the left support. Therefore, when proportioning the node, the length of the bearing face is set equal to 71% of the bearing plate length, l_b. The height of the back face, a, is assumed to be equivalent to the depth of the equivalent flexural stress block obtained from a typical flexural

analysis. Admittedly, assumptions used in a flexural analysis are not valid within a D-region, especially for very low a/d ratios. However, the proportioning procedure is well established in practice, and it is conservative. For a rectangular beam, a is calculated according to Equation 2-1.

$$a = \frac{\left(A_s f_s - A_s' f_s\right)}{0.85 b_w d} \qquad \text{Equation 2-1}$$

Where,

A_s = Area of tension reinforcement, in^2

A_s' = Area of compression reinforcement, in^2

b_w = Web width, in.

f_c' = Specified concrete compressive strength, psi

f_s = Stress in tension reinforcement, psi

f_s' = Stress in compression reinforcement, psi

The angle of the strut abutting the strut-to-node interface, θ, depends on the truss configuration. Based on the length of the bearing plate and height of the back face, the width of the strut-to-node interface, w_s, is determined according to the following equation:

$$w_s = l_b \sin\theta + a \cdot \cos\theta \qquad \text{Equation 2-2}$$

Where,

l_b = Length of bearing plate, in.

a = Height of back face of node, in.

θ = Angle of strut measured from the horizontal axis

Equation 2-2 is included in a figure of the ACI 318-08 code (ACI Figure RA.1.6), but not in the body of the code itself. According to MacGregor (2002), *future code committees should consider adding such equations to the Commentary*.

2.3.2 Proportioning a CCT Node

Refer to the CCT node shown in Figure 2-10. It has been magnified and is presented approximately to scale in Figure 2-14.

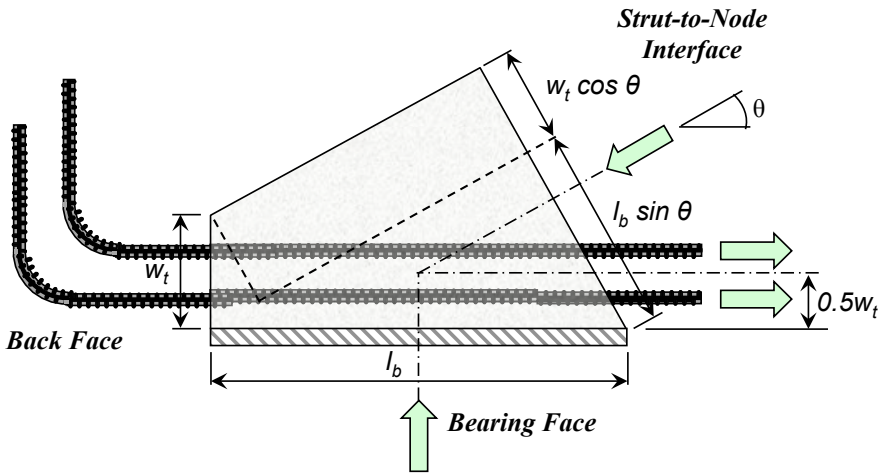

Figure 2-14. CCT Node.

The bearing face of a CCT node has the same dimensions as the bearing plate, l_b. The height of the back face, w_t, is taken as twice the distance from the near face of the beam to the centroid of the tension reinforcement. Finally, the angle of the strut abutting the strut-to-node interface depends on the truss configuration. Based on the given dimensions, the width of the strut-to-node interface, w_s, is determined the same as it is for a CCC node (Equation 2-2).

2.3.3 Proportioning a CTT Node

Refer to the CTT node shown in Figure 2-10. It has been magnified and is presented approximately to scale in Figure 2-15.

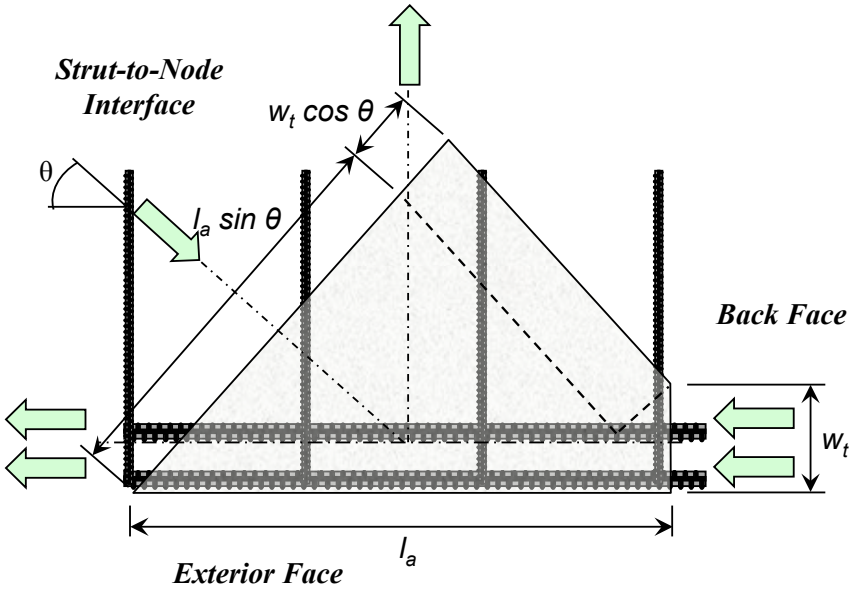

Figure 2-15. CTT Node.

Interior nodes, which are not bounded by a bearing plate, are often referred to as *smeared* nodes. Forces from compressive struts spread, or smear, and are equilibrated by multiple stirrups, or ties. Because a bearing plate does not abut the node, a proportioning technique must be employed to determine the extents of the exterior face, l_a. The method that is employed for the current project is that recommended by Wight and Parra-Montesinos (2003): the authors propose that any stirrup that intersects an adjacent strut at an angle greater than 25-degrees be engaged as part of the vertical tie of the CTT node (Figure 2-16).

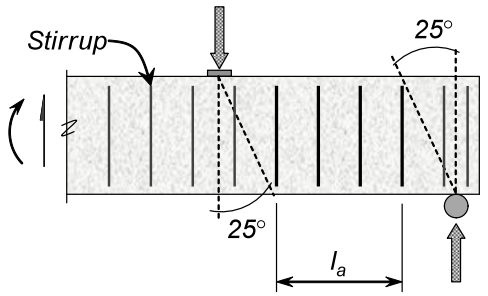

Figure 2-16. Determination of CTT vertical tie.

According to Wight and Parra-Montesinos (2003), it is conservative to assume that the exterior face, l_a, of the CTT node is as wide as the distance between the outermost stirrups included in the vertical tie.

The back face, w_t, of the node is calculated the same way as for a CCT node; twice the distance to the centroid of the tension steel, measured from the near face of the beam. Finally, the angle of the strut coming into the strut-to-node interface is based on the truss geometries. Based on the given dimensions, the width of the strut-to-node interface, w_s, is determined the same as for the CCC and CCT nodes (Equation 2-2).

2.3.4 Proportioning a Strut

Struts can be prismatic or bottle-shaped (Figure 2-9). A prismatic strut occurs within the compression zone of a beam's flexure region, and it is designed accordingly. Most struts are bottle-shaped and concentrate into the nodal regions. Therefore, the highest stress that a strut must resist occurs at the location where the strut and node abut one another, or the strut-to-node interface. Even if a strut is idealized as prismatic, the highest stress occurs at the strut to node interface. As such, the critical proportions of a strut are based on the nodal proportions. The critical capacity of a strut is taken to be identical to the capacity of the node-to-strut interface.

2.3.5 Proportions and Placement of Tie Reinforcement

Ties shown in a strut-and-tie model are simple representations of tensile stresses within a D-region. Proper placement of tie reinforcement is accomplished by matching the centroid and direction of the reinforcement with the axis of the tie in the truss model.

Tie details that deserve the most consideration are proper bar distribution, spacing, and development. In order to develop the reinforcing steel, ties must be properly anchored behind the nodal zones. Figure 2-17 illustrates the development length of a typical tie.

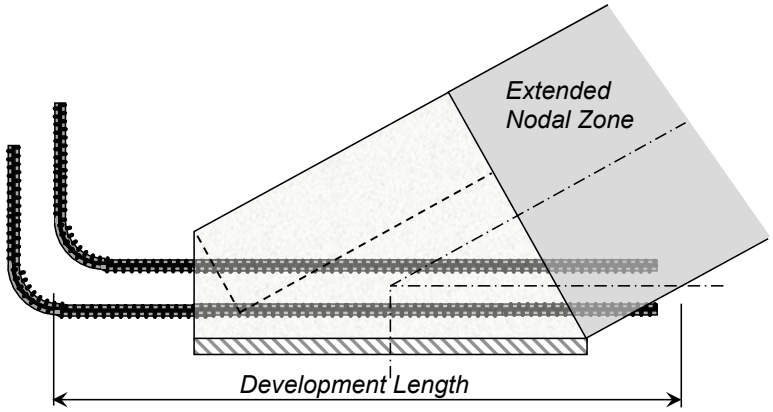

Figure 2-17. Development length of a tie.

ACI 318 allows the development length to be measured from the intersection of the extended nodal zone and the centroid of the bars, as shown in Figure 2-17. For the sake of simplicity, the development length can conservatively be taken from the edge of the bearing plate.

Proportioning nodes can be an iterative process. The size of the node is dependent on beam details such as bearing plate size and reinforcement location. It may be necessary to adjust beam geometry, reinforcement location, and bearing plate size such that the stress applied to a nodal region is less than its nominal capacity. Current STM design provisions: ACI 318-08 Appendix A; AASHTO

LRFD Bridge Design Specifications (2008); and *fib* Recommendations (1999) are presented next.

2.4 CURRENT CODE PROVISIONS FOR STM

The design provisions that are examined for this research program are the Building Code Requirements for Structural Concrete per the American Concrete Institute (ACI 318-08), the Bridge Design Specifications per the American Association of State Highway and Transportation Officials (AASHTO LRFD 2008 Interim), and the updated knowledge of the CEB/FIP 1990 Model Code per the International Federation for Structural Concrete (*fib* 1999). The recommendations of *fib* (1999) have been adopted by the European design standard, *Eurocode 2*. The reason that the *fib* (1999) provisions are evaluated rather than Eurocode 2 is because the *fib* (1999) provisions provide much more detailed information in regard to their recommended strut-and-tie modeling procedure.

The load carried by an element in an STM must be less than the capacity of the element (Equation 2-3). This is the basic premise for all STM provisions. The strength of an element in an STM is measured in terms of its *effectiveness* or *efficiency*. An efficiency factor, ν, is the ratio of the stress applied to an element at failure and its concrete compressive strength.

$$F_n \geq F_u \qquad \text{Equation 2-3}$$

Where,

$$F_n = f_{ce} \cdot A_{nz}$$

$$f_{ce} = \nu \cdot f_c'$$

A_{nz} = Area of the face of a nodal zone, in^2

F_n = Nominal strength of a node face, kip

F_u = Force acting on the face of a nodal zone, kip

f_c' = Specified compressive strength of concrete, psi

f_{ce} = Effective concrete strength, psi

ν = Efficiency factor

Efficiency factors as specified by ACI 318-08, AASHTO LRFD (2008), and the *fib* (1999) are presented in Section 2.4.2. It is important to note that differences exist between load, material, and strength reduction factors for the codes mentioned. Therefore, in order to maintain clarity when evaluating efficiency factors of different code provisions, reduction factors are not considered in the comparisons.

2.4.1 Design of Struts

In order to ensure adequate deformation capacity to develop the forces in a truss model, the orientation of a strut should not deviate excessively from 45-degrees. According to ACI 318-08, the minimum strut angle should not be taken as less than 25-degrees. Similarly, *fib* (1999) states that strut *angles smaller than 30-degrees are unrealistic and involve high incompatibility of strains*. AASHTO LRFD (2008) allows any strut angle but accounts for the ineffectiveness of shallow struts by reducing the efficiency factor accordingly.

ACI 318-08 and AASHTO LRFD (2008) designate a strut design separate from a node design and concurrently assign separate efficiency factors. This area of inconsistency is a source of confusion for designers when determining the capacity of the node-to-strut interface. Contrary to ACI 318-08 and AASHTO LRFD (2008), *fib* (1999) does not explicitly require the strut to be designed. *fib* (1999) recognizes the fact that the critical stress in a strut occurs at the strut-to-node interface. According to *fib* (1999):

> *Except for prismatic stress fields, the design strength of stress fields is, in fact, very rarely needed in practice…Critical concrete stresses in D-regions occur in the regions of concentrated nodes. These are…checked with the node design.*

For the purposes of comparison, the efficiency factors are presented in the following section for the three faces of a nodal region. The efficiency factor

assigned to a *strut* by ACI 318-08 and AASHTO LRFD (2008) is presented as the efficiency of the *node-to-strut interface*.

2.4.2 Design of Nodes: Nodal Efficiency Factors

In an STM design, the stress applied to each face of a node is kept less than its capacity. The capacity is taken as a fraction of its material strength. CCC nodes are usually assumed to have the highest capacity because concrete is subjected to biaxial or triaxial confining stresses. CCT and CTT nodes have reduced capacities because tensile strains across the nodal region are thought to reduce the compressive strength. Allowable stresses for nodal regions are listed in Sections 2.4.2.1 through 2.4.2.3.

2.4.2.1 CCC Nodal Zone

The three nodal faces in a CCC region are illustrated in Figure 2-13. The allowable capacities of the CCC nodal faces are presented in Table 2.1.

Table 2.1. Allowable Stresses for a CCC Node.

Node Face	Design Code	Efficiency Factor	Reduction Factor, ϕ_c
Back Face	ACI 318	$0.85 \cdot (1) = 0.85$	$\phi_c = 0.75$
	AASHTO	0.85	$\phi_c = 0.70$
	fib (1999)†	$0.85 \cdot \left(1 - f_c'/40ksi\right)$	$\alpha_c/\gamma_c = 0.5$††
Bearing Face	ACI 318-08	$0.85 \cdot (1) = 0.85$	$\phi_c = 0.75$
	AASHTO	0.85	$\phi_c = 0.70$
	fib (1999)†	$0.85 \cdot \left(1 - f_c'/40ksi\right)$	$\alpha_c/\gamma_c = 0.5$††
Strut-Node Interface	ACI 318	$0.85 \cdot (0.75) = 0.64$ when $\rho > \rho_{min}$††† $0.85 \cdot (0.60) = 0.51$ when $\rho < \rho_{min}$†††	$\phi_c = 0.75$
	AASHTO	0.85	$\phi_c = 0.70$
	fib (1999)†	$0.85 \cdot \left(1 - f_c'/40ksi\right)$	$\alpha_c/\gamma_c = 0.5$††

† *fib* (1999) includes a material variability factor, α_c, embedded within their efficiency factor expression. This factor varies depending on the strength of concrete (0.7 to 0.8 for 4000 to 7000-psi); it is not included as part of the efficiency factor for ease of comparison. An argument can be made for expressing the efficiency factor differently; however, the overall trend between code provisions will not be significantly affected.

†† Concrete compressive strength assumed to be 4000-psi.

††† ρ_{min} defined in Section 2.4.4

The back face and bearing face efficiency factors are the same for ACI 318 and AASHTO LRFD (i.e. 0.85). The *fib* (1999) factor is slightly lower and is reduced as the compressive strength of concrete increases.

A stress check at the back face of a CCC node is essentially the same procedure that is performed when checking a beam's flexural capacity. The maximum concrete compressive stress allowed for a flexural design is $0.85f_c'$. This is consistent with the efficiency factor allowed by ACI 318-08 and AASHTO LRFD (2008).

Similarly, the stress check at the bearing face of a CCC node is the same check that is conducted when determining the bearing capacity of concrete. According to ACI 318-08 and AASHTO LRFD (2008), the bearing capacity of unconfined concrete is equal to $0.85f_c'$ This is consistent with the bearing face efficiency factor.

Another trend to point out is that the efficiencies of all three faces in the CCC nodal zone are identical according to the AASHTO LRFD (2008) and *fib* (1999) provisions. The factor specified by ACI 318-08 is smaller at the node-to-strut interface. A discrepancy exists when the efficiency factor is the same at all three nodal faces: the capacity of a truss model will never be controlled by the capacity of the strut-to-node interface. Depending on the angle of the strut framing into the node, the stress at either the bearing or back face will be the most critical (Figure 2-13 and 2-14).

2.4.2.2 CCT Nodal Zone

The three nodal faces in a CCT region are illustrated in Figure 2-14. The allowable capacities of the CCT nodal faces are presented in Table 2.2.

Table 2.2. Allowable Stresses for a CCT Node.

Node Face	Design Code	Efficiency Factor	Reduction Factor, ϕ_c
Back Face	ACI 318	$0.85 \cdot (0.80) = 0.68$	$\phi_c = 0.75$
	AASHTO	0.75	$\phi_c = 0.70$
	fib (1999)†	$0.70 \cdot \left(1 - f_c' / 40ksi\right)$	$\alpha_c/\gamma_c = 0.5$††
Bearing Face	ACI 318-08	$0.85 \cdot (0.80) = 0.68$	$\phi_c = 0.75$
	AASHTO	0.75	$\phi_c = 0.70$
	fib (1999)†	$0.70 \cdot \left(1 - f_c' / 40ksi\right)$	$\alpha_c/\gamma_c = 0.5$††
Strut-Node Interface	ACI 318	$0.85 \cdot (0.75) = 0.64$ when $\rho > \rho_{min}$††† $0.85 \cdot (0.60) = 0.51$ when $\rho < \rho_{min}$†††	$\phi_c = 0.75$
	AASHTO	$\left(1 / 0.8 + 170\varepsilon_1\right) \leq 0.85$*	$\phi_c = 0.70$
	fib (1999)†	$0.70 \cdot \left(1 - f_c' / 40ksi\right)$	$\alpha_c/\gamma_c = 0.5$††

† *fib* (1999) includes a material variability factor, α_c, embedded within their efficiency factor expression. This factor varies depending on the strength of concrete (0.7 to 0.8 for 4000 to 7000-psi); it is not included as part of the efficiency factor for ease of comparison. An argument can be made for expressing the efficiency factor differently; however, the overall trend between code provisions will not be significantly affected.

†† Concrete compressive strength assumed to be 4000-psi.

††† ρ_{min} defined in Section 2.4.4

* Refer to Section 2.5 for more details of the equation used to calculate AASHTO LRFD interface efficiency factor.

The efficiency factors in the CCT nodal region are generally less than those in the CCC region because transverse tensile stresses are present, resulting in a reduction in the effective compressive strength of concrete. ACI 318-08 specifies the same efficiency factor at the node-to-strut interface in both the CCC and CCT regions.

The stress that must be resisted by the back face of a CCT node can be attributed to anchorage of the tie reinforcement, bearing from an anchor plate or headed bar, or external indeterminacy such as occurs at an interior node over a continuous support (Figure 2-18).

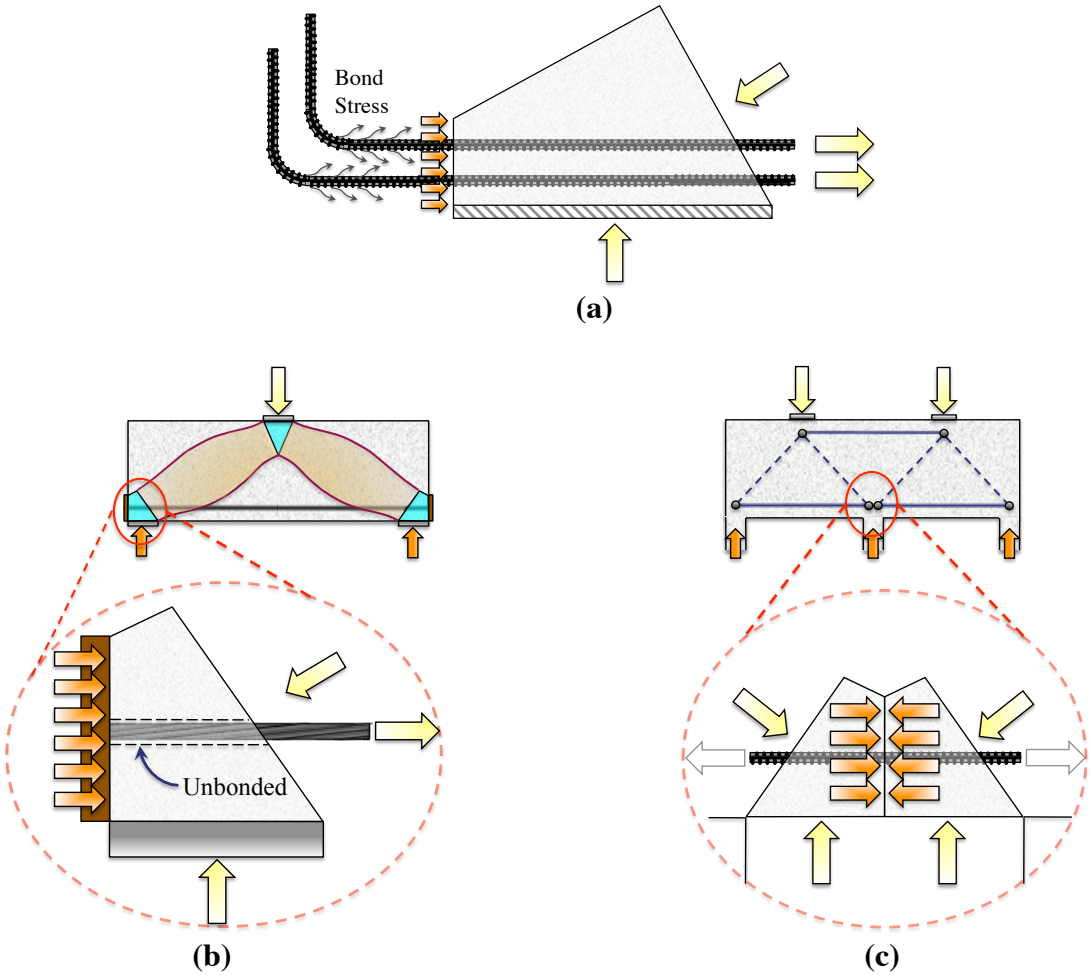

Figure 2-18. Stress condition at the back face of a CCT node: (a) bonding stress; (b) bearing of an anchor plate; (c) interior node over a continuous support.

The effectiveness of the back face of a CCT node is dependent on the stress condition. *fib* (1999) provisions recognize that the stress caused by the bonding of an anchored bar [Figure 2-18(a)] are not critical and need not be considered when evaluating the capacity of a CCT node. This fact is acknowledged by Thompson et al. (2003). According to the researchers:

> *The philosophy of the current code provisions for determining the capacity of CCT nodes may require reconsideration. The evidence from the tests*

shows that the failure of these nodes was primarily related to anchorage and that the current stress limits for nodes were unrealistic. It is possible that CCT nodes cannot fail in compression if anchorage of the tie bars is sufficient. The stress limits imposed by the code provisions may be unnecessary.

When the stress that is resisted by a CCT node is attributed to a condition other than anchorage, *fib* (1999) recommends the efficiency factor presented in Table 2.2 as follows:

In conclusion, it can be stated, that the concrete in the node [over an interior support] is under biaxial compression, but the horizontal compression is difficult to assess. On the other hand, tensile reinforcement penetrates the node region and is anchored there to some extent. Therefore, [the CCT bearing face efficiency] will again be applied here as design node strength, the [the CCC bearing efficiency] might eventually be considered.

ACI 318-08 and AASHTO LRFD (2008) provisions require that the stress attributed to the anchorage of a tie be applied to the back face of the CCT node as a concentrated force. The provisions do not distinguish between the stress conditions illustrated in Figure 2-18.

2.4.2.3 CTT Nodal Zone

The three nodal faces in a CTT region are illustrated in Figure 2-15. The allowable capacities of the CTT nodal faces are presented in Table 2.3.

Table 2.3. Allowable Stresses for a CTT Node.

Node Face	Design Code	Efficiency Factor	Reduction Factor, ϕ_c
Back Face	ACI 318	$0.85 \cdot (0.60) = 0.51$	$\phi_c = 0.75$
	AASHTO	0.65	$\phi_c = 0.70$
	fib (1999)†	NA	-
Exterior Face	ACI 318-08	$0.85 \cdot (0.60) = 0.51$	$\phi_c = 0.75$
	AASHTO	0.65	$\phi_c = 0.70$
	fib (1999)†	NA	-
Strut-Node Interface	ACI 318	$0.85 \cdot (0.75) = 0.64$ when $\rho > \rho_{min}$ ††† $0.85 \cdot (0.60) = 0.51$ when $\rho < \rho_{min}$ †††	$\phi_c = 0.75$
	AASHTO	$\left(1 / 0.8 + 170\varepsilon_1 \right) \leq 0.85$*	$\phi_c = 0.70$
	fib (1999)†	$0.60 \cdot \left(1 - f_c' / 40ksi \right)$	$\alpha_c / \gamma_c = 0.5$††

† *fib* (1999) includes a material variability factor, α_c, embedded within their efficiency factor expression. This factor varies depending on the strength of concrete (0.7 to 0.8 for 4000 to 7000-psi); it is not included as part of the efficiency factor for ease of comparison. An argument can be made for expressing the efficiency factor differently; however, the overall trend between code provisions will remain unchanged.

†† Concrete compressive strength assumed to be 4000-psi.

††† ρ_{min} defined in Section 2.4.4

* Refer to Section 2.5 for more details of the equation used to calculate AASHTO LRFD interface efficiency factor.

In general, the efficiency factors specified for a CTT nodal region are less than a CCT region due to the presence of additional tensile stresses. Again, ACI 318-08 specifies the same efficiency at the node-to-strut interface regardless of the type of nodal region.

Similar to the back face of a CCT node, *fib* (1999) recognizes that the back face and exterior face of a CTT node are typically not critical (provided bars are anchored properly). According to *fib* (1999):

> *If… bars are distributed over a great length of the main reinforcement, as is normally the case in beams, the node is of the "smeared" type and needs not be checked in detail.*

Schlaich et al. (1987) makes a similar point:

Since D-regions usually contain both smeared and singular nodes, the latter will be critical and a check of concrete stresses in smeared nodes is unnecessary.

2.4.3 Design of Ties

The design strength of ties is straightforward. The maximum capacity of a tie is simply taken as the specified yield strength of the reinforcement, f_y.

The important factors to consider when detailing a tie are proper bar distribution, spacing, and development length. Ties must be anchored behind the nodal zones with a minimum amount of development length as previously illustrated in Figure 2-17.

2.4.4 Minimum Transverse Reinforcement Requirements

A member designed using an STM must have sufficient deformation capacity in order to redistribute stresses into the assumed truss model. Providing a constant amount of transverse reinforcement is an efficient method for attaining deformation capacity. In general, a minimum amount of transverse reinforcement is required for both strength and serviceability. Reinforcement required for strength is quantified based on the amount necessary to maintain the integrity of the member after cracking has occurred. Reinforcement required for serviceability is determined based on the distribution of cracking and allowable crack widths desired under the action of service loads.

ACI 318-08 allows a designer to use unreinforced struts provided the efficiency factor is reduced. If a higher efficiency factor is desired, a minimum amount of transverse reinforcement is required. The amount is proportioned to act as a tie across the strut. Figure 2-19 illustrates the transverse tensile stresses developed in a bottle-shaped strut.

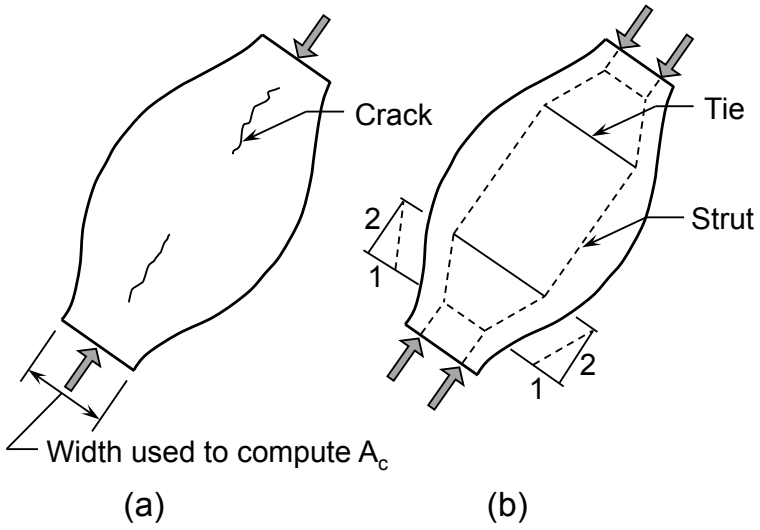

Figure 2-19. Bottle-shaped strut: (a) cracking of a bottle-shaped strut; and (b) strut-and-tie model of a bottle-shaped strut (ACI 318-08).

The ACI 318-08 requirement appears to be based on maintaining the integrity of a strut; therefore, it can be inferred that the provision is a *strength* requirement. According to ACI 318-08, §A.3.3:

> *…the axis of the strut shall be crossed by reinforcement proportioned to resist the transverse tensile force resulting from the compression force spreading in the strut. It shall be permitted to assume the compressive force in the strut spreads at a slope of 2 longitudinal to 1 transverse to the axis of the strut.*

According to ACI 318-08, in lieu of the preceding requirement, a minimally reinforced strut may contain the amount of reinforcement specified in Equation 2-4 and illustrated in Figure 2-20.

$$\rho_{\perp} = \sum \frac{A_{si}}{b_s \cdot s_i} \sin \alpha_i \geq 0.003 \qquad \text{Equation 2-4}$$

Where,

A_{si} = total area of surface reinforcement at spacing s_i in the i-th layer crossing a strut, with reinforcement at an angle α_i to the axis of the strut, in^2

b_s = width of strut, in.

s_i = center-to-center spacing of reinforcement of the i-th layer adjacent to the surface of the member, in.

α_i = angle between the axis of a strut and the bars in the i-th layer of reinforcement crossing that strut

$\rho_\perp$ = ratio of reinforcement perpendicular to the axis of the strut

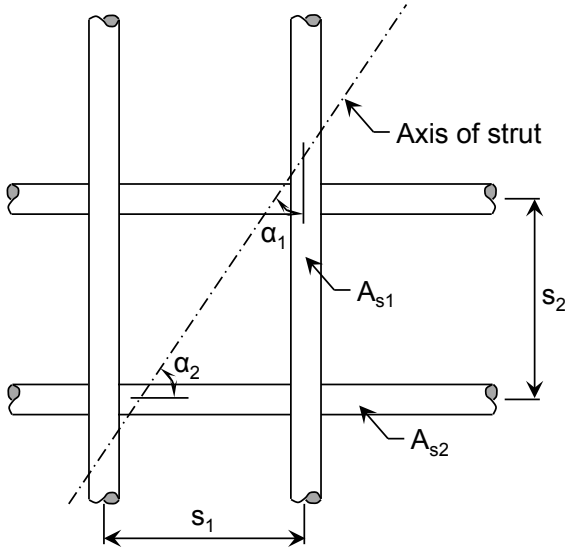

Figure 2-20. Reinforcement crossing a strut (taken from ACI 318-08).

If reinforcement is placed in orthogonal, evenly spaced grids and the strut is orientated at a 45-degree angle, the amount specified in Equation 2-4 is equivalent to 0.2% in each direction. Note, ACI 318-08 STM provisions do not specify a maximum spacing for the stirrups. Also, providing all of the reinforcement in a single transverse direction will satisfy the requirements of the provision. This may be an undesirable solution.

AASHTO LRFD (2008) §5.6.3.6 contains the following *crack control* provision regarding minimum reinforcement and maximum spacing:

Structures and components…except for slabs and footings…shall contain an orthogonal grid of reinforcing bars near each face. The spacing of the

bars shall not exceed 12 in. The ratio of reinforcement area to gross concrete area shall not be less than 0.003 in each direction. [i.e. 0.3%]

fib (1999) recommends the following minimum amount of reinforcement; they do not specify a maximum bar spacing:

…0.2% of the concrete cross-section in both orthogonal directions. These reinforcements… are arranged on both faces (0.1% for each face).

There is a discrepancy between the different provisions regarding the method used to calculate the percentage of horizontal reinforcement. The percentage specified in ACI 318-08 is based on bar spacing while the percentage specified by *fib* (1999) and AASHTO LRFD (2008) is based on the total cross-sectional area. This can result in a substantial difference. Take for example, the beam illustrated in Figure 2-21. The horizontal reinforcement ratio according to ACI 318-08 is 0.45%; according to AASHTO LRFD (2007) and *fib* (1999), the ratio of reinforcement for the same beam is 0.28%.

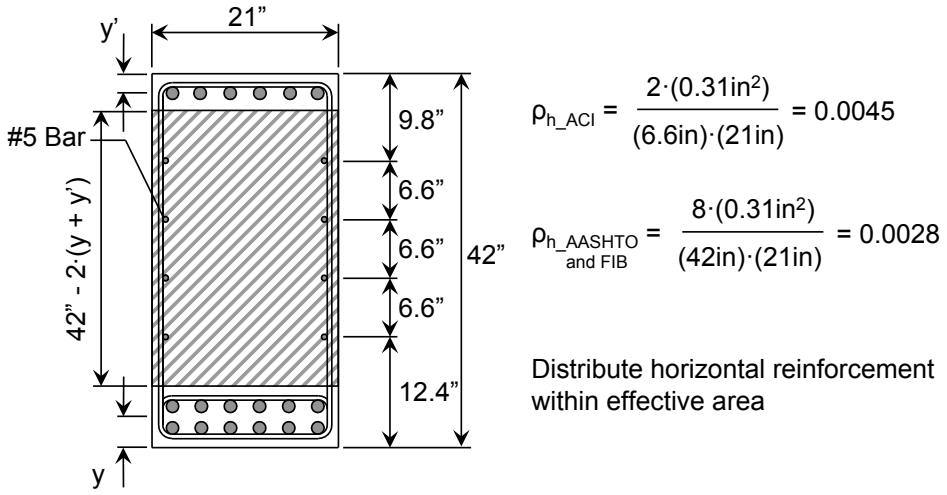

Figure 2-21. Horizontal reinforcement ratio calculated per ACI 318-08 vs. AASHTO LRFD (2007) and *fib* (1999).

For the sake of consistency, the horizontal reinforcement ratio used throughout the current research program is calculated based on the bar spacing (i.e. method employed by ACI 318-08). Based on a suggestion from a senior

TxDOT Bridge Engineer (communications with Dean Van Landuyt, 2006), it is recommended that the horizontal reinforcement be distributed vertically across the effective area shown in Figure 2-22. The extents of the area are based on the vertical projection of the strut. There is not a need to distribute the horizontal reinforcement in the compression zone of the beam or in the region defining the horizontal tie. Rather, the horizontal transverse reinforcement should be placed to control the cracks that form within the strut as shown in Figure 2-22.

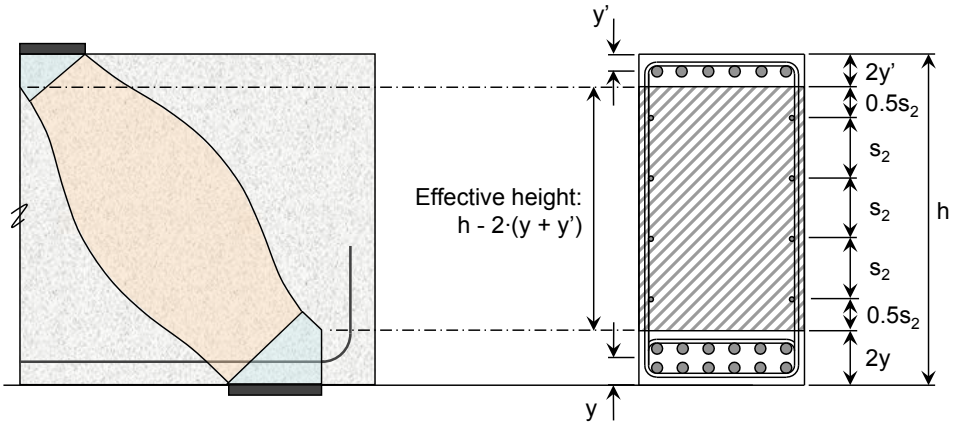

Figure 2-22. Effective height to use for the distribution of horizontal reinforcement.

Table 2.4 summarizes the minimum reinforcement requirements for ACI 318-08, AASHTO LRFD (2008), and *fib* (1999). Differences in the reinforcement requirements are discussed within a historical context in Sections 2.5 and 2.6. Section 2.5 presents a historical timeline of shear design provisions and their evolution in the U.S. Section 2.6 presents background information for the current STM design provisions found in ACI 318-08, AASHTO LRFD (2008), and *fib* (1999).

Table 2.4. Minimum Reinforcement Requirements

Design Provision	Minimum Reinforcement Requirement	Maximum Spacing
ACI 318	$\sum(\rho_v \cos\theta + \rho_h \sin\theta) \geq 0.3\%$	No Limit
AASHTO LRFD	$\rho_v \geq 0.3\%$ *and* $\rho_h \geq 0.3\%$	12-inches
fib (1999)	$\rho_v \geq 0.2\%$ *and* $\rho_h \geq 0.2\%$	No Limit

2.5 HISTORIC DEVELOPMENT OF SHEAR PROVISIONS

In 2002, *Appendix A, Strut-and-Tie Modeling* provisions were added to the ACI 318 building code. The chapter was introduced as a method for designing deep beams or other regions of discontinuity. Prior to 2002, deep beams were designed for shear based on an empirically derived formula. The evolution of these empirical shear provisions is presented next. The purpose of presenting the history of shear is to provide insight into current STM provisions.

Before 1963, provisions specific to the design of deep beams did not exist. Until that time, deep beams were most likely designed based on the prescriptive requirements specified for a wall design. These requirements can be traced back to the 1910 standard. In 1910, the National Association of Cement Users (NACU 1910) listed the following requirement for the design of concrete walls.

> *Concrete walls must be reinforced in both directions. The maximum spacing of reinforcing bars shall be 18 inches… Total reinforcement shall not be less than one-fourth of one percent [0.25%].*

This provision remained essentially unchanged until 1956. In the 1956 version of ACI 318, the minimum reinforcement ratio for walls in the vertical direction was reduced from 0.25% to 0.15% (ACI 318-56). The reason for the change is most likely due to the addition of a minimum reinforcement provision for beams. Based on advancements in shear research, the minimum amount of transverse web reinforcement for typical beams resisting shear was found to be 0.15%. Subsequently, a provision limiting the minimum amount of web reinforcement to 0.15% made its first appearance in Section *807-Minimum web*

reinforcement. Therefore, it can be assumed that the minimum reinforcement provision was changed in Section *1111-Reinforced concrete walls* in order to provide consistency between the two sections.

In 1963, the first provision specific to the design of deep beams appeared in the ACI 318 specifications. ACI 318-63 contains the first definition of a deep beam and explicitly requires a minimum amount of reinforcement. According to the requirements of ACI 318-63, deep beams are to be designed as follows:

> *Beams with depth/span ratios greater than 2/5 for continuous spans, or 4/5 for simple spans shall be designed as deep beams taking account of nonlinear distribution of stress, lateral buckling, and other pertinent effects. The minimum horizontal and vertical reinforcement in the faces shall be the same as in 2202(f) [0.25% and 0.15% respectively].*

Suggestions for the design of deep beams were based on recommendations from Chow et al. (1952). These studies determined the non-linear stress distribution in a deep beam based on a finite element analysis of a homogenous material. The researchers recognized the fact that concrete is a non-homogenous material. However, according to Chow et al. (1952), *a rigorous theoretical analysis of the stresses in such beams is hardly feasible*. As a result, Chow et al. (1952) recommended providing sufficient steel reinforcement in the tensile zones to *convert the beam, as closely as possible, to a homogenous beam*. The requirement in ACI 318-63 for the minimum amount of horizontal and vertical web reinforcement was taken to be the same as that required for walls based on the conventional construction practice at the time. According to the ACI 318-63 Commentary:

> *The empirical requirements [for walls] have been changed little since first presented in 1928 and have resulted in satisfactory construction.*

In 1971, entirely new provisions were included in the ACI code for the design of deep beams (ACI 318-71). Similar to a sectional shear design, the

nominal shear strength of a deep beam was taken as the sum of the concrete and steel contributions (Equation 2-5).

$$v_n = v_c + v_s \qquad \text{Equation 2-5}$$

Where,

$$v_c = \left(3.5 - 2.5\frac{M_u}{V_u d}\right)\left(1.9\sqrt{f_c'} + 2500\rho_w \frac{V_u d}{M_u}\right)$$

$$v_s = \frac{A_v f_y}{b_w s_1}\left(\frac{1+\frac{l_n}{d}}{12}\right) + \frac{A_{vh} f_y}{b_w s_2}\left(\frac{11-\frac{l_n}{d}}{12}\right)$$

A_v = area of shear reinforcement within a distance s_1, in^2

A_{vh} = area of shear reinforcement within a distance s_2, in^2

ϱ_w = ratio of main tensile reinforcement to $b_w d$

M_u = applied design moment at the critical section, in.-lb

V_u = applied design shear at the critical section, lb

f_c' = specified compressive strength of concrete, psi

f_y = specified tensile strength of reinforcement, psi

d = distance from extreme compression fiber to centroid of tension reinforcement, in.

b_w = web width, in.

s_1 = center-to-center spacing of vertical reinforcement, in.

s_2 = center-to-center spacing of horizontal reinforcement, in.

The concrete contribution, v_c, contains two terms in parentheses. The second term is the empirical formula for the diagonal cracking strength of concrete; the same equation that is used to this day for a sectional shear design. The first term provides an increase in shear strength above the diagonal cracking strength for an a/d ratio less than 2.0 and *shall not exceed 2.5*. According to ACI-

ASCE Committee 426 (1973), *this equation is based on the work by Crist (1966, 1967), and de Pavia and Siess (1965).*

The derivation of the web reinforcement contribution, v_s, is based on the shear friction capacity of the beam along the inclined crack. The shear friction equation is not normally applied to sections where there is a significant moment. However, for deep beams, there is significant shearing action along the critical inclined crack (ACI-ASCE 426-73). Normal forces on the inclined crack are developed by tension in the web reinforcing, and the tension in the web reinforcing is developed by the slip along the crack. If all of the web reinforcement is assumed to have yielded at ultimate load conditions, then the resistance can be derived based on the orientation and location of the reinforcement along the crack. Crist (1967) simplified the derivation of v_s based on a lower bound of test data. He expressed the trigonometric terms associated with crack inclination and the shear span in terms of overall span, l_n, and depth, d; resulting in the expression eventually adopted by ACI 318-71 (Equation 2-5).

The minimum requirement for horizontal and vertical web reinforcement remained unchanged from previous codes (0.25% and 0.15% respectively). However, a maximum spacing requirement was added (d/5 or 18-inches and d/3 or 18-inches in the horizontal and vertical directions, respectively).

The deep beam shear provisions remained essentially unchanged until the release of the 2002 version of the ACI 318 code (ACI 318-02). In 2002, the empirical deep beam shear equation (Equation 2-5) was completely removed from Chapter 11 and replaced with the following provision.

> *Deep beams shall be designed using either a nonlinear analysis… or Appendix A [Strut-and-Tie Models]*

The minimum amounts of horizontal and vertical web reinforcement were interchanged with one another (0.15% and 0.25% respectively) because *tests have shown that vertical shear reinforcement is more effective than horizontal reinforcement*. Also, the maximum spacing was reduced to d/5 or 12 in. for both

directions because *this steel is provided to restrain the cracks* (ACI 318-02). However, in lieu of the aforementioned minimum reinforcement and spacing requirements:

> *It shall be permitted to provide reinforcement satisfying A.3.3 [Section 2.4.4] instead of the minimum horizontal and vertical reinforcement specified [in Chapter 11].*

In summary, the *Deep Beam* section of the ACI 318 provisions (Chapter 11) requires a minimum amount of horizontal and vertical reinforcement; either by a prescriptive requirement (0.15% and 0.25%) or by the amount required in Section A.3.3. However, Section A.3.2 allows the use of unreinforced struts. This area of inconsistency is a point of confusion among designers and is addressed further within this research project.

The deep beam provisions in the current version of the ACI 318 code (ACI 318-08) have remained essentially unchanged since 2002. Next, a review of the background of STM procedures, including provisions specific to the current research program is presented.

2.6 HISTORIC DEVELOPMENT OF STRUT-AND-TIE MODEL PROVISIONS

The concept of idealizing reinforced concrete members using a truss model dates back to the end of the nineteenth century. In 1899, Wilhelm Ritter suggested a truss mechanism to explain the role of transverse reinforcement in resisting shear of a beam. Mörsch later refined Ritter's model in 1902. After 1927, truss modeling fell out of favor in the United States when Richart proposed a sectional method of shear design in which the concrete and steel contributions to shear strength were calculated independently (Brown et al. 2006).

In 1971, Lampert and Thürlimann developed a three-dimensional space truss to explain the combined actions of shear and torsion. Their torsion model was further refined by Mitchell and Collins (1971) and Ramirez and Breen (1983) so that the space truss could account for all combinations of shear, bending,

torsion, and axial loadings. Vecchio and Collins (1982) took the theory of plasticity a step further and derived the *modified compression field theory* – taking into account the deformation compatibility of the truss model. At this time, truss modeling re-emerged in American design standards. Based on the experimental program by Rogowsky et al. (1986), Rogowsky and MacGregor (1986) developed the *plastic truss theory*. This theory is an extension of the plasticity theory presented by Nielson et al. (1978) and Thürlimann (1978). At the same time, Marti (1985) and Schlaich et al. (1987) extended the truss modeling approach to overall discontinuity regions with a *strut-and-tie modeling* approach.

The STM provisions in the ACI 318-08 code are largely attributed to the work conducted by Rogowsky and MacGregor (1986), Ramirez and Breen (1991), Bergmeister et al. (1993), Schlaich et al. (1987), and Marti (1985). AASHTO LRFD (2008) provisions are based on the modified compression field theory (MCFT) proposed by Vecchio and Collins (1986). *fib* (1999) recommendations can be traced to the research conducted by Nielson et al. (1978) and Bergmeister et al. (1993). A summary of previous research findings is presented in Sections 2.6.1 through 2.6.3 .

2.6.1 Behavior of Struts (Strut-to-Node Interface)

There is a tremendous amount of research that has been conducted to determine the efficiency of concrete at the strut-to-node interface and numerous efficiency equations have been proposed. For detailed information on research programs that focused on the efficiency of a strut, refer to Brown et al (2006) and ACI 445R-99.

2.6.1.1 ACI 318-08 Strut Efficiency Factors

MacGregor (2002) presents a summary of the background of the efficiency factors ultimately selected by ACI 318-08 (Table 2.1, Table 2.2, and Table 2.3). According to MacGregor (2002):

…the values of the f_{cu} [effective concrete capacity] presented in the ACI Code were chosen to satisfy four criteria: Simplicity in application; Compatibility with tests of D-regions; Compatibility with other sections of ACI 318; Compatibility with other codes or design recommendations.

Because these four criteria lead to different values of f_{cu} for a given application, judgment was required in selecting the values of f_{cu}. The [values] are generally higher than those from other codes because more weight was given to [compatibility with the ACI Code and tests of D-regions] than was given to other codes.

ACI 318-08 efficiency factors at the strut-to-node interface are attributed to the research conducted by Rogowsky et al. (1986), Ramirez and Breen (1991), Bergmeister et al. (1993), Schlaich et al. (1987), and Marti (1985). A summary of their findings is presented in Sections 2.6.1.1.1 through 2.6.1.1.5.

2.6.1.1.1 Rogowsky and MacGregor (1986)

Rogowsky and MacGregor (1986) based their recommendations on an experimental program conducted by Rogowsky et al. (1986). The researchers tested 7 simply supported and 17 two-span continuous beams with various vertical and horizontal reinforcement ratios. They found that beams with significant amounts of vertical reinforcement were ductile and had consistent failure loads. The researchers recommended that the capacity of the stirrups crossing the diagonal of the shear span be greater than 30% of the applied shear force.

Also, Rogowsky and MacGregor (1986) observed that the selection of the truss model was more important than the selection of an efficiency factor. If the selected truss differs excessively from the elastic distribution of stresses, full redistribution may not occur and the truss may fail prematurely, giving the appearance of a low efficiency factor. For general use, they recommended the following efficiency factor.

$$\nu = 0.6$$ Equation 2-6

Finally, the researchers recommended a minimum strut angle similar to that recommended by Thürlimann (1978) and Ramirez and Breen (1991).

$$25° \le \theta \le 65°$$

2.6.1.1.2 Ramirez and Breen (1991)

Ramirez and Breen (1991) proposed a modified truss model that recognizes that concrete efficiency decreases as compressive strength increases. The strut efficiency factor that they recommended is expressed as follows:

$$\nu = \frac{30}{\sqrt{f'_c}}$$ Equation 2-7

Values range between 0.55 and 0.34 for 3000 to 8000-psi concrete. A comparison between the Ramirez and Breen (1991) recommendations and the current ACI 318-08 provisions is presented in Figure 2-23.

2.6.1.1.3 Bergmeister, Breen, Jirsa, and Kreger (1993)

Bergmeister et al. (1993) proposed the following efficiency factors. The researchers based the expression on a *large number of test results*. Also, they recognized that efficiency decreased as the compressive strength of concrete increased. The efficiency factor values range between 0.8 and 0.42 for 3000 to 8000-psi concrete (Equation 2-8 and Figure 2-23).

$$\nu = \begin{cases} 0.8\nu_{ed} \ if \ f'_c \le 4000\,psi \\ \left(0.9 - \dfrac{0.25 f'_c}{10{,}000\,psi}\right)\nu_{ed} \ if \ 4000\,psi < f'_c < 10{,}000\,psi \\ 0.65\nu_{ed} \ if \ f'_c \ge 10{,}000\,psi \end{cases}$$ Equation 2-8

Where,

ν_{ed} = 0.6 for compression diagonals (i.e. CCC and CCT strut-to-node interface)

1.0 otherwise (i.e. CCC and CCT back and bearing face)

A comparison between the Bergmeister et al. (1993) recommendations and the current ACI 318-08 provisions is presented in Figure 2-23.

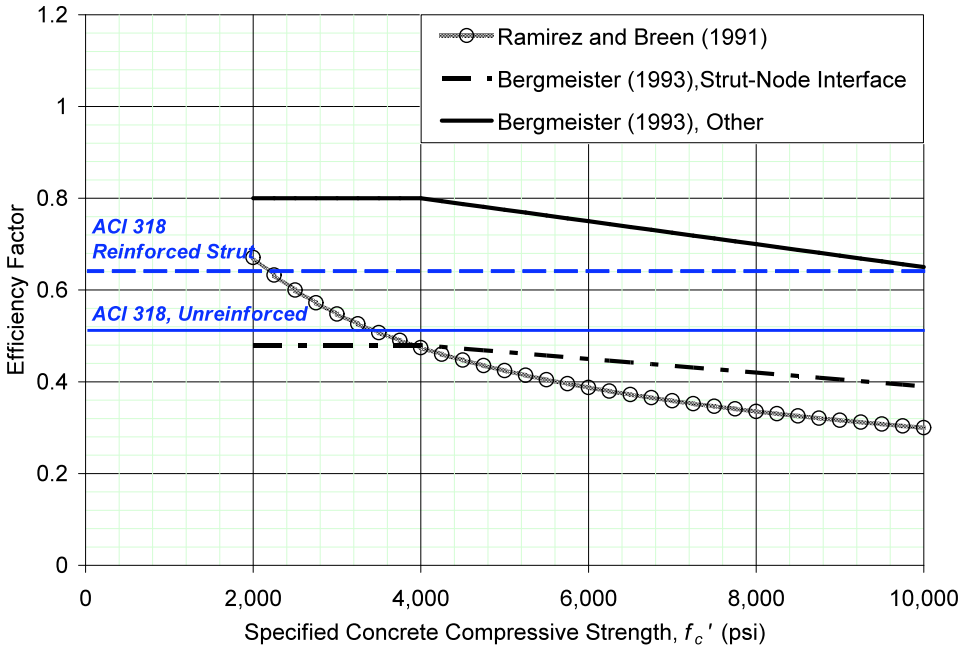

Figure 2-23. Comparison of strut efficiency factors: ACI 318-08

2.6.1.1.4 Marti (1986)

Based on comparisons with experimental research, Marti (1986) suggested that the following efficiency factor be used.

$$\nu = 0.6 \qquad \text{Equation 2-9}$$

Marti suggested this value as a *first start*. The efficiency factor may then be decreased or increased depending on details such as presence of distributed reinforcement or lateral confinement. Marti (1986) also pointed out that distributed minimum transverse reinforcement contributes significantly to the ability of a deep beam to redistribute internal forces after cracking.

2.6.1.1.5 Schlaich, Schäfer, and Jennewein (1987)

Sclaich et al. (1987) proposed that the efficiency factor reflect the fact that the strength of concrete is dependent on the multi-axial state of stress and on disturbances from cracks and reinforcement. The researchers stated that

confinement was favorable and could be provided by transverse reinforcement or by bulk concrete surrounding a relatively small compression field. They further stated that transverse tensile stresses were detrimental to the efficiency. For *reasons of practicality*, the researchers recommended the following efficiency factors:

$$\nu = 0.85 \cdot \beta_n$$

Where,

ν =	0.85, ($\beta_n = 1.0$),	for undisturbed, uniaxial state of compressive stress (CCC bearing and back face).
	0.68, ($\beta_n = 0.8$),	nodal regions where tension bars are anchored or crossing (CCT nodal regions).
	0.51, ($\beta_n = 0.6$),	if tensile strains result in cracking skewed to the strut (CTT nodal regions).
	0.34, ($\beta_n = 0.4$),	for skewed cracks with extraordinary crack width.

The recommendations proposed by Schlaich et al. (1987) are very similar to the efficiency factors adopted by the ACI 318-02 code.

2.6.1.2 AASHTO LRFD Strut Efficiency Factors: MCFT

The strut efficiency factors specified in the AASHTO LRFD (2008) specifications are based on the Compression Field Theory developed by Mitchell and Collins (1974) and, later, the Modified Compression Field Theory developed by Vecchio and Collins (1986). Vecchio and Collins (1986) suggested that the maximum compressive stress that concrete can resist reduces with the increase of cracking parallel to the compressive stress field. As a result, the stress limit recommended by Vecchio and Collins (1986) accounts for the principle tensile strain perpendicular to the axis of the strut. According to AASHTO LRFD (2008), the effective compressive strength of a strut is calculated as follows.

$$f_{cu} = \frac{f'_c}{0.8 + 170 \cdot \varepsilon_1} \leq 0.85 f'_c \qquad \text{Equation 2-10}$$

Thus, the efficiency factor is expressed as follows:

$$\nu = \frac{1}{0.8 + 170 \cdot \varepsilon_1} \leq 0.85$$

In which,

$$\varepsilon_1 = \varepsilon_s + (\varepsilon_s + 0.002) cot^2 \alpha_s$$

Where,

α_s = the smallest angle between the compression strut and adjoining tension tie, degrees

ε_s = the tensile strain in the concrete in the direction of the tensile tie

f_c' = specified compressive strength of concrete, psi

The tensile strain in concrete, ε_s, is attributed to the tensile strain in the adjacent tie. Thus, the efficiency factor diminishes in tension regions (CCT or CTT nodal regions). Also, due to equilibrium with the strut, the tie force increases as the strut becomes shallower. As a result, the tensile strain term increases for shallow struts; further reducing the efficiency factor.

In general, practitioners have reservations when it comes to calculating the tensile strain in concrete, ε_s, as the calculation is a somewhat tedious iterative process. The tensile strain in concrete may be estimated by dividing the tensile stress in the tie by the modulus of elasticity of steel However, the force in the tie depends on the compressive force in the strut This is turn depends on the efficiency factor. Hence, the calculation for the force in the strut, efficiency factor, and force in the tie must be reiterated until the values converge at a solution.

The AASHTO LRFD (2008) expression for strut efficiency has been derived by using hydrostatic nodes. Struts that are bounded by hydrostatic nodes increase proportionally with the a/d ratio (Figure 2-12). As a result, as the a/d ratio is increased, the efficiency factor must proportionally decrease in order to

counteract the increasing strut width. However, AASHTO LRFD (2008) §5.6.3.3.2 recommends the use of non-hydrostatic nodes. If non-hydrostatic nodes are used – as they typically are – then the STM capacity is reduced by both the diminishing efficiency factors and the diminishing strut width. Therefore, when non-hydrostatic nodes are employed, the efficiency of the strut-to-node interface is essentially penalized twice, possibly resulting in an overly conservative estimation of capacity.

2.6.1.3 fib (1999) Strut Efficiency Factors

fib (1999) provisions do not recommend separate stress checks between nodal zones and struts. They recognize the fact that the critical stress in a strut occurs at the node-to-strut interface. *fib* (1999) recommends using the same efficiency for all faces of a nodal region. Therefore, a background to the *fib* (1999) provisions is presented with the nodal zone efficiencies in Section 2.6.2.3.

2.6.2 Behavior of Nodal Zones

Few researchers distinguish between the efficiency of a strut or node. Typically, concrete efficiency is specified based on the degree of cracking, state of stress, or tensile strain within a compression field. However, the efficiency factors specified in ACI 318-08, AASHTO LRFD (2008), and *fib* (1999) are specific to individual elements (i.e. nodes and struts). This is primarily due to the fact that the degree of cracking and tensile straining are difficult to quantify from a designer's perspective.

In addition to the aforementioned design standards, it is of interest to examine the efficiency factors proposed by Brown et al. (2006) as part of TxDOT Project 4371. Project 4371 was the predecessor to the current project. A background of the development of nodal efficiency factors is presented as follows.

2.6.2.1 ACI 318-08 Nodal Efficiency Factors

The efficiency factors contained in ACI 318-08 are based on other sections of the ACI code, other codes, and experimental research. The efficiency factors that were adopted by ACI 318 are similar to those suggested by Schlaich et al. (1987) (Section 2.6.1.1.5); it can be assumed that they were selected accordingly. Also, MacGregor (2002) cites research conducted by Barton et al. (1991) as contributing to the nodal efficiency factors that were eventually selected.

2.6.2.1.1 Barton, Anderson, Bouadi, Jirsa, and Breen (1991)

Barton et al. (1991) conducted tests of ten isolated CCT and nine CTT nodal zones. Details of the isolated node specimens are shown in Figure 2-24.

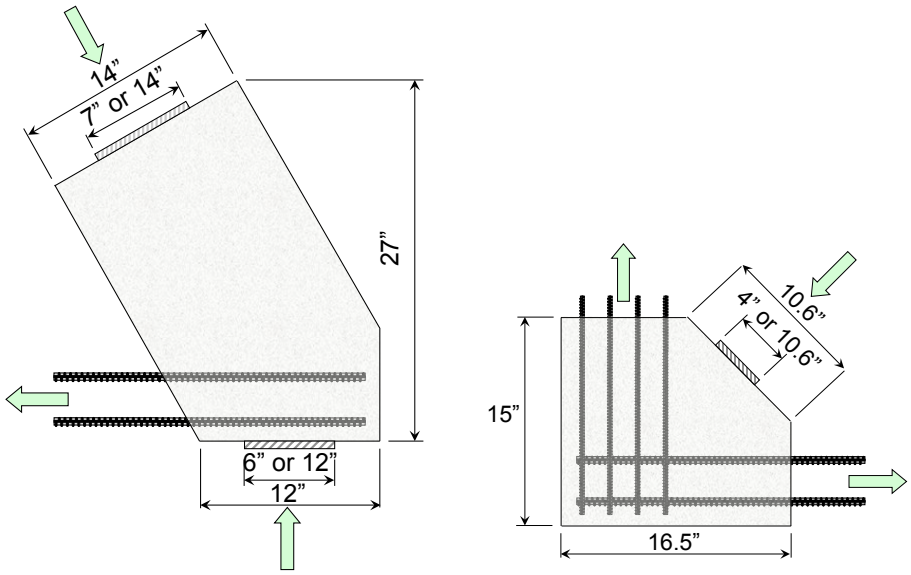

(a) CCT Node **(b) CTT Node**

Figure 2-24. Details of Isolated Node Specimens.

The researchers found that the ultimate strength of the CTT specimens was governed by yielding of the ties. Therefore, anchorage and reinforcement details had more of an impact on design strength rather than the efficiency factor.

Effective strength limits proposed by Schlaich et al. (1987) and Mitchell and Collins (1974) were found to be conservative. Six of the CCT specimens

experienced anchorage failures; the others failed due to the crushing of concrete at the support plate. Research conducted by Barton et al. (1991) indicated that an efficiency factor of 0.94 could be developed if reinforcement is properly detailed (MacGregor 2002).

2.6.2.2 AASHTO LRFD (2008) Nodal Efficiency Factors

The efficiency factor at the node-to-strut interface is based on the MCFT and described in detail in Section 2.6.1.2. At the CCC and CCT bearing and back face, the AASHTO LRFD (2007) nodal efficiency factors are similar to those selected by ACI 318-08. It can be assumed that they were selected in a similar fashion [i.e. per Schlaich et al. (1987)].

2.6.2.3 fib (1999) Nodal Efficiency Factors

Nodal efficiency factors suggested by *fib* (1999) are similar to those recommended by Nielson (1978) and Bergmeister et al. (1993). Both researchers recognize the fact that the efficiency of concrete decreases as its compressive strength increases.

2.6.2.3.1 Nielson (1978); Bergmeister, Breen, Jirsa, and Kreger (1993)

According to Bergmeister et al. (1993), Nielson (1978) developed the following empirical expression for the strength of concrete in beam webs.

$$\nu = 0.7 - \frac{f'_c}{29{,}000\,psi} \qquad \text{Equation 2-11}$$

Bergmeister et al. (1993) expanded upon Nielson's recommendation by developing efficiency factors for both undisturbed and disturbed regions (i.e. cracked and uncracked regions). The factors recommended by Bergmeister et al. (1993) for nodes are the same as those listed for struts (Equation 2-8). According to the researchers, *when compared with a large number of test results the function gave acceptable results*. The Nielson (1978) and Bergmeister et al. (1993) efficiency factors are presented along with those adopted by *fib* (1999) in Figure 2-25.

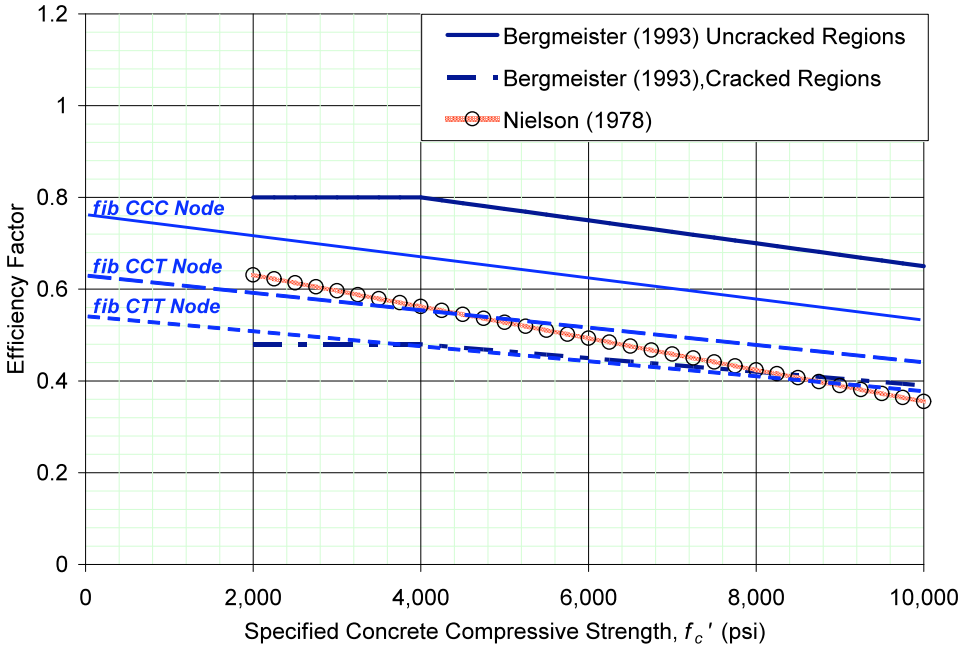

Figure 2-25. Comparison of nodal efficiency factors: *fib* (1999)

2.6.2.4 TxDOT Project 4371 Nodal Efficiency Factors: Brown et al. (2006)

Brown et al. (2006) examined both STM and sectional design methods for shear. As part of the experimental program, the researchers fabricated and tested a series of isolated strut specimens, and three series of deep beam specimens. Additionally, Brown et al. (2006) compiled a database of over 1200 shear tests. The database was used in combination with the experimental program to evaluate design expressions and develop a new strut-and-tie modeling procedure.

Brown et al (2006) recognized that the critical location of a strut is at the strut-to-node interface. The researchers recommend limiting the strength of concrete within a nodal zone according to the following efficiency factors:

$$\nu_R = \frac{27}{a/d\sqrt{f'_c}} \le \nu_{max} \qquad \text{Equation 2-12}$$

$$\nu_P = \frac{9}{a/d\sqrt{f'_c}} \le \nu_{max}$$

Where,

ν_{max} = 0.85 for a CCC Node

0.75 for a CCT Node

0.65 for a CTT Node

The higher value of efficiency factor, ν_R, is to be used for struts that are sufficiently reinforced per Equation 2-14 (Section 2.6.3.2). When examining the effect of their proposed efficiency factors, the researchers found that 95% of the beams in their database carried loads in excess of the calculated values.

Brown et al. (2006) derived the proposed efficiency factors assuming the beams in the database contain hydrostatic nodes. When non-hydrostatic nodes are used, the researchers recommended the following conversion factors:

$\nu_b = (1.0) \cdot \nu_R$, Bearing face of node Equation 2-13

$$\nu_t = \left(\frac{l_b}{w_t \cdot \tan\theta} \right) \cdot \nu_R, \quad \text{Back face of node}$$

$$\nu_s = \left(\frac{l_b}{w_s \cdot \sin\theta} \right) \cdot \nu_R, \quad \text{Node-to-strut interface}$$

Where,

w_s = Width of the strut-to-node interface (Equation 2-2), in.

w_t = Height of the nodal back face, in.

θ = Angle of strut with respect to horizontal plane, degrees

Given that the method was derived using hydrostatic nodes, the Brown et al. (2006) STM procedure may be unnecessarily conservative when non-hydrostatic nodes are used. A goal of the current project is to refine the method proposed by Brown et al. (2006) by evaluating design provisions through the use of non-hydrostatic nodes.

2.6.3 Minimum Transverse Reinforcement

As previously stated, the minimum amount of reinforcement required by ACI 318-08 and *fib* (1999) is approximately 0.2% in each direction. AASHTO

LRFD (2008) requires 0.3% in each direction. AASHTO LRFD (2008) explicitly states that the minimum reinforcement requirement is necessary for *crack control*.

It is difficult to find a derivation for the minimum reinforcement requirement prescribed by the different design provisions. Research that has examined the requirement is not often cited. Most likely, it is a product of the *rules of thumb* used since the early 20th century. Nonetheless, a study cited by MacGregor (2002) was used to validate the ACI 318-08 minimum reinforcement requirement. MacGregor (2002) cites the research conducted by Rogowsky (1983).

2.6.3.1 ACI 318 Minimum Transverse Reinforcement, MacGregor (2002), Rogowsky (1983)

In order for a strut to be considered minimally reinforced, ACI 318-08 requires that Equation 2-4 be satisfied (restated for the convenience of the reader):

$$\sum \frac{A_{si}}{b_s \cdot s_i} \sin \alpha_i \geq 0.003$$

The purpose of the equation is to provide a minimum percentage of tie reinforcement normal to the axis of the strut, thereby resisting the spreading of compressive stresses. Thus, the intent of Equation 2-4 is the resolve the components of the transverse reinforcement into a reinforcement ratio normal to the strut. However, from a geometric standpoint, Equation 2-4 is not correct. The sine term should be squared to correctly represent the stress components of the reinforcement. According to MacGregor (2002*), it has been expressed as shown to simplify the presentation*.

Also, according to MacGregor (2002), tests conducted by Rogowsky (1983) indicate that a vertical reinforcement ratio of at 0.35% is necessary for a two span continuous beam to reach its full plastic load capacity. In these tests, the strut angle was equivalent to 55-degrees. Therefore, according to Equation 2-4, the steel area was equivalent to 0.29% of the strut cross section (i.e. $0.0035 \cdot \sin 55° = 0.0029$).

Based on the findings of the researchers, it can be assumed that the ACI 318-08 requirement was calibrated to promote the yielding of the longitudinal steel before the onset of a shear failure.

2.6.3.2 TxDOT Project 4371 Min. Transverse Reinforcement: Brown et al. (2006)

Of interest to the current research program is the minimum transverse reinforcement proposed by Brown et al. (2006) as part of TxDOT Project 4371. Brown et al. (2006) derived the amount of reinforcement required in a strut completely on the basis of strength. They determined the amount of reinforcement required to maintain equilibrium as the compressive stresses disperse transversely. Based on the derivation, the minimum required amount of transverse reinforcement is calculated as follows.

$$\rho_{\perp,min} \geq \frac{k_s \cdot \nu \cdot f'_c \cdot A_c \sin\theta}{f_y \cdot b \cdot d \cdot m} \qquad \text{Equation 2-14}$$

Where,

A_c = minimum cross sectional area of the strut, in2

b = web width, in.

d = distance from extreme compression fiber to centroid of longitudinal reinforcement, in.

f_c' = specified compressive strength of concrete, psi

f_y = specified tensile strength of reinforcement, psi

k_s = non-hydrostatic node conversion factor (Equation 2-14)

m = slope of the dispersion of compression

θ = angle of strut respective to horizontal, degrees

ν = strut efficiency factor

According to the researchers, the minimum reinforcement requirement depends on the strength of the strut and will vary depending on which efficiency factors are used. The researchers stated that additional reinforcement might be

necessary to reduce crack widths. However, additional reinforcement would not reduce the level at which the first diagonal crack occurs.

According to Brown et al. (2006): based on a database of 1200 specimens, a minimum transverse reinforcement ratio of approximately 0.15% in each direction is sufficient to maintain equilibrium across the inclined crack. However, in keeping with the crack control requirements of the ACI 318 code, the researchers recommended that the minimum transverse reinforcement ratio be greater than or equal to 0.3% of the area of the inclined strut.

A background of the ACI 318-08, AASHTO LRFD (2008), and *fib* (1999) provisions has been presented. Next, a background on previous research specific to the objectives of the current project is presented. These objectives include the influence of distributed transverse reinforcement across the web, and the influence of triaxial confinement of the nodal regions.

2.6.4 Distribution of Transverse Reinforcement across the Web

According to the Commentary of ACI 318-08 (§ R11.5.7):

Research has shown that shear behavior of wide beams with substantial flexural reinforcement is improved if the transverse spacing of stirrup legs across the section is reduced.

The preceding recommendation only appears in the Commentary of the ACI 318-08 specifications; within the portion that includes sectional shear design provisions. Within the main body of the code and in Appendix A, the distribution of transverse reinforcement across the web is not required. The research cited by ACI 318-08 is that conducted by Leonhardt and Walther (1961); and Anderson and Ramirez (1989) and is presented in Sections 2.6.4.1 and 2.6.4.3, respectively.

According to Eurocode 2 (§ 9.3.2), the transverse spacing, s_{wt}, of shear reinforcement is limited to:

$s_{wt} \leq d \leq 31\text{-inches} \quad [V_u < 0.2\ V_n]$

$s_{wt} \leq 0.3 \cdot d \leq 8\text{-inches} \quad [V_u > 0.67\ V_n]$

The preceding requirement is for a conventionally loaded beam. It is not referenced in the deep beam portion of the code. The Eurocode 2 requirements are similar to the recommendation proposed by Leonhardt and Walther (1961). The background of this study is presented in Section 2.6.4.1.

AASHTO LRFD (2008) specifications contain a provision that directly penalizes a deep beam design if stirrups are not distributed across the web. According to AASHTO LRFD (2008), the width of a strut framing into a CTT node is reduced if stirrups are not distributed across the web. This requirement is illustrated in Figure 2-26. It is important to note that the requirement is only for a strut framing into a CTT node and only required in the STM section of the code.

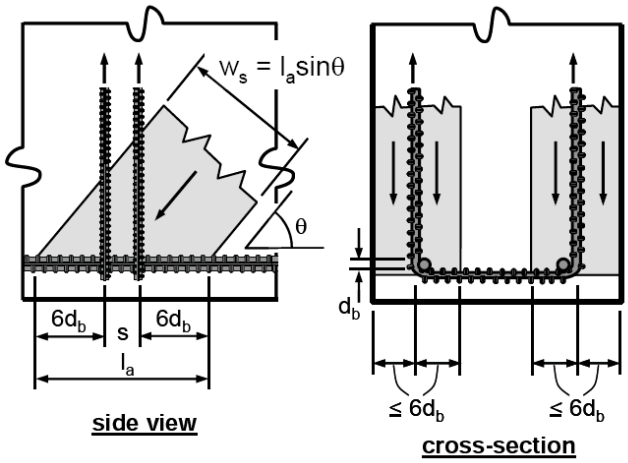

Figure 2-26. AASHTO LRFD requirement for a strut anchored by reinforcement (Brown et al. 2006).

Limiting the width of a strut framing into a CTT node may be unnecessarily conservative given that, in practice, most CTT nodes are smeared (Section 2.4.2.3). Also, this AASHTO LRFD (2008) provision is only applicable when designing a D-region. Yet, when the a/d ratio is less than two, a direct strut is the predominant mechanism of shear transfer. Thus, the use of a CTT node is not likely to be necessary. The applicability of using a direct strut or multiple-panel model for the design of a D-region is an issue that is further addressed as

part of this research project. One of the goals of the current research program is to investigate the AASHTO LRFD provision that limits the width of a strut framing into a CTT node. Previous research that has focused this issue is presented in Sections 2.6.4.1 to 2.6.4.3.

2.6.4.1 Leonhardt and Walther (1961)

Leonhardt and Walther (1961) theorized that an oblique strut in a deep beam acts like a beam supported at the stirrup legs (Figure 2-27). As a result, the researchers theorized that more intermediate supports (i.e. stirrup legs) would have the effect of increasing the shear capacity of the beam.

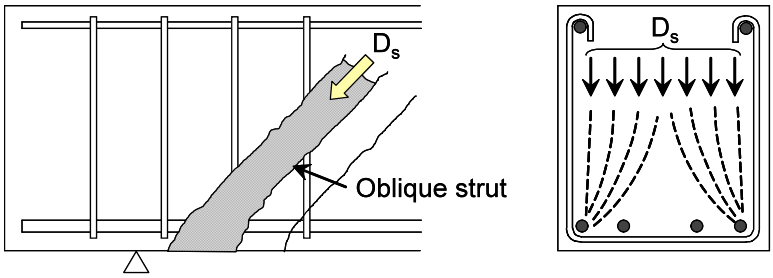

Figure 2-27. The oblique strut supported by vertical stirrup legs (taken from Leonhardt and Walther, 1961).

The researchers recommended spacing stirrups across the web at 20-cm (7.9-inches) for beams with high shear stresses and at 40-cm (15.7-inches) for beams with low shear stresses. Also, they recommended limiting the maximum spacing of stirrups across a beam web to a distance less than the beam's effective depth, *d*.

The experiments conducted by Leonhardt and Walther (1961) focused on sectional shear behavior. For the current study, it is of interest to examine the deep beam shear behavior for beams with stirrups distributed across the web. Also, the widest beam that the researchers tested was 12-inches. Leonhardt and Walther (1961) admitted that their tests were not sufficient to make a determination on the effect of stirrup distribution across the web:

More attention in the future will have to be paid to the distribution of the stirrups. These tests were concerned with fairly narrow webs (up to 12-inches).

2.6.4.2 Hsuing and Frantz (1985)

Hsuing and Frantz (1985) tested five beams with varying widths and stirrup distribution. Cross-sectional details of the beams are illustrated in Figure 2-28.

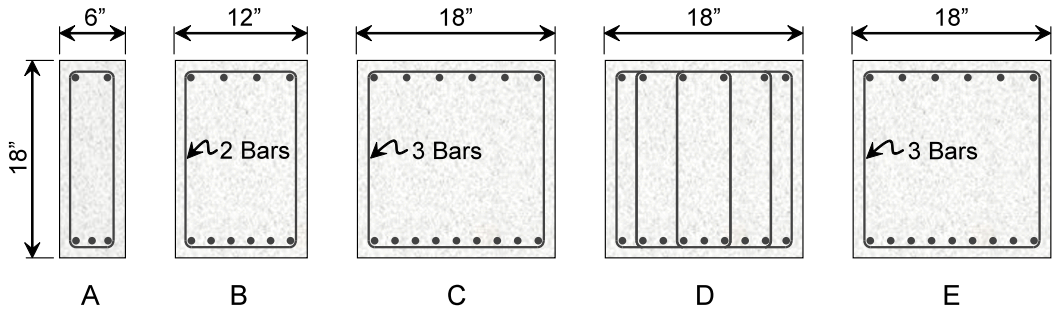

Figure 2-28. Details of specimens tested by Hsuing and Frantz (1985).

All of the specimens were tested with a shear span to depth ratio of 3.0. Each beam had identical longitudinal and transverse reinforcement ratios (1.8% tension, 0.2% compression, and 0.2% transversely). The stirrup spacing was held constant by bundling the stirrups for beams B, C, and E. The concrete strength was the same for all five specimens at the time of testing.

The ratio of measured to predicted capacities was 0.98, 0.89, 1.01, and 1.03 for beams A through D (Beam E was loaded to only 80% of its ultimate capacity). The researchers concluded that there was not a significant influence on the shear strength caused by the beam width or distribution of stirrups.

Hsuing and Frantz (1985) noted that Beam C had narrower crack widths than Beam D up to 90% of their respective capacities. They suggested that this was due to the fact that Beam C contained more reinforcement than Beam D at the location of crack measurement (i.e. at the beam surface).

In order to investigate the difference in crack widths between Beams C and D, Beam E was fabricated and loaded to 80% of its capacity; the main shear crack was epoxy injected; and the load was sustained as the epoxy cured. After the epoxy had cured, the beam was unloaded and the web was cored at the location of the main shear crack. The variation in crack width through the web was examined in order to ascertain if a lack of distributed stirrups results in wider interior crack widths. The researchers found that:

> *Although the center region of the cores usually contained the larger crack widths, it was not possible to conclude that a significant variation in crack width existed along the core length in this beam that had stirrups located only along the edges.*

The fact that crack widths did not vary through the web is inconsistent with the previous suggestion that the crack widths in Beam C were narrower than those of Beam D because more reinforcement was located at the surface. The researchers did not provide an explanation for this discrepancy.

The beams tested by Hsuing and Frantz (1985) had an a/d ratio of 3.0. The current research program is focused on deep beams with an a/d ratio less than 2.5. Therefore, the research conducted by Hsuing and Frantz (1985) is significant but inconclusive in regards to the effect that stirrup distribution has on the strength and serviceability behavior of deep beams ($a/d < 2.5$).

2.6.4.3 Anderson and Ramirez (1989)

Anderson and Ramirez (1989) tested four 16-inch wide specimens with varying stirrup distribution. All of the specimens were tested with a shear span to depth ratio of 2.65. Each beam had identical longitudinal and transverse reinforcement ratios (2.3% tension, 1.0% compression, and 0.4% transversely). Cross sectional details of the beams are illustrated in Figure 2-29.

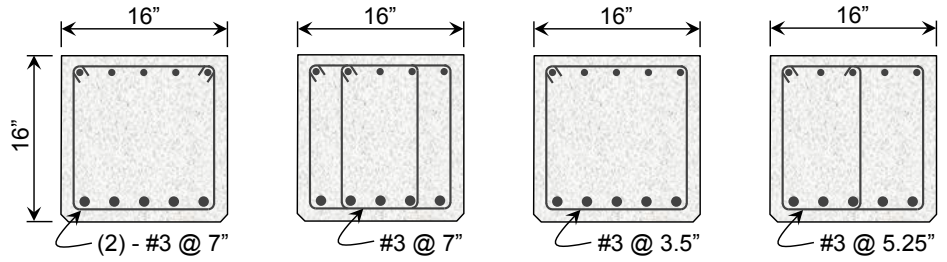

	W1	W2	W3	W4
V_{TEST}	103.4 kip	123.4 kip	113.4 kip	131.4 kip
V_{TEST} / V_{ACI}	1.05	1.23	1.13	1.30
f_c'	4230 psi	4670 psi	4690 psi	4900 psi

Figure 2-29. Details of specimens tested by Anderson and Ramirez (1989).

Anderson and Ramirez (1989) theorized that a lack of distributed stirrups could result in a concentration of compression stresses at the intersection between the stirrup and longitudinal tensile reinforcement. This situation could lead to premature failure due to the crushing of concrete within the nodal zone.

The beams tested by Anderson and Ramirez (1989) did not fail due to crushing in the CTT nodal zone. However, the researchers found that longitudinal bar strains were higher for interior bars when stirrups were distributed across the web; indicating that distributing the transverse reinforcement utilizes the interior longitudinal bars more effectively. As a result, the researchers concluded that stirrups should be distributed transversely across the web for wide beams with multiple longitudinal bars.

Upon examination of their data, the significance in the strength differences is found to be questionable (Figure 2-29). The ratio of measured to calculated capacities varied between 1.05 and 1.30 for beams W1 through W4. The multiple stirrup specimens (W2 and W4) had a relatively higher capacity beyond the nominal value; however, the compressive strength of concrete for these specimens was also relatively higher. If the beam capacities are normalized by their concrete compressive strength, the maximum difference in their normalized capacity is less than 8-percent (Figure 2-29). This is an insignificant amount given the degree of

scatter associated with shear testing. In addition, all of the specimens carried more shear than predicted by ACI 318-08. Therefore, considering that the strength of all the specimens was safely estimated and given the nominal difference in strength, the benefit of providing multiple stirrup legs is questionable.

Anderson and Ramirez (1989) did not specifically evaluate the strut width limitation specified by AASHTO LRFD (2008). AASHTO LRFD (2008) allows the designer to use an effective strut width equal to six bar diameters from the centroid of a stirrup (Figure 2-26). Based on this requirement, the effective strut width that may be used for the beams tested by Anderson and Ramirez (1989) was greater than the width of the web (i.e. *6·(1.125") + 2(1.5") = 16.5" > 16"*). In other words, the effective strut width that was evaluated by Anderson and Ramirez (1989) was less than six bar diameters (Figure 2-30).

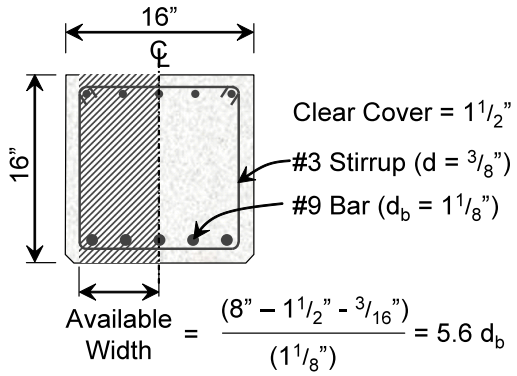

Figure 2-30. Effective strut width of specimens tested by Anderson and Ramirez (1989).

Finally, the specimens tested by Anderson and Ramirez (1989) had an a/d ratio of 2.65. These beams are not considered deep beams and would be designed using sectional methods. It is not necessary to use STM to design these beams. As a result, an effective strut width limitation is not required according to AASHTO LRFD (2008). In summary, it can be concluded that the previous research did not evaluate the effects of distributing transverse reinforcement in deep beams.

2.6.5 Triaxially Confined Nodal Zones

Another objective of the current research program is to determine the effect of triaxially confined nodal regions on the strength and serviceability behavior of deep beams. It is a well-known fact that the strength and ductility of concrete is higher under triaxial compression than it is under uniaxial compression (Figure 2-31).

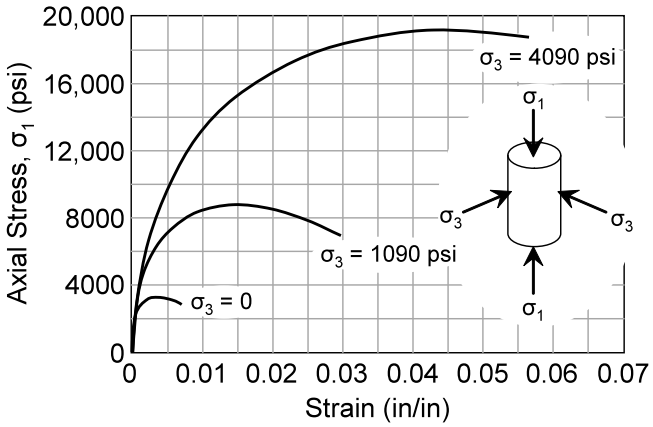

Figure 2-31. Stress-strain curve for concrete cylinder under triaxial compression (MacGregor and Wight, 2005).

In concrete structures, confining stresses are achieved with closely spaced hoops or spiral reinforcement, or additional concrete surrounding the loaded area. When concrete is loaded uniaxially, it expands in the transverse direction. If reinforcement or additional concrete is provided to confine the expansion, the offsetting transverse stresses provide triaxial confinement. As a result, the strength of the confined region is increased.

In STM, nodal zones are generally either biaxially or triaxially confined. Biaxial or two-dimensional confinement occurs when a load plate extends between opposite sides of a loaded area (Figure 2-32b). As a result, the lateral spread of compression is confined in a single plane. Triaxial confinement occurs when a load plate is surrounded by concrete on all sides. In this case, the lateral spread of compression is confined in two directions transverse to the loading

direction. Figure 2-32 illustrates the differences between biaxial and triaxial confinement.

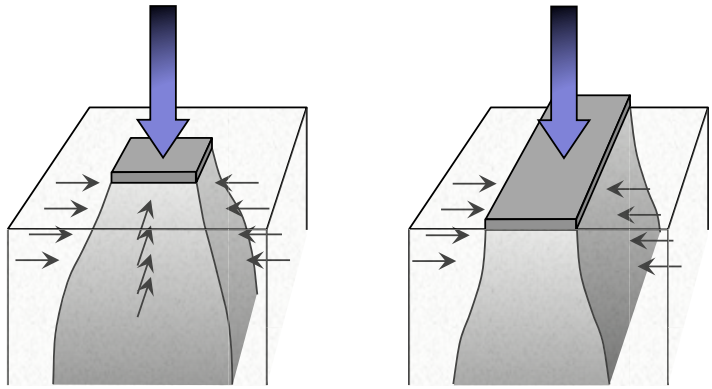

(a) **(b)**

Figure 2-32. Bearing load under (a) triaxial (b) biaxial confinement.

Many researchers recognize the fact that the bearing capacity of triaxially confined concrete can be increased. ACI 318-08 and AASHTO LRFD (2008) contain provisions permitting an increase in the design bearing strength of concrete when the loaded area is smaller than the supporting area. The AASHTO LRFD (2008) specifications express the effective compressive strength of concrete in bearing, f_{cb}, as follows (the ACI 318-08 expression is essentially identical).

$$f_{cb} = 0.85 f'_c \cdot m \qquad \text{Equation 2-15}$$

$$m = \sqrt{\frac{A_2}{A_1}} \le 2$$

Where,

m = confinement modification factor

f_c' = specified compressive strength of concrete, psi

The definition of A_2 and A_1 is illustrated in Figure 2-33.

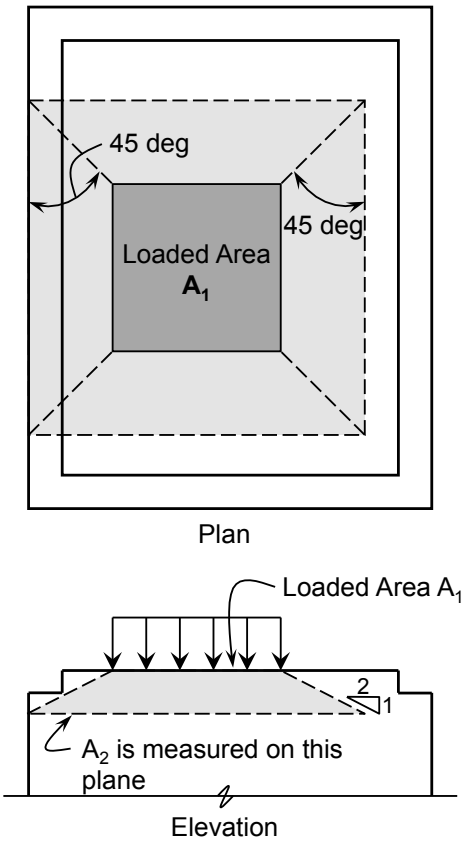

Figure 2-33. Application of frustum to find A_2 in stepped or sloped supports (taken from ACI 318-08).

The ACI 318-08 and AASHTO LRFD (2008) specifications allow the bearing capacity of concrete to be increased due to triaxial confinement. However, these design provisions do not explicitly allow a similar increase in the nodal regions of a strut-and-tie model. Both provisions contain the following note with regard to triaxial confinement:

> *Unless confining reinforcement is provided within the nodal zone and its effect is supported by tests and analysis, the calculated effective compressive stress… shall not exceed the value given…[in Table 2.1 and Table* 2.2*].*

The preceding provision is attributed to the research conducted by Bergmeister et al. (1993). The researchers made recommendations for the design

of bursting reinforcement required around a post-tensioned anchorage zone. Their design expression allows an increase in the bearing capacity of an anchorage zone when closed stirrups and hoops are provided

In contrast to ACI 318 and AASHTO LRFD, *fib* (1999) contains the following provision allowing the designer to increase the effective strength of concrete at all nodal boundaries when triaxial confinement is present:

> *For nodes with secured triaxial compression due to local compression… the increased strength values for multiaxial states of stress may be applied to individual node surfaces…*

The confinement factor specified in fib (1999) is expressed in Equation 2-16 and illustrated Figure 2-34.

$$\beta = min\left(\frac{b}{b_1} \; or \; \frac{a}{a_1}\right) \leq 4 \qquad \text{Equation 2-16}$$

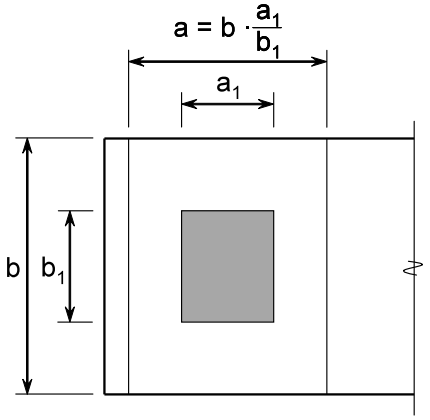

Figure 2-34. Definition of triaxial confinement geometries used in *fib* (1999).

Current STM efficiency factors have been mostly calibrated with beams whose bearing plates extended the full width of the beam. Often times, bearing plates do not extend the full width. As a result, if a designer is using ACI 318-08 or AASHTO LRFD (2008) for a deep beam design, excessively large bearing plates (or closed stirrups) may be necessary, as provisions do not explicitly allow for an increase in nodal strength due to the triaxial confinement provided by

surrounding concrete. A goal of the current research program is to examine the influence that triaxial confinement has on the strength and serviceability behavior of deep beams. Past research related to this topic is presented in Sections 2.6.5.1 through 2.6.5.3.

2.6.5.1 Leonhardt and Walther (1961), Furuuchi et al (1998)

Leonhardt and Walther (1961) and Furuuchi et al. (1998) investigated the effects of reduced load plate size on the shear strength of *deep slab* specimens. The cross-sectional dimensions of the test specimens were 8"x20" (Figure 2-35).

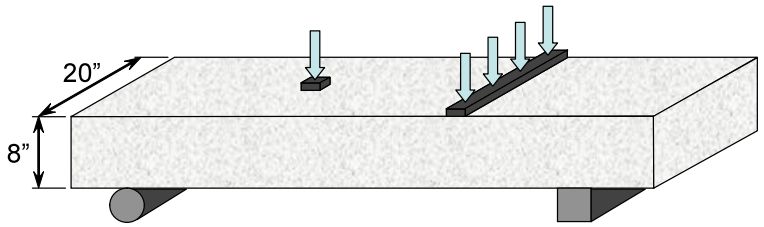

Figure 2-35. Detail of Leonhardt and Walter (1961) and Furuuchi et al. (1998) test specimens.

The specimens tested by Leonhardt and Walther (1961) contained longitudinal reinforcement in the tensile zone and were otherwise unreinforced. The a/d ratio varied between 2.5 and 4.4. The specimens tested by Furuuchi et al. (1998) contained longitudinal reinforcement in the top and bottom side of the beam, but did not contain any shear reinforcement. The a/d ratio varied between 1.25 and 2.25.

The Leonhardt and Walther (1961) specimens failed at both the concentrated and line-load side. According to the researchers:

> *…since there appears to be no special reason for this different failure behavior… it must be assumed that the shear strength does not differ much for the two types of loading and that the occurrence of failure on the one or other side is probably decided by minor local differences in the quality of concrete.*

Furuuchi et al. (1998) derived an expression for effectively increasing the load plate width. The researchers found that the effective width of the load or support plate could be increased by a factor ranging between two and three.

The specimens tested by Leonhardt and Walther (1961) and Furuuchi et al. (1998) can not be used to fully address one of the primary objectives of this research project; an examination of the effects of triaxial confined nodal regions. Specimens tested by Leonhardt and Walther (1961) were only tested under sectional shear forces. As such, it is expected that the size of the plate would have little influence on the shear capacity. A goal of the current research program is to examine the effect of varying both the load plate and the support plate for deep beams. Furuuchi et al. (1998) tested beams with an a/d ratio less than 2.5 and varied both support and load plates. However, these specimens were only 6-inches deep and did not contain transverse reinforcement. An objective of the current research program is to test large-scale specimens that are a realistic representation of deep beams used in practice.

2.6.5.2 Hawkins (1968)

Hawkins (1968) tested 230 concrete cubes in uniaxial compression and developed an expression to predict their capacity. The loading geometry, specimen size, and type and strength of concrete were varied. The majority of the specimens were 6-inch cubes. The cubes were loaded with a ¾-inch thick bearing plate with an area that was between one to thirty-six times smaller than the area of the cube face.

Based on the findings of the research program, Hawkins (1968) proposed an increase in the compressive strength of concrete according to the following expression.

$$1 + \frac{K}{\sqrt{f'_c}}\left(\sqrt{\frac{A_2}{A_1}} - 1\right) \qquad \text{Equation 2-17}$$

Where,

K = constant depending on concrete characteristics

According to Hawkins (1968), the material constant, *K*, varies between 50 and 65. Accordingly, if the compressive strength of concrete is equal to 2500 to 4000-psi; then the $\frac{K}{\sqrt{f'_c}}$ term is essentially equal to 1.0 (i.e. $\sqrt{2500} = 50$ and $\sqrt{4000} = 63$). By setting the $\frac{K}{\sqrt{f'_c}}$ term equal to one, Equation 2-17 is simplified such that the bearing strength factor is equal to $\sqrt{\frac{A_2}{A_1}}$; which is the same factor adopted by the ACI 318-08 and AASHTO LRFD (2008) provisions for bearing (Equation 2-15).

2.6.5.3 Brown et al. (2006)

Brown et al. (2006) conducted ten tests on seven specimens with reduced support plate widths. An illustration of the beams tested by the researchers is shown in Figure 2-36. The beam cross-sections were either 18"x18" or 30"x18".

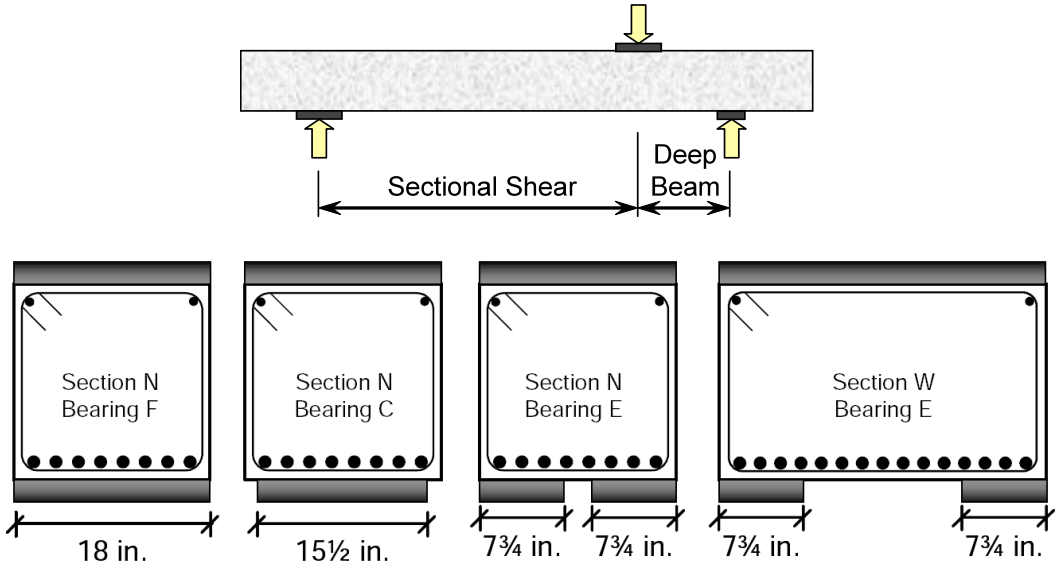

Figure 2-36. Detail of specimens tested by Brown et al. (2006).

The researchers varied the width of the beam specimens and kept the bearing plates the same size. According to the provisions of STM, if the strut width is kept constant, then the beams should have the same strength regardless of their width. This was not the case; the wider beam specimens carried almost twice the load. Unfortunately, all of the wide beam specimens failed in sectional shear in the *long span* (Figure 2-36) whereas the narrow beams failed in deep beam shear in the *short span* (Figure 2-36). The researchers addressed this discrepancy by demonstrating that the amount of shear force carried by the wide specimens in the deep beam side was more than twice shear carried by the narrow beams. Additionally, only the CCT node was investigated by Brown et al. (2006). Therefore, the results of the tests cannot be used to fully address the objectives of this research study.

In summary, previous research studying the effects of triaxial confinement on the behavior of deep beams is found to be inconclusive for the purpose of this research study. The current research program is designed to provide the necessary additional information.

2.7 SERVICEABILITY CONSIDERATIONS

As presented in Section 2.4.4, differences exist between the various design provisions as to the amount of transverse reinforcement required for a deep beam design using STM. As a result, one of the objectives of the current research program is to examine the amount of minimum transverse reinforcement necessary to provide adequate strength and serviceability performance. The findings for the minimum reinforcement study are presented by Birrcher (2008).

Tests discussed in this report were primarily developed to investigate the influence of multiple stirrup legs and of triaxial confinement. However, these beams were also designed to contain the following two reinforcement ratios of interest: 0.2% and 0.3%. Differences in deep beam performance are noted for both amounts of reinforcement within the current report. However, the findings of the minimum transverse reinforcement task are presented by Birrcher (2008).

2.8 DEEP BEAM DATABASE

In addition to the experimental portion of the current research program, a database containing 904 deep beam shear tests ($a/d \leq 2.5$) has been compiled (including the 36 specimens tested as part of the current project). The purpose of the database is to supplement the experimental program and provide an additional means of examining design provisions. This database is an expansion of the database originally compiled by Brown et al. (2006). All of the tests from the Brown et al. (2006) database with an a/d ratio greater than 2.5 have been removed; the remaining dataset has been rechecked and additional deep beam tests have been added. This database will subsequently be referred to as the *collection database*. The collection database was compiled based on the research papers cited in Appendix D.

298 beams in the collection database were removed due to what is considered to be inadequate details reported by the authors. The remaining database containing 606 beams is referred to as the *filtered database*. A

description of the criteria used to develop the filtered database is described as follows.

2.8.1 Filtered Database

In order to evaluate the current STM design provisions, it is necessary to have an accurate description of bearing plate geometries. 284 of the specimens in the collection database were not accompanied with adequate, verifiable bearing plate dimensions.

Only beams that were tested with one or two point loads were considered; thus, uniformly loaded beams were filtered from the database. The definition of the a/d ratio for a uniformly loaded beam is not straightforward. Also, determination of a truss model is slightly more complicated. Therefore, seven uniformly loaded beams were filtered from the database.

Of the remaining specimens, three failed due to crushing of their stub columns rather than failure of the beam. For these specimens, stub columns were used at the bearing points to support the beam and apply the load. Failure of a stub column is not an appropriate mechanism for evaluating strut-and-tie provisions with respect to shear behavior; as a result, these beams were filtered out of the deep beam database.

Finally, four specimens were removed from the remaining dataset due to the fact that the compressive strength of concrete at the time of testing was less than 2000-psi. For concrete to be considered *structural*, it must have a compressive strength greater than or equal to 2000-psi.

In summary, the filtered database contains 606 specimens. These specimens have adequate details necessary to evaluate strut-and-tie modeling provisions. Next, it was of interest to the research team to only consider beams that better represent actual beams used in the field. Of the 606 specimens in the filtered database, 428 were filtered out based on their dimensions and reinforcement details. The remaining 178 specimens constitute what is referred to

as the *evaluation database*. A description of the filtering criteria used to develop the evaluation database is presented as follows.

2.8.2 Evaluation Database

Due to the limitations of testing capacity and/or research budgets, most of the specimens in the filtered database are unrealistically scaled and proportioned. In order to illustrate this point, the specimens in the filtered database are plotted in Figure 2-37 by their shear area ($b_w \cdot d$) along the y-axis and aspect ratio of their cross-section (d/b_w) along the x-axis.

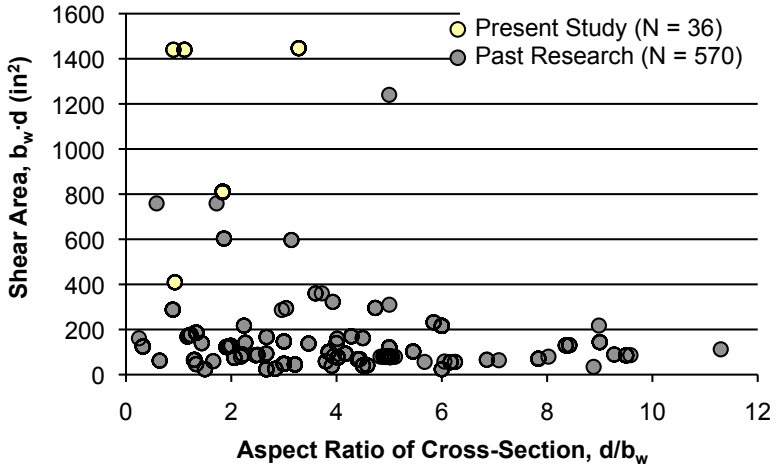

Figure 2-37. Summary of beam proportions in filtered database (N=606).

The majority of the specimens in the filtered database have an area less than 200-in^2. Yet, bent caps in the State of Texas are typically on the order of 1400-in^2 and greater. Also, a significant number of beams in the filtered database have an aspect ratio greater than four – some have a depth over 8 times greater than their width. Such a high aspect ratio is unrealistic. Conventional beams have an aspect ratio of approximately one to three.

In addition to specimen size, a significant number of the beams in the filtered database do not have any or contain unrealistically low amounts of transverse reinforcement. Although testing specimens without any transverse reinforcement may be interesting from an academic standpoint, most beams in the

field, particularly deep beam regions, contain a minimum amount of transverse reinforcement. Therefore, unreinforced beams are not used to evaluate STM provisions. However, it is of interest to evaluate specimens that have less transverse reinforcement than the minimum required by design specifications. By examining the trends of *lightly reinforced* specimens, a determination can be made as to an adequate amount of reinforcement necessary to maintain the integrity or strength of a D-region.

As stated, it is the goal of the research program to only consider those beams that better represent actual bent caps. This criterion was given the most weight when forming the evaluation database. In addition, it was necessary that the number of remaining beams in the evaluation database was statistically significant. Accordingly, the following criteria were used to remove 428 of the *less representative* specimens from the filtered database:

- **Beam width, b_w, greater than 4.5-inches:** 222 specimens had a width less than 4.5-inches.
- **Shear area, $b_w \cdot d$, greater than or equal to 100-in^2:** of the remaining dataset, 73 specimens had a shear area less than 100-in^2.
- **Depth, d, greater than or equal to 12-inches**: of the remaining dataset, 13 specimens had a depth less than 12-inches.
- **Transverse reinforcement ratio, $\Sigma\rho_\perp$, greater than 0.1%** (ACI 318 definition, Equation 2-4): of the remaining dataset, 120 specimens had $\Sigma\rho_\perp$ less than 0.1%.

The remaining database is referred to as the *evaluation database* and contains 178 specimens; 34 of which have been tested as part of the current research program (2 specimens from this study were filtered out of the evaluation database because they did not contain any transverse reinforcement). Specimens in the evaluation database are considered to more realistically represent deep beams used in the field. The data from these beams were used throughout the remainder of the current research program in evaluating and formulating STM

design provisions. A complete description of the beams in the evaluation database is presented in Appendix E.

2.9 SUMMARY

In order to accomplish the research goals, an extensive review of deep beam tests has been conducted. Few tests exist that specifically address the research objectives.

As part of the current study, 36 specimens were fabricated and tested. Cross-sectional dimensions of the specimens are as follows: 21”x23”, 21”x42”, 21”x44”, 21”x75”, and 36”x48”. These specimens represent some of the largest deep beam shear tests ever conducted. In addition to the experimental program, a database of over 904 deep beam shear tests was compiled. Of those 904 tests, 178 were considered to be more representative of TxDOT bent caps in terms of size and reinforcement details. Specifics on the need for the current study are summarized as follows.

2.9.1 Need for this Research Study

One of the objectives of the current research program is to determine how the strength and serviceability behavior is affected by the distribution of transverse reinforcement (i.e. multiple stirrup legs) across a beam’s web. There are significant inconsistencies between current design provisions regarding this topic. AASHTO LRFD (2008) requires distributed reinforcement in deep beam regions in order for a designer to utilize the full beam’s width as the width of the strut framing into a CTT node. However, the applicability of a CTT nodal zone (i.e. multiple-panel truss model) is questionable when the a/d ratio is less than two. ACI 318-08 does not require multiple stirrup legs in deep beam regions. However, ACI 318-08 includes language in the commentary on sectional shear stating the benefit of distributing stirrups across the web. Eurocode 2 also limits the transverse spacing of stirrups, but the provision is only included in the sectional shear portion of the code. The studies cited by ACI 318-08 and

Eurocode 2 (Leonhardt and Walther, 1961; and Anderson and Ramirez, 1989) are not conclusive as to the advantage of multiple stirrup legs. *fib* (1999) states that CTT nodes are generally smeared and need not be checked. The study conducted by Hsuing and Frantz (1985) concluded that stirrup distribution had little to no influence on the strength or crack widths for the specimens in their testing program.

Another objective of the current research program is to determine how the strength and serviceability behavior of a deep beam is affected when the size of a bearing plate is reduced, resulting in a triaxially confined nodal zone. The size of a bearing plate has a pronounced effect on the nominal capacity of a beam determined with a truss model. Most researchers recognize that the confinement provided by concrete around a node will significantly increase its effective strength. However, the ACI 318-08 and AASHTO LRFD (2008) provisions do not allow for a similar increase in the strength of a nodal region. A reason that STM provisions for triaxially confined nodes have not been implemented can be attributed to the limited research that has directly investigated the issue. Other than a deep slab study conducted by Furuuchi et al. (1998) and a few beams tested by Brown et al. (2006), there are no other tests investigating the effect of triaxially confining a node of a deep beam shear specimen.

A final objective of this research study is to examine current STM design provisions in ACI 318-08, AASHTO LRFD (2008), and *fib* (1999) and recommend a simple STM design methodology. The evaluation database is used to evaluate the code provisions. Ultimately, the purpose of the evaluation is to recommend a design procedure that is useful to practitioners. A useful design procedure is simple, practical, transparent, and should be consistent with other parts of the code.

CHAPTER 3

Experimental Program

3.1 OVERVIEW

The purpose of the experimental program is to investigate how the strength and serviceability of a deep beam is influenced by: (i) the distribution of stirrups across the web of a beam; (ii) triaxial confinement of the CCC and CCT nodes (load and support bearing plates); (iii) varying shear span-to-depth ratios; (iv) varying transverse reinforcement ratios; and (v) increasing depth. The testing program was developed in order to investigate the aforementioned variables as well as to supplement the existing data in the literature.

In order to address the objectives of the research program, 37 tests were conducted on 19 specimens. One of these tests was not a valid shear failure. Therefore, it was not included in the collection database. However, the information obtained from the test is relevant with regard to a project objective. Thus, the beam data is presented in this document. The information presented in this chapter is intended to provide all of the important details relevant to the design, fabrication, and testing of these specimens.

Additional information regarding the development of the testing program is presented in Section 3.2. Relevant details of all of the specimens are presented including the load plate, geometry and reinforcement configuration. Next, details regarding the test setup are presented in Section 3.3 including the configuration of the testing frame, instrumentation, measurement of loads, and measurement of displacements. Finally, details of the fabrication and construction of the specimens is presented in Section 3.4 including specific information on the properties of the materials used to construct each beam.

3.2 TESTING PROGRAM

In order to accomplish the goals of the current research program, it was necessary to test specimens that were considerably larger than those that have been tested in the past. In general, previous research has been conducted on beams that are too narrow to realistically represent actual bents and deep beams used in the field. This point is illustrated in Figure 3-1.

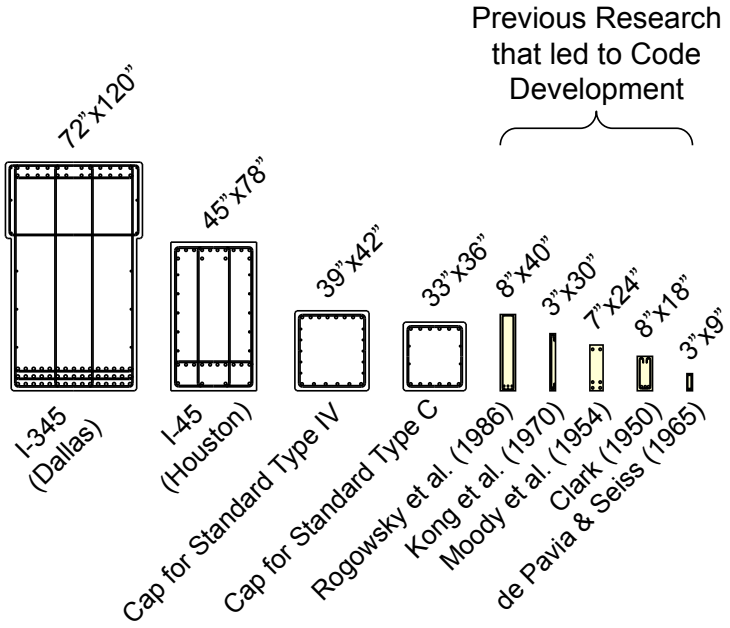

Figure 3-1. Comparison between actual bent caps and beams included in past research programs.

Bent caps used in the State of Texas are illustrated to scale in Figure 3-1 alongside beams that have been tested as part of past research studies. The beams shown from the previous studies are taken from research papers that were used for the development of deep beam shear design provisions. Because of this considerable difference in size, specimens in the current research program were scaled in order to more realistically represent deep beams and to adequately address the research objectives.

The research objectives were: examine the influence that (i) the distribution of stirrups across the web of a beam; (ii) triaxial confinement of the CCC and CCT nodes; (iii) reinforcement ratio, (iv) shear span-to-depth ratio; (v) and depth has on the strength and serviceability performance of deep beams. In order to isolate the primary test variables of the research program, the experimental portion was divided into five separate testing series. A summary of these five testing series is presented as follows and in Table 3.1.

- Series I: Distribution of stirrups through the beam web
- Series II: Triaxially confined nodal regions
- Series III: Reinforcement and shear span-to-depth ratio
- Series IV: Effect of depth
- Series M: Multiple purpose

An overview of the development of the testing program is presented in Sections 3.2.1 through 3.2.6.

Table 3.1. Testing Program.

Testing Series	b in.	d in.	Support Plate†	Load Plate†	No. of Stirrup Legs	ϱ_v	ϱ_h	a/d ratio
Series I 2 vs. 4 Stirrup	21	38.5	16”x21”	20”x21”	2	0.003	0.003	1.84
					4			
					2	0.002	0.002	
					4			
Series II Bearing Plate Size	21	38.6	10”x21”	20”x21”	2	0.003	0.003	1.84
			10”x21”	10”x7”				
			10”x21”	36”x21”				
			5”x7”	36”x21”				
			5”x7”	36”x21”		0.002	0.002	
			10”x21”	10”x7”				
			10”x21”	10”x21”				
			5”x21”	20”x21”				
Series III a/d Ratio Reinforcement Ratio	21	38.6	16”x21”	20”x21”	2	0.000	0.000	1.84
								2.47
						0.002	0.002	1.84
						0.0025	0.0015	
						0.003	0.003	
						0.001	0.001	
						0.003	0.003	
						0.002	0.002	
						0.002	0.002	1.20
						0.003	0.003	
						0.002	0.002	2.49
						0.003	0.003	
Series IV Depth	21	68.9	16”x21”	29”x21”	2	0.002	0.002	1.85
						0.003	0.003	
				24”x21”		0.002	0.002	2.50
						0.002	0.002	1.20
		19.5		16.5”x21”		0.003	0.003	1.85
						0.002	0.002	
				15.5”x21”		0.002	0.002	2.50
				18”x21”		0.002	0.002	1.20
Series M Mult. Purpose	36	40	16”x36”	24”x36”	4	0.003	0.003	1.85
				8”x12”		0.003	0.003	
				24”x36”		0.009	0.003	
				24”x36”		0.002	0.002	
				24”x36”	2	0.003	0.003	

† Plate dimensions: [in direction of span] x [transverse to direction of span]

3.2.1 Series I: Distribution of Stirrups across Beam Web

For a deep beam design, AASHTO LRFD (2008) requires the use of multiple stirrup legs in order to fully utilize the entire width of a beam. More background on this issue is presented in Section 2.6.4.

In order to investigate these provisions further, four tests were conducted on specimens with a 21"x44" cross-section. For each beam, the transverse reinforcement ratio and stirrup spacing was held constant. The only difference was the distribution of stirrups across the web. According to AASHTO LRFD (2008), the width of a strut anchored by stirrups is limited to a distance equal to six bar diameters from the centroid of the stirrups. Therefore, multiple stirrup legs must be provided to fully utilize the section. The reinforcement for Series I specimens was configured to specifically evaluate this AASHTO LRFD effective strut width provision. An overview of the effective strut widths of Series I specimens is shown in Figure 3-2. Key beam details are presented in Section 3.2.1.1. Complete details are summarized in Section 3.2.6.

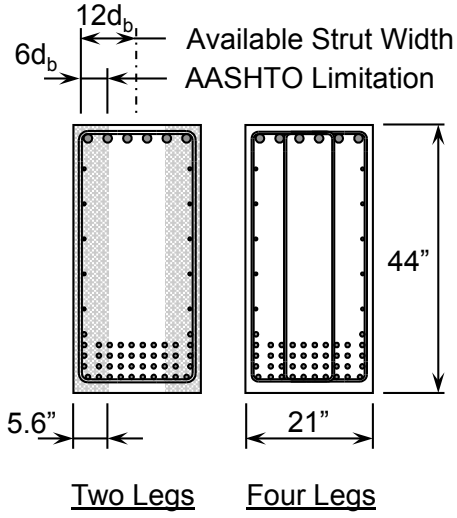

Figure 3-2. Effective width of strut anchored by reinforcement at the CCT node.

The 21"x44" test specimens were designed such that shear was the critical mode of failure. The specimen width was selected to be as wide as possible, while

keeping it narrow enough to ease installation and removal from the test setup. In order to evaluate the effective strut width provisions, the test specimens were proportioned such that a significant difference existed between the two and four-leg stirrup configurations. For example, the difference between the effective widths of the struts supported by two and four stirrup legs is 11.3 and 21-inches respectively (Figure 3-2); a 46-percent difference.

The longitudinal reinforcement was proportioned so that shear would be the dominant failure mode. The transverse reinforcement ratio was proportioned in order to study the two different ratios of interest: 0.2% and 0.3%. The vertical stirrup spacing was kept constant so that the only variable between companion tests was the number of stirrups distributed across the web.

3.2.1.1 Series I: Beam Details

In order to distinguish Series I specimens from one another, the nomenclature presented in Figure 3-3 was developed. Each numeral is a variable within the testing series. Beam details other than those shown in the specimen I.D. (Figure 3-3) remained constant and are presented in Section 3.2.6.

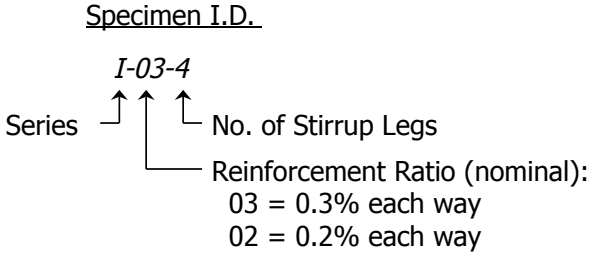

Figure 3-3. Series I: description of nomenclature used for Specimen I.D.

Geometric and reinforcement details for all of the beams tested within Series I are presented in Figure 3-4 and Table 3.2. A discussion of the results of the Series I testing program is presented in Chapter 4.

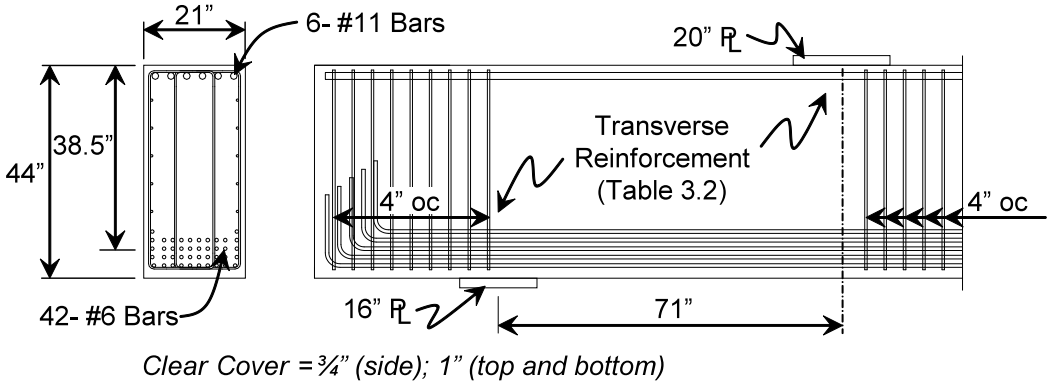

Figure 3-4. Series I beam details.

Table 3.2 Series I test specimen details.

Name	f'_c †† (psi)	ρ_v	ρ_h	d (in.)	a/d ratio	Stirrup Spacing	No. Legs	Strut Width†
I-03-4	5240	0.0030	0.0033	38.5	1.84	#3@7	4	21”
I-03-2	5330	0.0029	0.0033	38.5	1.84	#4@6.5	2	11.3”
I-02-4	3950	0.0021	0.0020	38.5	1.84	#3@10	4	21”
I-02-2	4160	0.0020	0.0020	38.5	1.84	#4@9.5	2	11.3”

† Effective strut width according to AASHTO LRFD (i.e. $\pm 6 \cdot d_b$ from centroid of stirrup)
†† Compressive strength of concrete measured at the time of testing (Section 0)

3.2.2 Series II: Triaxially Confined Nodal Zones

Researchers [Hawkins (1968); Bergmeister et al. (1993); MacGregor and Wight (2005)] agree that triaxial confinement can increase the compressive strength of concrete. However, ACI 318-08 and AASHTO LRFD (2008) lack explicit provisions allowing an increase in the strength of a nodal zone when triaxial confinement due to surrounding concrete is present. Triaxial confinement within nodal zones is an important issue as the size of a bearing plate can have a pronounced affect on the capacity predicted from an STM. Detailed information regarding this issue is presented in Section 2.6.5.

In order to investigate the effects of triaxial confinement within a deep beam nodal zone, eight tests were conducted on specimens with a 21”x42” cross-section. The testing program was planned so that a reinforcement ratio of 0.2% and 0.3% could be compared. Beam details were consistent between tests. The

only test variable was either the size of the load or support plates. An overview of the bearing plate sizes that were studied for the 21"x42" specimens are shown in Figure 3-5. Key beam details are presented in Section 3.2.2.1. Complete details are summarized in Section 3.2.6.

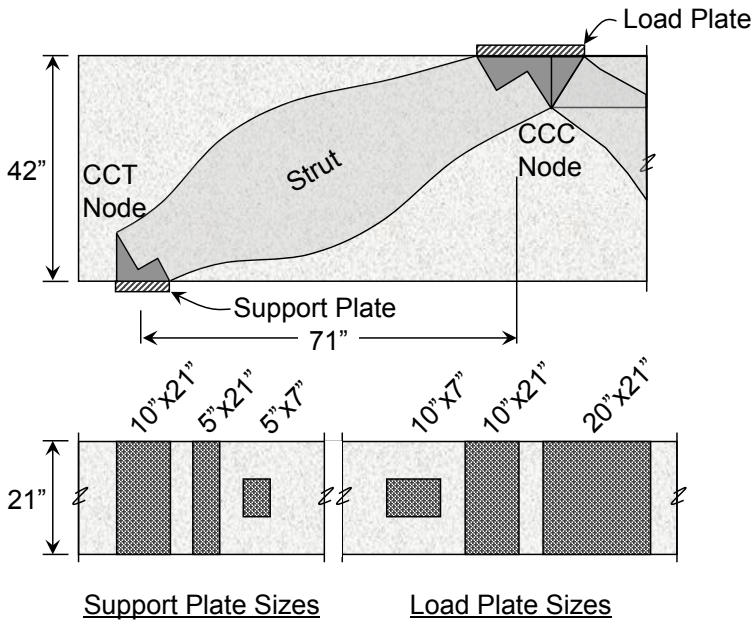

Figure 3-5. Plate sizes investigated within Series II.

In order to investigate the effect of triaxial confinement in the nodal regions, identical tests were conducted in which the only variable was the size of the bearing plate. For a plate to be triaxially confined, its width must be substantially less than that of the beam. Concurrently, it was important that the width of the test specimen was large enough such that there was a significant difference between a reduced and full size bearing plate. For the specimens tested as part of this study, the width of the bearing plates used to study triaxially confined nodes was three times narrower than the width of the beam (i.e. from 21-inches to 7-inches). Triaxial confinement was investigated at both the load (CCC node) and support (CCT node) bearing plates. Other variables were kept constant. Plate sizes are illustrated in Figure 3-5.

The 21-inch wide specimens were designed in the same manner as the Series I specimens; i.e. so shear would be the dominant mode of failure. The transverse reinforcement ratio was proportioned in order to study the two different ratios of interest: 0.2% and 0.3%.

3.2.2.1 Series II: Beam Details

In order to distinguish Series II beams from one another, the nomenclature presented in Figure 3-6 was developed. Each numeral is a variable within the testing series. Beam details other than those shown in the specimen I.D. (Figure 3-6) remained constant and are presented in Section 3.2.6.

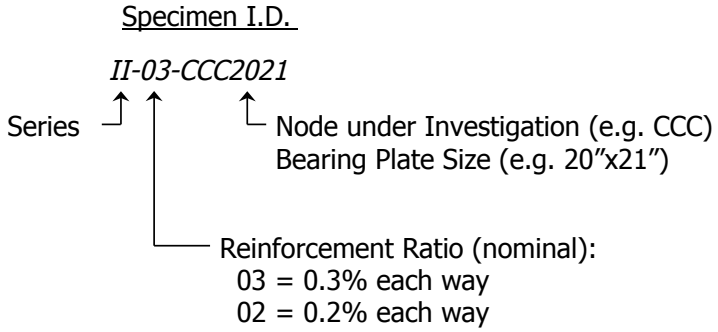

Figure 3-6. Series II: Description of nomenclature used for Specimen I.D.

Geometric and reinforcement details for all of the beams tested within Series II are presented in Figure 3-7 and Table 3.3. A discussion of the results of the Series II testing program is presented in Chapter 5.

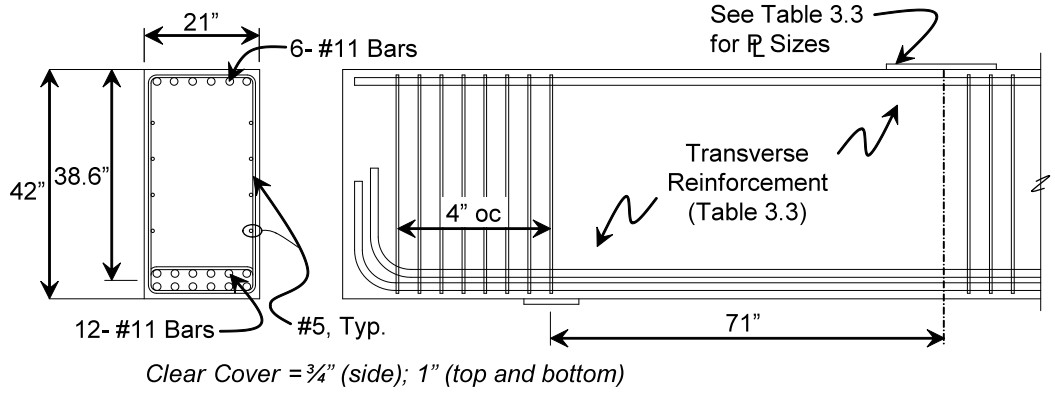

Figure 3-7. Series II beam details.

Table 3.3. Series II test specimen details.

Name	f'_c †† (psi)	ϱ_v	ϱ_h	d (in.)	a/d ratio	Load Plate† (in.)	Support Plate† (*in.*)
II-03-CCC2021	3290	0.0031	0.0031	38.6	1.84	20x21	10x21
II-03-CCC1007	3480	0.0031	0.0031	38.6	1.84	10x7	10x21
II-03-CCT1021	4210	0.0031	0.0031	38.6	1.84	36x21	10x21
II-03-CCT0507	4410	0.0031	0.0031	38.6	1.84	36x21	5x7
II-02-CCT0507	3120	0.0020	0.0020	38.6	1.84	36x21	5x7
II-02-CCC1007	3140	0.0020	0.0020	38.6	1.84	10x7	10x21
II-02-CCC1021	4620	0.0020	0.0020	38.6	1.84	10x21	10x21
II-02-CCT0521	4740	0.0020	0.0020	38.6	1.84	20x21	5x21

† Load plate dimensions: [in direction of span] x [transverse to direction of span]
†† Compressive strength of concrete measured at the time of testing (Section 0)

3.2.3 Series III: Reinforcement and Shear Span-to-Depth Ratio

Twelve tests were conducted on beams with 21"x42" cross-sections. The purpose of Series III specimens was to examine the differences in shear strength and serviceability behavior caused by varying a beam's transverse and skin reinforcement ratio; and a/d ratio. Reinforcement ratios of 0.2% and 0.3% and a/d ratios of 1.2, 1.85, and 2.5 were the primary variables under investigation.

Additional details with regard to the design and a discussion of results for Series III specimens are presented by Birrcher (2008). However, because many of the specimen details were consistent between all testing series, it was possible to make comparisons among different test series. The details of these specimens are summarized in Section 3.2.6. An overview of the details and nomenclature used to distinguish beams within Series III is presented next.

3.2.3.1 Series III: Beam Details

In order to distinguish Series III beams from one another, the following nomenclature was developed. Each numeral is a variable within the testing series. Beam details other than those shown in the specimen I.D. (Figure 3-6) remained constant and are presented in Section 3.2.6. An overview of the beams tested within Series III is presented in Figure 3-9.

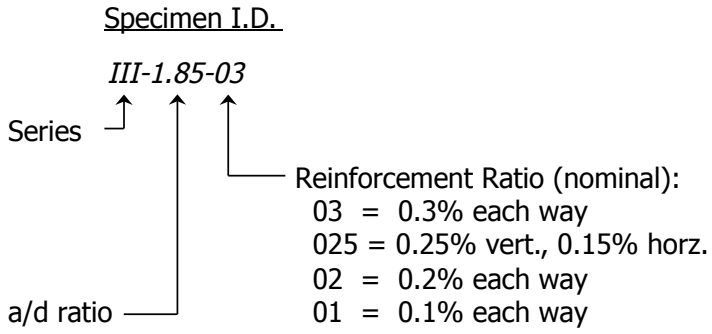

Figure 3-8. Series III: Description of nomenclature used for Specimen I.D.

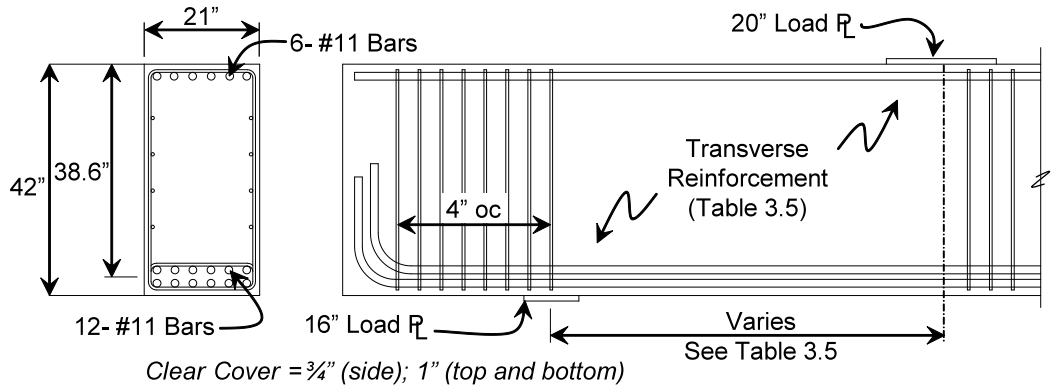

Figure 3-9. Series III beam details.

3.2.4 Series IV: Depth Effect

Four tests were conducted on beams with 21"x75" cross-sections and four tests were conducted on beams with 21"x23" cross-sections. The purpose of these specimens was to examine the differences in shear strength and serviceability behavior caused by variations in beam depth. The behavior of the Series IV specimens can be directly compared that of the 42-inch Series III specimens. The testing program was planned so that the behavior of beams with transverse reinforcement ratios of 0.2% and 0.3% could be compared to one another for 23, 42, and 75-inch deep beams.

Additional details with regard to the design and a discussion of results for Series IV specimens are presented by Birrcher (2008). However, because these specimens are part of the overall research program, their details are presented here

and the specimens are included in the evaluation database. Complete specimen details are summarized in Section 3.2.6. An overview of the nomenclature used to distinguish beams within Series IV is presented next.

3.2.4.1 Series IV: Beam Details

In order to distinguish Series IV beams from one another, the nomenclature presented in Figure 3-10 was developed. Each numeral is a variable within the testing series. An overview of the beams tested within Series IV is presented in Figure 3-11. A detailed description of the specimens is summarized in Section 3.2.6.

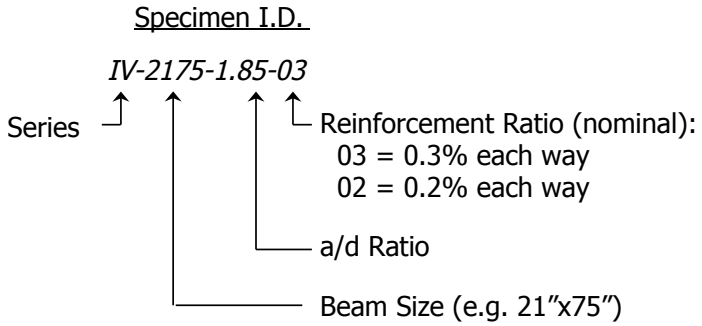

Figure 3-10. Series IV: Description of nomenclature used for Specimen I.D.

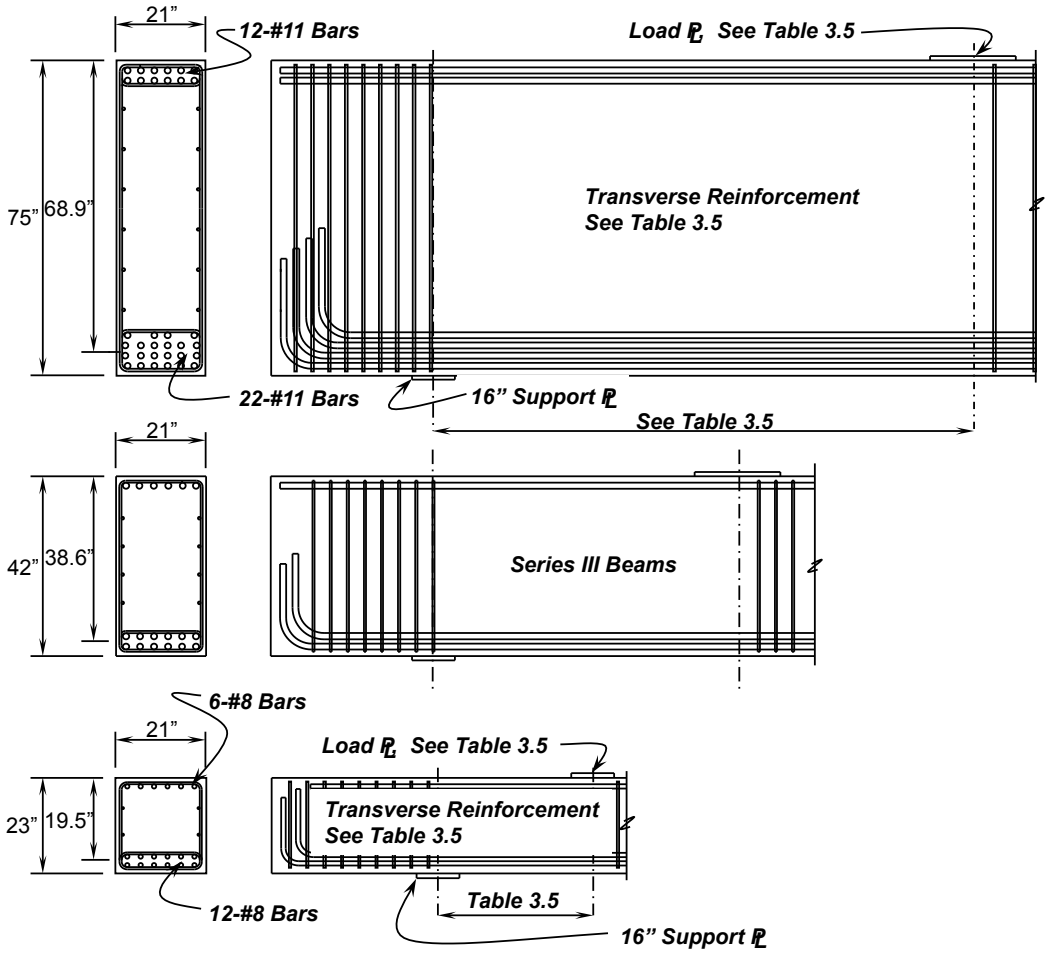

Figure 3-11. Series IV beam details.

3.2.5 Series M: Multiple Purpose

Five tests were conducted on specimens with a 36"x48" cross-section. The purpose of Series M specimens was to validate the findings obtained in the other testing series for 36"x48" beams.

Series M specimens were designed in the same manner and for the same purpose as beams within other testing series. For this part of the experimental program, two Series M tests are evaluated: one Series M specimen provided an additional triaxially confined node comparison for a beam with 0.3% transverse reinforcement in each direction; the other Series M specimen provided a comparison between beams reinforced with 0.3% transverse reinforcement in

each direction with either two or four stirrups legs. Details of these four tests are presented in Figure 3-12.

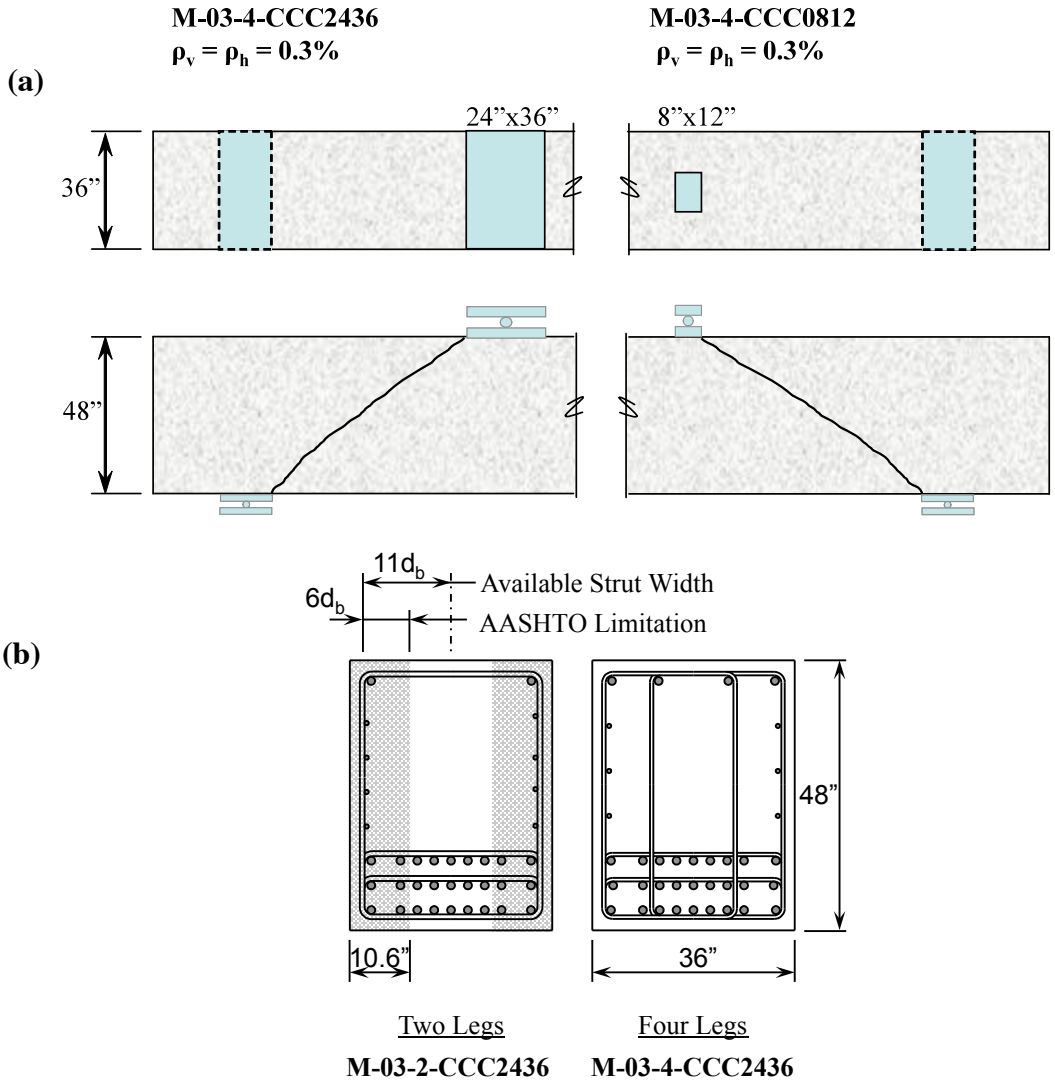

Figure 3-12. Series M: (a) Triaxially confined load plate and (b) 2 versus 4 stirrup leg comparison.

As previously mentioned, Specimen M-03-2-CCC2436 did not fail in shear. Therefore, results from this test are not included in the filtered database. However, the data collected from this experiment has value and is of interest to the current research. The purpose of testing Specimen M-03-2-CCC2436 was to

correlate the findings from the tests conducted on 21-inch wide specimens with those conducted on 36-inch wide specimen. Therefore, results for this specimen are presented in Chapter 4 along with the Series I results.

A detailed discussion of the fabrication and testing of Series M specimens is presented by Huizinga (2007). Specimen details are summarized in Section 3.2.6. The nomenclature used to distinguish the beams within Series M and other details specific to their purpose is presented in Section 3.2.5.1.

3.2.5.1 Series M: Beam Details

In order to distinguish Series M beams from one another the nomenclature presented in Figure 3-13 was developed. Each numeral is a variable within the testing series. Other beam details remain constant and are summarized in Section 3.2.6. Geometric and reinforcement details for all of the Series M tests are presented in Figure 3-14 and Table 3.4.

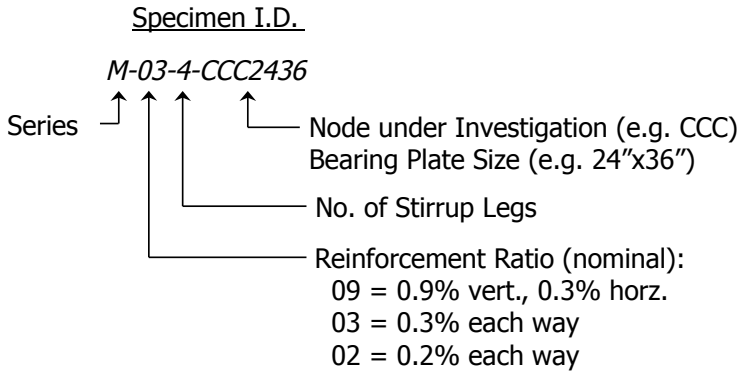

Figure 3-13. Series M: description of nomenclature used for Specimen I.D.

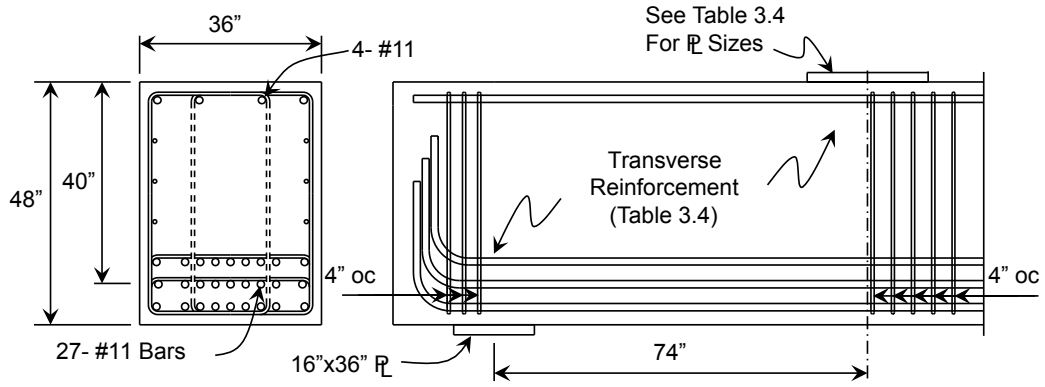

Figure 3-14. Series M beam details.

Table 3.4. Series M test specimen details.

Name	f'_c ††	ϱ_v	ϱ_h	a/d ratio	Stirrup Spacing	Load Plate† (*in.*)	Purpose
M-03-4-CCC2436	4100	0.0031	0.0030	1.85	#5@11"	24x36	*Control*
M-03-4-CCC0812	3000	0.0031	0.0030	1.85	#5@11"	8x12	*Triaxial Node*
M-03-2-CCC2436	4900	0.0031	0.0030	1.85	#7@11"	24x36	*2 vs. 4 Stirrups*
M-09-4-CCC2436	4100	0.0086	0.0030	1.85	#5@4"	24x36	*Reinf. Ratio*
M-02-4-CCC2436	2800	0.0022	0.0022	1.85	#4@10"	24x36	*Reinf. Ratio*

† Load plate dimensions: [in direction of span] x [transverse to direction of span]
†† Compressive strength of concrete measured at the time of testing (Section 0)

3.2.6 Summary of All Testing Series

A summary of the details for all 37 tests of the experimental program is presented in Table 3.5. A discussion of results for Series I and II specimens is presented in Chapters 4 and 5, respectively. For the convenience of the reader, beam details are presented along with the experimental results for all 37 of the test specimens in Appendix E.

Table 3.5. Summary of all beam details.

Beam I.D.	b in.	h in.	d in.	ρ_l	ρ_l'	ρ_v	ρ_h	Stirrup Spa. in.	l_b † in.	b_b † in.	l_l † in.	b_l † in.	a/d ratio
Series I Distribution of Stirrups through beam web													
I-03-2	21	44	38.5	0.0229	0.0116	0.0029	0.0033	6.5	16	21	20	21	1.84
I-03-4	21	44	38.5	0.0229	0.0116	0.0030	0.0033	7.0	16	21	20	21	1.84
I-02-2	21	44	38.5	0.0229	0.0116	0.0020	0.0020	9.5	16	21	20	21	1.84
I-02-4	21	44	38.5	0.0229	0.0116	0.0021	0.0020	10.0	16	21	20	21	1.84
Series II Triaxial Confinement of Nodal Regions													
II-03-CCC2021	21	42	38.6	0.0231	0.0115	0.0031	0.0045	9.5	10	21	20	21	1.84
II-03-CCC1007	21	42	38.6	0.0231	0.0115	0.0031	0.0045	9.5	10	21	10	7	1.84
II-03-CCT1021	21	42	38.6	0.0231	0.0115	0.0031	0.0045	9.5	10	21	36	21	1.84
II-03-CCT0507	21	42	38.6	0.0231	0.0115	0.0031	0.0045	9.5	5	7	36	21	1.84
II-02-CCT0507	21	42	38.6	0.0231	0.0115	0.0020	0.0019	15.0	5	7	36	21	1.84
II-02-CCC1007	21	42	38.6	0.0231	0.0115	0.0020	0.0019	15.0	10	21	10	7	1.84
II-02-CCC1021	21	42	38.6	0.0231	0.0115	0.0020	0.0019	15.0	10	21	10	21	1.84
II-02-CCT0521	21	42	38.6	0.0231	0.0115	0.0020	0.0019	15.0	5	21	20	21	1.84
Series III Reinforcement and a/d Ratio													
III-1.85-00	21	42	38.6	0.0231	0.0115	0.000	0.000	-	16	21	20	21	1.84
III-2.5-00	21	42	38.6	0.0231	0.0115	0.000	0.000	-	16	21	20	21	2.47
III-1.85-02	21	42	38.6	0.0231	0.0115	0.0020	0.0019	14.5	16	21	20	21	1.84
III-1.85-025	21	42	38.6	0.0231	0.0115	0.0024	0.0014	12.0	16	21	20	21	1.84
III-1.85-03	21	42	38.6	0.0231	0.0115	0.0029	0.0029	10.0	16	21	20	21	1.84
III-1.85-01	21	42	38.6	0.0231	0.0115	0.0010	0.0014	18.0	16	21	20	21	1.84

† l_b = length of support plate, along the length of the beam; l_l = length of load plate, along length of the beam
b_b = width of support plate, transverse to the beam; b_l = width of support plate, transverse to the beam

Table 3.5 (cont.'d). Summary of all beam details

Beam I.D.	b in.	h in.	d in.	ρ_l	ρ_l'	ρ_v	ρ_h	Stirrup Spa. in.	l_b† in.	b_b† in.	l_l† in.	b_l† in.	a/d ratio
Series III, continued…													
III-1.85-03b	21	42	38.6	0.0231	0.0115	0.0031	0.0029	6.0	16	21	20	21	1.84
III-1.85-02b	21	42	38.6	0.0231	0.0115	0.002	0.0018	9.5	16	21	20	21	1.84
III-1.2-02	21	42	38.6	0.0231	0.0115	0.002	0.0018	9.5	16	21	20	21	1.20
III-1.2-03	21	42	38.6	0.0231	0.0115	0.0031	0.0029	9.5	16	21	20	21	1.20
III-2.5-02	21	42	38.6	0.0231	0.0115	0.002	0.0018	9.5	16	21	20	21	2.49
III-2.5-03	21	42	38.6	0.0231	0.0115	0.0029	0.0042	9.5	16	21	20	21	2.49
Series IV Depth Effect													
IV-2175-1.85-02	21	75	68.9	0.0237	0.0129	0.0021	0.0018	9.5	16	21	29	21	1.85
IV-2175-1.85-03	21	75	68.9	0.0237	0.0129	0.0031	0.0029	9.5	16	21	29	21	1.85
IV-2175-2.5-02	21	75	68.9	0.0237	0.0129	0.0021	0.0021	14.25	16	21	24	21	2.50
IV-2175-1.2-02	21	75	68.9	0.0237	0.0129	0.0021	0.0021	14.25	16	21	24	21	1.20
IV-2123-1.85-03	21	23	19.5	0.0232	0.0116	0.0030	0.0030	6.25	16	21	16.5	21	1.85
IV-2123-1.85-02	21	23	19.5	0.0232	0.0116	0.0020	0.0017	5.25	16	21	16.5	21	1.85
IV-2123-2.5-02	21	23	19.5	0.0232	0.0116	0.0020	0.0017	5.25	16	21	15.5	21	2.50
IV-2123-1.2-02	21	23	19.5	0.0232	0.0116	0.0020	0.0017	5.25	16	21	18	21	1.20
Series M Multiple Purpose													
M-03-4-CCC2436	36	48	40	0.0293	0.0043	0.0031	0.0030	11	16	36	24	36	1.85
M-03-4-CCC0812	36	48	40	0.0293	0.0043	0.0031	0.0030	11	16	36	8	12	1.85
M-03-2-CCC2436	36	48	40	0.0293	0.0022	0.0032	0.0030	11	16	36	24	36	1.85
M-09-4-CCC2436	36	48	40	0.0293	0.0043	0.0086	0.0030	4	16	36	24	36	1.85
M-02-4-CCC2436	36	48	40	0.0293	0.0043	0.0022	0.0022	10	16	36	24	36	1.85

† l_b = length of support plate, along the length of the beam; l_l = length of load plate, along length of the beam
b_b = width of support plate, transverse to the beam; b_l = width of support plate, transverse to the beam

3.3 TESTING FRAME

In order to apply loads high enough to fail large-scale deep beams, a new test setup was designed and constructed in the Phil M. Ferguson Structural Engineering Laboratory. A key component of the new testing frame was a 96,000-pound steel platen or *strong floo*r. The strong floor was salvaged from a six-million pound testing frame that had been decommissioned by the Navy and donated to the Ferguson Laboratory. An illustration of the final test setup is presented in Figure 3-15. The construction and installation of the strong floor is presented in Figure 3-16. In addition, a picture of the test setup immediately prior to a test is presented in Figure 3-16. Further details on the design and construction of the testing frame are presented by Huizinga (2007).

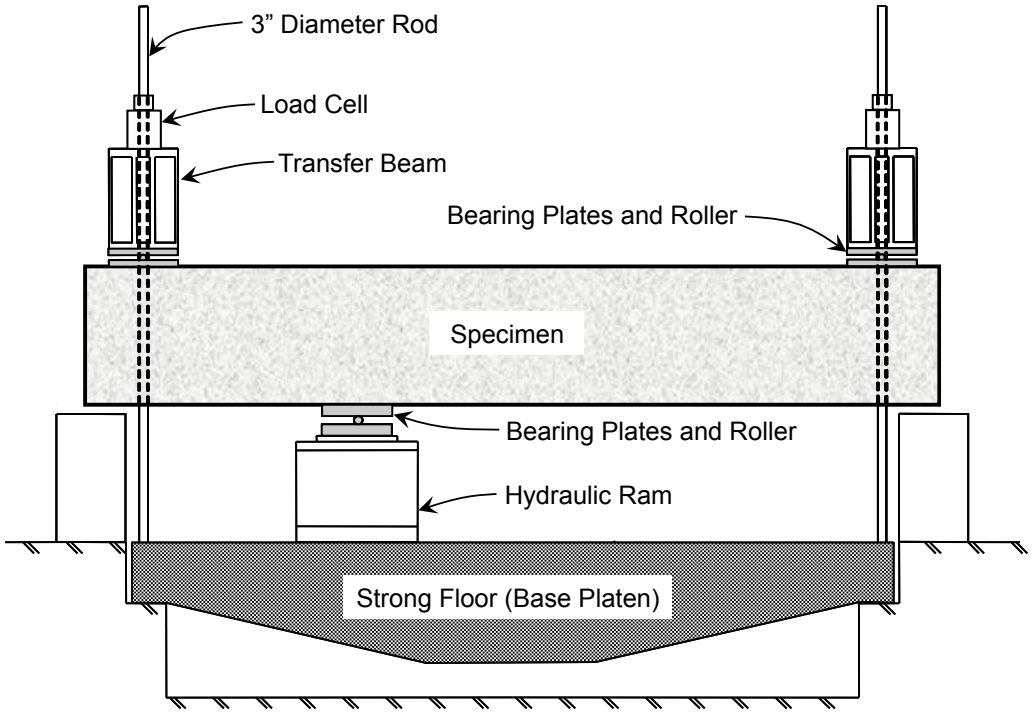

Figure 3-15. Elevation view of test setup [Huizinga (2007)].

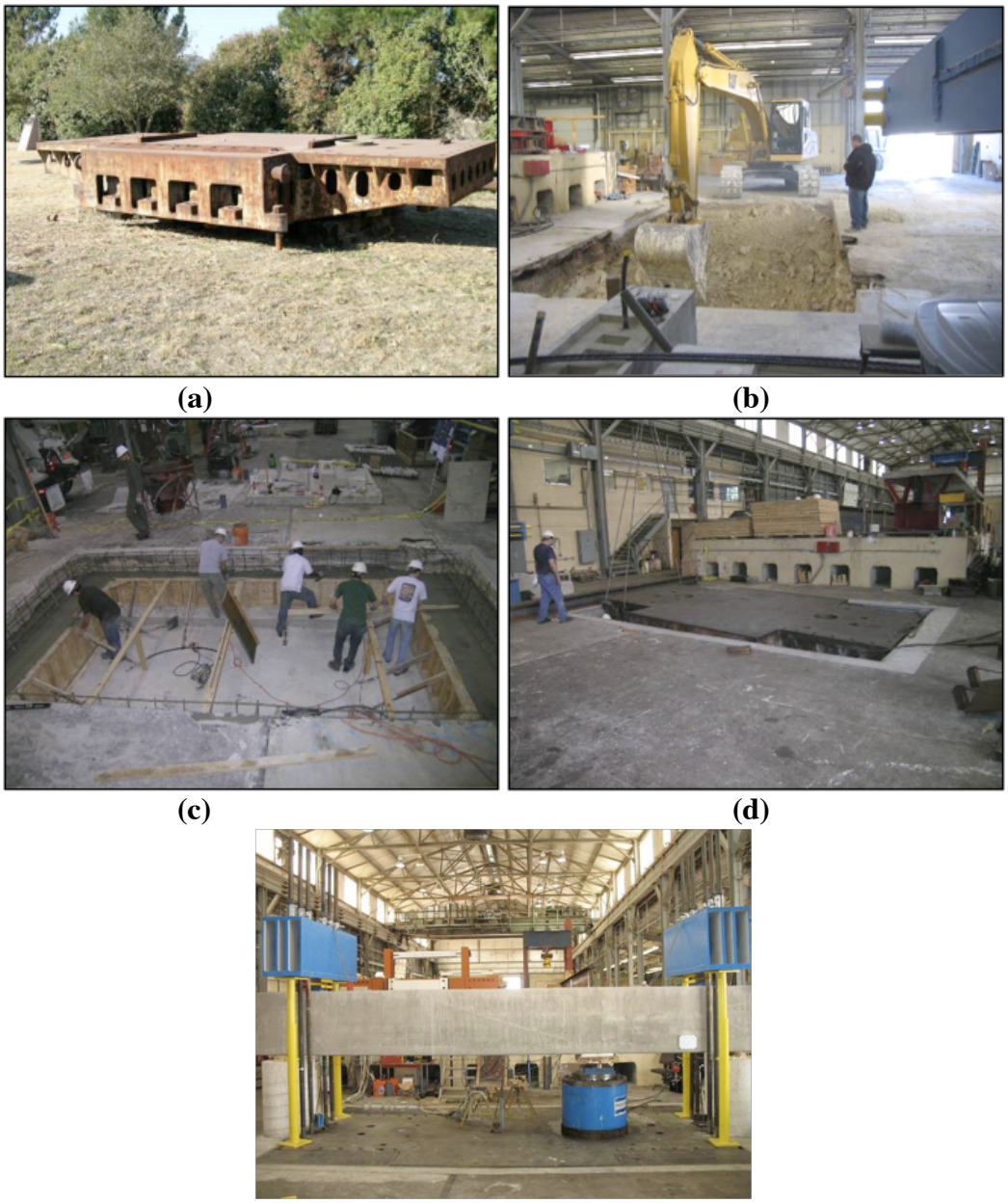

Figure 3-16. Installation of strong floor: (a) steel platen (b) floor excavation (c) fabrication of platen support (d) lowering of platen into position, and (e) test setup.

3.4 FABRICATION OF SPECIMENS

Specimens were constructed using conventional materials. The use of steel formwork accelerated the fabrication process and provided dimensional accuracy. In general, the assembly of the reinforcement cage, installation of strain gauges, placement of concrete, and removal of formwork took about two weeks to complete per specimen. Beams were tested a minimum of 28-days after concrete placement. Additional details regarding the materials, assembly, and testing of the beam specimens are presented in Sections 3.4.1 through 3.4.3.

3.4.1 Steel Reinforcement

Steel reinforcement was domestic Grade 60 deformed bars meeting the requirements of ASTM A615. Cross sectional dimensions of the bars complied with the nominal sizes given in ASTM A615.

Each rebar order delivered to the Ferguson Laboratory was accompanied with a set of four coupons of each bar size. The tensile strength of the coupons was measured in accordance with ASTM A370. At least three of the coupons were tested for each bar size. The tensile strength of the longitudinal and transverse reinforcement for Series I, II, and M test specimens are summarized in Table 3.6.

Table 3.6. Steel reinforcement material properties.

Beam Name	Bar Type			Yield Strength		
	long.	vert.	horz.	f_{yl} †	f_{yv} ††	f_{yh} †††
M-03-4-CCC2436	#11	#5	#5	67	61	61
M-03-2-CCC2436	#11	#7	#5	65	63	63
M-03-4-CCC0812	#11	#5	#5	65	64	63
I-03-2	#6	#4	#4	73	67	67
I-03-4	#6	#3	#4	73	73	67
I-02-2	#6	#4	#4	73	67	67
I-02-4	#6	#3	#4	73	73	67
II-03-CCC2021	#11	#5	#5	64	65	65
II-03-CCC1007	#11	#5	#5	64	65	65
II-03-CCT0507	#11	#5	#5	66	71	71
II-03-CCC1021	#11	#5	#5	66	71	71
II-02-CCT0507	#11	#5	#4	69	64	63
II-02-CCC1007	#11	#5	#4	69	64	63
II-02-CCC1021	#11	#5	#4	69	67	62
II-02-CCT0521	#11	#5	#4	69	67	62

† f_{yl} = yield strength of longitudinal reinforcement measured per ASTM A370
†† f_{yv} = yield strength of vertical transverse reinforcement measured per ASTM A370
††† f_{yh} = yield strength of horizontal transverse reinforcement measured per ASTM A370

3.4.2 Concrete Mixture Design

Typically, TxDOT engineers specify the compressive strength of concrete used for a bent to be in the range between 3600 to 5000-psi. As a result, the specified compressive strength of concrete used for the experimental program was designed to be within the same range. The actual measured compressive strength of concrete ranged between 3120 and 5330-psi. Concurrent with the placement of concrete for each beam, standard 4”x8” cylinders were prepared in accordance with ASTM C31 and tested in accordance with ASTM C39. Proportions of the concrete mixture are presented in Table 3.7.

Table 3.7. Concrete mixture proportions

Material	Quantity
Type I Portland Cement	300 to 317 lb/cy
Fly Ash	79 to 83 lb/cy
CA: ¾" or 1" River Rock	1800 to 1850 lb/cy
FA: Sand	1370 to 1515 lb/cy
Water	29 to 31 gallons/cy
HRWR* Admixture	15 to 20 oz/cy
Set Retardant Admixture	6 oz/cy
Water/Cement Ratio	0.62 to 0.68
Slump	4 to 8 inches

* *HRWR:* High Range Water Reducing (i.e. *Superplasticizer*)

3.4.3 Construction of Specimens

The concrete used to fabricate the beams specimens was provided from a local ready-mix supplier. Upon the arrival of concrete at the Ferguson Laboratory, a slump test was conducted according to ASTM C143. If necessary, additional water was added to increase the slump to approximately 6 ± 2-inches. In all of the cases where water was added, the additional amount did not exceed the amount of water that was held back at the batch plant (as indicated on the batch tickets). Twelve to twenty 4-inch diameter cylinders were prepared in accordance with ASTM C31. The cylinders were covered with a plastic sheet and cured under the same ambient conditions as the beam specimens.

Large-scale beams could be fabricated relatively quickly and with accurate dimensional tolerances due to the use of steel formwork. All specimens were fabricated using the same steel formwork. External pneumatic vibrators attached to a bracket that moved along the length of the formwork were used to consolidate the concrete. After the placement of concrete, the beams were covered with a plastic sheet and cured under the ambient laboratory conditions. An illustration of the fabrication procedure from assembly of reinforcing cages to removal of formwork is presented in Figure 3-17.

Figure 3-17. Fabrication of a typical beam: (a) assembly of reinforcement cage (b) placement of cage in formwork (c) forms in place prior to concrete placement (d) placement of concrete (e) beam curing (f) test specimen after the removal of forms.

3.5 TESTING OF SPECIMENS

Beams were loaded in 50 to 75-kip increments with a 6-million pound capacity double-acting hydraulic ram. After each load increment, cracks were marked and the width of the widest diagonal shear crack on each face of the beam was recorded. Photographs were taken after each load increment and the entire test was recorded with a video camera.

Each end of each beam was tested, resulting in two tests per beam. This was made possible by securing the inclined crack at the failure location with an external, post-tensioned, clamp. After a shear failure was attained, external post-tensioned clamps were installed to strengthen the inclined failure crack. After securing the failure crack, the hydraulic actuator was moved to the opposite span of the beam and positioned based on the desired a/d ratio. An illustration of the process of testing one side of a beam; securing of the failure zone with clamps; and testing the other side is presented in Figure 3-18.

(a)

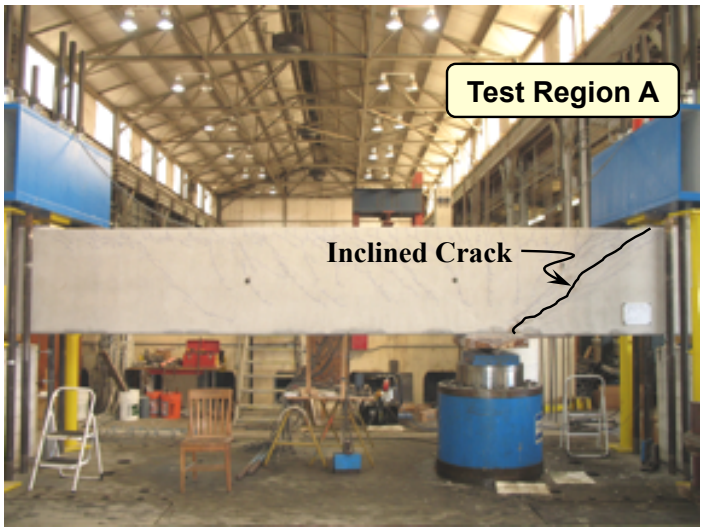

(b)

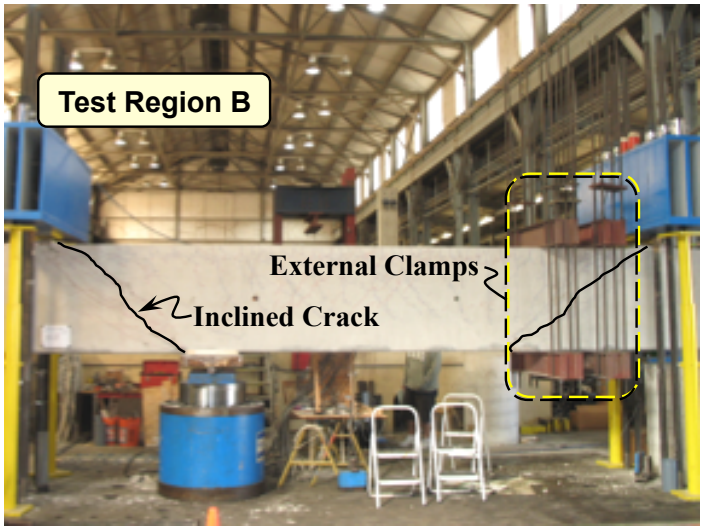

Figure 3-18. Each end of a beam is loaded to failure resulting in two tests: (a) shear failure is attained in Test Region A (b) external post-tensioned clamps in place and shear failure is attained in Test Region B.

The test specimens can be considered as upside-down simply supported beams subjected to an asymmetric concentrated load. Therefore, the tension reinforcement was located along the top-side of each beam, and the compression reinforcement along the bottom. The applied force, *load*, was applied upward

from the bottom of the beam and the *supports* were at the top, resisting the upward movement.

The orientation of the beam was taken into account when determining the amount of shear the beam was resisting. Load cells were positioned at the supports (i.e. on top of the transfer beam), so they were only able to measure the amount of applied live load, P_L. The weight of each transfer beam, P_{TR}, was approximately 7.7-kips. The amount of internal shear resisted by the beam varied along the length due to its self weight, ω_{DL}. Location and determination of the critical shear force, V_{test}, is illustrated in Figure 3-19.

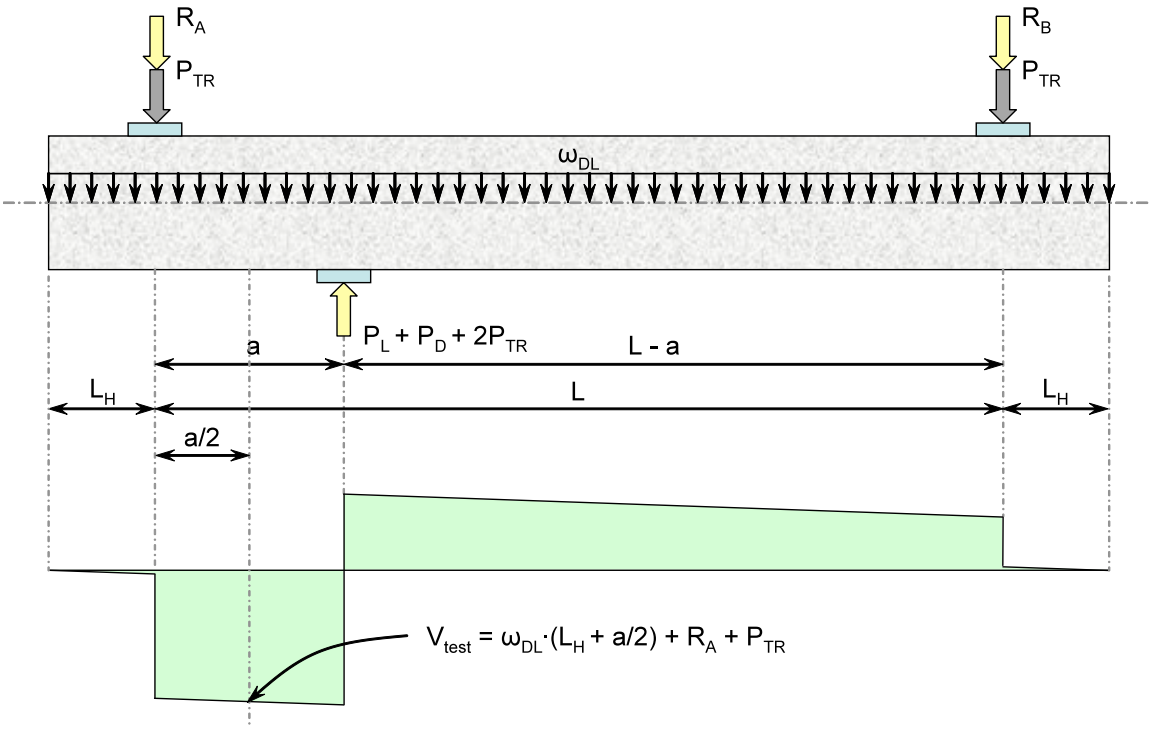

WHERE,

$P_L = R_A + R_B$	L = 255.25”	ω_{36x48} = 1.80 kip/ft
$P_D = \omega_{DL}\cdot(2L_H + L)$	L_H = 38.375”	ω_{21x42} = 0.92 kip/ft
	P_{TR} = 7.7 kip	ω_{21x44} = 0.96 kip/ft

Figure 3-19. Force and shear force diagram for typical beam test.

The shear at the critical section is determined based on the reaction measured directly from the nearby load cells. The critical shear in the beam is equivalent to the reaction in the near support, R_A, plus the weight of the transfer beam, P_{TR}, and a portion of the self weight of the specimen, $\omega_{DL}\cdot(L_H + a/2)$. Section 3.5.3 presents additional information on the load cells.

It is important to note that photographs and figures presented in this document are typically presented upside-down so that the beams are viewed in a conventional manner; i.e. with the tension steel at the bottom of the beams and the load applied from the top. Details on the photograph location are presented in Figure 3-20.

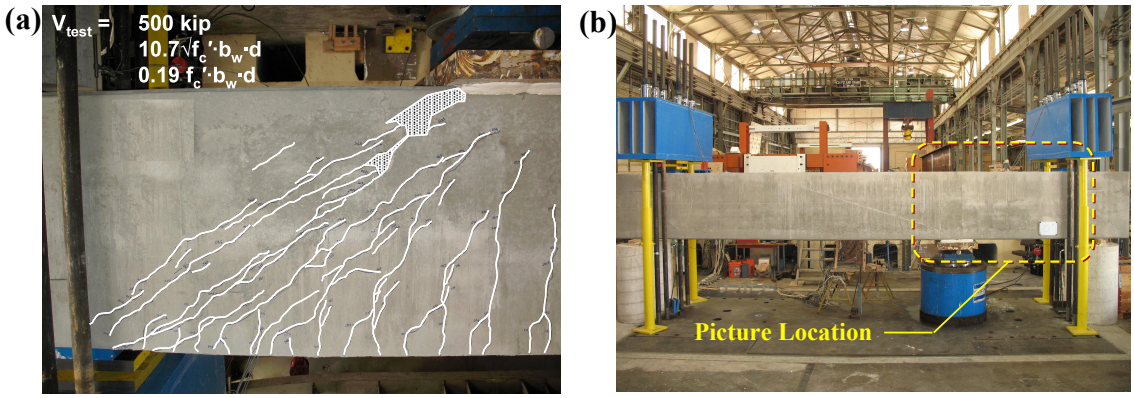

Figure 3-20. (a) Photographs are orientated upside-down in order to present test results in a conventional manner; (b) actual picture location.

3.5.1 Strain Measurements: Reinforcing Bars

Strain gauges were affixed to the transverse and longitudinal reinforcement (Figure 3-21).

Figure 3-21. Installation of strain gauge for measuring steel strains.

The location of the gauges for Series I and II specimens is illustrated in Figure 3-22. The 36"x48" Series M beams had internal gauges located in similar locations; more detailed information regarding the Series M beams is presented by Huizinga (2007).

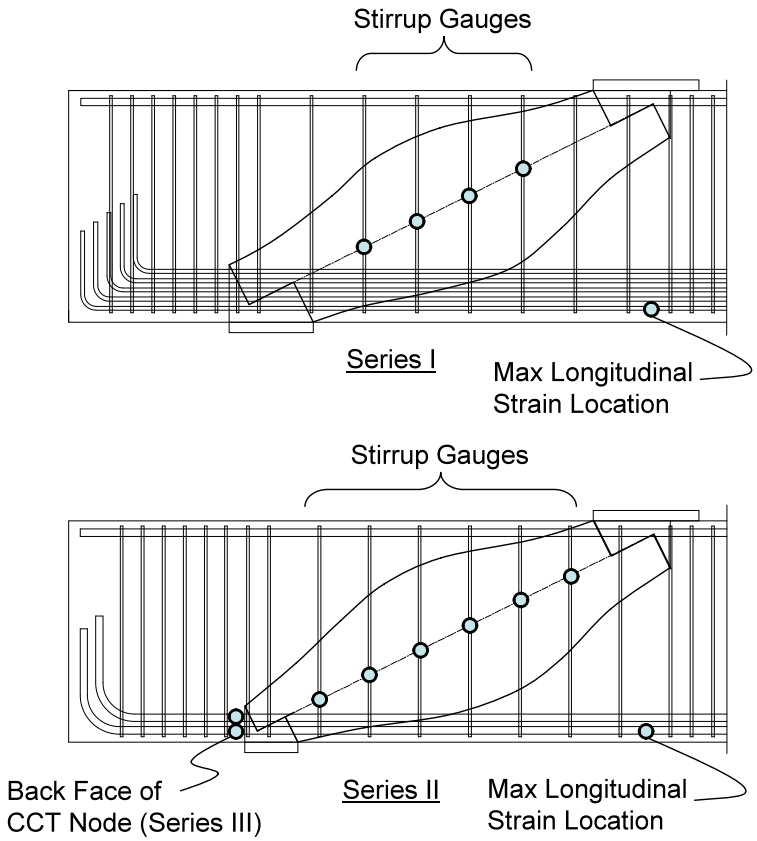

Figure 3-22. Series I and II typical strain gauge locations.

The locations of strain gauges attached to stirrups were based on the assumed centerline of the inclined strut. The purpose of locating a gauge along the

strut centerline is to measure steel strains at or close to the primary diagonal splitting crack. Four stirrups were instrumented within the test regions of the Series I beams. In each of these locations, both external and internal stirrups legs were instrumented. None of the Series II beams contained internal stirrups. For Series II beams, both legs of each stirrup shown in Figure 3-22 were instrumented.

The maximum longitudinal reinforcing bar strain was measured at the bottom-most longitudinal bar directly below the load point. All six of the bottom longitudinal bars were instrumented for specimens II-03-CCC2021 and II-03-CCC1007. For all other tests, every other bottom bar was instrumented. The purpose of providing gauges along the longitudinal tension steel was to monitor the yielding of the longitudinal reinforcement (if any) as the beam was loaded to failure in shear. With regard to the Series I specimens, it was of interest to measure the amount of tension force that was being distributed to the internal longitudinal bars. Recall, Anderson and Ramirez (1989) reported that beams with multiple leg stirrups were more effective at evenly distributing tension to the internal longitudinal reinforcement (Section 2.6.4.3).

Finally, all twelve of the #11 bars were instrumented at the back face of the CCT node for the following two specimens: III-1.85-02 and III-1.85-025. The depth of the back face of a CCT node is commonly assumed equivalent to twice the distance from the exterior of the beam to the centroid of the tension reinforcement (Section 2.3). Often times, the distance is quite small; resulting in a small area to resist the applied force assumed from a STM. By measuring the internal straining of the bars, the amount of stress applied to the back face of the CCT node could be quantified. Similar strain measurements were taken from strain gauges applied to the concrete's surface. A description of the concrete gauges follows.

3.5.2 Strain Measurements: Concrete Surface

Strain gauges were affixed to the beam's surface to measure the change in strain (Figure 3-23).

Figure 3-23. Installation of a concrete surface gauge for measuring concrete strains.

The back face of CCT nodes were instrumented with strain gauges for all of the Series I specimens and the following specimens within Series II and III: II-03-CCT1021 and II-03-CCT0507; III-1.85-00, III-1.85-02, and III-1.85-025. The location of these concrete gauges is illustrated in Figure 3-24.

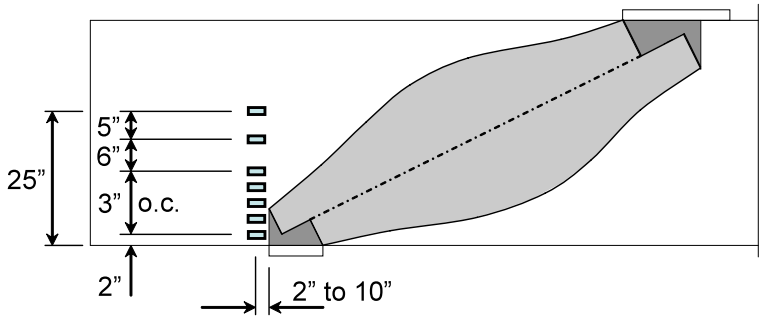

Figure 3-24. Concrete strain gauge locations

The purpose of measuring external strains was to verify the modeling assumption used to proportion the back face of a CCT node. By measuring the concrete strain, the accuracy and conservatism of hydrostatic and non-hydrostatic node geometry assumptions could be examined. The strain gauges affixed to the reinforcement at the CCT back face (Section 3.5.1) were located in the same plane as the surface gauges in order to compare the values from the two locations.

3.5.3 Load and Displacement Measurements

500-kip capacity load cells were placed between the transfer beam and the reaction nuts at all twelve of the rod locations (Figure 3-25). Therefore, it was possible to directly measure the load reaction at each support. Figure 3-25 illustrates the position of the load cells on top of a transfer beam.

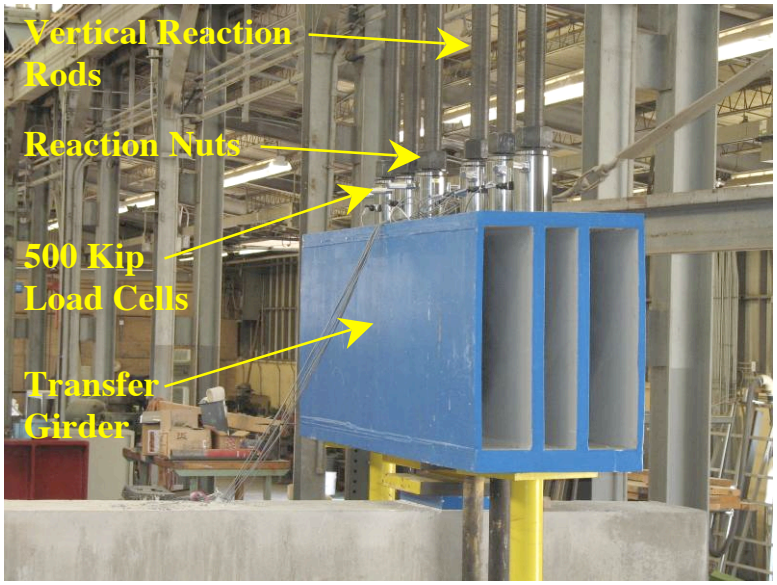

Figure 3-25. Load cells measure the reaction in each rod.

Four 6-inch linear potentiometers were used to measure the displacement of a beam during testing. Linear potentiometers were located at the supports, load point, and centerline of the beam. The locations of the linear potentiometers are shown in Figure 3-26. A photograph of the linear potentiometer used to measure the load plate displacement is presented in Figure 3-27.

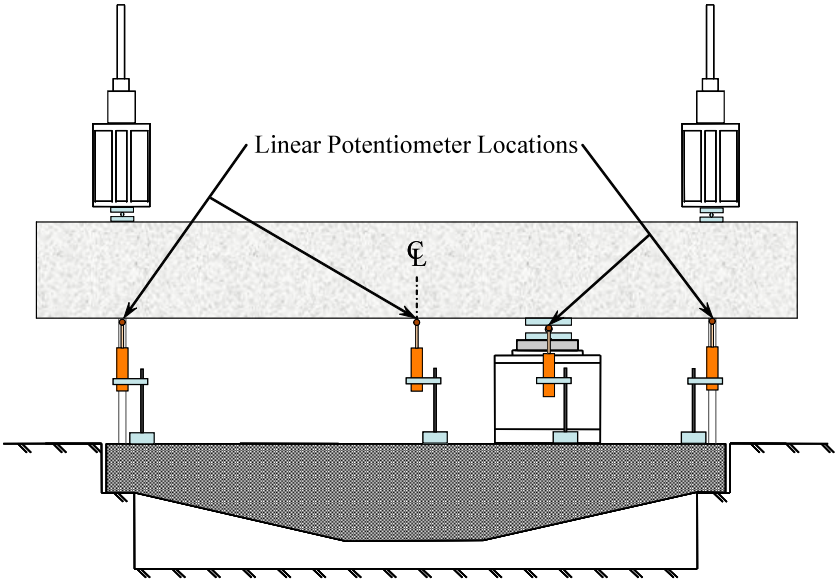

Figure 3-26. Linear potentiometer locations.

Figure 3-27. Linear potentiometer used to measure the displacement at the load point.

The purpose of the linear potentiometers was to measure the deflections of the beam specimens due to shear and flexural stresses. The test specimens also underwent rigid body motion as they were lifted off their supports and as the 3-inch vertical reaction rods elongated. The displacement measured at the supports

was used to subtract the rigid body motion from the beam deformations. An illustration of the rigid body motion and beam deformation is presented in Figure 3-28. The beam displacement at the location of the load, Δ_{BEAM}, was determined according to Equation 3-1.

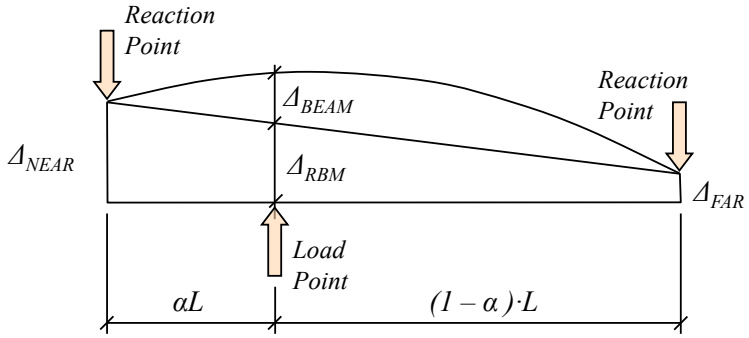

Figure 3-28. Diagram of beam displacements due to rigid body motion and flexural and shear deformations

$$\Delta_{RBM} = \Delta_{FAR} + (1-\alpha)\cdot(\Delta_{NEAR} - \Delta_{FAR}) \qquad \text{Equation 3-1}$$

$$\Delta_{BEAM} = \Delta_{LOAD} - \Delta_{RBM}$$

Where,

Δ_{RBM} = Displacement due to rigid body motion

Δ_{NEAR} = Recorded displacement at near reaction point

Δ_{FAR} = Recorded displacement at far reaction point

Δ_{LOAD} = Recorded displacement at load point

Δ_{BEAM} = Displacement due to flexural and shear deformations

3.5.4 Serviceability Data

Serviceability data was collected from all of the specimens tested as part of the experimental program. The serviceability information that was collected included: the load at which the first diagonal crack formed; and the width of the maximum diagonal crack measured at each load increment.

Two separate measurements of the maximum diagonal crack were taken after each load increment on both faces of the test region using a crack comparator card. The maximum diagonal crack widths presented in this document are measured at both the north and south face of a specimen. The values are an average of the two measurements taken at each load increment.

The first diagonal crack was measured both by visual observation and from data obtained from strain gauges affixed to the stirrups. The beam was inspected after each load increment. In general, the first diagonal crack formed at a 45-degree angle with respect to the load plate. Strain gauge data was used to more accurately determine the shear at which the crack formed. Upon examination of the data, the first cracking load was recorded at the point in time when the stirrup strains increased significantly. The visual observation of the first cracking load was used to verify the more accurate results determined from the strain gauges. The recorded first cracking load for Specimen I-02-2 is presented in Figure 3-29 along with the subsequent strain gauge data.

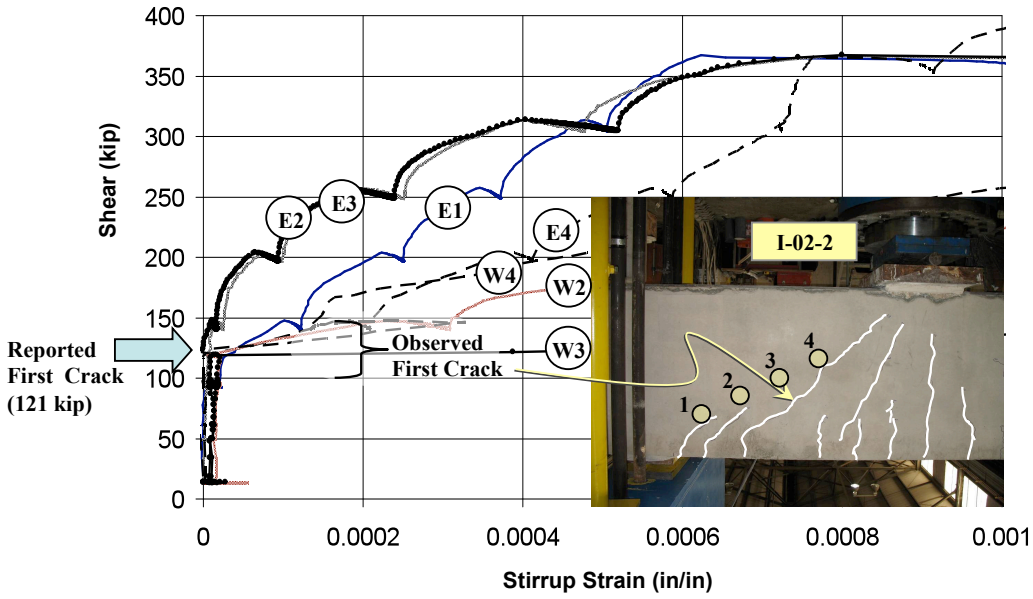

Figure 3-29. Visual and experimental determination of first cracking load.

When a specimen was loaded to failure, the *untested* side of the beam was subjected to loads that were approximately 40-percent of the ultimate capacity. Therefore, it was only possible to measure the first cracking load for the first test conducted on each beam. Results from tests that were conducted as the second test of a beam are denoted as *pre-cracked* in order to indicate that cracks were present prior to testing.

3.6 SUMMARY

The test setup, design of test specimens, reinforcing bar details, material properties, and information on the instrumentation used to gather data are described in this chapter. In order to accomplish the goals of the current study, beams of significant size were designed and fabricated. These beams are more representative of actual transfer girders and bridge bents used in practice. The strength of such large-scale beams necessitated the use of a high-capacity testing frame. As a result, the base platen of a 6-million pound testing frame was salvaged and utilized in the test setup of the current research study.

A total of 12 tests were conducted on the Series I and Series II beams; 20 tests were conducted on the Series III and Series IV beams; and 5 tests were conducted on the Series M beams. Strength and crack width (i.e. serviceability) data was collected during the testing of all specimens. The beams tested as part of the current study represent some of the largest deep beam shear tests ever conducted. The difference in specimen size between the current and past studies is illustrated in Figure 3-30 and Figure 3-31. Bent caps used in the State of Texas are illustrated in Figure 3-30 alongside beams that have been fabricated and tested as part of the current and past research projects. A comparison between all beams in the collection database and the beams of the current study is presented in Figure 3-31.

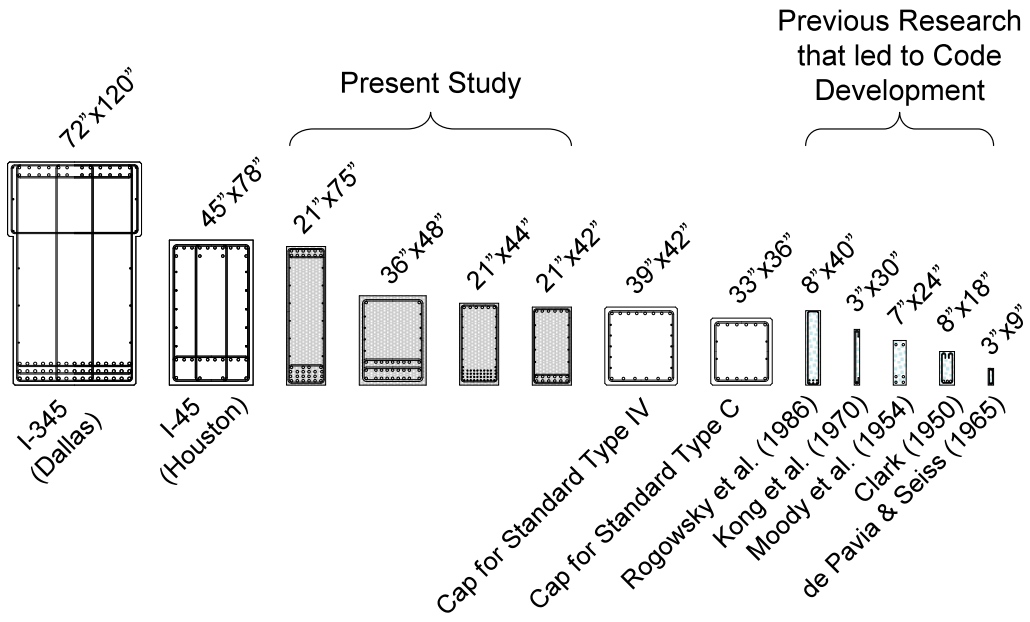

Figure 3-30. Comparison of actual bent caps and beams included in current and past research programs.

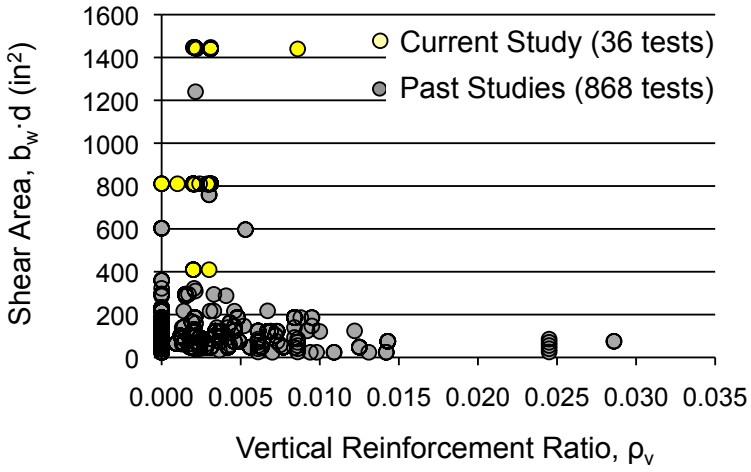

Figure 3-31. Comparison of beams sizes between current and past studies.

Details and discussion of results for Series I and II specimens are presented in Chapters 4 and 5 respectively. Information on Series III and IV specimens are presented by Birrcher (2008).

CHAPTER 4

Distribution of Stirrups across the Web

4.1 OVERVIEW

The purpose of the Series I and M testing programs were to evaluate the benefit of distributing stirrups across the web for beams subjected to deep beam shear. In order to accomplish this objective, six tests were conducted on the three beams illustrated in Figure 4-1. All pertinent details of the test specimens are presented in Table 3.5.

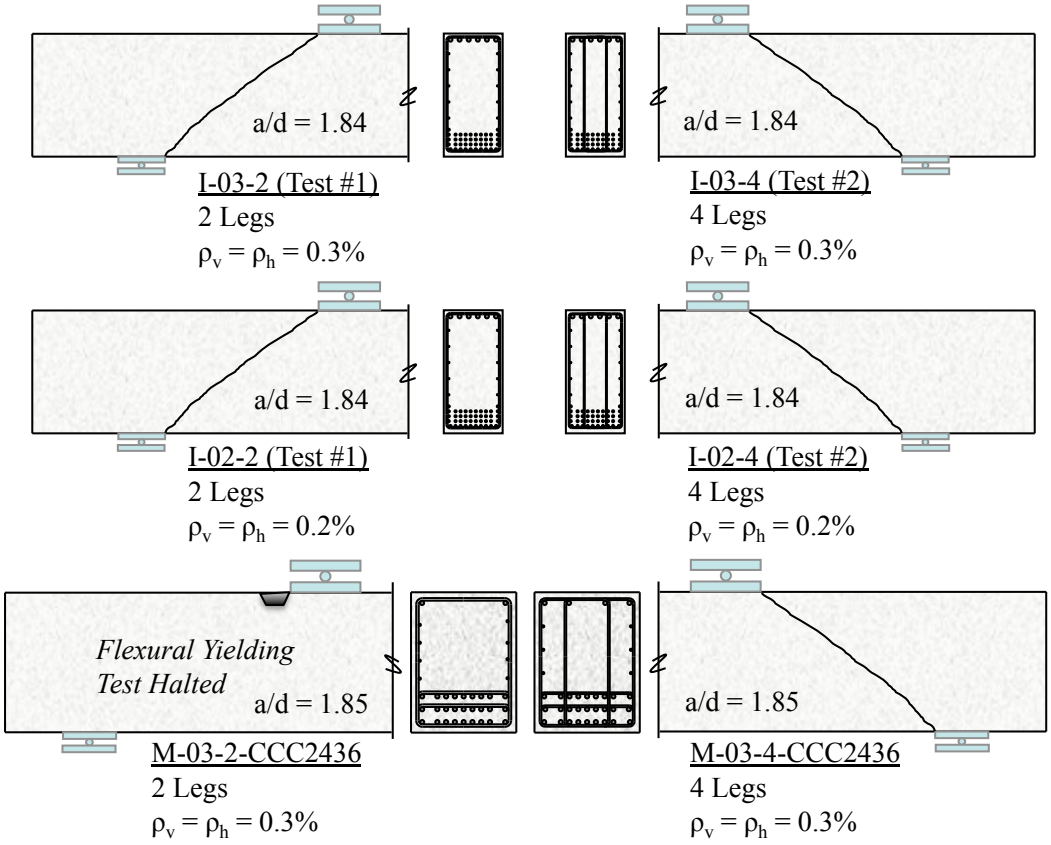

Figure 4-1. Summary of tests: 2 versus 4 stirrup legs

The test specimens illustrated in Figure 4-1 were designed and detailed such that the only variation between each side of a beam was the number of stirrup legs distributed across the web. For each beam, the transverse

reinforcement ratio (ρ_v and ρ_h) and stirrup spacing were kept the same. Details on the design, fabrication and testing of the Series I and M test specimens are given in Chapter 3. The stirrup configuration was selected in order to evaluate the AASHTO LRFD (2008) provision described in Section 2.6.4. In summary, the provision limits the width of a strut framing into a CTT node to six times the diameter of the main longitudinal reinforcement. Based on this requirement, Series I specimens that contain two stirrup legs have an effective strut width of 5.6-inches on each side of the beam (Figure 4-2). If a designer wishes to utilize the full beam width, then four stirrup legs must be provided. Cross sectional details of the specimens that contain stirrups with two and four legs are illustrated in Figure 4-2.

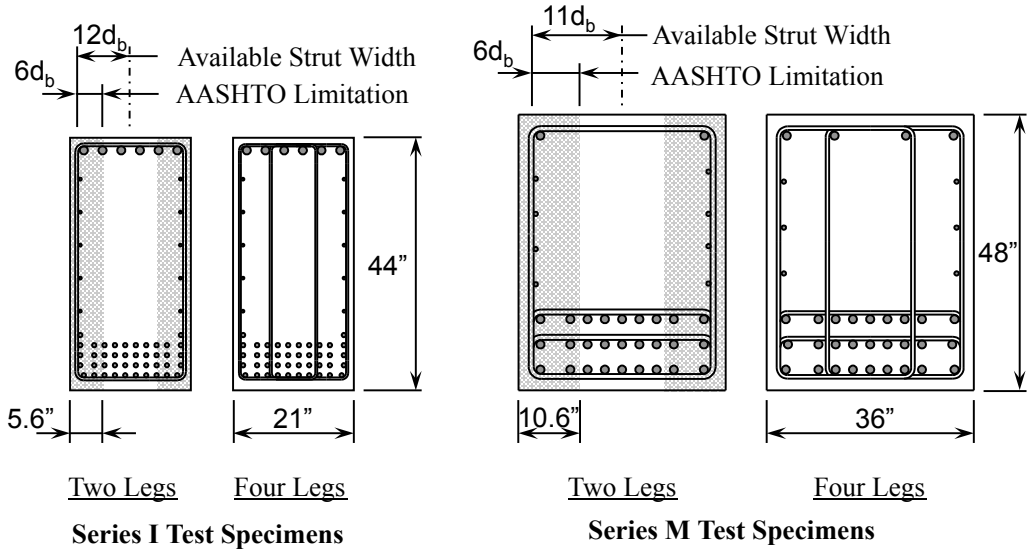

Figure 4-2. Effective strut width of a two-leg vs. a four leg specimen.

Strength and serviceability data was collected for each test. An analysis of the data and a discussion of the results are presented as follows.

4.2 RESULTS OF SERIES I AND M TESTS

A shear failure can be characterized as either a one-panel (deep beam) or two-panel (sectional shear) mechanism as described in Section 2.2. For low a/d ratios, the crushing of a single strut dominates the failure mode. For high a/d

ratios, the splitting in tension of a multi-panel truss model is the primary failure mode. As seen in Figure 4-1, the a/d ratio was approximately 1.85 for all six tests. This shear span-to-depth ratio is within the transition region between a single-panel (crushing) mode and a double panel (splitting) mode. An illustration of these two failure modes is presented in Figure 2-6 and Figure 2-7 respectively. For the purpose of comparison, the reported shear capacity is normalized by the compressive strength and the square root of the compressive strength of concrete at the time of testing (Table 4.1).

Table 4.1. Test Results: Series I and M

Specimen I.D.	f_c' (psi)	V_{test} † (kip)	$\frac{V_{test}}{\sqrt{f'_c}\, b_w d}$	$\frac{V_{test}}{f'_c\, b_w d}$	V_{crack} (kip)	$\frac{V_{crack}}{\sqrt{f'_c}\, b_w d}$
I-03-2	5240	569	9.7	0.13	144	2.5
I-03-4	5330	657	11.1	0.15	-	-
I-02-2	3950	454	8.9	0.14	121	2.4
I-02-4	4160	528	10.1	0.16	-	-
M-03-2-CCC2436	4900	1096[f]	10.9	0.16	-	-
M-03-4-CCC2436	4100	1128	12.2	0.19	354	3.8

† See Section 3.5 for determination of critical shear value, V_{test}

f Test was stopped prior to failure of the specimen due to the onset of yielding of the tensile reinforcement and crushing of concrete in the compression zone

It is important to note that Specimen M-03-2-CCC2436 did not experience shear failure. The test was halted upon the onset of yielding of the flexural tensile reinforcement and crushing of the concrete in the compression region. As a result, the maximum shear value reported (V_{test}) in Table 4.1 is the amount of shear carried in the beam upon the onset of flexural failure. Specimen M-03-2-CCC2436 is not a valid deep beam shear test. Nonetheless, results are reported for this specimen because they are note-worthy with regard to a 36-inch wide deep beam reinforced with two and four stirrup legs.

4.2.1 Normalization of Shear Values

In order to compare the capacity of different test specimens with one another, the shear values are normalized by the cross-sectional dimensions and the

strength of concrete. In general, strength values are normalized by either the compressive strength of concrete (i.e., dividing the value by f_c') or by the tensile strength of concrete (i.e., dividing the value by $\sqrt{f_c'}$) depending on the mechanism of failure.

For deep beam tests conducted as part of the current experimental program, cracking patterns at failure indicated that a direct strut was the predominant mechanism for shear transfer and the mode of failure. Parallel cracks between the load point and support delineated the boundary of the strut. Crushing occurred in the compression region adjacent to the load point and along the strut. Thus, normalizing strength values by the compressive strength of concrete is more appropriate than normalizing by the tensile strength of concrete ($\sqrt{f_c'}$).

The load at which the first diagonal crack formed was normalized by the tensile strength of concrete or $\sqrt{f_c'}$. Diagonal cracking is a result of the tensile splitting of concrete within the test region. Thus, it is more appropriate to normalize these values by the tensile strength of concrete ($\sqrt{f_c'}$).

4.2.2 Shear Capacity

The shear capacity of the four Series I specimens is presented with the final cracking patterns in Figure 4-3. The side of each beam with two stirrup legs was tested first; the side with four stirrup legs was tested second. Therefore, the specimens that contained four stirrup legs are denoted as *pre-cracked* to indicate that cracks were present prior to testing. Additional discussion on the Series M tests are presented by Huizinga (2007).

The crack patterns at failure as shown in Figure 4-3 indicate that a direct strut or single-panel mechanism was the predominant mechanism for shear transfer and the mode of failure.

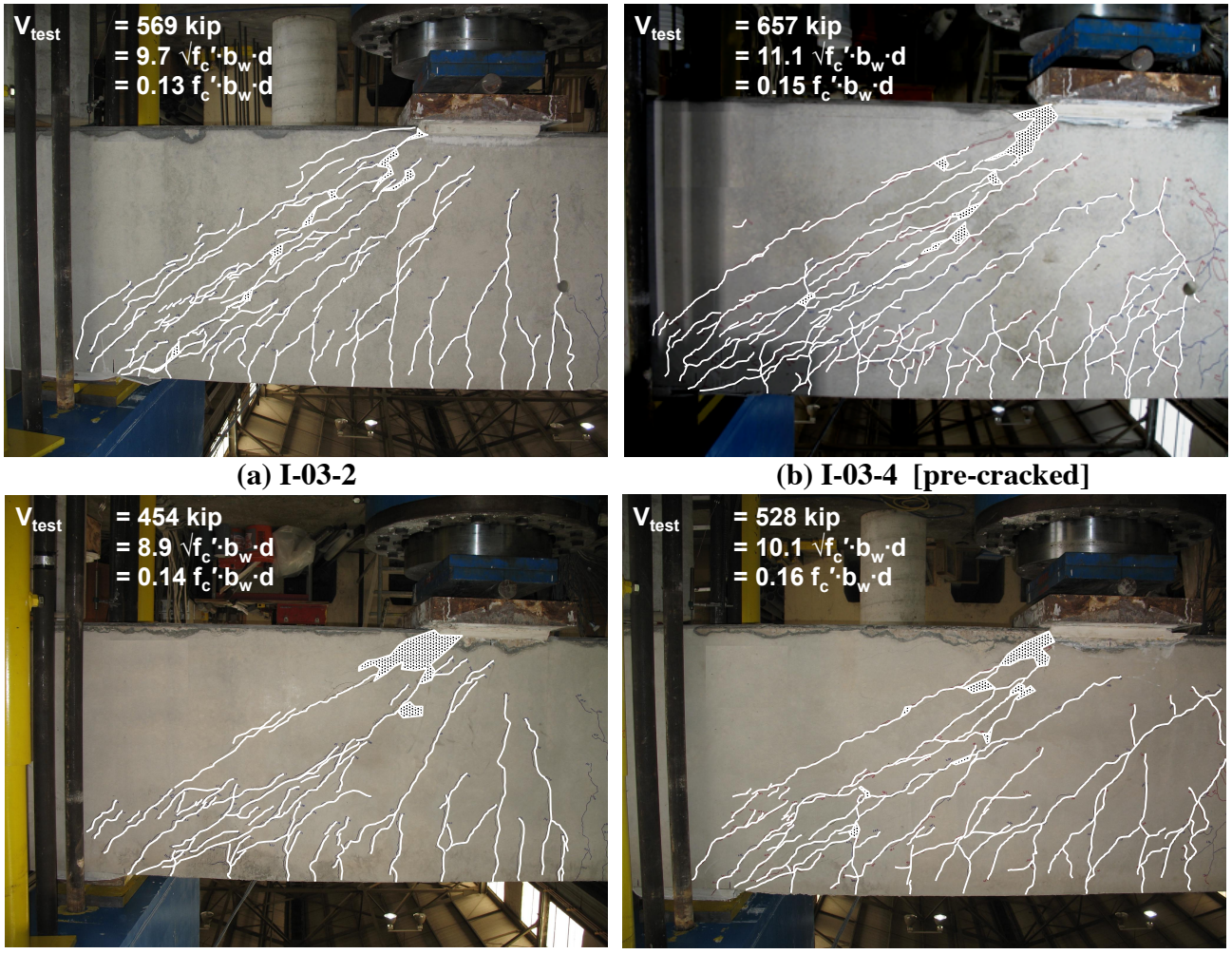

(a) I-03-2 **(b) I-03-4 [pre-cracked]**

(c) I-02-2 **(d) I-02-4 [pre-cracked]**

Figure 4-3. Series I test specimens at failure.

The normalized capacity of the Series I specimens varied between 0.13 and $0.16f_c'\cdot b_w\cdot d$ (Table 4.1). In order to quantify the expected range of scatter associated with shear testing, the results from ten similar beams are compared to one another. All of these beams have been tested as part of the current experimental program and are presented in Appendix E. Other than the transverse reinforcement ratio, all of the other pertinent variables are identical: web width, depth, a/d ratio, bearing plate sizes, and longitudinal reinforcement ratio. Complete details are presented in Table 3.4. The range of scatter in shear capacity that can be expected from similar tests is illustrated in Figure 4-4.

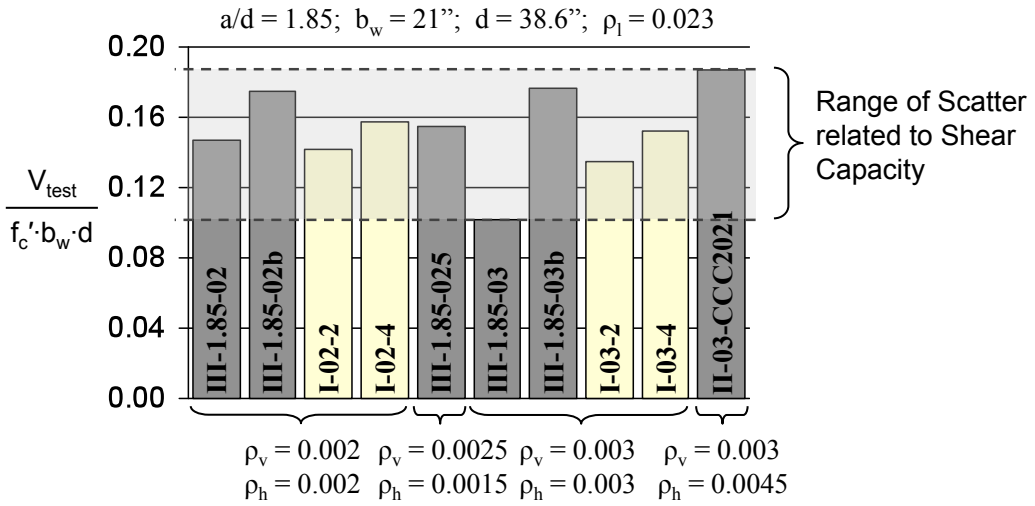

Figure 4-4. Comparison of shear capacity for similar test specimens.

Given that the range of strength values for the Series I tests are within the range of scatter associated with essentially identical shear tests (Figure 4-4), it can be concluded that distribution of stirrups across a web does not have a significant influence on the shear capacity.

A similar conclusion can be reached based on examination of the two Series M test specimens. The test with four stirrups leg, M-03-4-CCC2436, had a normalized shear capacity of $0.19\cdot f_c'\cdot b_w\cdot d$ and the maximum shear carried for the beam with two stirrup legs was $0.16\cdot f_c'\cdot b_w\cdot d$. Again, based on the range of scatter in shear capacity for 21"x44" specimens (Figure 4-4), it can be inferred that the

difference in shear capacity between the two 36”x48” specimens was trivial. As a result, stirrup distribution did not appear to have an influence on the capacity of a 36-inch wide deep beam.

Additionally, increasing the amount of transverse reinforcement from 0.2% to 0.3% in each direction did not significantly influence the strength of the test specimens. This is expected for a beam in which the predominant shear transfer mechanism can be idealized with a single-panel truss model. In other words, the capacity of a single-panel truss model is directly related to the strength of the concrete strut and nodal regions rather than the quantity of transverse reinforcement.

4.2.3 Effectiveness of Longitudinal Tension Reinforcement

Anderson and Ramirez (1989) tested the effectiveness of distributing stirrups across a beam’s web for 16”x16” specimens (Section 2.6.4). The researchers concluded that stirrups should be distributed across the web. The main justification for their recommendation was the observation that strains on interior longitudinal bars were higher for beams with distributed stirrups than for those without. Note, the research conducted by Anderson and Ramirez (1989) investigated the effect of distributed reinforcement on the behavior of beams loaded in sectional shear (a/d = 2.65). Stirrups are more effective in a sectional shear region (i.e. multiple-panel truss model) than a deep beam region (i.e. single-panel truss model). Series I beams were loaded in deep beam shear (a/d = 1.85). Thus, stirrup distribution is expected to have an even lesser effect on the behavior of these specimens.

In concurrence with Anderson and Ramirez (1989), the magnitudes of the strains at the outer-most layer of the longitudinal bars were measured. The strain data is presented in Figure 4-5. Upon examination of the strain data presented in Figure 4-5, it can be concluded that the detailing of stirrups had no influence on the distribution of longitudinal strains for the Series I test specimens.

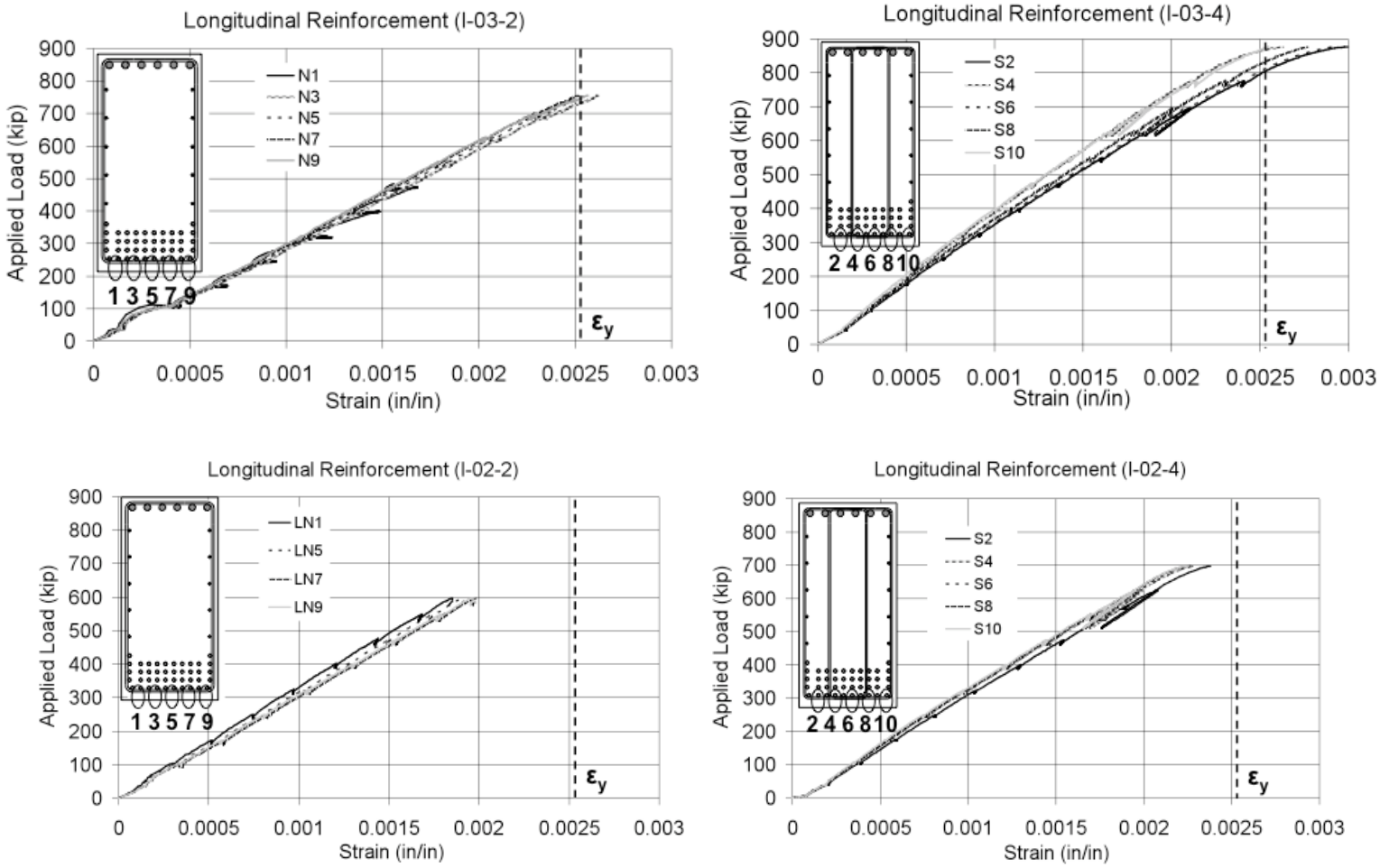

Figure 4-5. Measured longitudinal strains within the outermost layer of tension reinforcement

4.2.4 Serviceability Performance

First cracking and crack width data was collected from Series I test specimens. It was not possible to compare the first cracking load of specimens with two stirrup legs to those with four stirrup legs because both tests were conducted on opposite sides of the same beam. In other words, the second test region was pre-cracked during the first test. Therefore, the first cracking load was collected from both of the specimens with two stirrup legs (I-02-2 and I-03-2). The specimens with four stirrup legs are denoted as *pre-cracked* because they had experienced approximately 40% of their ultimate capacity prior to testing.

The first cracking load for all specimens (Table 4.1) was above the minimum value attributed to the diagonal tensile strength of concrete (i.e. 2 $\sqrt{f_c'}b_w d$). In order to quantify the expected range of scatter associated with the first cracking load, the results from six similar beams are compared to one another. The results for these beams are taken from the current experimental program and are presented in Appendix E. Other than the transverse reinforcement ratio, all of the other pertinent details are identical. The range of scatter associated with the first diagonal cracking load for similar specimens is presented in Figure 4-6.

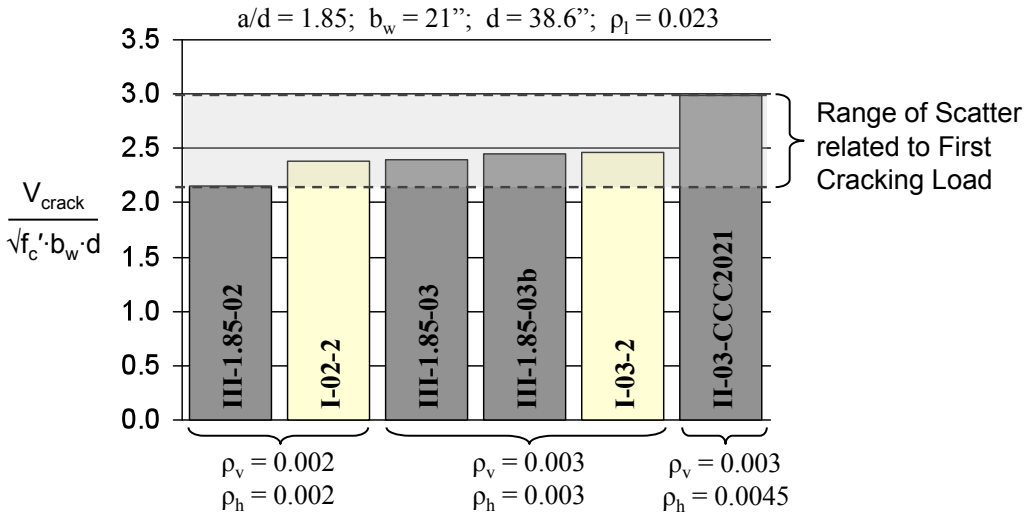

Figure 4-6. Comparison of first cracking load between similar test specimens.

Since the difference in cracking load between Specimen I-02-2 and I-03-2 is within the range of scatter associated with otherwise similar specimens, it can be concluded that the quantity of transverse reinforcement did not have a notable influence on the first cracking load. For additional discussion relating the first cracking load to the applied service level stress, refer to Birrcher (2008).

Crack patterns at approximately 90% of capacity and corresponding crack width data are presented in Figure 4-7 for specimens with 0.3% transverse reinforcement in each direction and in Figure 4-8 for specimens with 0.2% in each direction. The crack widths measured on each beam face are presented at individual load increments and normalized by the ultimate capacity of the specimen. The purpose of presenting the crack data in Figure 4-7 and Figure 4-8 is to present a relative comparison between specimens with two and four stirrup legs. For information with regard to an acceptable crack width and corresponding serviceability load level, refer to Birrcher (2008).

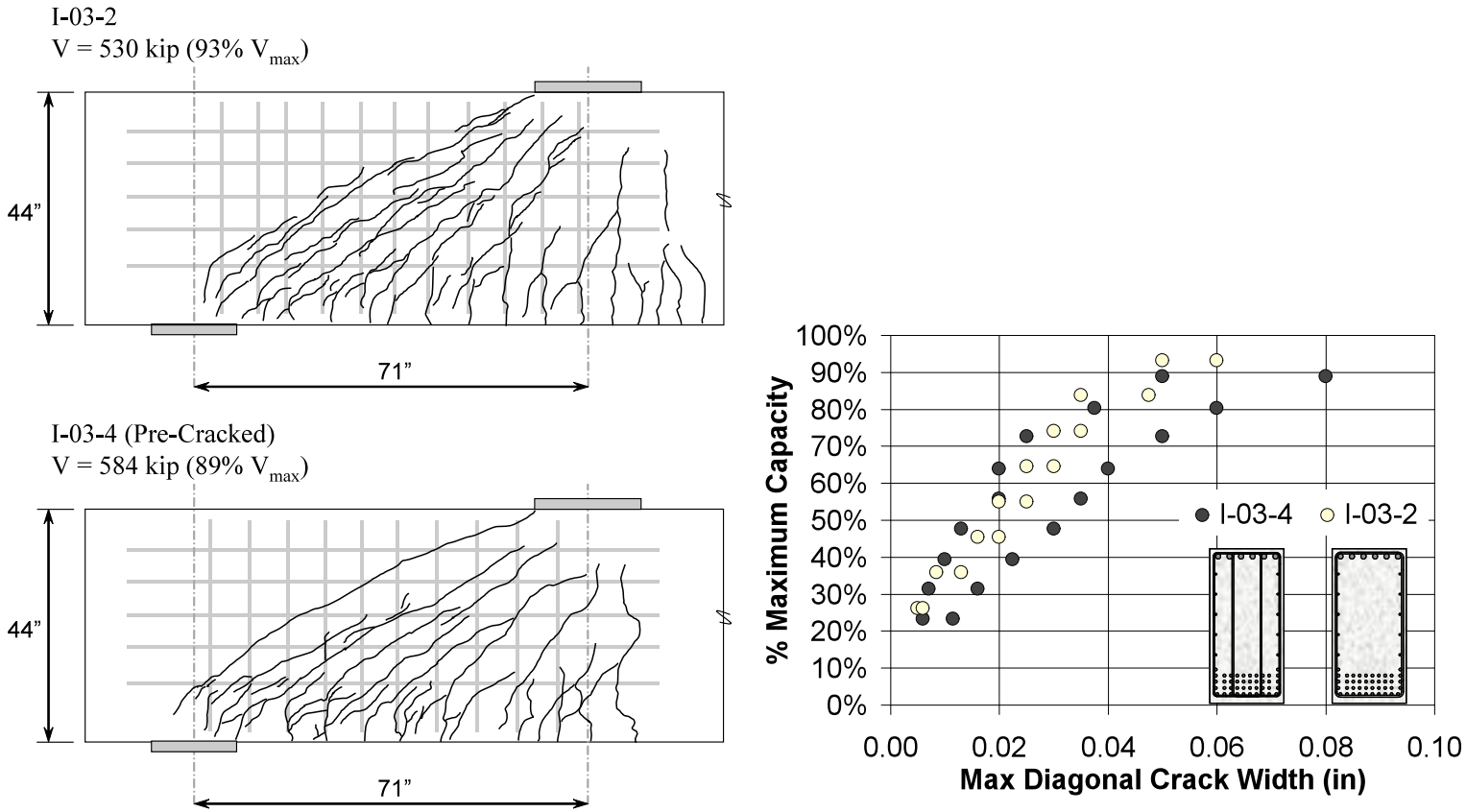

Figure 4-7. Crack pattern at approximately 90% of capacity and crack width behavior: 0.3% transverse reinforcement in each direction.

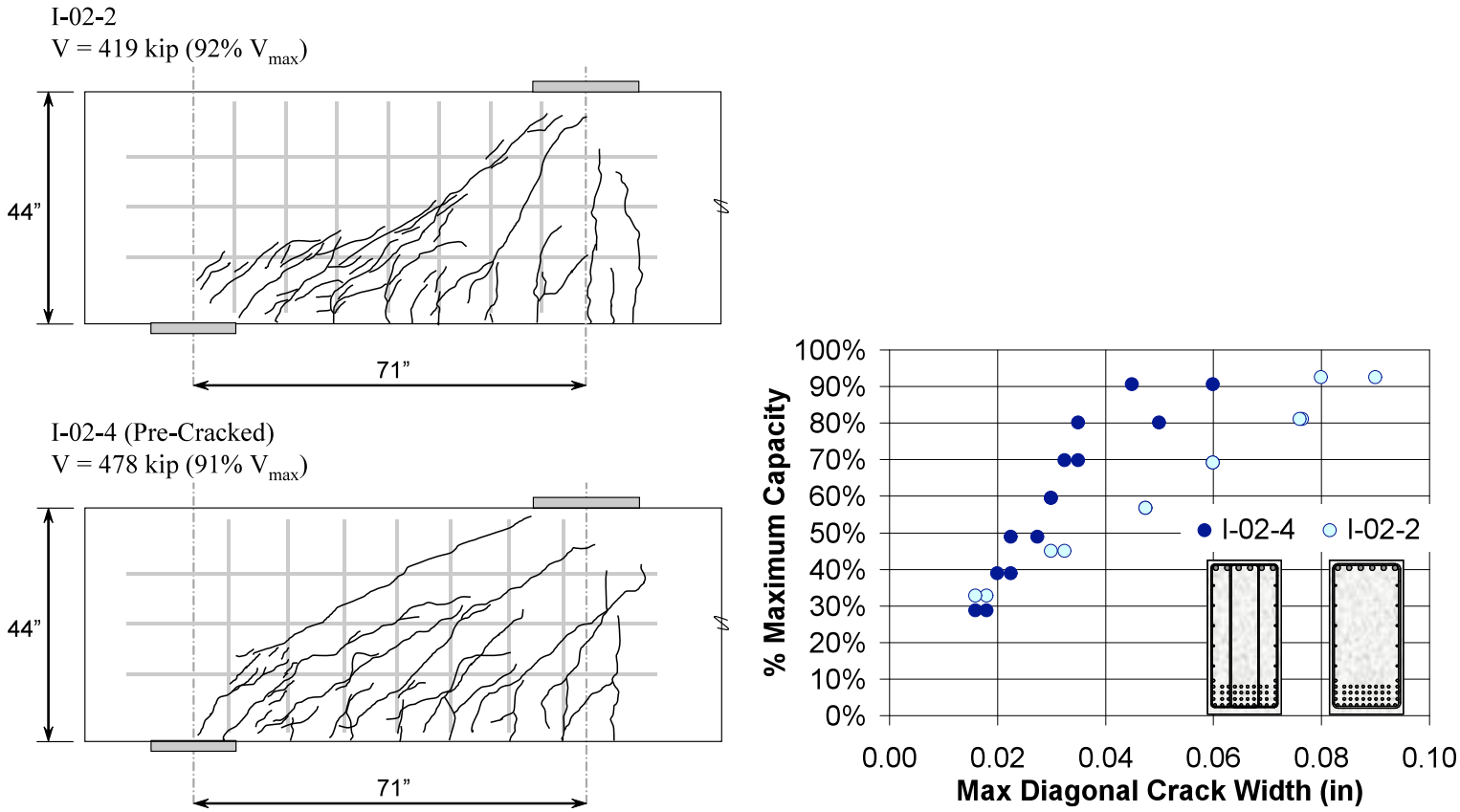

Figure 4-8. Crack pattern at approximately 90% of capacity and crack width behavior: 0.2% transverse reinforcement in each direction.

Upon a comparative examination of the crack width data and crack maps of specimens with 0.3% transverse reinforcement in the vertical and horizontal directions (Figure 4-7), the following conclusion can be reached: the serviceability performance of beams with two stirrup legs in equivalent to those with four stirrup legs.

Upon an examination of the crack width data and crack maps of specimens with 0.2% transverse reinforcement in the vertical and horizontal directions (Figure 4-8), the following conclusion can be reached: specimens detailed with four stirrup legs demonstrated narrower diagonal crack widths with more crack distribution compared to specimens detailed with two stirrup legs.

Similarly, crack width data for the Series M specimens is presented in Figure 4-9. Cracking data for the specimens presented in Figure 4-9 is not normalized by their shear capacity, as Specimen M-03-2-CCC2436 did not experience a shear failure. Additional details are presented by Huizinga (2007).

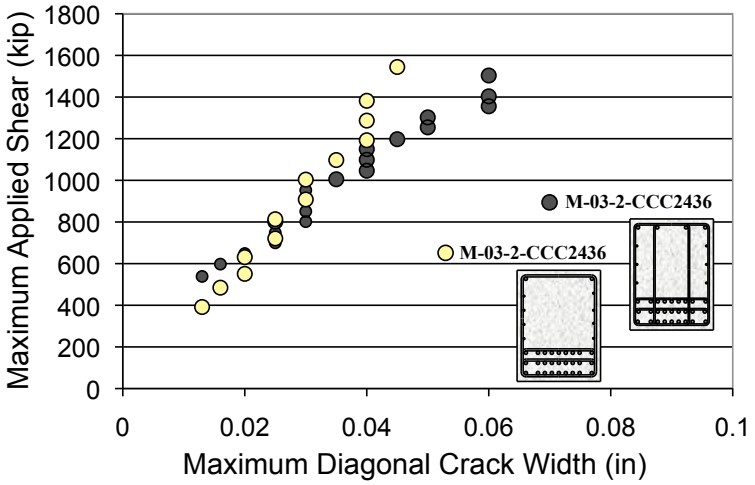

Figure 4-9. Shear carried in a test specimen versus the corresponding maximum diagonal crack width.

Upon examination of the crack width data presented in Figure 4-9 it can be concluded that the serviceability performance for these beams was not

detrimentally affected by reducing the distribution of stirrups from four to two legs across the web.

The objective of the Series I and M testing programs were to investigate the strength and serviceability effects caused by the distribution of stirrups across the web. For additional information relating the quantity of transverse reinforcement to the corresponding serviceability behavior, refer to Birrcher (2008). The author discusses the effects of transverse reinforcement and makes recommendations as to the minimum required amount.

4.2.5 Evaluation of Specimens with Current Code Expressions

A comparison between the experimental shear strength and nominal capacity calculated per the ACI 318-08 and AASHTO LRFD (2008) STM provisions is illustrated in Figure 4-10 for both a one-panel and two-panel truss model. The values were normalized by the compressive strength of concrete at the time of testing. The difference in the estimations obtained from one-panel truss models is attributed to the different efficiency factors specified in the ACI 318-08 and AASHTO LRFD (2008) provisions. The strength estimations obtained with a two-panel truss model were the same for the ACI 318-08 and AASHTO LRFD (2008) provisions as the estimate is governed by the yield capacity of the vertical tie (i.e. stirrups).

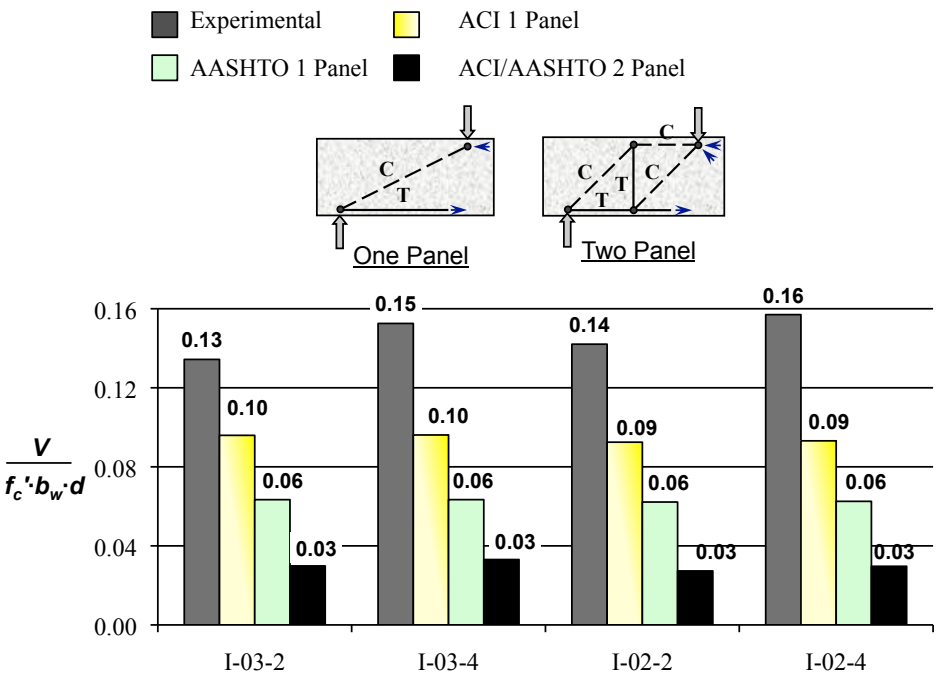

Figure 4-10. Comparison of experimental capacity with ACI 318 and AASHTO LRFD one and two-panel STM calculations.

Upon comparison of the experimental and estimated capacities presented in Figure 4-10, it can be concluded that the shear capacity estimated by the ACI 318-08 and AASHTO LRFD (2008) STM provisions was conservative for beams that contained 0.2% and 0.3% reinforcement. In addition, both provisions estimated similarly conservative capacities regardless of whether or not two or four stirrup legs were provided.

The difference between experimental and calculated shear capacities presented in Figure 4-10 illustrates the inappropriateness of using a two-panel truss model in a deep beam region. The nominal capacity calculated using a two-panel model was approximately five times less than the actual capacity. Also, the failure of the Series I specimens was preceded by the crushing of concrete near the load plate and along the strut (Figure 4-3). This type of behavior is better represented by a one-panel STM. As a result, the nominal capacity calculated using a one-panel model was more appropriate.

This point can be illustrated with the following example presented in Figure 4-12.

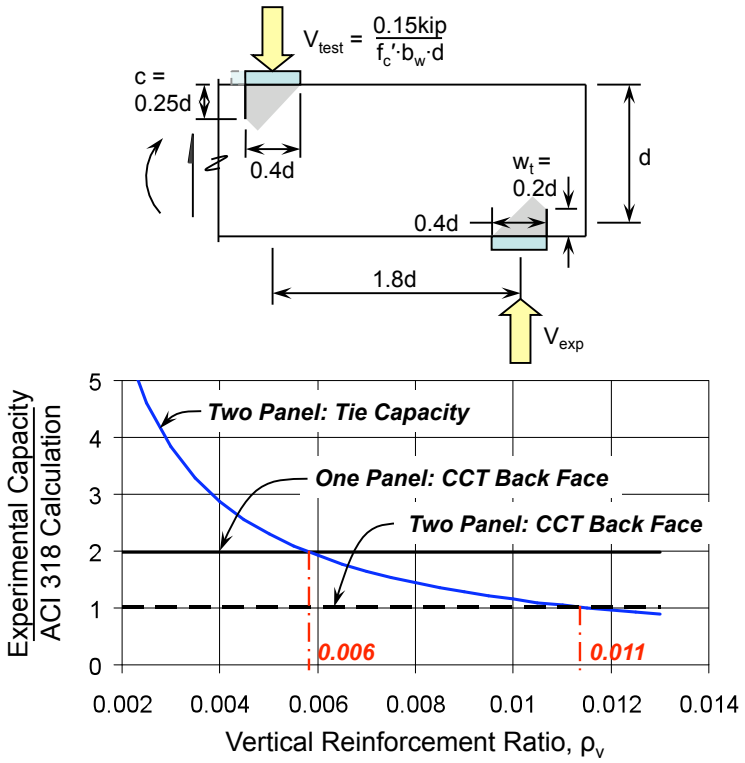

Figure 4-12. Comparison between one and two-panel STM: per ACI 318.

For the example shown, the capacity of a two-panel STM is controlled by the vertical tie if the transverse reinforcement ratio is less than 1.1%; an unrealistically high percentage. In other words, the capacity of the preceding D-region is usually controlled by the capacity of the vertical tie when modeled with a two-panel STM.

For this example, in order for the capacity calculated from a two-panel truss model to govern over that calculated from a one-panel truss model, a vertical reinforcement ratio of over 0.6% would have to be provided; a fairly large amount. In general, a one-panel truss is more appropriate than a two-panel truss when modeling a deep beam region ($a/d < 2$) with a STM.

4.3 SUMMARY

The purpose of the Series I testing program was to investigate the benefit gained from distributing stirrup legs across the width of a deep beam; from both a strength and serviceability standpoint. Four tests were conducted on beams with a 21"x44" cross-section and a shear span-to-depth ratio of 1.85. Stirrup details with two or four legs were investigated, for transverse reinforcement ratios of 0.2% and 0.3%. Based on the test results, the following conclusions are reached:

- The use of additional stirrup legs across the width of the web did not have a significant influence on the strength of a specimen.
- The use of additional stirrup legs across the width of the web did not have a significant influence on the serviceability performance of beams with at least 0.3% transverse reinforcement in both the horizontal and vertical directions.
- The use of additional stirrups across the width of the web improved the serviceability behavior of beams reinforced with 0.2% transverse reinforcement in both the horizontal and vertical directions.

The current research program is the first to investigate the influence of stirrups with multiple legs on the strength and serviceability behavior of deep beam regions (a/d < 2). From a theoretical standpoint, the quantity and detailing of stirrups does not have a significant impact on the strength of a deep beam region as the ultimate capacity is controlled by a direct strut forming between the load and support plates. Therefore, the data obtained from the testing of the Series I beams are justified from both a theoretical and experimental standpoint.

As for serviceability behavior, the quantity and detailing of transverse reinforcement has been observed to have a more pronounced influence on crack widths as the a/d ratio transitions from deep beam to sectional shear behavior (Birrcher 2008). Based on data from the Series I tests (a/d = 1.85), the detailing of stirrups did not affect crack width behavior provided a reinforcement ratio of at least 0.3% in the horizontal and vertical direction was present.

The impetus for this research task was to evaluate the AASHTO provision that limits the width of a CCT node in a deep beam. Based on the findings of the experimental program, the AASHTO LRFD (2008) provision was found to be inappropriate. The provision only is applicable when a multiple panel truss model is used. However, a single panel model is generally more appropriate when the a/d ratio is less than two. Additionally, if a two-panel STM is used to model a D-region, the capacity of the interior vertical tie force is typically likely to govern. This further illustrates the inappropriateness of the provision.

From a serviceability standpoint, a difference in behavior was not observed for both the 21-inch or 36-inch wide specimens provided the specimens contain 0.3% transverse reinforcement in the vertical and horizontal directions. As such, the width limitation at the CTT strut-to-node interface should be removed from the AASHTO LRFD Bridge Design Specifications (2008).

CHAPTER 5

Triaxially Confined Nodal Zones

5.1 OVERVIEW

The purpose of the Series II testing program was to evaluate and quantify the benefits provided by triaxial confinement in the nodal regions of a beam subjected to deep beam shear. To achieve this goal, five beams were fabricated and tested in the Ferguson Structural Engineering Laboratory. Two ends of a beam were tested resulting in a total of ten tests. Eight tests were conducted on beam specimens with a 21"x42" cross-section. Two tests were conducted on larger beams with a 36"x48" cross-section (Series M). As explained earlier, Series M beam specimens were designed as multiple purpose test specimens. Two tests conducted on Series M test specimens relate to triaxially confined nodes. Therefore, the results of these tests are included in the comparative analysis presented in this chapter.

Within the Series II testing program, most of the details of the beam specimens were kept constant. The primary experimental variables were the size of the load and support plates and the amount of transverse reinforcement. The two transverse reinforcement ratios that were investigated were 0.3% and 0.2% in the vertical and horizontal direction. For the experimental program, the *length* of a bearing plate is defined as the dimension of the plate measured along the span; the *width* of a bearing plate is defined as the dimension measured transverse to the span. All plate dimensions are reported with the length-dimension first, then the width-dimension (i.e. *length* x *width*). Details of the fabrication and testing of the Series II and Series M beams are included in Section 3.1.2. A summary of the ten tests is illustrated in Figure 5-1 and 5-2.

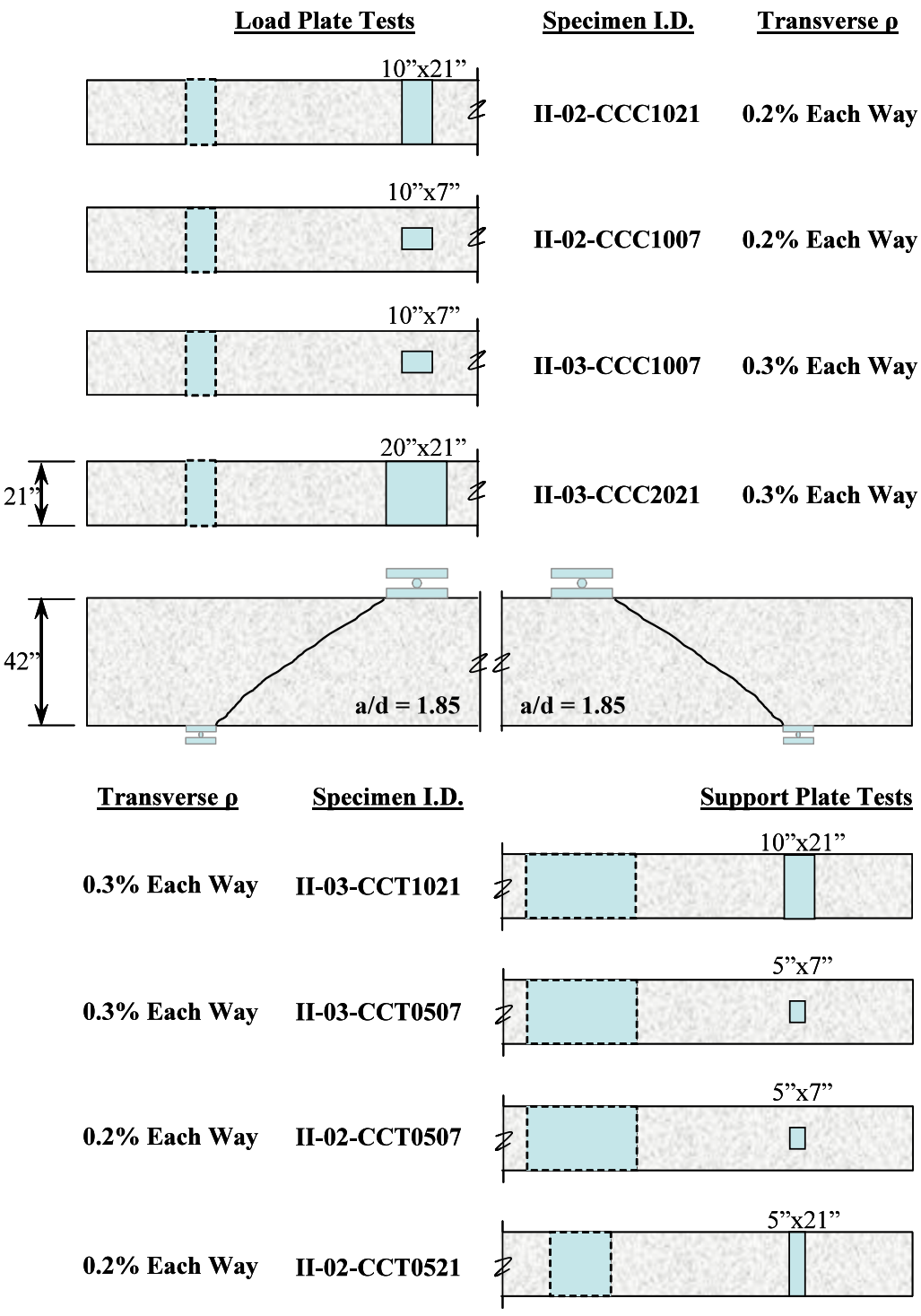

Figure 5-1. Summary of tests within Series II: 21”x42” specimens.

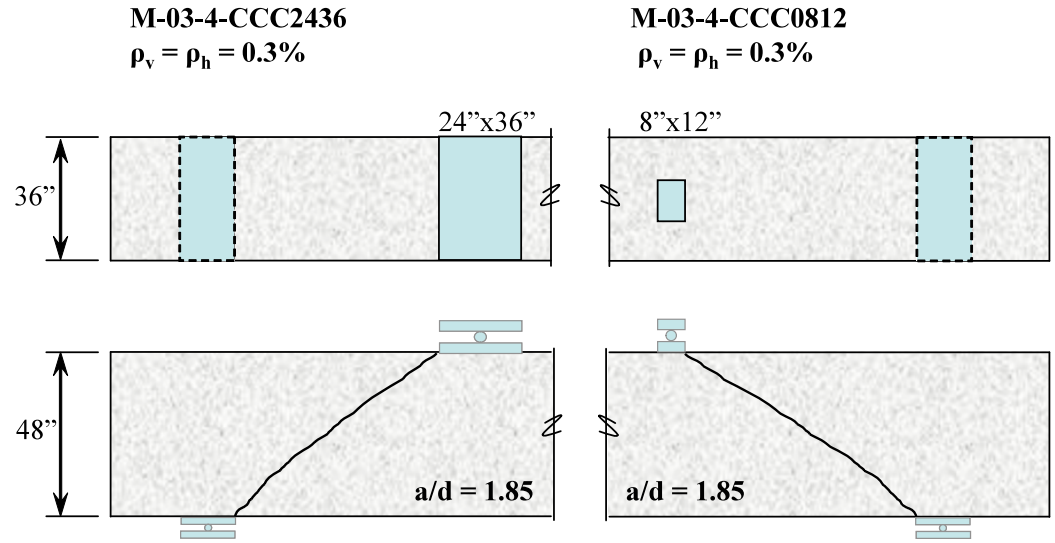

Figure 5-2. Summary of tests within Series M: 36"x48" specimens.

Note, for three of the CCT nodal tests shown in Figure 5-1, the size of the non-critical load plate (CCC node) was 36"x21". A very large load plate was purposely selected in order to ensure that the CCT nodal region would be critical. The non-critical load plate for specimen II-02-CCT0521 was smaller (20"x21"). However, it was large enough to ensure that the CCT nodal region was critical as evident from the shear capacity and serviceability performance of these test specimens (Sections 5.2.1 and 5.2.2).

Currently, STM provisions in ACI 318-08 and AASHTO LRFD (2008) do not explicitly allow the designer to increase the permissible concrete compressive strength at all nodal faces when triaxial confinement due to surrounding concrete is present. The strength of a beam calculated using STM provisions is directly related to the size of the nodal region; which is a function of the bearing plate size. As a result, designers have a great difficulty in satisfying the stress limits of a deep beam that is loaded by or supported on bearing plates much narrower than the beam. It is important to point out that the use of bearing pads narrower than the width of a deep beam is common in design practice, particularly for bent caps.

5.2 RESULTS OF SERIES II AND SERIES M TESTS

In order to address the research objective related to triaxially confined nodes, strength and serviceability data was collected for each test. A summary of the strength results and first diagonal cracking loads are presented for Series II and M beams in Table 5.1. Values are normalized by the compressive strength and square root of the compressive strength of concrete in the same manner as described in Section 4.2.1. First diagonal cracking loads are not presented for the second test conducted on each specimen.

Table 5.1. Test Results: Series II

Specimen I.D.	f_c' (psi)	V_{test} (kip)	$\frac{V_{test}}{f'_c b_w d}$	V_{crack} (kip)	$\frac{V_{crack}}{\sqrt{f'_c} b_w d}$	f_b/f_c' †
II-03-CCC2021	3290	500	0.19	139	3.0	0.50
II-03-CCC1007	3480	478	0.17	-	-	2.71
II-02-CCC1007	3140	335	0.13	-	-	2.11
II-02-CCC1021	4620	329	0.09	132	2.4	0.47
II-03-CCT1021	4410	636	0.18	-	-	0.69
II-03-CCT0507	4210	598	0.18	146	2.8	4.05
II-02-CCT0507	3120	401	0.16	94	2.1	3.68
II-02-CCT0521	4740	568	0.15	-	-	1.14
M-03-4-CCC2436	4100	1128	0.19	354	3.8	0.45
M-03-4-CCC0812	3000	930	0.22	-	-	4.55

† f_b/f_c' = maximum stress in bearing over specified concrete compressive strength

5.2.1 Shear Capacity

The shear capacity of the Series II specimens is presented with the cracking patterns at failure in Figure 5-3 and Figure 5-4. Recall, two tests were conducted on each beam specimen. The second test conducted on each specimen is marked as *pre-cracked* to indicate that some cracks were present prior to testing.

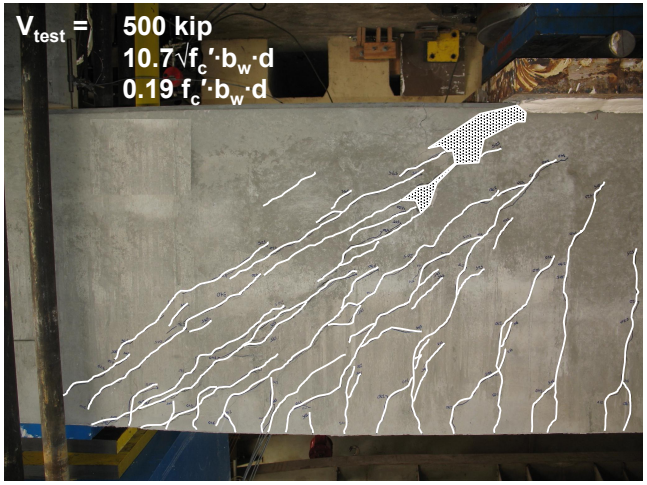

(a) II-03-CCC2021

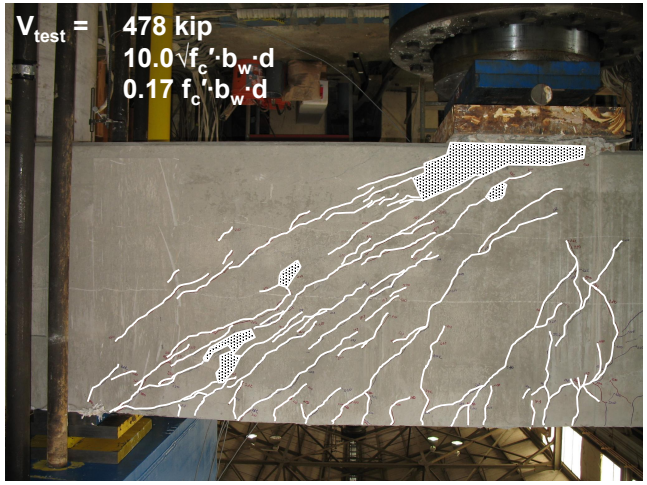

(b) II-03-CCC1007 [pre-cracked]

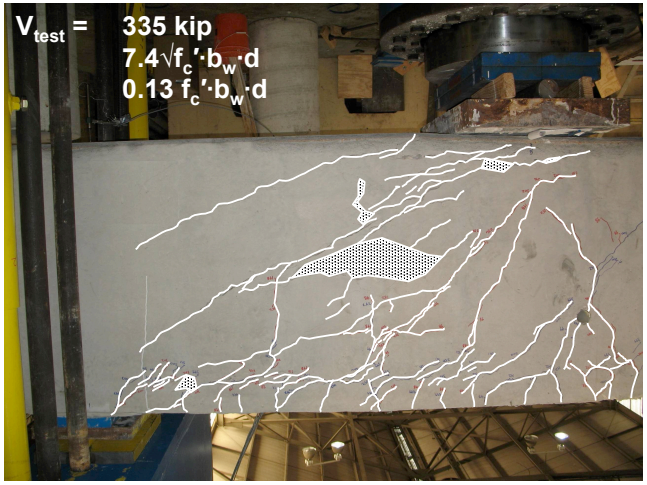

(c) II-02-CCC1007 [pre-cracked]

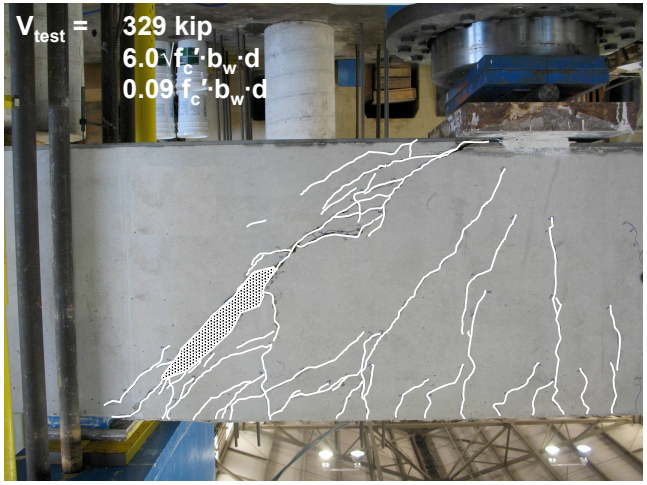

(d) II-02-CCC1021

Figure 5-3. Series II specimens with various bearing plate sizes at the CCC node at failure.

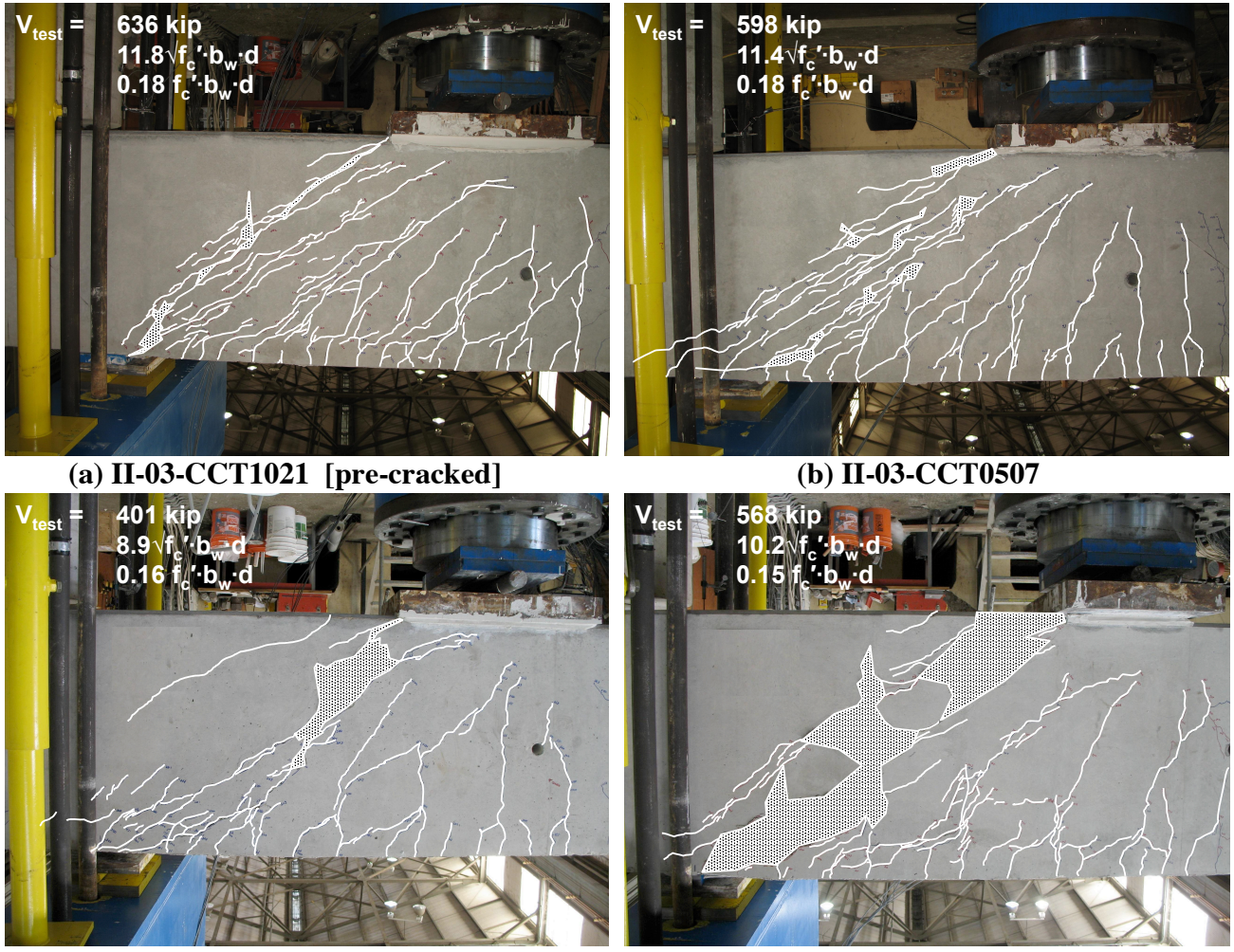

(a) II-03-CCT1021 [pre-cracked] (b) II-03-CCT0507

(c) II-02-CCT0507 (d) II-02-CCT0521 [pre-cracked]

Figure 5-4. Series II specimens with various bearing plate sizes at the CCT node at failure.

The crack patterns at failure (shown in Figure 5-3 and Figure 5-4) indicate that the formation of a direct strut was the predominant shear transfer mechanism. Parallel cracks between the load point and support delineate the approximate boundary of the strut. Crushing occurred in the compression region adjacent to the load point and along the strut. Therefore, normalizing the capacity values by the compressive strength of concrete is more appropriate than the square root of the compressive strength. Normalization is necessary to account for the unintended differences in the compressive strength of concrete of the specimens at the time of testing.

The normalized capacity of specimens with different support plate (CCT node) dimensions varied between 0.15 and $0.18 f_c' \cdot b_w \cdot d$ (Table 5.1). This difference is within the range of scatter associated with shear testing, as previously illustrated in Figure 4-4. At failure, the stress applied to the bearing plate was 0.7 to $1.1 \cdot f_c'$ for cases in which the CCT nodes were unconfined; and 0.45 to $0.5 \cdot f_c'$ for cases in which the CCC nodes were unconfined. For cases in which confinement was provided at the CCT and CCC nodes, the applied bearing stress was as high as 4.1 and $4.6 \cdot f_c'$, respectively. Therefore, it can be concluded that triaxial confinement allowed the application of bearing stresses much higher than the compressive strength of concrete.

The difference in capacity between the beams supported on 5"x21" and 10"x21" support plates (Table 5.1) was also within the range of scatter associated with shear strength data (Figure 4-4). This small difference indicated that a reduction in the length of a full-width support plate for specimens with CCT nodes that were not triaxially confined did not significantly influence the shear capacity.

The normalized capacity of specimens with different load plate (CCC node) dimensions varied between 0.09 and $0.19 f_c' \cdot b_w \cdot d$ (Table 5.1). Such a significant difference must be attributed to more than the scatter associated with shear testing. Both load plate dimensions and reinforcement details varied among

these specimens. In order to examine these tests further, the specimens are paired based on their details and presented in Table 5.2. Table 5.2 presents pairs of specimens considered nominally identical to each other in all aspects other than the load plate size. Upon further examination, it can be concluded that the shear capacity of the specimens where the CCC nodes were triaxially confined benefitted from this triaxial confinement.

Table 5.2. Effect of Triaxial Confinement for CCC Specimens.

Specimen Comparison	**Load Plate Size** ***(l x w)***	$\frac{V_{test}}{f'_c b_w d}$	f_b / f_c' †
M-03-4-CCC2436	24”x36”	0.19	0.45
M-03-4-CCC0812	8”x12”	0.22	4.55
II-03-CCC2021	20”x21”	0.19	0.50
II-03-CCC1007	10”x7”	0.17	2.71
II-02-CCC1021	10”x21”	0.09	0.47
II-02-CCC1007	10”x7”	0.13	2.11

† f_b/f_c' = maximum stress in bearing over specified concrete compressive strength

The shear capacity was significantly influenced by the length of the load plate. Upon comparison of specimens II-03-CCC2021 and II-02-CCC1021, it is observed that a reduction in the length of an unconfined load plate from 20”x21” to 10”x21” significantly reduced the shear capacity. It must be noted that both of these specimens contained different amounts of transverse reinforcement (0.3% versus 0.2%). However, it was previously illustrated in Figure 4-4 that the differences in shear capacity associated with 0.3% or 0.2% transverse reinforcement are small enough to be considered insignificant when taken in context with the scatter associated with shear testing. Therefore, it can be concluded that the length of an unconfined load plate at a CCC node has a significant influence on the shear capacity of a deep beam. This phenomenon is consistent with the principle of strut-and-tie modeling. That is, the capacity of a D-region is related to the stress condition in the nodal regions. Providing a

smaller, unconfined load plate results in much higher stresses. Thus, a lower capacity is to be expected.

5.2.2 Serviceability Data

First cracking loads and crack width data were collected from Series II test specimens. The initial diagonal cracking load was only recorded for the first test conducted on each beam specimen. The measured first cracking load (Table 5.1) was always above the minimum value attributed to the diagonal tensile strength of concrete (i.e. $2\sqrt{f_c'} \cdot b_w \cdot d$). Also, the difference in cracking load among the Series II specimens was within the magnitude of scatter associated with otherwise similar specimens (Table 4.6). Upon examination of the data summarized in Table 5.1, it can be concluded that the quantity of transverse reinforcement did not have a significant influence on the first diagonal cracking load. For additional discussion relating the first cracking load to the applied service level stress, refer to Birrcher (2008).

Crack patterns at approximately 90% of capacity and corresponding crack width data are presented in Figure 5-5 through Figure 5-8. The crack widths measured on each face are presented at individual load increments and normalized by the ultimate capacity of the test specimen. The purpose of presenting the crack data in Figure 5-5 through Figure 5-8 is to present a relative comparison between specimens with confined and unconfined bearing plates. For information with regard to an acceptable crack width and corresponding serviceability load level, refer to Birrcher (2008).

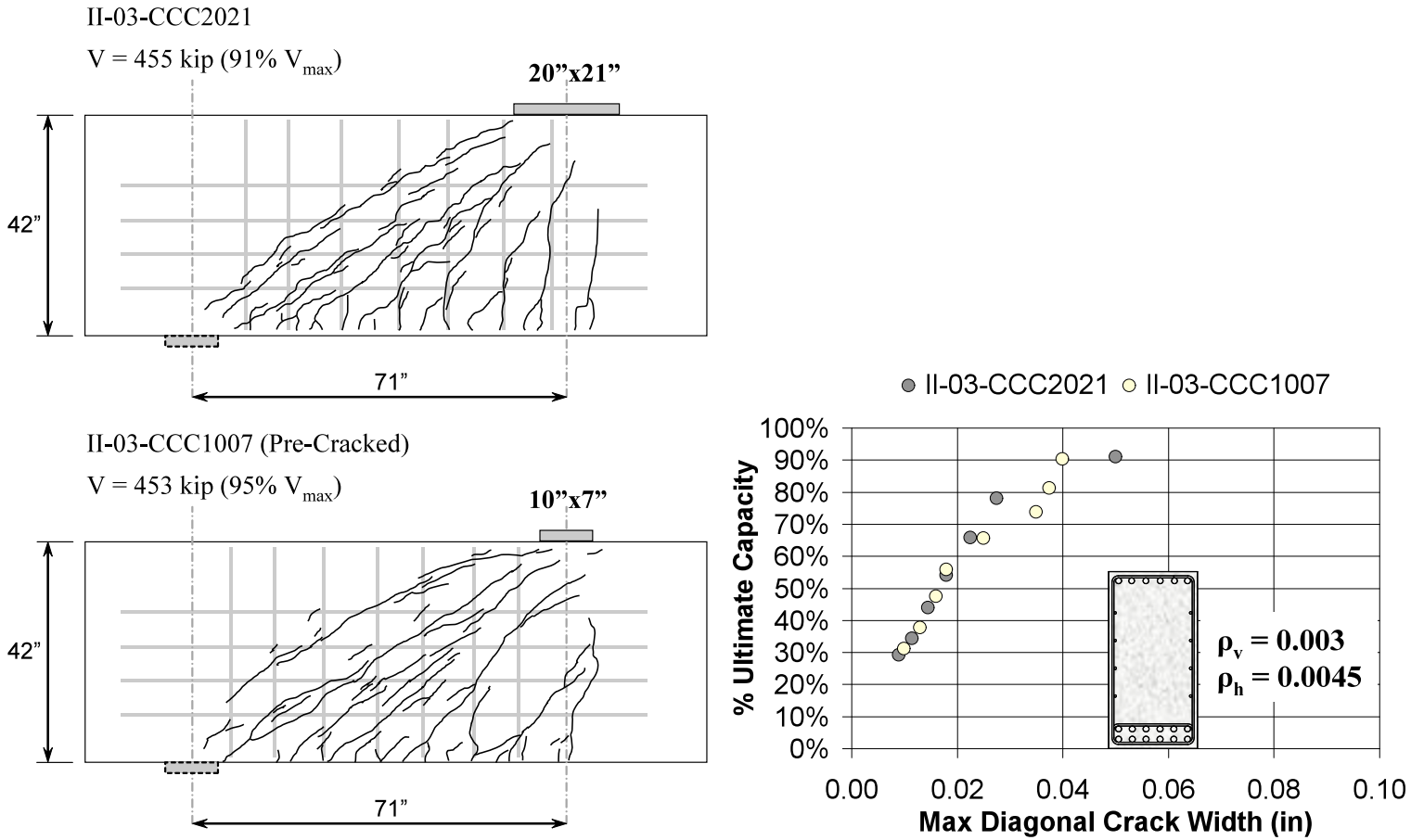

Figure 5-5. Serviceability data for triaxially confined CCC nodes: Crack patterns and widths at approximately 90% of capacity; 0.3% transverse reinforcement in each direction.

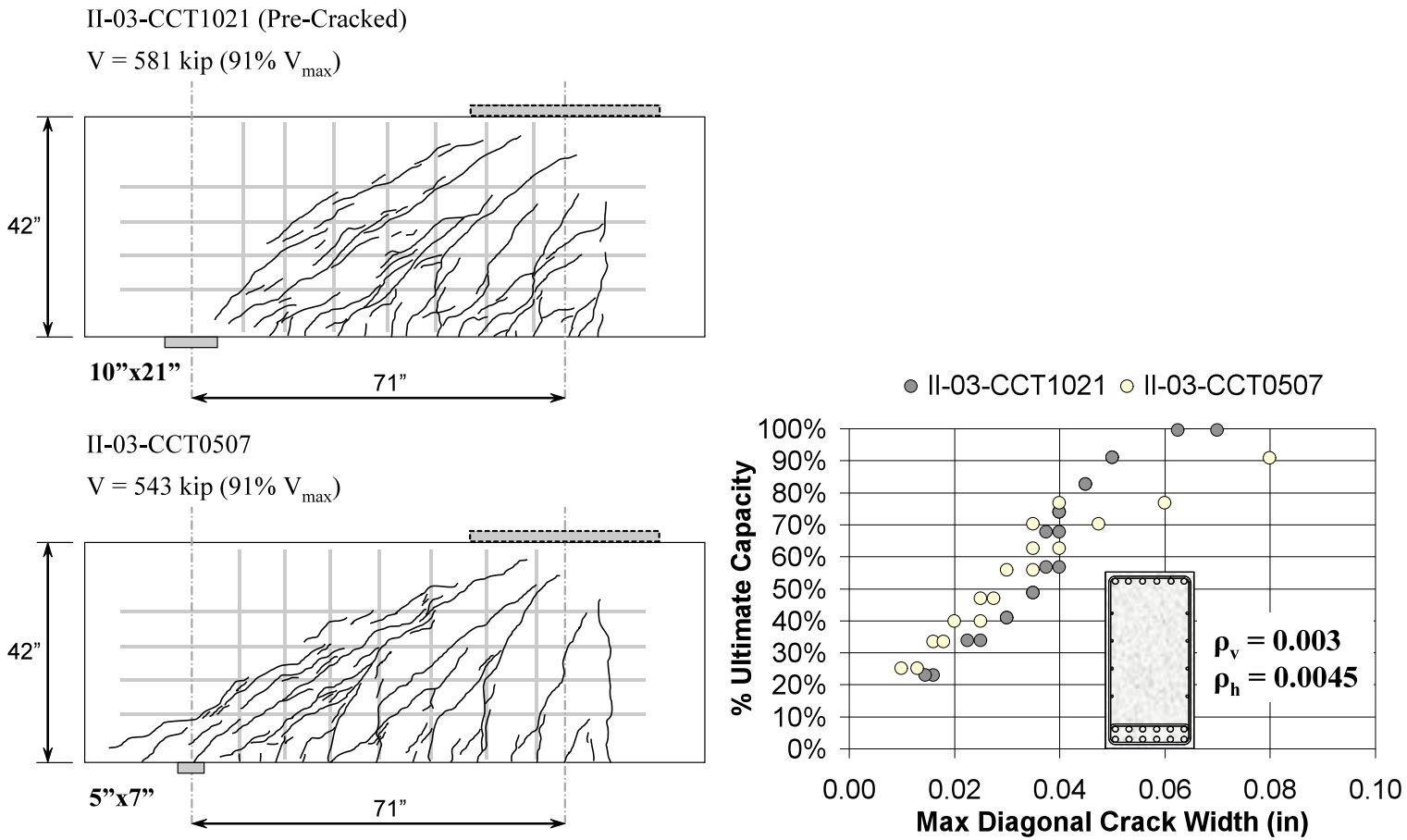

Figure 5-6. Serviceability data for triaxially confined CCT nodes: Crack patterns and widths at approximately 90% of capacity; 0.3% transverse reinforcement in each direction.

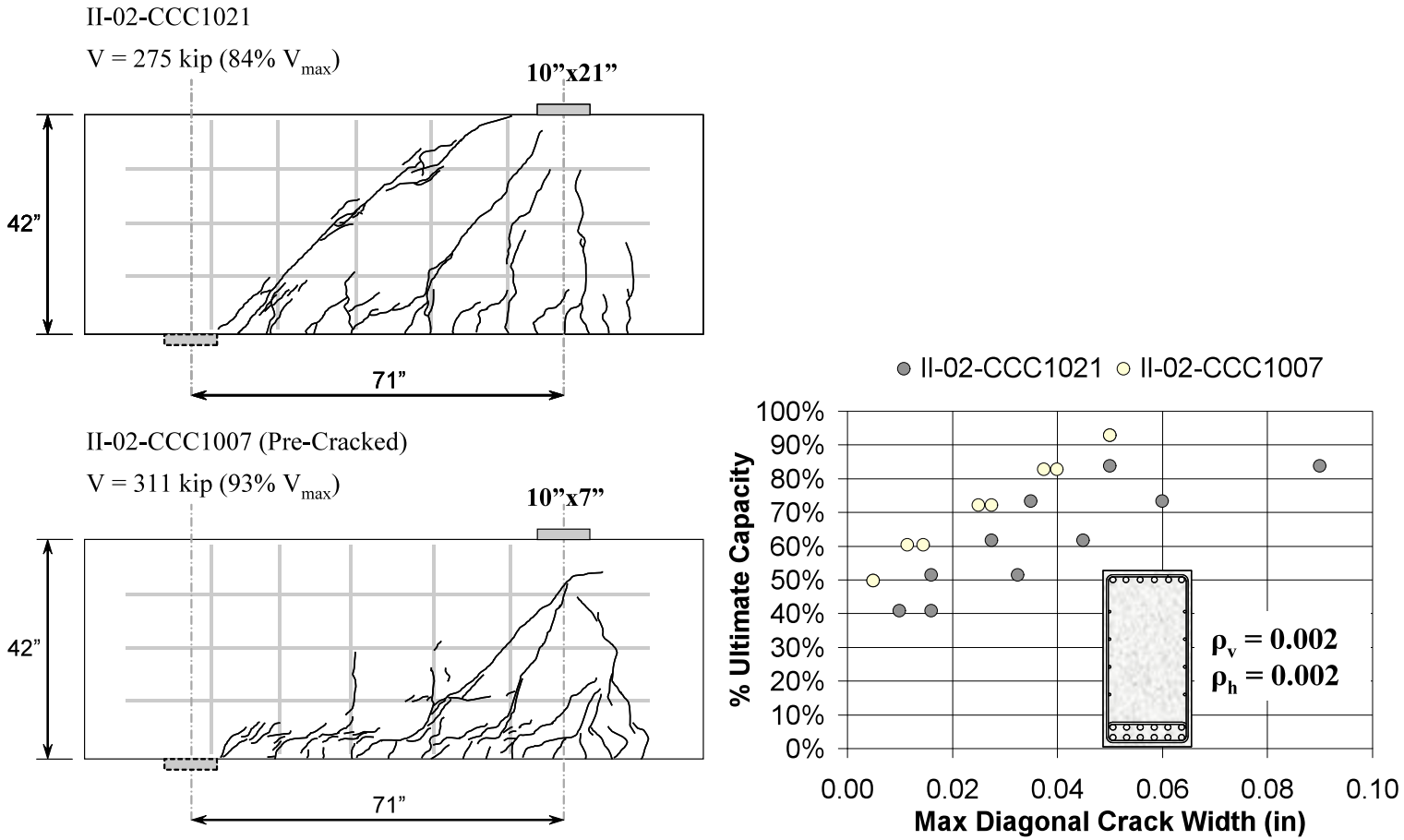

Figure 5-7. Serviceability data for triaxially confined CCC nodes: Crack patterns and widths at approximately 90% of capacity; 0.2% transverse reinforcement in each direction.

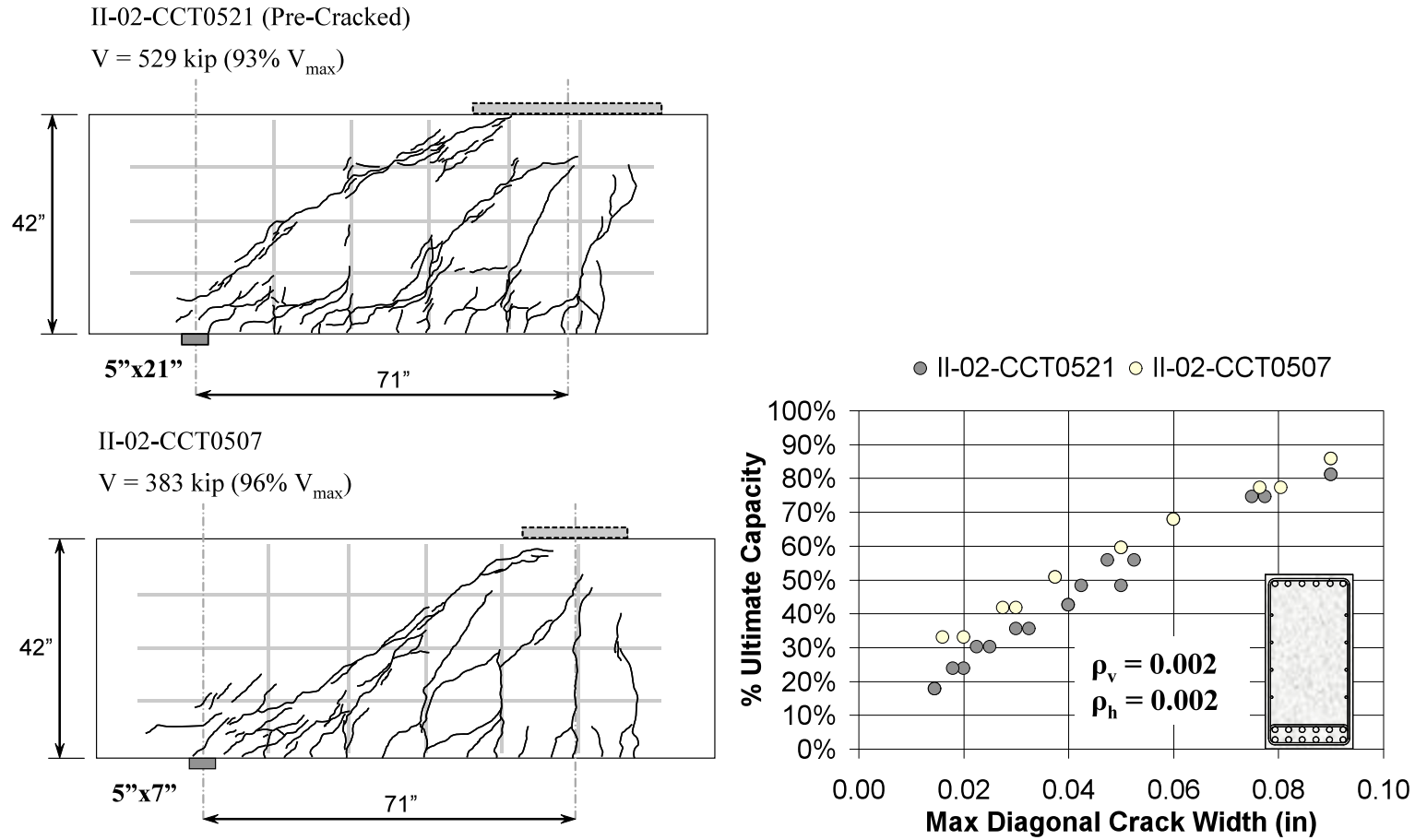

Figure 5-8. Serviceability data for triaxially confined CCT nodes: Crack patterns and widths at approximately 90% of capacity; 0.2% transverse reinforcement in each direction.

Upon examination of the crack width data presented in Figure 5-5 through Figure 5-8, the following observations can be made. For specimens reinforced with a transverse reinforcement ratio of 0.3% in each direction, the size of the load or support plate – triaxially confined or not – did not have a significant influence on the serviceability behavior. For specimens reinforced with a transverse reinforcement ratio of 0.2% in each direction, the serviceability performance as quantified by crack patterns and widths was less regular or predictable. Therefore, in terms of serviceability behavior as affected by bearing plate size, a transverse reinforcement ratio of 0.3% in each direction provided a more desirable and consistent performance.

The objective of the Series II testing program is to investigate the strength and serviceability effects caused by the triaxial confinement in the nodal regions. For additional information relating the quantity of transverse reinforcement to the corresponding serviceability behavior, refer to Birrcher (2008). The author discusses the effects of transverse reinforcement and makes recommendations as to the minimum required amount.

5.2.3 Experimental vs. Calculated Capacities

A comparison between the experimental capacities and nominal capacities calculated per the ACI 318-08 and AASHTO LRFD (2008) provisions is illustrated in Figure 5-9 for the specimens with varying load plate dimensions at the CCC node; and in Figure 5-10 for the specimens with varying support plate dimensions at the CCT node. The values were normalized by the compressive strength of concrete at the time of testing. The difference in the capacities estimated by using the ACI 318-08 and AASHTO LRFD (2008) provisions is attributed to the different efficiency factors for a single-panel truss model.

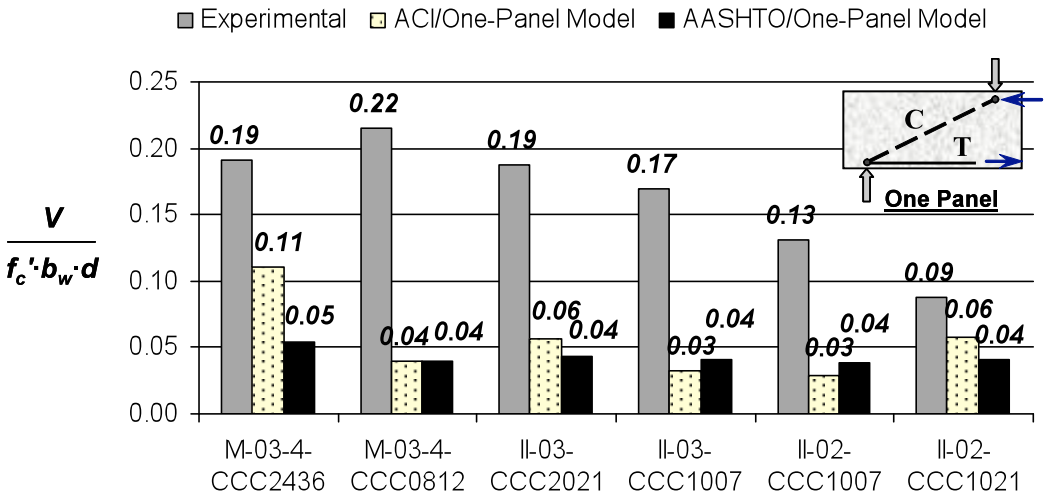

Figure 5-9. Comparison of experimental capacity with ACI 318-08 and AASHTO LRFD (2008) one-panel STM calculations: CCC specimens.

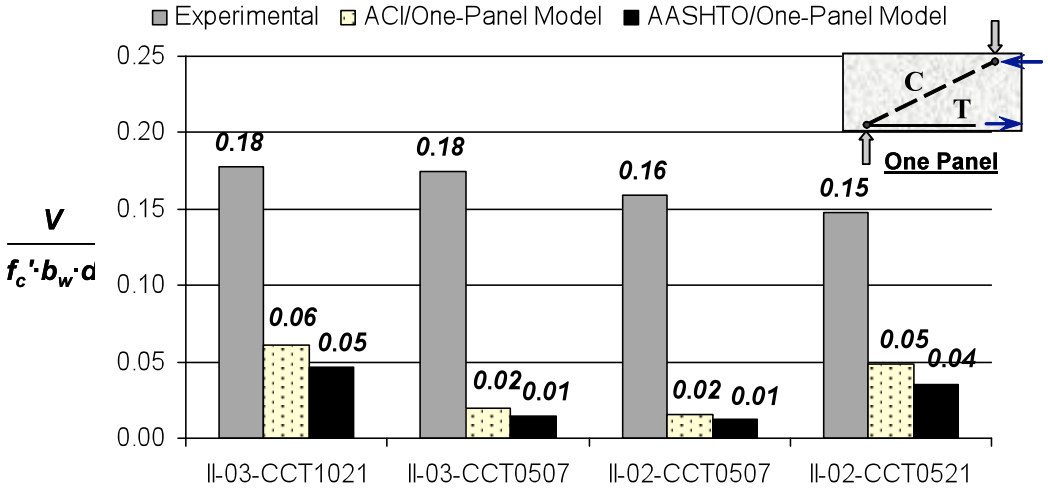

Figure 5-10. Comparison of experimental capacity with ACI 318-08 and AASHTO LRFD (2008) one-panel STM calculations: CCT specimens.

Upon examination of the experimental and calculated capacities presented in Figure 5-9 and 5-10, the following observations can be made.

The AASHTO LRFD (2008) STM provisions are generally more conservative than ACI 318-08. This is likely a result of the fact that the AASHTO

LRFD (2008) efficiency factor at the CCT strut-to-node interface reduces as the a/d ratio increases.

The calculated capacity of Specimen II-03-CCC1007 and II-02-CCC1007 was controlled by the efficiency of the strut-to-node interface at the CCC node. The efficiency factor at this boundary is 0.85 according to AASHTO LRFD (2008) and 0.64 according to ACI 318-08. Thus, for this case, ACI 318-08 is more conservative than AASHTO LRFD (2008)

The nominal capacity calculated per the ACI 318-08 and AASHTO LRFD (2008) provisions are overly conservative. The conservatism increases substantially when small bearing plates that triaxially confine the CCC or CCT nodes are provided. This is due to the fact that the capacity calculated by using a STM is directly related to the size of the nodal regions (i.e. size of the bearing plates). Based on these observations, it is proposed that the allowable stresses in triaxially confined nodal regions be increased according to Equation 5-1.

$$m = \sqrt{A_2 / A_1} \leq 2 \qquad \text{Equation 5-1}$$

$m =$ triaxial confinement modification factor

The definition of A_2 and A_1 is illustrated in Figure 2-28.

ACI 318-08 §10.14 and AASHTO LRFD (2008) Article 5.7.5 allow for an increase in the bearing capacity of concrete when triaxial confinement is present (Section 2.6.5). However, there is not a provision in place within the STM provisions allowing for a similar increase in the capacity of all six nodal faces in a STM. Thus, it is proposed that the allowable stress at each face of a triaxially confined nodal region be increased by the factor specified in ACI 318-08 and AASHTO LRFD (2008) allowing an increase in the bearing capacity of concrete (Equation 5-1). The implications of increasing the capacity according to Equation 5-1 are presented in Figure 5-11 for ACI 318-08 and Figure 5-12 for AASHTO LRFD (2008).

The ratio of experimental to calculated capacities are presented for all beams within Series II and M whose bearing plates were narrower than the width of the beam (note, a value greater than one represents a beam whose nominal design strength was conservatively estimated).

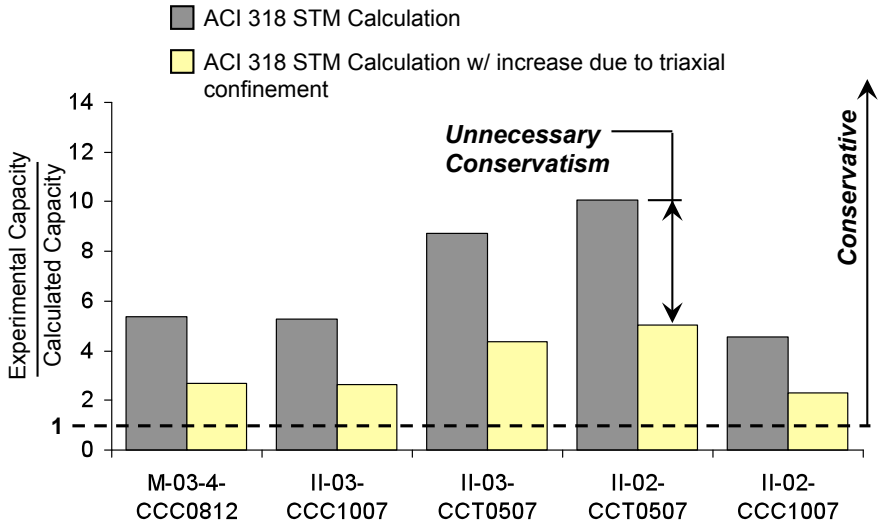

Figure 5-11. Conservatism of ACI 318 STM calculation with and without an increase in capacity due to triaxial confinement.

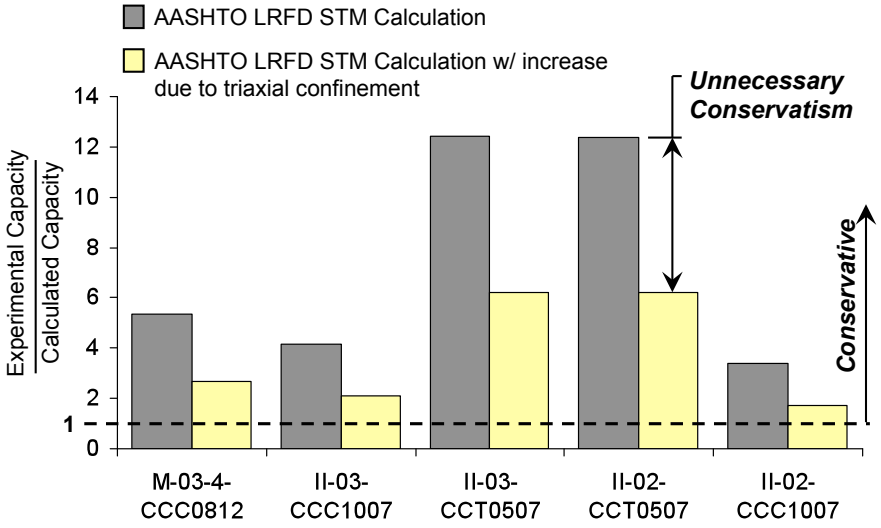

Figure 5-12. Conservatism of AASHTO LRFD STM calculation with and without an increase in capacity due to triaxial confinement.

Based on the data and results of calculations presented in Figure 5-11 and 5-12, it can be concluded that the proposal of increasing the permissible capacity of triaxially confined nodal regions results in more accurate and adequately conservative estimations. A similar comparison is conducted for all the beams in the filtered database that have a bearing plate narrower than their width (i.e. specimens with triaxially confined nodes). The results from these specimens are illustrated in Figure 5-13 for ACI 318-08 and Figure 5-14 for AASHTO LRFD (2008). Once again, it can be concluded that calculations that allow for an increase in nodal capacity due to triaxial confinement are more accurate and adequately conservative.

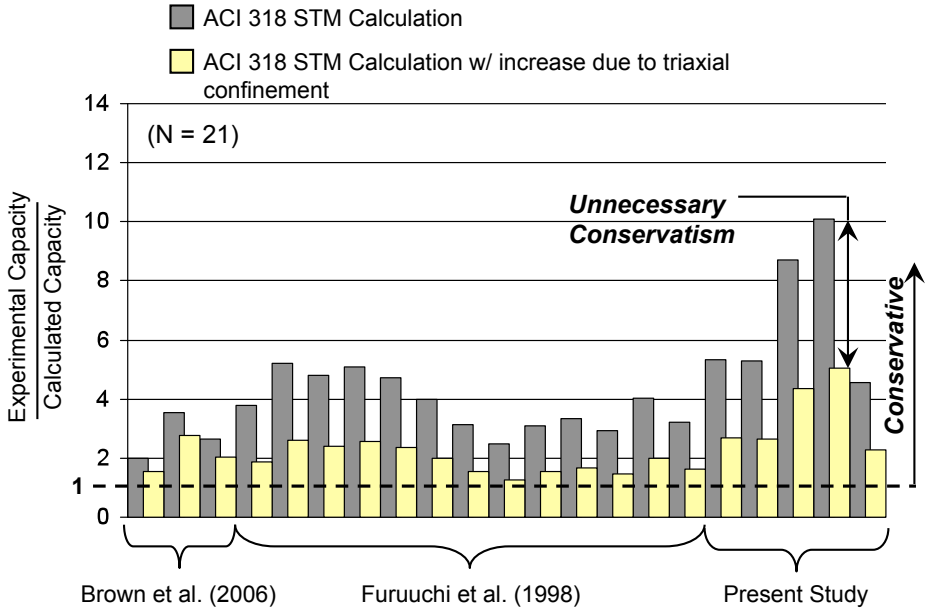

Figure 5-13. ACI 318-08 STM calculations for all beams in database that contain triaxially confined nodal regions (N = 21).

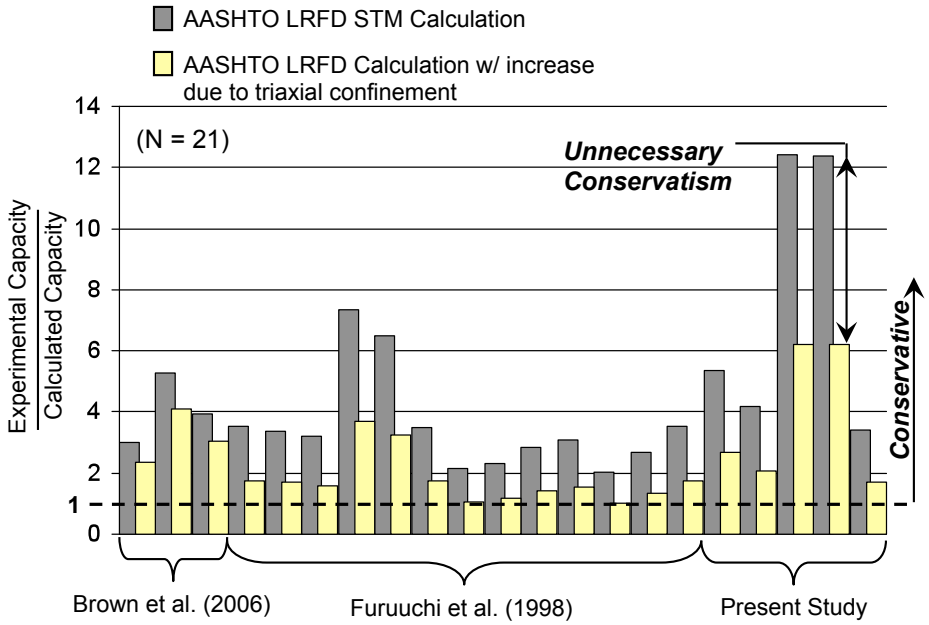

Figure 5-14. AASHTO LRFD (2008) STM calculations for all beams in database that contain triaxially confined nodal regions.

5.3 SUMMARY

The purpose of the Series II testing program was to investigate the effects of triaxial confinement in CCC and CCT nodal regions. Two tests on a 36"x48" beam specimen and eight on 21"x42" specimens were conducted at a shear span-to-depth ratio of 1.85. Two transverse reinforcement ratios were investigated: 0.2% and 0.3% in the vertical and horizontal directions.

Based on the results of the testing program, the following conclusions are reached:

- A CCC or CCT node, triaxially confined by surrounding concrete, can achieve bearing stresses much higher than the compressive strength of concrete.
- Reducing the length of a full-width load plate at the CCC node significantly reduced the shear capacity. Reducing the length of a full-width support plate at the CCT node did not have a significant influence on the shear capacity.

- The serviceability performance of a deep beam (a/d = 1.85) was not influenced by the size of the bearing plate at the CCC or CCT node, nor was it influenced by presence or absence of triaxial confinement of the bearing plate – provided that the beam contained a ratio of 0.3% transverse reinforcement in each direction.
- For specimens that contained a ratio of 0.2% transverse reinforcement in each direction, the serviceability behavior was more sensitive to the bearing plate configuration and reinforcement details.
- Increasing the ACI 318-08 or AASHTO LRFD (2008) efficiency factors prescribed at all nodal faces by the bearing capacity factor [i.e. triaxial confinement modification factor, *m,* (Equation 5-1)], results in more accurate STM calculations with less unnecessary conservatism (Figure 5-11 through Figure 5-14).

The research program summarized in this chapter was the first to investigate the influence of triaxial confinement on the shear capacity of reinforced concrete deep beams. Based on the findings of this testing series, an improved strut-and-tie methodology is proposed. Chapter 6 presents a new STM design methodology that takes advantage of the triaxial confinement modification factor.

CHAPTER 6

STM Design Method

6.1 OVERVIEW

In a strut-and-tie model, the complex state of stress in a D-region is idealized as a series of compression and tension members within a truss. When establishing an STM design procedure, consideration is given to: simplicity; coordination with experimental data; and coordination between the various design provisions.

In developing an STM procedure, it is first necessary to explicitly define the model. This step cannot be over-emphasized as the performance of a strut-and-tie model and corresponding efficiency factors are intrinsically linked to the geometry of the nodal regions. In addition, an evaluation of a STM procedure must be made in a comprehensive manner. In other words, the entire procedure must be considered as a whole. Often times, researchers in the past have made recommendations for a single aspect of strut-and-tie modeling. However, the efficiencies of each component are linked to one another.

Based on the preceding requirements, the approach taken in this study in developing a STM method is to comprehensively evaluate the STM procedures specified according to ACI 318, AASHTO LRFD, *fib* (1999), and TxDOT Project 4371. An established and consistent truss model is used in order to evaluate each provision in an unbiased manner. The selection process used to determine this standard truss model is outlined as follows.

6.2 SELECTION OF STRUT-AND-TIE MODEL

One of the benefits of strut-and-tie modeling is its versatility. The method can be used for any structural configuration and results in a conservative design. However, in part, because of the flexibility of strut-and-tie modeling, current provisions lack explicit guidance and consistency. As a result, design engineers often express apprehension towards these current STM procedures. Therefore, it

is a goal of the research project to clearly define a STM procedure and alleviate some of the confusion attributed to current methods.

Many types of discontinuities can be classified as D-regions. Common examples of D-regions include: deep beams (e.g. transfer girders, bridge bents), shear walls, corbels, post-tensioned anchorage zones, and pile supported footings (pile caps). Examples of a few of these D-regions are illustrated in Figure 6-1.

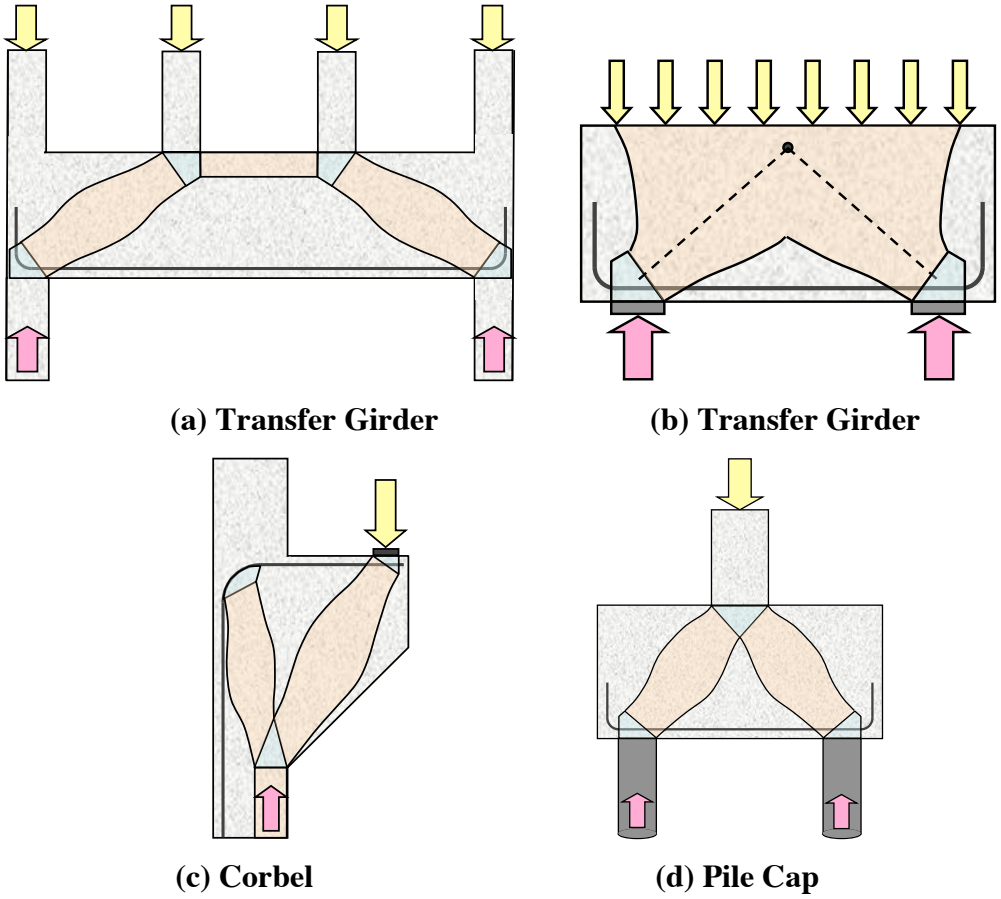

(a) Transfer Girder **(b) Transfer Girder**

(c) Corbel **(d) Pile Cap**

Figure 6-1. Examples of D-regions.

Truss models used to represent different types of D-regions may slightly vary from one another depending on the type of structure. Consequently, a STM procedure may yield different results based on the type of structure that is analyzed. A STM procedure that is valid for different types of D-regions must be based on well-established theoretical principles. Based on this philosophy, the

STM procedure proposed in this chapter is based on the fundamental principles established through past research and contained in the ACI 318-08, AASHTO LRFD, and *fib* (1999) design provisions.

With regard to the development of the proposed STM procedure, the 178 deep beam shear tests contained in the evaluation database are used for calibrating design efficiency factors. The advantage of using a deep beam shear test to calibrate efficiency factors is that these structures contain the fundamental components of a strut-and-tie model. These components are: (i) a direct strut, (ii) a tie, (iii) a CCC node, (iv) and a CCT node. Based on the results from 178 specimens, the three STM design provisions are evaluated an efficiency factors are calibrated at the CCC and CCT nodal regions. Subsequently, the current design provisions are significantly improved with regard to the modeling of deep beam shear behavior. Since the fundamental principles of strut-and-tie modeling are maintained, it is strongly believed that the findings of the proposed procedure are valid for other types of D-regions. The efficiency factors specified herein are calibrated similar to the method employed by ACI 318-08, AASHTO LRFD (2008), and *fib* (1999). That is, they have been determined based on theoretical principles, data from tests of D-regions, and regularity with other parts of the code. However, it is believed that the approach taken for the development of the proposed STM methodology is more comprehensive and transparent than what currently exists.

Nodal geometries of the D-regions shown in Figure 6-1 can be determined based on the techniques outlined in Section 2.3. By using these unambiguous rules for proportioning a strut-and-tie model, it is possible to comprehensively examine the resulting efficiency factors and draw conclusions based on the trends and differences. A single-panel truss with non-hydrostatic nodal zones was selected to represent all of the beams in the evaluation database for the purposes of examining current design provisions and calibrating new efficiency factors. Figure 6-2 illustrates the details of such a model.

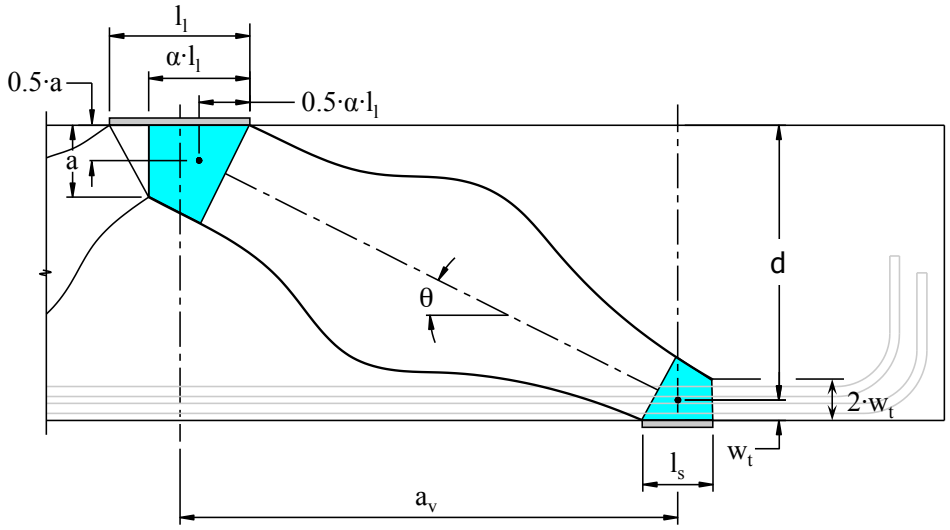

Figure 6-2. Non-hydrostatic single-panel strut-and-tie model.

The dimensioning techniques necessary to proportion this model are established in the ACI 318-08, AASHTO LRFD (2008) and *fib* (1999) provisions and have been outlined in Section 2.3. For the reader's convenience, these techniques are summarized in Figure 6-3.

(a)

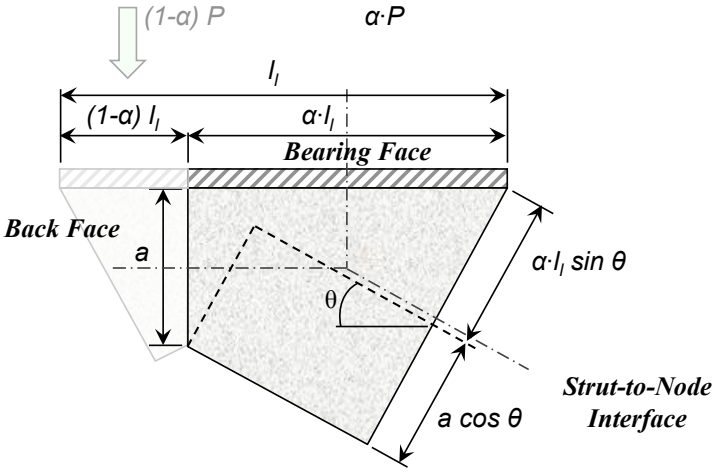

(b)

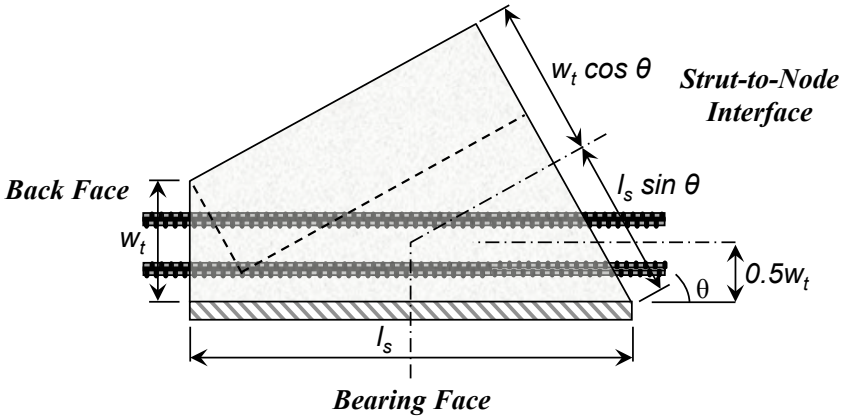

Figure 6-3. Definition of the geometry of a (a) CCC Node (b) CCT Node

Where,

a = depth of equivalent rectangular stress block (Equation 2-1)

d = distance from extreme compression fiber to centroid of longitudinal tension reinforcement

l_l = length of the bearing plate at the CCC node

l_s = length of the bearing plate at the CCT node

w_t = twice the distance from extreme tension fiber to centroid of longitudinal tension reinforcement

α = proportion of applied load that flows to near support

θ = angle of strut measured from the horizontal axis

When selecting a standard model, the two decisions affecting nodal efficiencies include: (i) whether the nodal regions are to be defined with hydrostatic or non-hydrostatic nodes; (ii) whether a one-panel or two-panel truss is to be used. A single-panel non-hydrostatic model was selected because it is simple, straightforward, and the most practical. Justification for using a single-panel non-hydrostatic model along with the corresponding implications is presented in Sections 6.2.1 and 6.2.2.

6.2.1 Single-Panel Truss Model

When modeling a D-region, it is common knowledge that a direct strut forms between the load and support for *low* a/d ratios: (i) according to Kani et al. (1979), beams with a shear span-to-depth ratio less than about 2.5 carry the load by a direct strut; (ii) research conducted as part of the current research program has shown that a direct strut is the primary shear transfer mechanism when the a/d ratio is equal to 1.85 (Birrcher 2008). In addition, ACI 318-08 allows a designer to use a single-panel strut when the a/d ratio is less than or equal to 2.1 [note, this is accomplished indirectly as the strut angle is limited to 25-degrees (i.e. $a/d = 1/\tan 25^\circ = 2.1$)]. As a result, it can be concluded that using a single-panel truss to evaluate STM provisions is well founded for specimens with an a/d ratio less than or equal to two based on experimental observations, past research, and current design provisions.

As the a/d ratio exceeds two, a beam can no longer transfer the shear forces by maintaining a direct strut. Thus, a two-panel truss mechanism governs. The specimens in the evaluation database have an a/d ratio as large as 2.5, yet they are being evaluated with a single-panel truss model. Admittedly, a single-panel truss is not a representative shear mechanism when the a/d ratio is between 2.0 and 2.5. However, it is a goal of this study to provide design engineers with a

STM procedure that can be confidently used in the transition region between sectional and deep beam shear (2.0 < a/d < 2.5). Therefore, STM provisions are evaluated using a single-panel truss model for a/d ratios up to 2.5. In this way, the trends observed in the experimental data for deep beam shear can be integrated with sectional design procedures.

6.2.2 Non-Hydrostatic Nodal Regions

When the a/d ratio of a beam is in the range of one to two, and if a single-panel truss model is used, the strut width associated with non-hydrostatic nodes is more realistic than that obtained when using hydrostatic nodes. As an example, consider the hydrostatic and non-hydrostatic truss models illustrated in Figure 6-4.

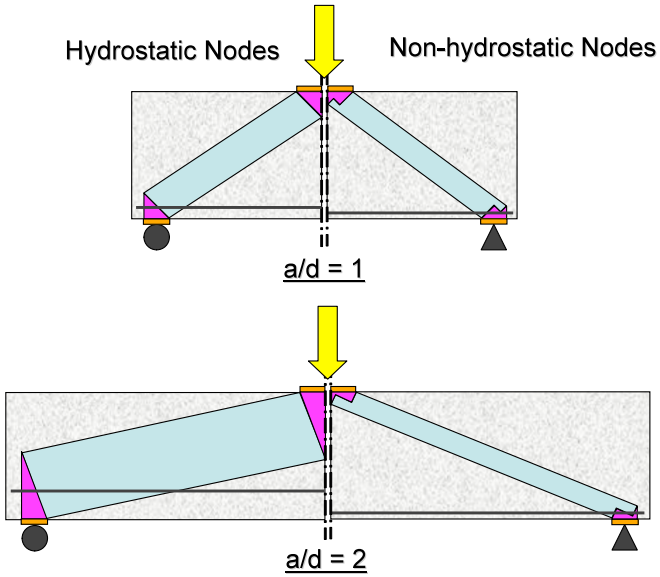

Figure 6-4. Difference between hydrostatic and non-hydrostatic nodes as a/d ratio increases.

The width of a strut abutting a hydrostatic node increases substantially as the a/d ratio increases. Whereas, the width of a strut abutting a non-hydrostatic node decreases slightly as the a/d ratio increases. If hydrostatic nodes are used, coordinating the centroid of the tie reinforcement with the centroid of a

hydrostatic CCT node is illogical and unrealistic. Similarly, it is difficult to coordinate the aforementioned unrealistic placement of flexural reinforcement with the depth of a beam's flexural compression zone, i.e. the back face of a CCC node.

It is well established that the shear strength of a beam decreases as the a/d ratio increases (MacGregor and Wight, 2005; Kani et al., 1979; ACI-ASCE 1973). The reduction in shear strength associated with an increasing a/d ratio is accounted for when non-hydrostatic nodes are used (Figure 6-4). In contrast, as discussed in Section 2.2.3, when hydrostatic nodes are used, the corresponding efficiency factors must decrease in a manner that is at least inversely proportional to the a/d ratio to counteract the increasing size of the strut. This is why STM methods that have been derived using hydrostatic nodes – such as AASHTO LRFD (2008) – have a strut efficiency factor that decreases as the a/d ratio increases. On the other hand, when non-hydrostatic nodes are used the strut size diminishes slightly as the a/d ratio increases, thereby, accounting for the reduction in shear strength. These differences in nodal dimensions are illustrated in Figure 6-5 for the example presented in Figure 6-4.

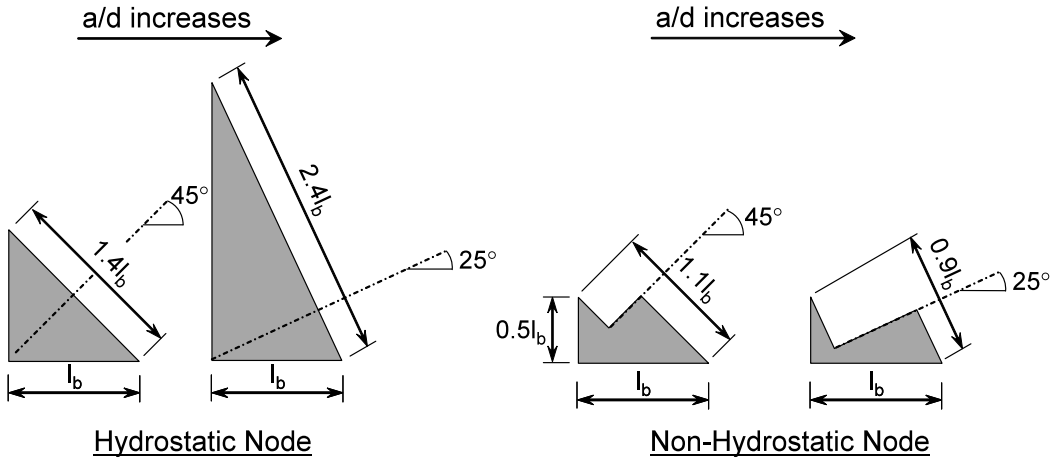

Figure 6-5. Typical difference in node dimensions between an a/d ratio of one and two.

Both ACI 318-08 and AASHTO LRFD (2008) include provisions that direct a designer towards using non-hydrostatic nodes (ACI 318-08, Figure RA.1.5; and AASHTO LRFD (2008), Figure 5.6.3.3.2-1). Not to mention, most designers use non-hydrostatic nodes, as it is difficult to coordinate the dimensions of a hydrostatic node with other beam details.

In summary, the use of either hydrostatic or non-hydrostatic nodes is an assumption – a design tool intended to provide a simple method for proportioning a STM. Each nodal dimensioning technique has its theoretical strengths and weaknesses. For example, a hydrostatic state of stress is typically associated with materials that cannot resist shear; yet, concrete has the ability to resist shear stresses. As such, it is reasonable to assume that the nodal region in a concrete beam is in a non-hydrostatic state of stress. On the other hand, the dimensioning technique used to proportion a non-hydrostatic node can be overly simplified and overly conservative, as is suggested to be the case at the back face of the CCT node (Section 6.4.2). Nonetheless, the benefits of using non-hydrostatic nodes are that they allow for the use of constant efficiency factors and they consider additional details such as reinforcement location and flexural capacity

In order to directly compare STM provisions with one another, an explicitly defined truss model (Figure 6-2) is used. Using a consistent model to evaluate code provisions is essential as the resulting nodal stresses (i.e. efficiencies) are dependent on the model.

6.3 EVALUATION OF CURRENT DESIGN PROVISIONS

A comparison between the ACI 318-08 STM, AASHTO LRFD (2008), *fib* (1999), ACI 318-99 [empirical provisions in lieu of STM (Equation 2-5)], and TxDOT Project 4371 (Sections 2.4 and 2.5) design provisions for deep beam shear is made. A single-panel strut-and-tie model was analyzed using the nodal geometries presented in Figure 6-3. An outline of the calculations performed for each STM procedure is located in Appendix F. In summary, the following seven

stress checks are conducted for all of the beams in the database: **1)** Back face of CCC and **2)** CCT nodes; **3)** Bearing face of CCC and **4)** CCT nodes; **5)** Strut-to-node interface at the CCC and **6)** CCT nodes; and **7)** stress in the tie reinforcement. The locations of these seven stress checks are illustrated in Figure 6-6.

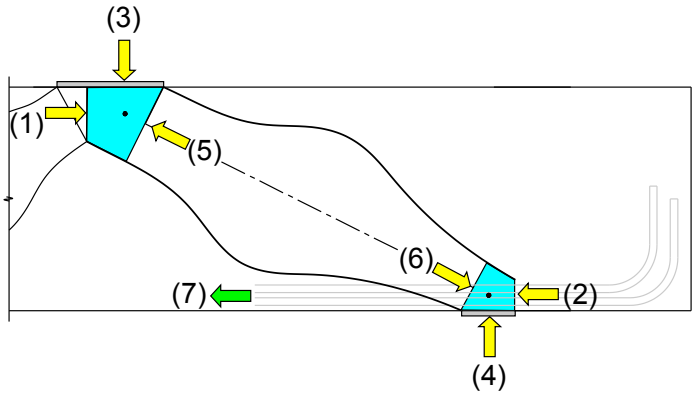

Figure 6-6. Seven stress checks used to evaluate STM procedures.

In addition to the seven stress checks shown above, failure of the D-region may be attributed to the longitudinal splitting of the strut. This failure mechanism is not directly checked. However, failure of the strut due to splitting is indirectly accounted for as all of the beams in the evaluation database contain a minimum amount of transverse reinforcement. Minimum transverse reinforcement provides a strut with the deformation capability necessary to prevent premature splitting of the strut. The minimum amount of reinforcement required for a D-region to realize its maximum shear capacity is introduced in Section 6.5.4 and discussed by Birrcher (2008).

Design provisions are compared to one another based on the experimental results of the 178 beams in the evaluation database (34 contributed from the current study). A description of the filtering criteria used to form the evaluation database is located in Section 2.8. The primary attributes of the evaluation database are summarized in Figure 6-7; details are included in Appendix E.

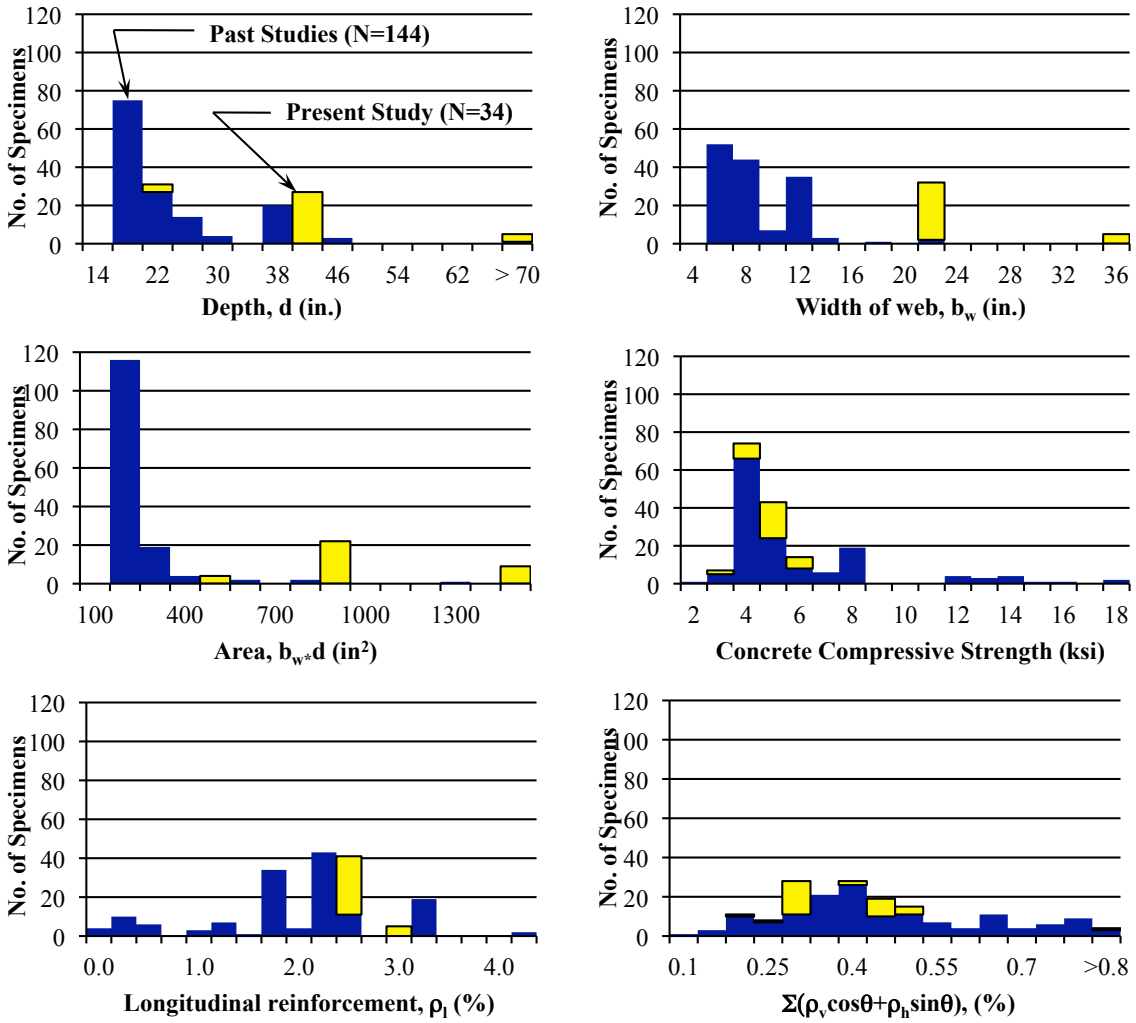

Figure 6-7. Primary attributes of the specimens in the evaluation database.

The purpose of comparing the provisions is to establish a basis for an improved design method. Figure 6-8 and Table 6.1 present a summary of the accuracy and conservatism of the five design procedures. The ratio of experimental to calculated shear capacity was determined for the beams in the evaluation database. A histogram of the findings is presented as follows.

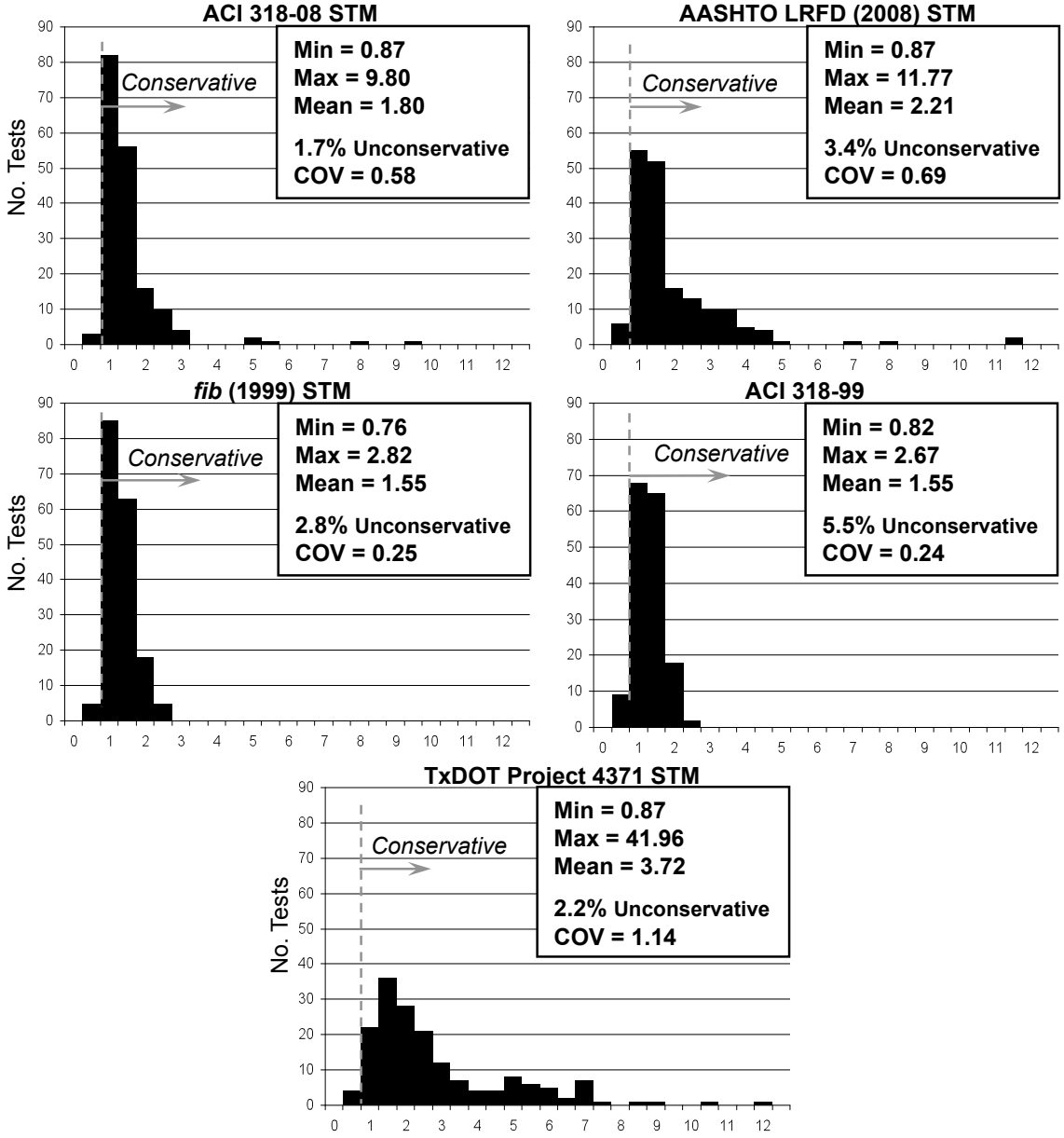

Figure 6-8. Range of experimental/calculated values determined using evaluation database (178 data points).

Table 6.1. STM Provisions: Evaluation Database

N = 178	Experimental/Calculated				
Design Provision	**Max**	**Min**	**Mean**	**% Unconservative†**	**COV††**
ACI 318 STM	9.80	0.87	1.80	1.7%	0.58
AASHTO LRFD	11.77	0.87	2.21	3.4%	0.69
fib (1999)	2.82	0.76	1.55	2.8%	0.25
ACI 318-99*	2.67	0.82	1.55	5.5%	0.24
Project 4371	41.96	0.87	3.72	2.2%	1.14

† Unconservative = Experimental/Predicted Value < 1.0
†† *COV* = Coefficient of Variation = Standard Deviation/Mean
* Equation 2-5

Based on a comparison of the five sets of design provisions presented in Figure 6-8, the empirical equation removed from the ACI 318 provisions (Equation 2-5) in 2002 and the STM provisions recommended by *fib* (1999) are the most accurate (COV of 0.24 and 0.25 respectively).

The reason that a strut-and-tie method is preferred over an empirical equation is because a STM is more versatile and the emphasis of a truss model is on the critical details. Details that are often the cause of a deep beam shear failure include: development length, nodal bearing stresses, stresses at the back face of a CCC node and stress in the tie. If the ACI 318 empirical equation is used to design a deep beam region, the bearing stresses and flexural capacity of the beam also need to be checked. However, if a STM is used to design a deep beam region, then the model accounts for these potentially critical bearing and flexural stresses.

The AASHTO LRFD (2008) and TxDOT Project 4371 methods are sufficiently conservative. However, there is a large amount of scatter associated with the two methods. The reason for the large amount of scatter and conservatism can be attributed to the derivation of these methods. The derivation is based on using hydrostatic nodes. As a result, the efficiency factors for these methods diminish as the a/d ratio increases. As presented in Section 2.2.3, when non-hydrostatic nodes are used in combination with efficiency factors that

diminish as the shear span increases, the result is overly conservative estimations of shear capacity.

The efficiency factors specified by ACI 318-08 and *fib* (1999) are similar in magnitude. However, the *fib* (1999) method is much more accurate [COV of 0.25 for *fib* (1999) versus 0.58 for ACI 318-08]. The difference in accuracy between the two procedures can be attributed to the following:

- *fib* (1999) explicitly allows the allowable stress at all faces of a nodal zone to be increased when triaxial confinement due to surrounding concrete is present.
- *fib* (1999) states that a stress check at the back face of a CCT due to bond stresses is not necessary – provided bars are anchored properly.
- The efficiency factors recommended by *fib* (1999) decrease as the compressive strength of concrete increases.

It is a major goal of this research study to make improvements to the ACI 318-08 and AASHTO LRFD (2008) STM procedures. According to MacGregor (2002), the selection of efficiency factors shall satisfy the following four criteria:

- Simplicity in application.
- Compatibility with tests of D-regions.
- Compatibility with other sections of ACI 318-08 and/or AASHTO LRFD (2008)
- Compatibility with other codes or design recommendations.

Based on the accuracy of the *fib* (1999) procedure, it was decided to pursue this method further. The *fib* (1999) provisions provide an engineer with an accurate and safe procedure for the design of a deep beam region. However, the *fib* (1999) provisions are not consistent with ACI 318-08 or AASHTO LRFD (2008). Therefore, minor improvements are recommended in order to make the *fib* (1999) provisions more consistent with ACI 318-08 and AASHTO LRFD (2008). An improved STM approach is presented in Section 6.4 and summarized in Section 6.6.

6.4 PROPOSED METHOD

As detailed in Section 6.2, a single-panel non-hydrostatic truss model (Figure 6-2) is used to evaluate a dataset of 178 specimens and make a recommendation for an improved STM procedure. For the selected model, a STM procedure consists of the seven stress checks illustrated in Figure 6-6.

The stress at each nodal face is compared to its respective allowable efficiency factor. The face that controls the calculated capacity is the one with the largest stress to efficiency ratio. If the stress in the tie controls the beam's capacity, then that particular specimen is not used to calibrate efficiency factors. The controlling efficiency of each of the six nodal faces is examined for all beams in the database in Sections 6.4.2 through 6.4.5 and a recommendation at each face is made accordingly.

6.4.1 Triaxial Confinement

Based on the test results from the specimens with triaxially confined CCC and CCT nodes (i.e. Series II specimens discussed in Chapter 5), it was concluded that the effective compressive strength of all faces of a triaxially confined node can be increased by the bearing capacity modification factor specified in the ACI 318-08 and AASHTO LRFD (2008) provisions. According to ACI 318-08 §10.14 and AASHTO LRFD §5.7.5 the allowable bearing capacity of concrete can be expressed as follows.

$$P_n = m \cdot 0.85 \cdot f_c' \cdot A_1 \qquad \text{Equation 6-1}$$

Where,

P_n = nominal bearing resistance

m = bearing capacity (triaxial confinement) modification factor, $\sqrt{\frac{A_2}{A_1}} \le 2$

The definition of A_2 and A_1 is illustrated in Figure 6-9.

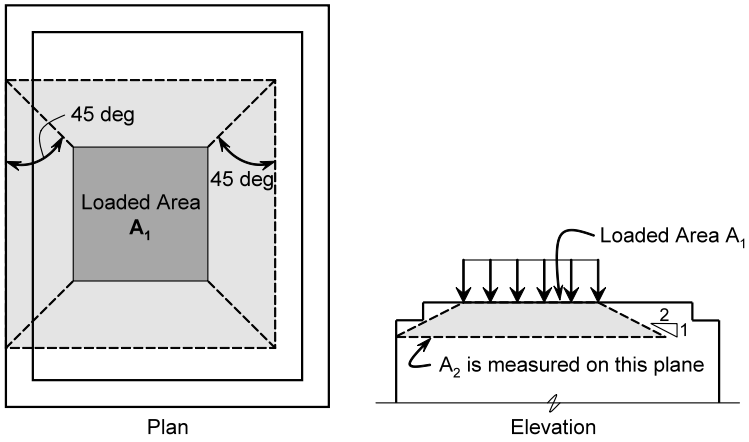

Figure 6-9. Application of frustum to find A_2 in stepped or sloped supports (ACI 318-08).

From a theoretical standpoint, when a nodal zone is triaxially confined, the compressive strength of concrete is increased in the entire region. Therefore, it is reasonable to assume that the compressive strength of all nodal faces is increased when triaxial confinement is present. This phenomenon is verified with beams fabricated and tested as part of the current study and past studies. Figure 6-10 presents a summary of calculations carried out by using the ACI 318-08 STM provisions both with and without an increase in nodal capacity due to triaxial confinement. The ratio of experimental capacity to the calculated capacity is presented for all beams in the filtered database whose bearing plate width was smaller than the width of the beam. The result of increasing the allowable capacity of a nodal region is presented for beams designed per the ACI 318-08 STM specifications; similar conclusions can be drawn from the AASHTO LRFD (2008) STM provisions (Figure 5-14).

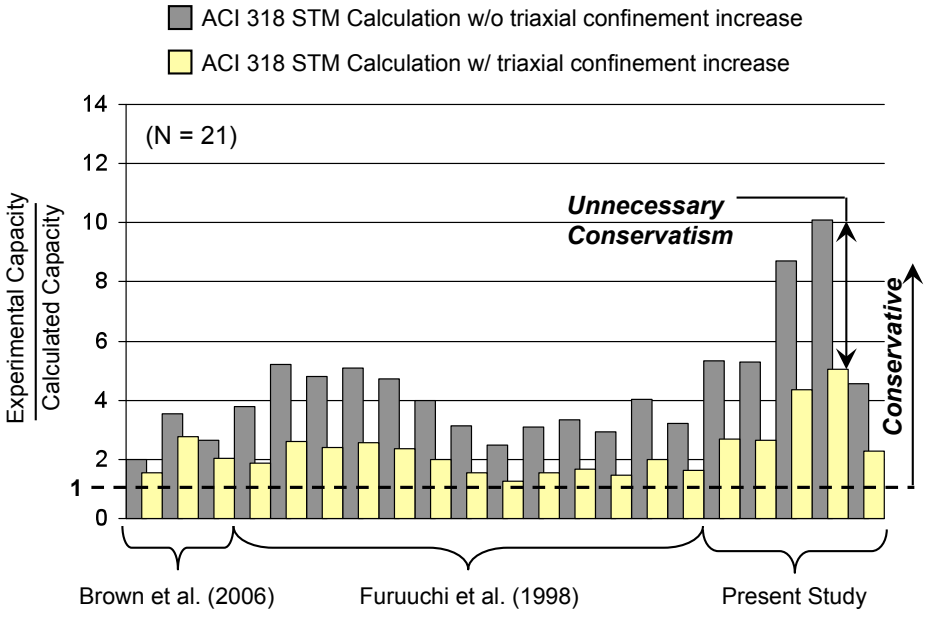

Figure 6-10. The effect of triaxial confinement: (ACI 318-08).

Brown et al. (2006) tested three beams whose load plates had a width less than the width of the beam (Section 2.6.5.4). Furuuchi et al. (1998) tested a series of deep slabs with varying load and support plate dimensions (Section 2.6.5.1). Specimens tested by Furuuchi et al. (1998) were 6-inch deep, 20-inch wide, and did not contain any shear reinforcement. Based on their aspect ratio and lack of stirrups, these beams are considered the worst-case scenario when evaluating triaxial confinement provisions. Upon examination of Figure 6-10, it can be concluded that an increase in the capacity of all triaxially confined nodal faces improves the accuracy of a STM prediction without diminishing its conservatism. This conclusion is justified on a theoretical and experimental basis.

6.4.2 Back Face of the CCT Node

In a strut-and-tie model, the height of the back face of a CCT node is taken as twice the distance from the exterior beam surface to the centroid of the reinforcement that defines the tie (Figure 6-11).

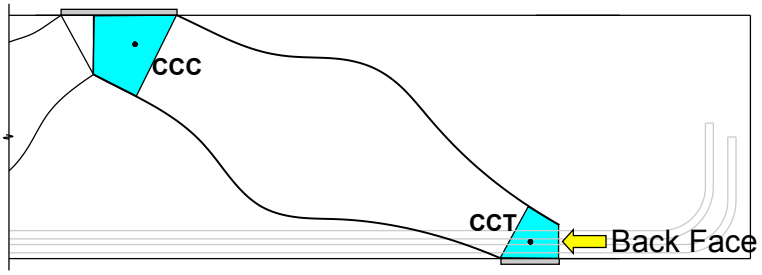

Figure 6-11. Back face of a CCT node.

As discussed in Section 2.4.2.2, the efficiency of the back face of a CCT node is dependent on the stress condition. Stress at this surface can be attributed to the bonding stress that results from the anchorage of a tie, bearing stress of an anchor plate or headed bar, or an external indeterminacy such as occurs at an interior node over a continuous support. An example of these configurations is presented in Figure 6-12.

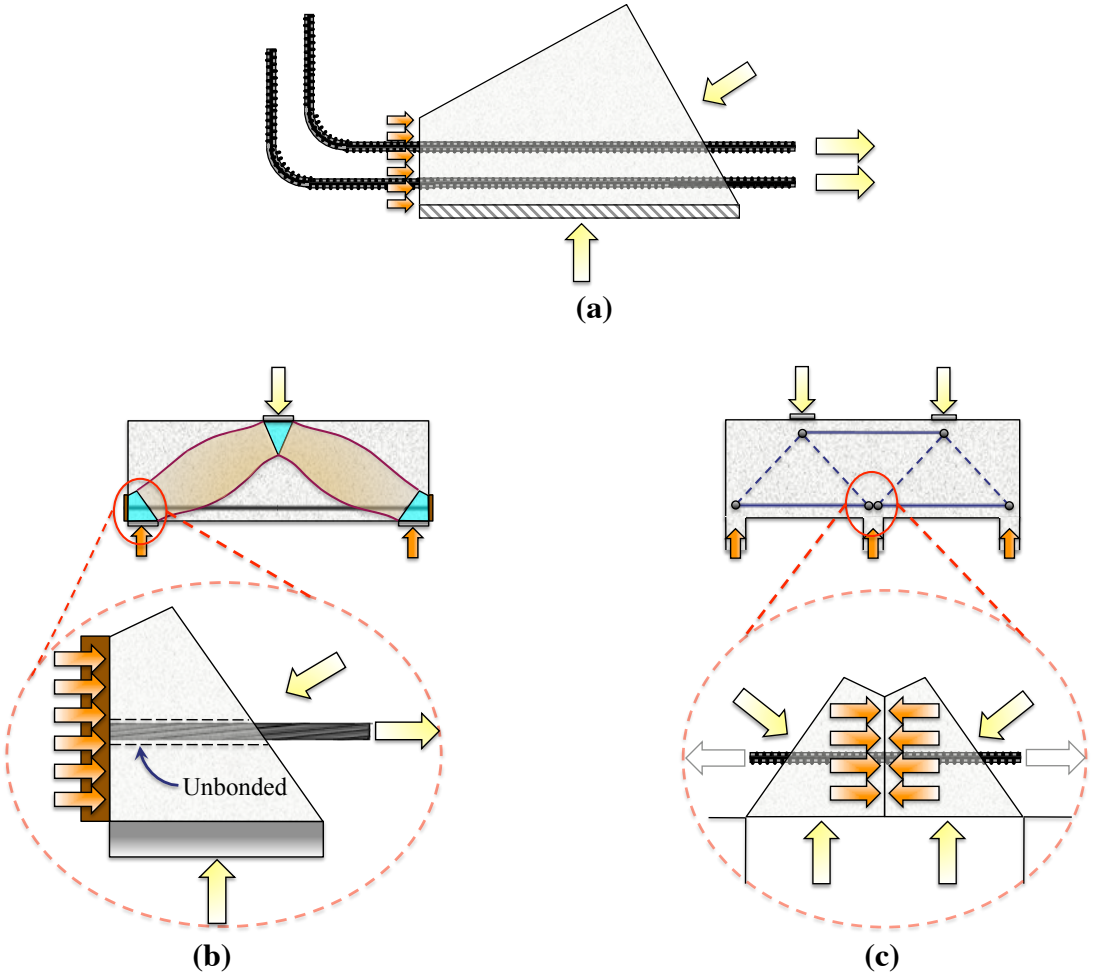

Figure 6-12. Stress condition at the back face of a CCT node: (a) bonding stress; (b) bearing of an anchor plate; (c) interior node over a continuous support.

The effectiveness of a CCT node to resist bonding stresses [Figure 6-12 (a)] is investigated separately from the other stress conditions shown. The results of this study are presented in Section 6.4.2.1. The effectiveness of the back face to resist bearing stresses caused by conditions other than anchorage is discussed in Section 6.4.2.2.

6.4.2.1 Effectiveness of Back Face to Resist Bonding Stresses

According to the ACI 318-08 and AASHTO LRFD (2008) STM provisions, stresses at the back face of a CCT must always be checked. Alternatively, the *fib* (1999) provisions do not require a check at the back face of a CCT node if the applied force is the resultant of the bond stress attributed to the anchorage of a tie (provided that the tie is sufficiently developed).

In general, the technique used to proportion the back face of a CCT node typically results in an excessively small face. As a result, it often controls the nominal capacity of a truss model. If the tie is anchored properly, crushing of concrete at the back face of the support is unlikely and should not be used to determine the capacity of a CCT node. Thompson et al. (2003) investigated stresses in CCT nodal regions and reached a similar conclusion:

> *The philosophy of the current code provisions for determining the capacity of CCT nodes may require reconsideration. The evidence from the tests shows that the failure of these nodes was primarily related to anchorage and that the current stress limits for nodes were unrealistic. It is possible that CCT nodes cannot fail in compression if anchorage of the tie bars is sufficient. The stress limits imposed by the code provisions may be unnecessary.*

In order to investigate the criticality of stresses at the back face of the CCT node, the capacity of beams estimated per the ACI 318-08 provisions was examined in further detail. The node face that determined the capacity of each beam in the database was found according to the ACI 318-08 STM provisions. Then, the capacity of each of the beams in the database was determined per the ACI 318-08 STM provisions except that the stress at the back face of the CCT node was ignored. As a result, not considering the stress at the back face of the CCT node had an insignificant impact on the conservatism of the ACI 318-08 provisions. This point is illustrated in Figure 6-13.

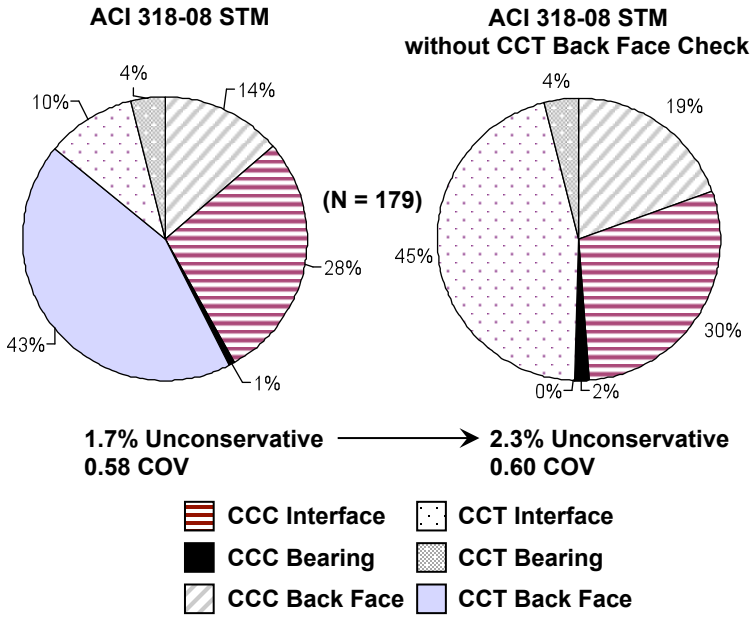

Figure 6-13. Governing node face with and without a stress check at the back face of the CCT node: ACI 318.

As can be observed in Figure 6-13, if ACI 318-08 STM provisions are used without any modifications, the stress check performed at the back face of the CCT node controls the capacity for 43% of the beams in the evaluation database. If the stress at the back face of the CCT node is not checked, the amount of unconservative predictions increases from 1.7% to 2.3% and the coefficient of variation increases from 0.58 to 0.60. This is a minor change considering that the CCT back face stress check originally controlled the design of almost half the beams in the database. Therefore, it can be concluded that checking the stresses at the back face of the CCT node minimally improves the accuracy and conservatism of the ACI 318-08 STM design provisions.

In order to gather more information on the stress distribution at the back face of the CCT nodes, concrete strain gauges were affixed behind the support plate of beams tested as part of the current experimental program, as illustrated in Section 3.5.2. The purpose of collecting strain data at the back face of the CCT

node was to determine the magnitude and distribution of stresses in the region and compare these results with typical modeling assumptions.

The back face of a CCT node is taken as twice the distance from the exterior face of the beam to the centroid of the longitudinal reinforcement. For the Series I and III specimens, that distance is equal to approximately 11" and 7" respectively. According to ACI 318-08 and AASHTO LRFD (2008), the limiting efficiency factor at the back face of a CCT node is 0.68 and 0.75, respectively. In other words, the allowable stress at the back face is $0.68 \cdot f_c'$ and $0.75 \cdot f_c'$. The assumed CCT nodal geometries and allowable stress at the back face are presented in Figure 6-14 for the Series I and III specimens. An allowable stress of $0.70 \cdot f_c'$ is assumed and shown for illustration purposes.

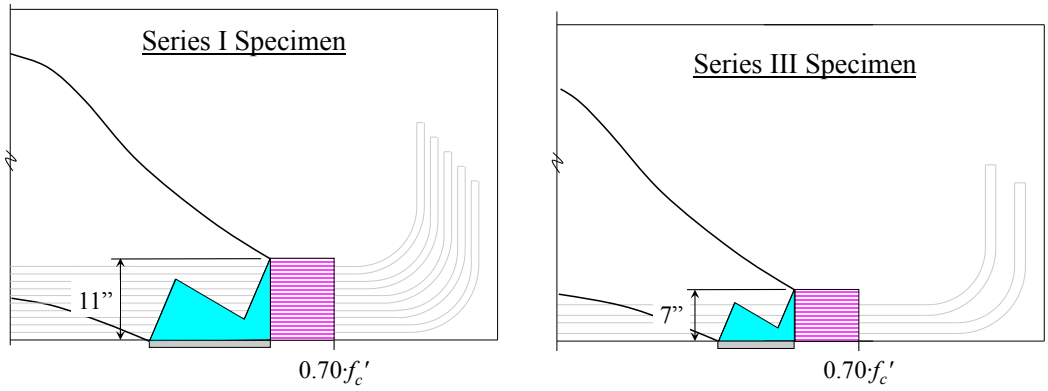

Figure 6-14. Assumed nodal dimensions and allowable stress distribution at back face of CCT node.

Strain gauges were applied behind the support plate (Section 3.5.2) for all of the Series I specimens and the following Series III specimens: III-1.85-0, III-1.85-02, and III-1.85-025. The strain distribution at 90% of ultimate capacity is presented for specimens I-02-4 and I-02-2; and for specimens III-1.85-0, III-1.85-02, and III-1.85-025 in Figure 6-15. In addition, the theoretical stress at the back face based on the assumed nodal geometry is presented.

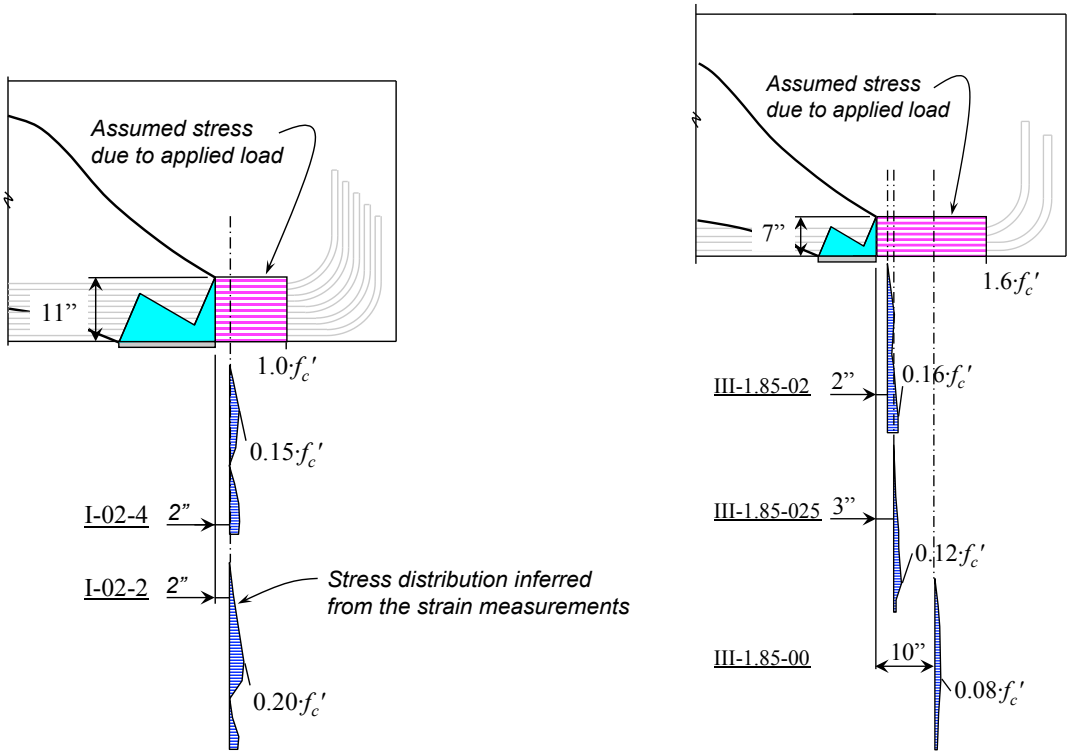

Figure 6-15. Strain distribution measured behind the support plate at 90% of ultimate capacity.

Based on the strain data measured behind the CCT nodal region, it can be concluded that the technique used to proportion the back face of a non-hydrostatic CCT node is unrealistic and should not be used to determine the capacity of a truss model if reinforcement is anchored properly. For this condition, crushing of concrete at the back face of a CCT node is not a realistic failure mechanism. Crushing of concrete at the back face of the CCT nodes was not observed in any of the tests conducted within this research program nor those reported in the literature.

In order to verify data obtained from concrete gauges, steel strain gauges were applied to all twelve of the main longitudinal bars for specimens III-1.85-02 and III-1.85-025 as described in Section 3.5.1. The rebar gauges were located in the same plane as the concrete surface gauges. The force in the steel reinforcement was inferred based on the experimentally measured strains,

modulus of elasticity of steel, and nominal area of the reinforcing bars. The force applied to the same plane of concrete was inferred based on the area under the strain profile curve shown in Figure 6-15, the width of the beam, and the modulus of elasticity of concrete taken as $57{,}000\sqrt{f_c'}$. The resulting force measured in the reinforcement was within 10% of the value measured with the concrete surface gauges for both specimens. Thus, it can be concluded that the surface gauge data was reliable.

6.4.2.2 Effectiveness of Back Face to Resist Direct Stresses

Conditions exist where the stress applied to the back face of a CCT node is attributed to forces other than those caused by the bonding of anchored reinforcement. An example of such conditions are at the CCT node over an interior support or at a CCT node where the anchorage of the reinforcement is provided by a bearing plate or headed bar (Figure 6-12).

When the stress at the back face of a CCT node is the result of a condition other than the transfer of bonding stresses, the nodal dimension must be proportioned accordingly so that the crushing of concrete does not occur. The *fib* (1999) design provisions recognize the complication of this stress condition:

> *In conclusion, it can be stated, that the concrete in the node [over an interior support] is under biaxial compression, but the horizontal compression is difficult to assess. On the other hand, tensile reinforcement penetrates the node region and is anchored there to some extent. Therefore, [the CCT bearing face efficiency] will again be applied hear as design node strength, the [the CCC bearing efficiency] might eventually be considered.*

Based on the recommendations of *fib* (1999), Schlaich et al. (1987), and Thompson et al. (2003), the bonding stresses attributed to the anchorage of a tie are not critical and need not be applied to the back face of a CCT node provided that the tie meets the necessary anchorage requirements. If the force applied to the

back face of a CCT node is attributed to stresses other than those caused by anchorage, the effectiveness of the node to resist crushing must be checked. In this case, an efficiency factor consistent with the CCT bearing face (Section 6.4.4) should be used.

If the stress applied to the back face of a CCT node is the result of a combination of both anchorage and a discrete force from another strut framing into the node, it is only necessary to proportion the node to resist the direct compression stresses. In other words, stresses due to anchorage are indirectly accounted for with an adequately developed tie and need not be considered. It is believed that the small amount of stress that may indirectly occur in the nodal region due to anchorage is accounted for by the excessively small dimension of the CCT node and the respective efficiency factor.

6.4.3 Efficiency of the Bearing and Back Face of CCC Node

The dimensions of the bearing and back face of a CCC node, as shown in Figure 6-16, is proportioned according to the method presented in Figure 6-3.

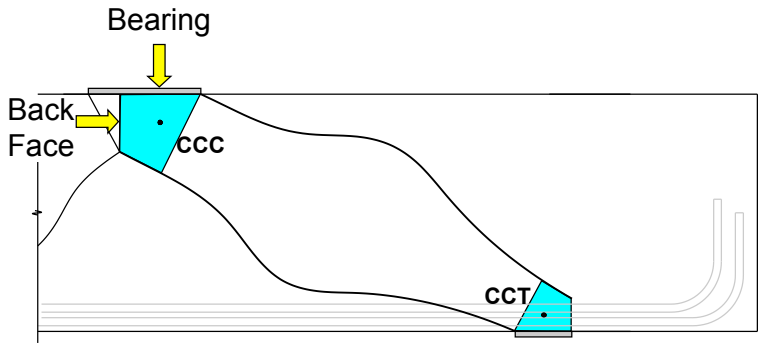

Figure 6-16. Bearing and back face of a CCC node.

The height of the back face of the CCC node is based on the depth of the equivalent compression block determined from flexural mechanics. This dimension is justified, as the crushing of the back face of a CCC node is the same failure mode observed in a flexural failure. In a flexural analysis, it is assumed that the compression block is loaded uniaxially. Similarly, it is assumed that the bearing face of the CCC node is uniaxially loaded in compression. According to

both ACI 318-08 and AASHTO LRFD (2008), the efficiency of concrete in an undisturbed state of uniaxial compression is typically taken as a constant value of 0.85. Therefore, for purpose of maintaining consistency with the ACI 318-08 and AASHTO LRFD (2008) specifications, it is proposed that the efficiency of the undisturbed uniaxial compression stress field associated with the back face of the CCC node be set to a constant value of 0.85.

The efficiency of the bearing face of the CCC node is established in a similar manner. This recommendation is consistent with what is currently done in the ACI 318-08 and AASHTO LRFD (2007) specifications.

The implications of these proposals are examined within the evaluation database. The normalized stress at the back and bearing face of the CCC node is plotted for beams where said nodal boundaries control the design (Figure 6-17). Based on the results obtained from the database and illustrated in Figure 6-17, a constant efficiency of 0.85 is an appropriate value.

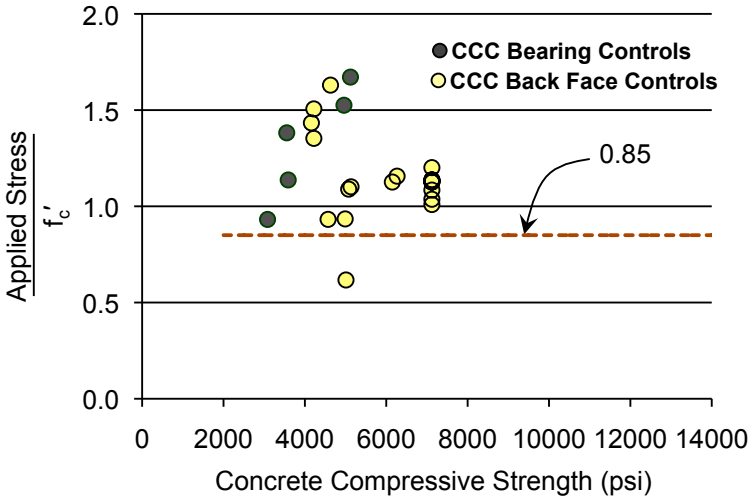

Figure 6-17. CCC back (N = 19) and bearing face (N = 6) efficiency factor: Proposed Method.

The efficiency factor specified by *fib* (1999) is also considered an appropriate value. However, a constant efficiency factor is recommended for the bearing and back face of the CCC node based on following: (i) in the interest of

maintaining consistency with other sections of ACI 318-08 and AASHTO LRFD (2008); and (ii) in the interest of having the simplest code provision that captures the trends (or lack thereof) of the data presented in Figure 6-17.

6.4.4 Efficiency of the Bearing Face of CCT Node

The dimension of the bearing face of a CCT node, as shown in Figure 6-18, is proportioned according to the method presented in Figure 6-3.

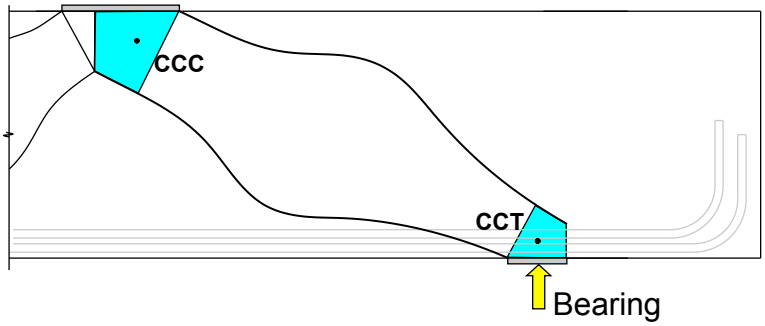

Figure 6-18. Bearing face of a CCT node.

According to Vecchio and Collins (1986), the effective compressive strength of concrete decreases with the accumulation of transverse tensile strains (i.e. a CCT nodal region). The philosophy that concrete has a reduced efficiency in the CCT nodal region has been adopted by ACI 318-08, AASHTO LRFD (2008), and *fib* (1999). In accordance with ACI 318-08, AASHTO LRFD (2008), and *fib* (1999) it is proposed that the efficiency at the bearing face of the CCT node be set to a constant value of 0.70.

The conservativeness of this proposal is examined by using the evaluation database. The normalized stress at the bearing face of the CCT node is plotted for beams where said boundary controls the STM calculations (Figure 6-19).

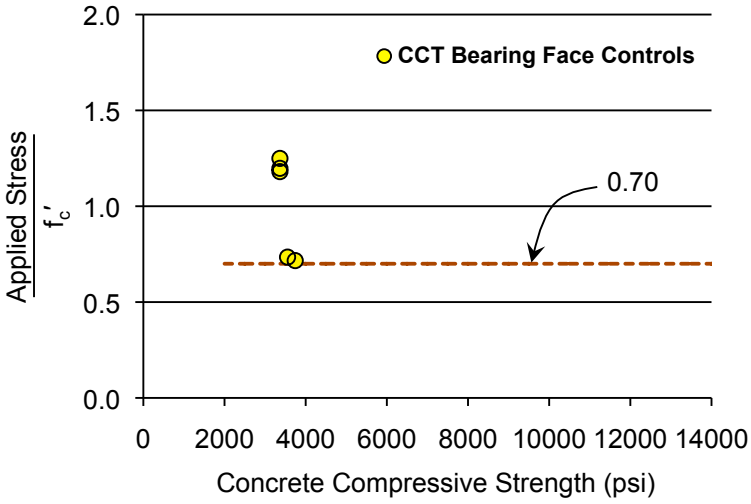

Figure 6-19. CCT bearing face efficiency factor (N = 5): Proposed Method.

Admittedly, there are a sparse number of beams in the database that are controlled by the CCT bearing face. Nevertheless, based on the results obtained from the database, and in accordance with ACI 318-08 and AASHTO LRFD (2008), a constant efficiency of 0.70 is appropriate.

6.4.5 Efficiency of the Strut-to-Node Interface

The dimension of the CCC and CCT strut-to-node interface, as shown in Figure 6-20, is proportioned according to the method presented in Figure 6-3.

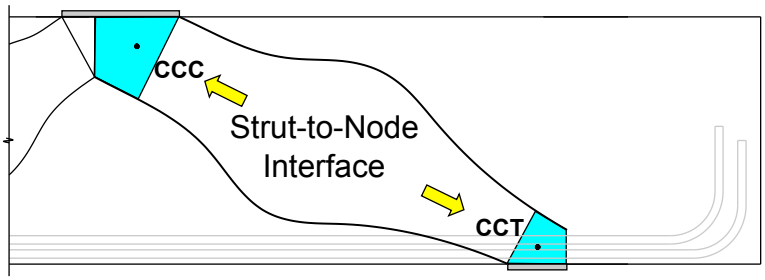

Figure 6-20. CCC and CCT strut-to-node interface.

AASHTO LRFD (2008) and *fib* (1999) specify a concrete efficiency at the CCT interface lower than at the CCC interface for the same reason cited for the bearing faces; i.e. the presence of transverse tensile stresses diminish the

compressive strength of concrete. ACI 318-08, on the other hand, specifies the same efficiency at both the CCC and CCT interface.

Although the efficiency of a CCT region has been shown to be lower than that of a CCC region, the diminishing effect is accounted for by non-hydrostatic nodal geometries. In other words, the smaller proportion of the CCT node-to-strut interface indirectly accounts for the reduction in efficiency. Consider, for example, the beams in the database whose calculated capacities are controlled by the ACI 318-08 stress checks at the CCC or CCT node-to-strut interface (Figure 6-21).

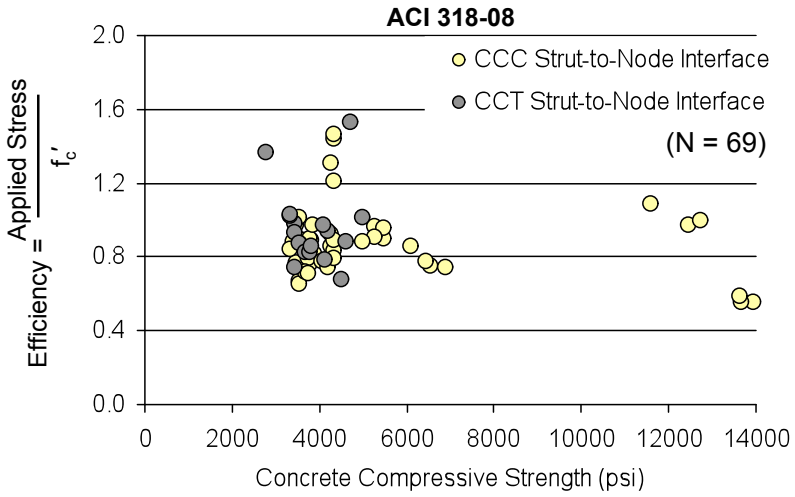

Figure 6-21. Experimental efficiency vs. ACI 318-08 at the CCC and CCT strut-to-node interface.

As seen in Figure 6-21, the efficiency at the strut-to-node interface is defined as the ratio of the applied stress at said interface to the compressive strength of concrete. Upon examination of the capacity of the beams in the database as estimated by the ACI 318-08 STM provisions, the CCC strut-to-node interface governed the capacity for 50 beams while the CCT strut-to-node interface governed for 19 beams. It is important to observe that the data for the 69 beams controlled by the CCC and CCT strut-to-node interface is equally scattered and with a similar lower bound.

Accordingly, it can be concluded that efficiency of the CCC or CCT strut-to-node interface is equivalent when those interfaces control the capacity calculations (per ACI 318-08). A similar conclusion can be reached for the calculations carried out by the AASHTO LRFD (2008) STM specifications (Figure 6-22).

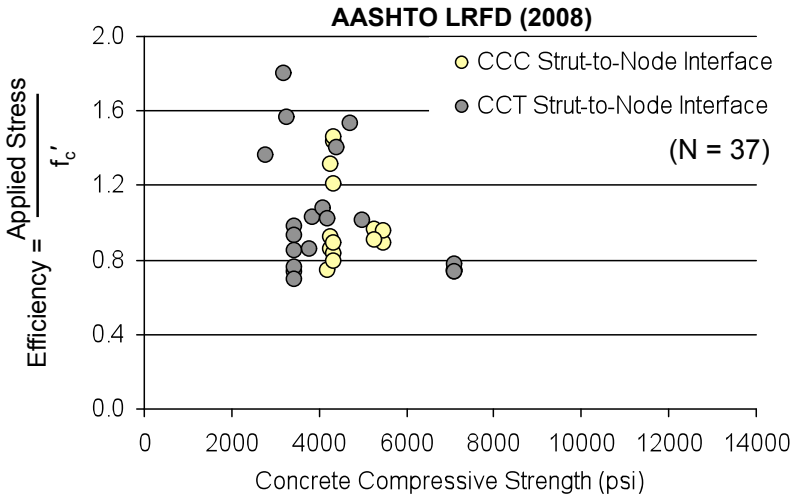

Figure 6-22. Experimental efficiency vs. AASHTO LRFD (2008) at the CCC and CCT strut-to-node interface.

In light of the data presented in Figure 6-21 and Figure 6-22, there is no reason to specify a lower efficiency factor at the CCT strut-to-node interface.

Efficiency factors recommended by *fib* (1999) are a function of concrete compressive strength. High strength concrete has a lower efficiency because of the corresponding reduction in shear transmitted along the main diagonal crack. The strength of the cement paste in high-strength concrete is more than that of the aggregate. When shear cracks form in high-strength concrete, the resulting cracks are transmitted through rather than around the aggregate. As a result, the main inclined crack is smoother, so it has a lower interface shear capacity. Additionally, research conducted by Nielson (1978), Ramirez and Breen (1991), Bergmeister et al. (1993) Brown et al. (2006) support the use of an interface efficiency factor that diminishes as concrete compressive strength increases.

Figure 6-23 illustrates the results of the calculations performed on the specimens in the evaluation database by using the *fib* (1999) efficiency factors.

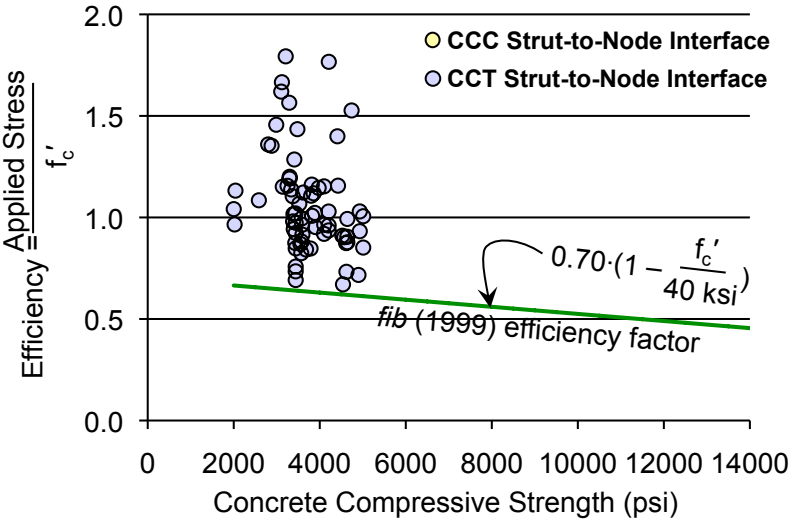

Figure 6-23. Experimental efficiency vs. *fib* (1999) recommendations at the CCC and CCT strut-to-node interface.

As seen in Figure 6-23, the CCC strut-to-node interface never controls the capacity of a deep beam estimated per the *fib* (1999) STM provisions. This is attributed to the geometric proportions that define the CCC nodal zone. The bearing and back face of the CCC node are always smaller than the interface and the *fib* (1999) recommended efficiency is the same at all three nodal faces. As a result, the critical stress cannot occur at the node-to-strut interface. It will always occur at either the back face or bearing face depending on the strut angle. The same phenomenon does not occur in the CCT nodal zone because a stress check is not required at the back face.

Given that the experimental stress at the CCC and CCT strut-to-node interface is equivalent when estimated per ACI 318-08 and AASHTO LRFD (2008) (Figure 6-21 and Figure 6-22); and given that the capacity of a beam estimated per *fib* (1999) STM provisions is never controlled by the stress at the CCC strut-to-node interface; it is proposed that the efficiency factor assigned to the CCC strut-to-node interface also be assigned to the CCT node-to-strut

interface. This recommendation is consistent with the general philosophy of the ACI 318-08 provisions.

It has previously been determined that the nodal efficiency is independent of the a/d ratio when non-hydrostatic nodes are used and dependent on the compressive strength of concrete. Therefore, in accordance with *fib* (1999), it is proposed that the efficiency at the node-to-strut interface diminish as the compressive strength of concrete increases. Modifications to the *fib* (1999) efficiency factor are suggested as follows.

The *fib* (1999) strut-to-node efficiency factor is equal to 0.43 when the compressive strength of concrete is 14,000-psi. In general, concrete is considered *high-strength* when the compressive strength is greater than 8,000-psi. Given that there is not much data available in the high-strength range, it is proposed that the efficiency be capped at a lower value of 0.45 for compressive strengths greater than 8,000-psi. Similarly, it is proposed that the efficiency be capped at an upper value of 0.65 [the *fib* (1999) factor is equal to 0.63 when the compressive strength of concrete is 4000-psi]. Finally, it is proposed that the efficiency linearly decrease between 4,000 and 8,000-psi. As such, the proposed CCC and CCT strut-to-node interface efficiency factor, ν, is expressed as follows:

$$\nu = \quad 0.45 \leq \ 0.85 - \frac{f_c'}{20ksi} \leq 0.65 \qquad \text{Equation 6-2}$$

The conservativeness of this proposal is examined by using the evaluation database (Figure 6-24). The efficiency factors at the CCC and CCT strut-to-node interface are plotted for beams whose capacity is calculated by using the proposed method.

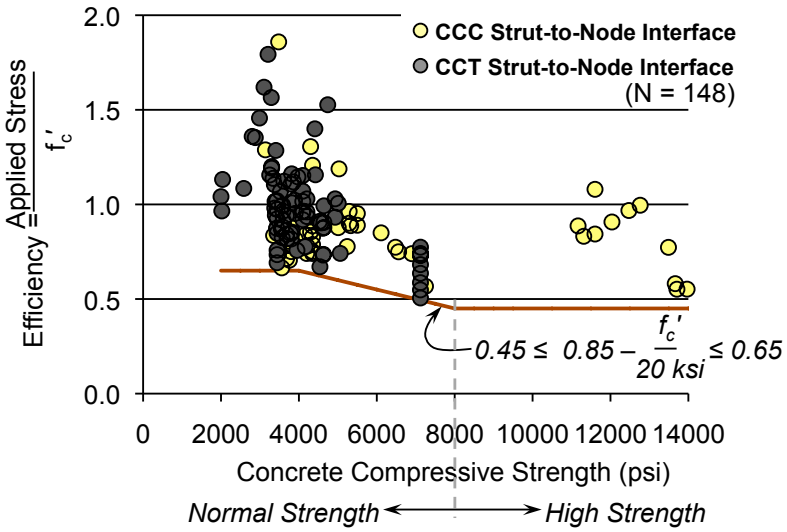

Figure 6-24. Experimental vs. proposed efficiency at the CCC and CCT strut-to-node interface.

Based on the results obtained from the evaluation database, the efficiency factor proposed for the determination of the capacity of the CCC and CCT strut-to-node interface (Equation 6-2) is an appropriate expression.

The recommendations outlined by *fib* (1999) were used to formulate a new STM design procedure. In accordance with *fib* (1999), the following attributes of the proposed STM provisions are consistent with the *fib* (1999) STM provisions:

- Disregard the stress check at the back face of the CCT node when the applied force is the resultant of bonding stresses from a sufficiently anchored tie.
- Increase the allowable stress in triaxially confined nodal regions.
- At the CCC and CCT strut-to-node interface, the efficiency of concrete decreases as the compressive strength increases.

The following attributes of the proposed STM provisions are consistent with the ACI 318-08 and AASHTO LRFD (2008) provisions:

- A triaxial confinement modification factor is used to account for the increase in nodal capacity due triaxial confinement. The modification factor is expressed the same as for bearing capacity (Equation 6-1).
- In accordance with ACI 318-08, the efficiency of the CCC and CCT node-to-strut interfaces are identical.
- At the bearing and back face of the CCC node, the efficiency of concrete is a constant value of 0.85.
- At the bearing face of the CCT node, the efficiency of concrete is a constant value of 0.70.

Based on the fundamental principles of strut-and-tie modeling given in the ACI 318-08, AASHTO LRFD (2008), and *fib* (1999) design provisions, and based on tests of the D-regions analyzed using the evaluation database, a new STM provision is proposed. The details of the proposed provision are summarized in Figure 6-25. The proposed STM procedure is compared to ACI 318-08, AASHTO LRFD (2007), and *fib* (1999) in Section 6.5. A complete outline of the new procedure is presented in Section 6.6.

$\varphi F_n > F_u$

$F_n = m \cdot \nu \cdot f_c' \cdot A_{nz}$

Where,

$m = \sqrt{A_2 / A_1}$ (Equation 6-1)

STM Proposed Efficiency Factors, ν

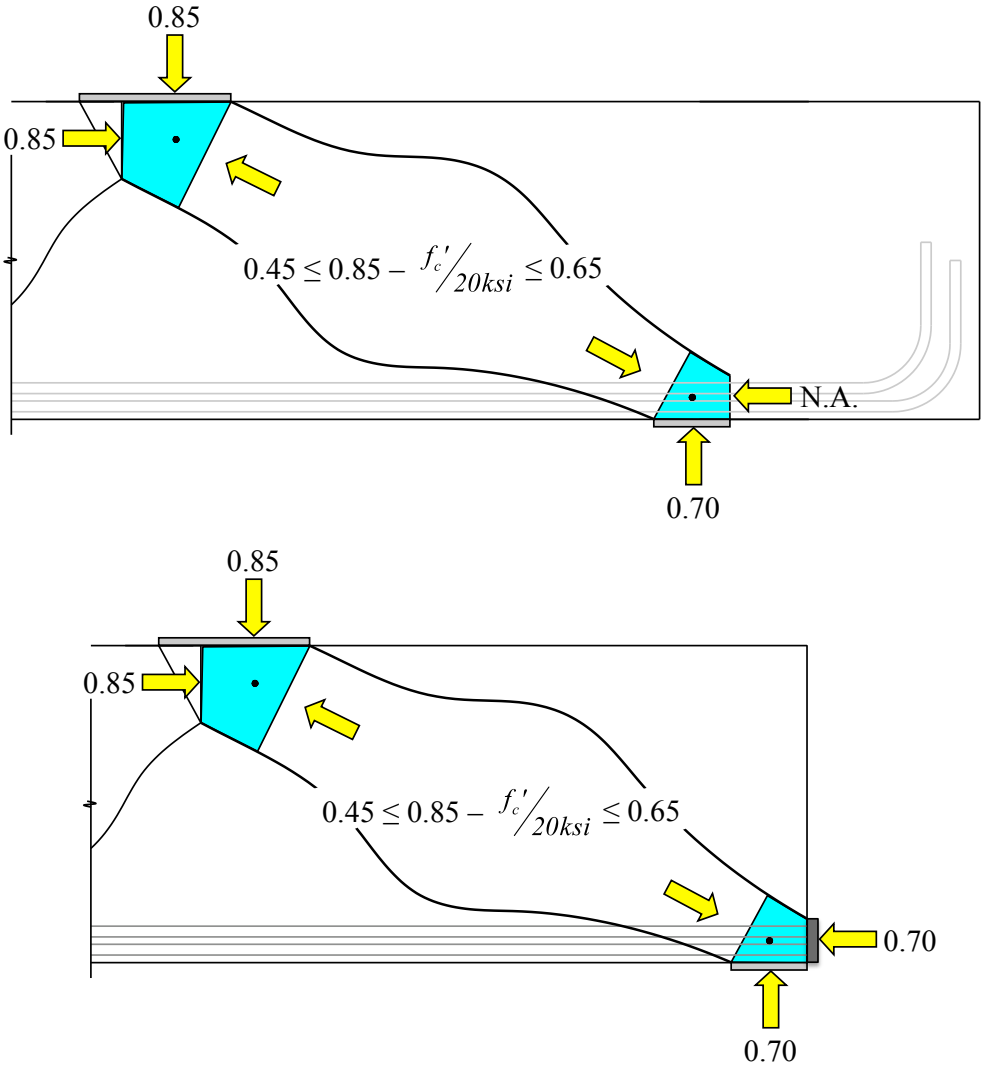

Figure 6-25. Proposed STM design provision.

6.5 ASSESSMENT OF PROPOSED METHOD

6.5.1 Evaluation Database

An assessment of the proposed method based on the experimental results of the beams in the evaluation database is presented in Table 6.2 and Figure 6-26.

Table 6.2. STM Provisions: Evaluation Database

N = 178	Experimental/Calculated				
Design Provision	**Max**	**Min**	**Mean**	**% Unconservative†**	**COV††**
ACI 318	9.80	0.87	1.79	1.7%	0.58
AASHTO LRFD	11.77	0.87	2.21	3.4%	0.69
fib (1999)	2.82	0.76	1.55	2.8%	0.25
ACI 318-99*	2.67	0.82	1.55	5.5%	0.24
Project 4371	41.96	0.87	3.72	2.2%	1.14
PROPOSED	***4.14***	***0.73***	***1.54***	***0.6%***	***0.28***

† *Unconservative* = Experimental/Calculated Value < 1.0

†† *COV* = Coefficient of Variation = Standard Deviation/Mean

* Equation 2-5

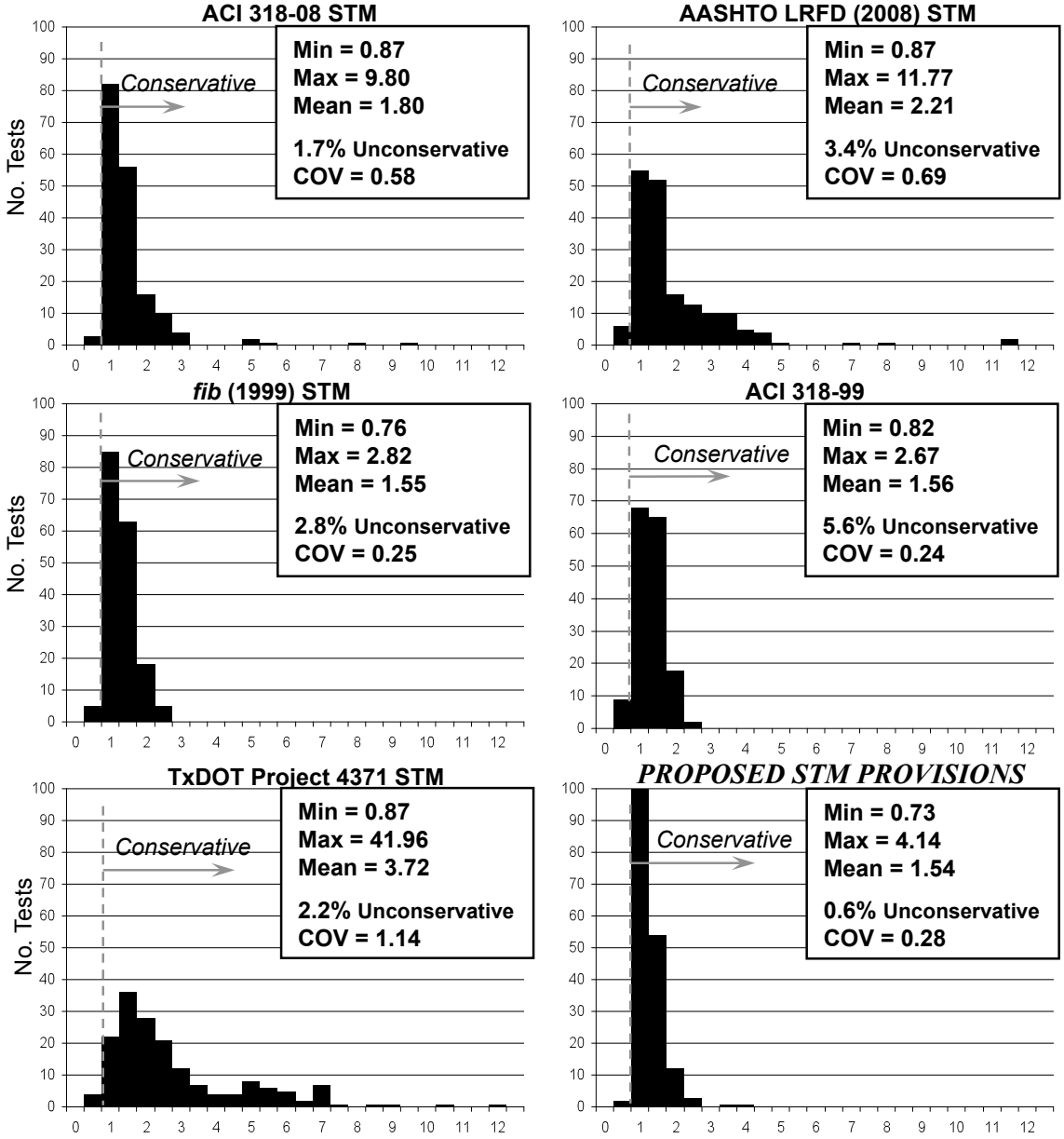

Note: In accordance with ACI 318-08 and AASHTO LRFD (2008), the proposed method contains a limit on the triaxial confinement modification factor equal to 2 (Equation 6-1); whereas, fib (1999) limits this factor to 4 (Equation 2-17). The proposed method would perform slightly better than fib (1999) if the triaxial confinement modification limit were increased to 4 [Mean = 1.51, 0.6% unconservative, COV = 0.22].

Figure 6-26. Comparison of proposed STM provisions with other design provisions (Evaluation Database = 178 data points).

As shown, the proposed strut-and-tie modeling procedure is a significant improvement over the current ACI 318-08 and AASHTO LRFD (2008) procedures. The amount of unconservative estimations using the proposed provisions is slightly less than the *fib* (1999) provisions, but the *fib* (1999) methodology is slightly more accurate than the proposed procedure. However, if both methods contained the same limit on the triaxial confinement modification factor, then the proposed procedure would have a COV equal to 0.22, a slight improvement compared to the *fib* (1999) provisions. As it is, the proposed triaxial confinement factor is consistent with the ACI 318-08 and AASHTO LRFD (2008) bearing capacity provisions.

6.5.2 Filtered Database

The specimens in the *evaluation database* were selected from a larger dataset based on their geometry and proportions. It was the intent of the research team to formulate design recommendations based on test specimens that best represented actual structural members. As a result, the larger beams contained in the evaluation database were used to calibrate the recommended nodal efficiencies. Upon derivation of the proposed STM methodology, it is of interest to compare the performance of the procedure with a larger dataset; i.e. a dataset that contains data other than those that were used to calibrate the proposed STM procedure. Therefore, the performance of the proposed STM provisions are compared with the other design provisions for the tests that are contained in the *filtered database*.

As previously discussed, the STM model that was used to evaluate deep beam design provisions indirectly accounts for failure controlled by the longitudinal splitting of the strut by only considering beams that contain a minimum amount of reinforcement. Therefore, only those beams in the filtered database that contain a minimum amount of transverse reinforcement are evaluated. An assessment of the proposed provisions is presented in Figure 6-27. The data presented in Figure 6-27 is based on the experimental results of the

beams in the filtered database with a minimum reinforcement ratio greater than or equal to 0.1% (i.e. $\rho_{\perp} > 0.1\%$).

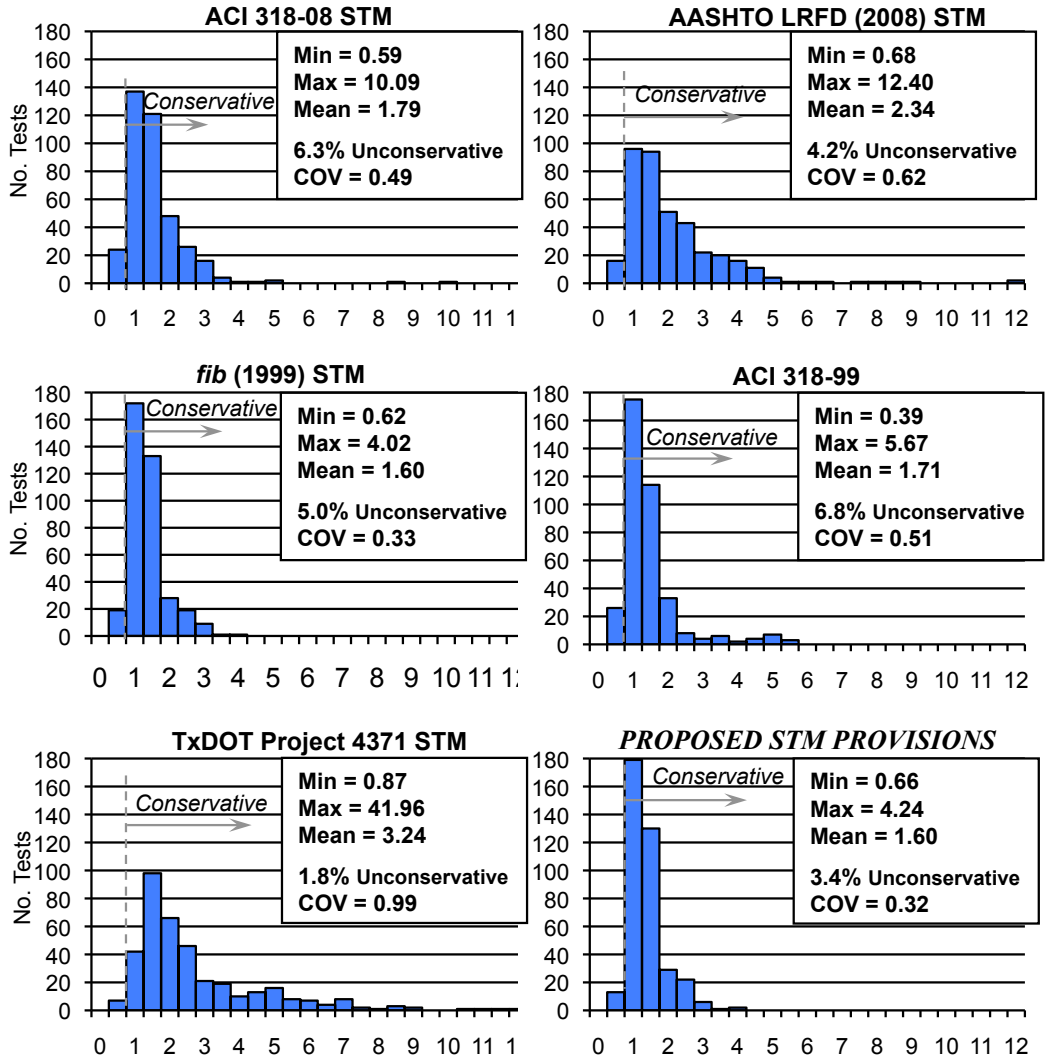

Note: If the triaxial confinement modification limit of the proposed method were increased to 4 [Mean = 1.59, 3.4% unconservative, COV = 0.31].

Figure 6-27. Comparison of proposed STM provisions with other design provisions (Filter Database with $\rho_{\perp} > 0.1\%$ = 381 data points)

Upon observation of Figure 6-27, it can be concluded that the trends between the design provisions are consistent when a similar evaluation is conducted using the beams in the filtered database. Again, the proposed STM

procedure is a significant improvement over the ACI 318-08 and AASHTO LRFD (2008) provisions.

Many of the specimens in the filtered database were not used to calibrate the proposed STM provisions. However, the proposed procedure estimates the capacity of the beams in the filtered and evaluation database with an equivalent amount of accuracy. The reason that the procedure performs as well for the specimens in the filtered database can be attributed to the fact that is has been mostly derived according to the theoretical principles of strut-and-tie modeling.

6.5.3 Shear Span to Depth Ratio: a/d < 2.5

Recall, the proposed procedure was calibrated using non-hydrostatic nodes for beams with an a/d ratio up to 2.5. The purpose of considering specimens with a/d ratios between 2.0 and 2.5 is to address the discontinuity in shear provisions within the transition region between deep beam and sectional shear design. The fact that the shear strength of a member is reduced as the a/d ratio increases is accounted for by the diminishing dimension of the non-hydrostatic strut-to-node interface. The capacities of all specimens in the evaluation database were estimated using the newly proposed STM provisions, and the AASHTO LRFD (2008) STM provisions to study the transition from deep beam shear to sectional shear. The results of this analysis are summarized Figure 6-28.

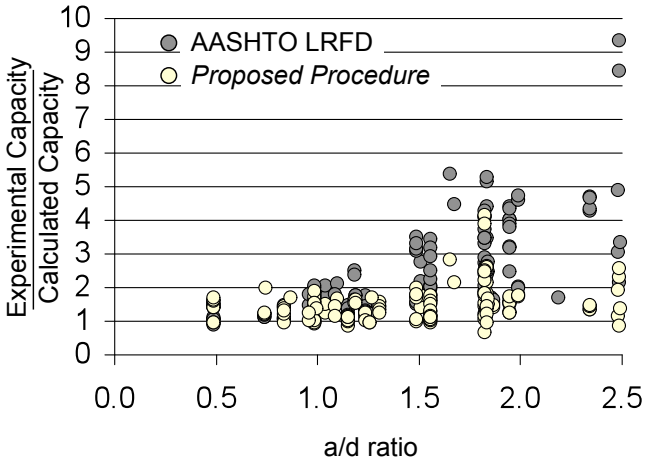

Figure 6-28. AASHTO LRFD (2008) STM provisions vs. the proposed STM provisions for various a/d ratios.

The fact that the AASHTO LRFD (2008) method was derived using hydrostatic nodes results in excessively conservative strength estimations for beams with high a/d ratios (a/d greater than 1.5, approximately). As a result, a large discrepancy exists between deep beam and sectional shear provisions. It is worth noting that the capacities of 14 of the 179 specimens in the evaluation database were over-estimated per the AASHTO LRFD (2007) provisions by at least a factor of 4 for an a/d ratio greater than 1.5. The fact that the proposed procedure was calibrated using non-hydrostatic nodes for beams with an a/d ratio up to 2.5 allows for a smoother transition in calculated shear capacity between deep beam and sectional shear provisions. In other words, the level of conservatism is roughly constant for all a/d ratios as shown in Figure 6-28.

6.5.4 Transverse Reinforcement Ratio: $\rho_{\perp} > 0.1\%$

The proposed procedure was based on beams with a minimum transverse reinforcement ratio of 0.1% perpendicular to the strut (i.e. $\rho_{\perp} \geq 0.1\%$). This is considerably less than what is required by ACI 318-08 and AASHTO LRFD (2008).

When a deep beam is designed by using a strut-and-tie model, transverse reinforcement is required in order to provide sufficient deformation capacity for the assumed *plastic* truss model to develop. Additionally, transverse reinforcement is also necessary to ensure adequate serviceability behavior. The quantity of reinforcement that is required for strength and serviceability is a primary research objective and is discussed in detail by Birrcher (2008).

According to Brown et al. (2006), the amount of transverse reinforcement necessary to maintain the equilibrium of a strut due to spreading of compression is approximately 0.15% in each direction; *fib* (1999) requires a minimum amount of 0.2% in each direction without specifying whether this amount is required for strength, serviceability, or both; and AASHTO LRFD (2008) requires 0.3% in each direction and explicitly denotes it as crack control reinforcement. ACI 318-08 allows the use of unreinforced struts. For a strut to be considered reinforced a minimum amount of 0.3% reinforcement perpendicular to the strut ($\rho_{\perp}$) must be provided.

All design provisions evaluated as part of the current research program were examined using specimens with $\rho_{\perp}$ values as low as 0.1%; i.e. much less than required by ACI 318-08, AASHTO LRFD (2007), or *fib* (1999). In addition, the proposed method summarized in Section 6.6 was calibrated based on the same lightly reinforced specimens. The implications of considering beams with a transverse reinforcement ratio, $\rho_{\perp}$, as low as 0.1%, are presented in Table 6.3 and Figure 6-29.

Table 6.3. Influence that Transverse Reinforcement Ratio has on Accuracy of STM Provision

	$\Sigma\rho_{\perp} \geq 0.001$ *No. = 179*		$\Sigma\rho_{\perp} \geq 0.003$ *No. = 127*		$\rho_v = \rho_h \geq 0.002$ *No. = 44*		$\rho_v = \rho_h \geq 0.003$ *No. = 25*	
	% NG[†]	COV	% NG[†]	COV	% NG[†]	COV	% NG[†]	COV
ACI 318-08	1.7%	0.58	2.4%	0.54	2.3%	0.69	4.0%	0.82
AASTHO LRFD (2008)	3.4%	0.69	1.6%	0.68	0.0%	0.76	0.0%	0.88
fib (1999)	2.8%	0.25	2.4%	0.25	0.0%	0.23	0.0%	0.24
Proposed Method	0.6%	0.28	0.0%	0.27	0.0%	0.33	0.0%	0.36

[†] *%NG* = percentage of beams with Experimental/Calculated ratio < 1.0.

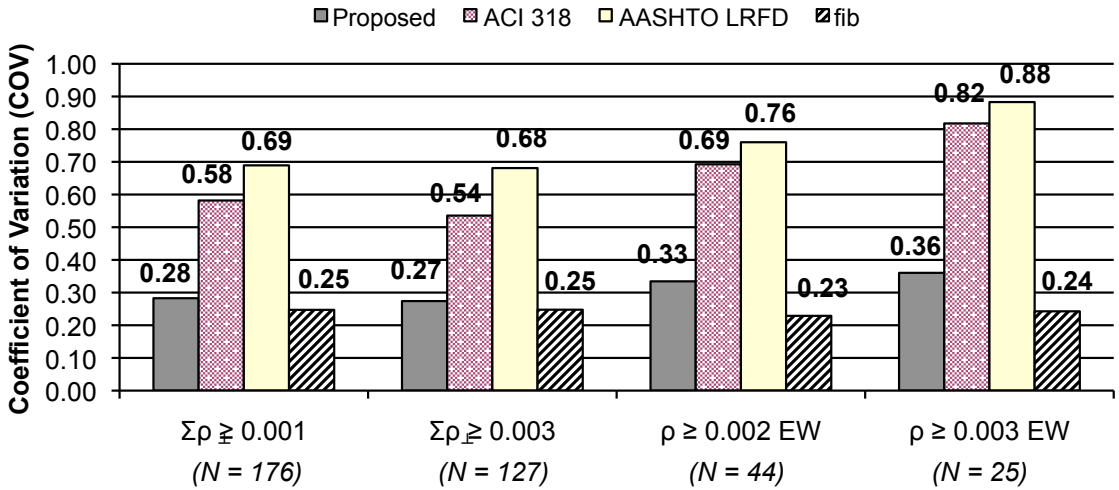

Note: In accordance with ACI 318-08 and AASHTO LRFD (2007), the proposed method contains a limit on the triaxial confinement modification factor equal to 2 (Equation 6-1); whereas, fib (1999) limits this factor to 4 (Equation 2-17). The proposed method would perform slightly better than shown if the triaxial confinement limit were increased to 4 [COV = 0.22; 0.22; 0.24; and 0.24 respectively, for the reinforcement ratios presented in Table 6.3 *and Figure 6-29].*

Figure 6-29. Influence that transverse reinforcement ratio has on the COV of various STM provisions.

The purpose of comparing the performance of the proposed STM provisions for differing amounts of minimum transverse reinforcement is to determine whether the earlier observations in regards to conservatism and accuracy remain valid for the proposed STM methodology. The difficulty with evaluating the provisions for beams with, for example, the AASHTO minimum of 0.3% transverse reinforcement in each direction, is that only a sparse number of beams meet the criteria. More specifically, only 44 beams meet the *fib* (1999) minimum requirement (0.2% in each direction) and only 25 meet the AASHTO LRFD requirement (0.3% in each direction). Therefore, significant conclusions should not be inferred from statistical comparisons based on such small data sets. Nonetheless, upon comparison of the various STM design provisions, it can be seen that the performance of each provision (as indicated by the COV) is relatively equivalent to each another regardless of the minimum amount of reinforcement. As a result, it can be concluded that the lightly reinforced specimens in the evaluation database provide a valid basis of comparison among different STM provisions. In other words, the conclusions remain valid for beams with a higher percentage of crack control reinforcement.

Upon observation of the number of unconservative predictions for the proposed method, it could be concluded that, from a strength standpoint, a transverse reinforcement ratio of $\rho_{\perp} = 0.1\%$ is adequate to ensure that the strength of more than 95% of the specimens in the dataset. However, one of the beams tested as part of the experimental program (Specimen III-1.85-01) had 0.1% vertical and 0.14% horizontal reinforcement ($\rho_{\perp} = 0.15\%$), yet the ratio of experimental to estimated capacity was 0.73 when using the proposed provisions. This low strength value should not be overlooked despite all of the statistical analyses. Therefore, based on the findings of the experimental program, a transverse reinforcement ratio of at least 0.2% in each direction is recommended in order to ensure adequate strength. If less reinforcement is provided, then the chance increases that the capacity will be unconservatively estimated.

The amount of transverse reinforcement required to ensure adequate serviceability behavior is examined in detail and presented by Birrcher (2008). In accordance with the current recommendations by Birrcher (2008), the following minimum required amount of transverse reinforcement and bar spacing is proposed:

$$A_v = 0.003 \cdot b_w \cdot s_1 \qquad \text{Equation 6-3}$$

$$A_{vh} = 0.003 \cdot b_w \cdot s_2$$

$$s_i \leq \begin{pmatrix} d/5 \\ 12in. \end{pmatrix}$$

Where,

A_v = Area of shear reinforcement perpendicular to the flexural tension reinforcement, in^2

A_{vh} = Area of shear reinforcement parallel to the flexural tension reinforcement, in^2

b_w = Width of beam web, in.

s_1 = Center-to-center spacing of transverse reinforcement in the vertical direction, in.

s_2 = Center-to-center spacing of transverse reinforcement in the horizontal direction, in.

It is recommended that the horizontal reinforcement be distributed vertically across the effective area shown in Figure 6-30. The extents of the area are taken as the extents of the direct strut.

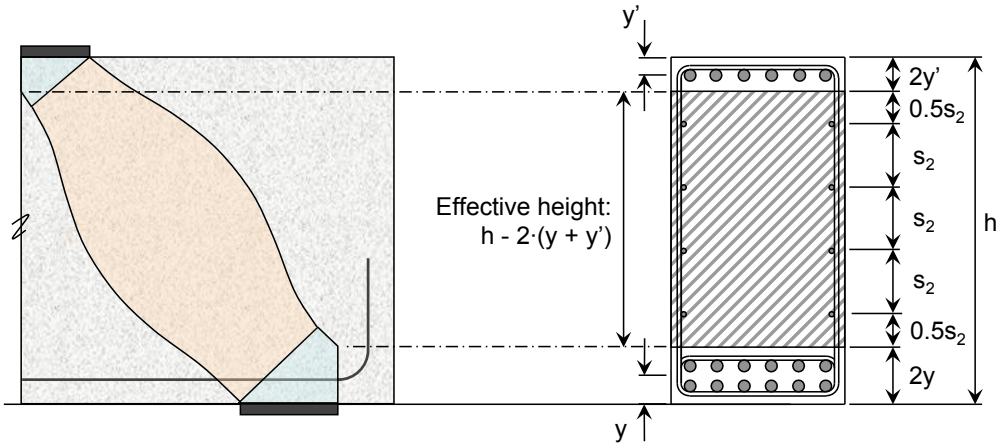

Figure 6-30. Distribution of horizontal reinforcement within effective height.

The extents of the effective height shown are proportioned in order to provide horizontal reinforcement across the area of a deep beam containing the bottle-shaped strut; thereby controlling the crack widths induced by the lateral spreading of compression (Section 2.4.4).

6.6 OUTLINE OF PROPOSED STRUT-AND-TIE MODELING PROCEDURE

A detailed examination of the ACI 318-08, AASHTO LRFD (2008), and *fib* (1999) provisions was conducted and recommendations were discussed for the newly proposed strut-and-tie modeling procedure. For the reader's convenience, the proposed STM procedure is summarized as follows.

6.6.1 Step 1: Define Critical Nodal Regions

Stresses in a D-region concentrate into nodal zones. Failure of a D-region is typically due to crushing of concrete in the nodal region (i.e. strut-to-node interface, bearing face) or anchorage failure. The advantage of a strut-and-tie model over a sectional model for the design of a D-region is that the focus of the design is on the critical nodal regions rather than the less relevant cross-sectional behavior. Efficiency factors are directly dependent on the assumed proportions of the nodal region. The proposed strut-and-tie method is based on the non-hydrostatic node proportions outlined in Section 2.3 and illustrated in Figure 6-31.

(a)

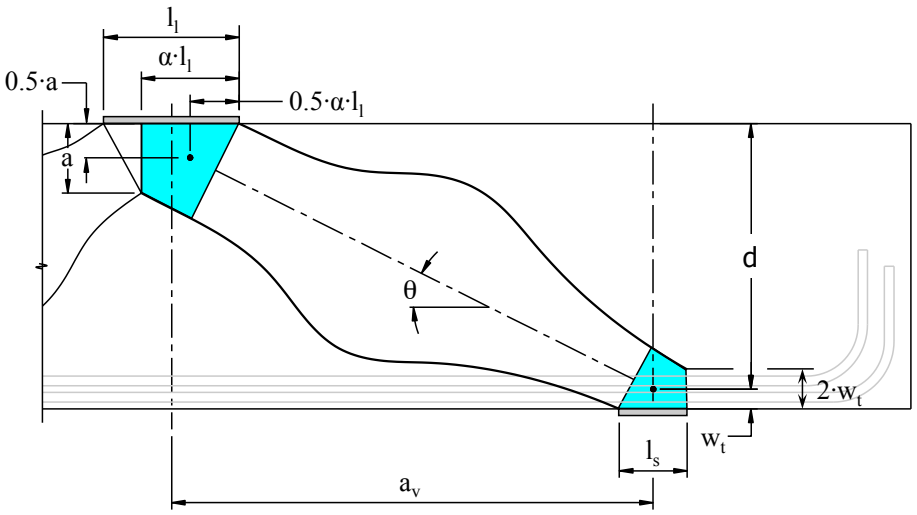

(b)

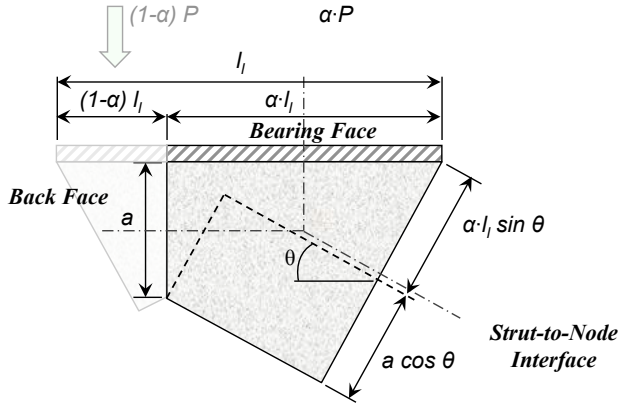

(c)

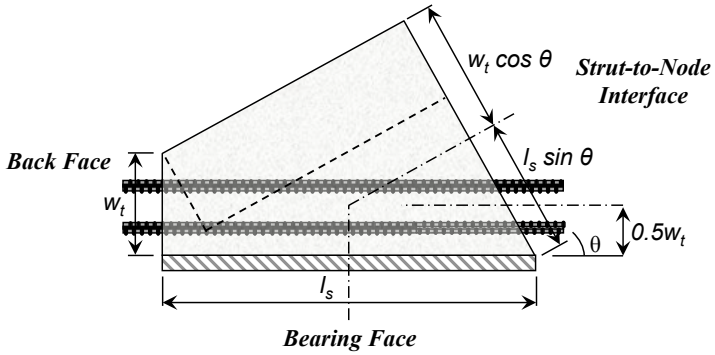

Figure 6-31. (a) Single-panel STM (b) CCC Node (c) CCT Node

Bond stresses in a smeared node region (CTT nodes) and at the back face of the CCT node are not critical if the anchorage of longitudinal bars or stirrups is adequately developed.

6.6.2 Step 2: Design Nodal Regions

The nominal compression strength of a nodal zone, F_n, shall be as follows.

$$F_n = f_{ce} \cdot A_{nz} \qquad \text{Equation 6-4}$$

Where,

f_{ce} = effective compressive strength of concrete in nodal zone, psi

A_{nz} = the area of the face of the nodal zone, in^2

The effective compressive stress, f_{ce}, on the face of a nodal zone shall not exceed the following value.

$$f_{ce} = m \cdot \nu \cdot f_c' \qquad \text{Equation 6-5}$$

Where,

f_c' = Specified compressive strength of concrete, psi

$m = \sqrt{A_2 / A_1} \le 2$, Triaxial confinement modification factor.

Definition of A_2 and A_1 is illustrated in Figure 6-32

ν = 0.85, Bearing and Back Face of CCC node.

0.70, Bearing Face and Back Face of CCT node.

It is not necessary to apply the resultant of bonding stresses directly to the back face of a CCT node provided that tie is adequately anchored.

$\left(0.85 - f_c' / 20ksi\right)$, CCC and CCT Strut-to-Node Interface

Not to exceed 0.65 nor less than 0.45.

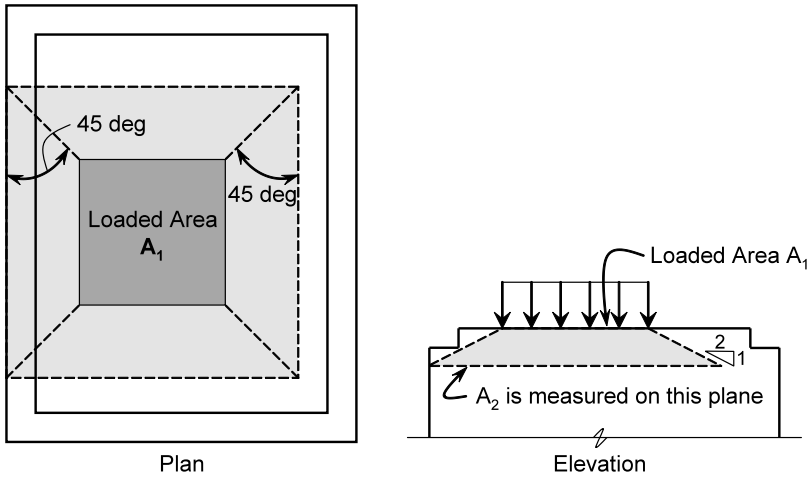

Figure 6-32. Application of frustum to find A_2 in stepped or sloped supports (ACI 318-08).

6.6.3 Step 3: Proper Detailing of Reinforcement

Anchorage, transverse reinforcement, and bar spacing requirements are listed as follows.

6.6.3.1 Anchorage Requirements

Proper placement of tie reinforcement involves distribution of the reinforcement across the width of the tensile zone. The centroid and direction of the reinforcement should coincide with the axis of the tie in the truss model. Ties shall be properly anchored behind the nodal zones. The development length may be measured from the intersection of the extended nodal zone and the centroid of the bars (Figure 6-33). For the sake of simplicity, it may be conservatively measured from the face of the bearing plate.

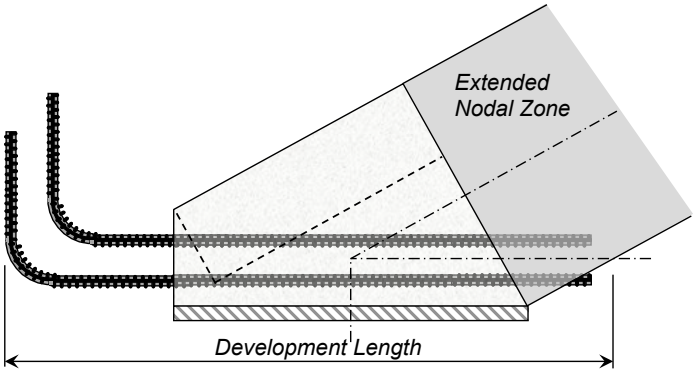

Figure 6-33. Tie development length.

6.6.3.2 Minimum Transverse Reinforcement

The following amount of transverse reinforcement shall be provided to provide integrity and ensure adequate serviceability behavior (Birrcher 2008).

$$A_v = 0.003 \cdot b_w \cdot s_1$$

$$A_{vh} = 0.003 \cdot b_w \cdot s_2$$

$$s_i \leq \begin{pmatrix} d/5 \\ 12in. \end{pmatrix}$$

Where,

A_v = Area of shear reinforcement perpendicular to the flexural tension reinforcement, in^2

A_{vh} = Area of shear reinforcement parallel to the flexural tension reinforcement, in^2

b_w = Width of beam web, in.

s_1 = Center-to-center spacing of vertical reinforcement, in.

s_2 = Center-to-center spacing of horizontal reinforcement, in.

Horizontal reinforcement, s_2, should be distributed within the effective area illustrated in Figure 6-30.

6.7 SUMMARY

A new STM design procedure was developed for the design of deep beams and D-regions. The fundamental principles of the proposed STM methodology

have been derived from existing procedures in ACI 318-08, AASHTO LRFD (2008), and *fib* (1999). The efficiency factors recommended for the proposed procedure have been calibrated using the results of experimental tests, while maintaining consistency with current design provisions. Although the efficiency factors of the proposed procedure were calibrated based on tests of deep beams, they were also calibrated based on maintaining consistency with current design provisions, and theoretical principles. Thus, it is strongly believed that the proposed STM method is valid for other types of structures.

The new method provides a significant improvement in accuracy over the ACI 318-08 and AASHTO LRFD (2008) procedures. Thus, based on the new STM provisions, it is proposed that the ACI 318-08 and AASHTO LRFD (2008) provisions be modified accordingly. A summary of the proposed changes to AASHTO LRFD (2008) and ACI 318-08 is presented in Appendix A and Appendix B respectively. An example problem that illustrates the differences between the existing and proposed provisions is presented in Appendix C.

CHAPTER 7

Summary and Conclusions

7.1 SUMMARY

Since the inclusion of Strut-and-Tie Modeling (STM) provisions in the AASHTO LRFD specifications in 1994, TxDOT engineers have been examining the impact that the provisions have on their design of bent caps. In general, the provisions are considered *confusing* as a result of discrepancies that exist between the current AASHTO LRFD (2008) specifications and the previous AASHTO Standard Specifications (2002). In addition, bents in the State of Texas are experiencing diagonal cracking problems with increasing frequency. These field related issues, taken in combination with discrepancies in the AASHTO LRFD provisions, were the impetus for TxDOT to fund the current project. As a result, the overall objective for the project is to develop safe and consistent design guidelines in regards to both strength and serviceability of bent caps and other deep beams.

In order to accomplish the aforementioned goals, the scope of the project was divided into the following two parts, containing a total of seven specific tasks:

PART I: Tasks presented and investigated in this dissertation.

1. Determine the influence that the distribution of stirrups across the width of a beam web has on the strength and serviceability behavior of a deep beam (Chapter 4).
2. Determine the influence that triaxially confined bearing plates has on the strength and serviceability behavior of a deep beam (Chapter 5).
3. Propose a simple STM design methodology for the design of deep beams (Chapter 6)

PART II: Tasks that will be presented by Birrcher (2008):

4. Determine the influence that the amount of transverse reinforcement has on the strength and serviceability behavior of a deep beam; for varying a/d ratios and depths.
5. Investigate the effectiveness of an STM model in the transition region between deep beam and sectional shear (i.e. at a/d = 2).
6. Recommend a methodology for determining the stress that causes the first diagonal crack for a deep beam.
7. Recommend a methodology for relating the maximum diagonal crack width of a deep beam to its residual capacity.

To achieve the primary research objectives outlined above in the form of specific research tasks, a database containing 904 deep beam specimens was compiled. Of these 904 tests, 36 were conducted as part of the current project; therefore, data from 868 specimens were collected from previous research. It was a goal of the research program to only consider those beams that best represent actual bent caps. In addition, it was necessary to consider a high enough number of beams such that statistically significant conclusion may be reached. As a result, filtering criteria were used to remove 726 beams from the database. The criteria were chosen to consider only beams that best represent bent caps designed in practice. In other words, in order to accomplish the goals of the current project, it was necessary to examine beams whose size and construction was more representative of those used in the field. The remaining 178 tests constitute what is referred to as the *evaluation database*. Of these 178 specimens, 34 were conducted as part of the current project.

7.2 CONCLUSIONS

The conclusions of the current study are presented in this section. The following conclusions are based on the experimental and analytical research conducted in this study.

7.2.1 Distribution of Stirrups across the Web of a Beam

The purpose of this task is to investigate the AASHTO LRFD (2008) STM provision (Section 2.6.4 of this document) that limits the width of a strut framing into a CTT node. Four tests were conducted on beams with a 21"x44" cross-section, and two tests were conducted on beams with a 36"x48" cross-section. Both sets of tests had a shear span-to-depth ratio of 1.85. Stirrup details with two or four legs were investigated. A transverse reinforcement ratio of 0.2% and 0.3% in each direction was investigated. The relative serviceability performance between stirrups with four legs and two legs was compared to one another. A discussion of the influence of reinforcement ratio is presented by Birrcher (2008).

- **The AASHTO LRFD (2008) provision requiring designers to limit the width of a CTT node within a D-region is unnecessary.** Singular node regions are more critical than smeared node regions [*fib* (1999); Schlaich et al. (1987)]. Thus, the focus of a STM design should be placed on the more critical singular node regions. The AASHTO LRFD (2008) CTT node limitation rarely is applicable for the design of a beam region with an a/d ratio less than two. This fact has been validated by experimental tests conducted as part of the current research program for beams as wide as 36-inches. It is proposed that the provision be removed from AASHTO LRFD (2008).
- **The use of additional stirrups across the width of the web did not improve serviceability behavior of beams up to 36-inches wide when 0.3% transverse reinforcement was provided in each direction. However, additional stirrup legs improved the serviceability behavior of beams with 0.2% in each direction.** When 0.3% transverse reinforcement was provided in each direction, the serviceability performance of beams tested as part of the current program was not influenced by the distribution of stirrups across the web. However, crack widths for beams that were reinforced with 0.2% transverse reinforcement in each direction were significantly smaller and more distributed than for beams that contained four stirrup legs.

- **The shear stress at which the first diagonal crack formed was not influenced by the quantity of transverse reinforcement.** The difference between the first cracking loads for specimens containing stirrups with two legs and reinforced with 0.2% and 0.3% transverse reinforcement was within the range of scatter associated with the diagonal cracking capacity of concrete.

7.2.2 Triaxial Confinement of Load and Support Plates (CCC and CCT Nodes)

The purpose of this task is to investigate the influence that triaxial confinement of the load or support plate (CCC or CCT node) has on the shear strength and serviceability behavior of a deep beam. Eight tests were conducted on beams with a 21"x42" cross-section and two were conducted on beams with a 36"x48" cross-section. The shear span-to-depth ratio of all specimens was 1.85. Triaxial confinement of the load and support plates (CCC and CCT nodes) was and a transverse reinforcement ratio of 0.2% and 0.3% in each direction was investigated. The relative serviceability performances between confined and unconfined bearing plates were compared to one another. A discussion of the influence of reinforcement ratio is presented by Birrcher (2008).

- **The capacity of all faces of the CCC and CCT nodal region can be increased by the bearing capacity factor, $\sqrt{A_2/A_1}$, included in the AASHTO LRFD (2008) and ACI 318-08 provisions.** ACI 318-08 §10.14 and AASHTO LRFD (2008) Article 5.7.5 allow for an increase in the bearing capacity of concrete when triaxial confinement is present. Based on the experimental and analytical results of this research program, it was found that an increase in the capacity of the CCC or CCT nodal region by a similar factor provided for more accurate STM estimations with less unnecessary conservatism.
- **For specimens that contained a ratio of 0.2% transverse reinforcement in each direction, the serviceability behavior was more sensitive to the bearing plate configuration and reinforcement details.** In general, the crack

widths and crack distribution for beams with 0.2% transverse reinforcement in each direction were wider and more erratic than beams reinforced with 0.3% transverse reinforcement in each direction.

- **The shear stress at which the first diagonal crack formed was not influenced by triaxial confinement of the load or support plate.** The difference between the first cracking loads for specimens containing 0.2% and 0.3% transverse reinforcement was within the range of scatter associated with the diagonal cracking capacity of concrete.

7.2.3 Newly Proposed STM Design Provisions

A new STM design procedure was developed for the design of deep beams. The new method was formulated based on the methodology used in *fib* (1999) while maintaining consistency with ACI 318-08 and AASHTO LRFD (2008). In addition, the proposed method was calibrated based on beams that were considered more representative of beams designed in practice – in terms of their size and reinforcement details.

In developing an STM procedure, it was necessary to explicitly define the truss geometries. This step cannot be over-emphasized as the performance of an STM methodology and its efficiency factors are intrinsically linked to the geometry of the nodal regions. Thus, the following proposal is based on an explicitly defined single-panel truss model with non-hydrostatic nodes. This model was used to define all of the beams in the evaluation database.

Another important aspect of the new STM design methodology is that it was comprehensively derived based on all the stress checks that constitute an STM design. Stress checks at all six nodal faces (three faces at CCC and three faces at CCT nodes) and in the longitudinal tie were performed for all of the beams in the evaluation database. The splitting of the strut was indirectly accounted for by only considering those beams that contained a minimum amount of transverse reinforcement. The results of the stress checks were used to formulate the new STM design provisions. Thus, the newly proposed design

procedure considers every facet of an STM design. Accordingly, the following conclusion can be made:

- **The newly proposed STM procedure is: (i) simpler; (ii) more accurate and (iii) more conservative than the ACI 318-08 and AASHTO LRFD (2008) STM design provisions.** The procedure is based on the fundamental principles of STM and on the procedures established in ACI 318-08, AASHTO LRFD (2008), and *fib* 1999. Thus, it has been derived based on theoretical principle, tests of D-regions, and by maintaining consistency with current design provisions. The procedure is practical and has been derived in a comprehensive and transparent manner. Implementation of the new design provisions into AASHTO LRFD (2008) and ACI 318-08 is recommended and presented in Appendix A and B, respectively.

APPENDIX A

Proposed Changes to the AASHTO LRFD (2008) Bridge Design Specifications

A.1 INTRODUCTION

The STM design methodology presented in Chapter 6 can be incorporated into the AASHTO LRFD (2008) strut-and-tie provisions. The advantage of the proposed methodology is that the procedure significantly simplifies the current AASHTO LRFD (2008) STM provisions because the determination of the tensile strain transverse to the CCT node is no longer required. In addition, the proposed procedure is significantly more accurate than the current AASHTO LRFD method, as illustrated in Chapter 6. Finally, the proposed method removes unnecessary conservatism of the AASHTO LRFD (2008) provisions at high shear span-to-depth ratios ($2.0 \geq a/d \geq 1.5$)

Proposed changes to the AASHTO LRFD (2008) provisions are presented as follows. An explanation of the changes is presented as in Section A.3.

A.2 PROPOSED CHANGES TO AASHTO LRFD BRIDGE DESIGN SPECIFICATIONS

5.6.3 Strut-and-Tie Model

5.6.3.1 General

Strut-and-tie models may be used to determine internal force effects near supports and the points of application of concentrated loads at strength and extreme event limit states.

The strut-and-tie model should be considered for the design of deep footings and pile caps or other situations in which the distance between the centers of applied load and the supporting reactions is less than about twice the member **depth**.

The angle between the axes of any strut and any tie entering a single node shall not be taken as less than 25 degrees.

If the strut-and-tie model is selected for structural analysis, Articles 5.6.3.2 through 5.6.3.6 shall apply.

C5.6.3.1

Where the conventional methods of strength of materials are not applicable because of nonlinear strain distribution, strut-and-tie modeling may provide a convenient way of approximating load paths and force effects in the structure. The load paths may be visualized and the geometry of concrete and steel **reinforcement** selected to implement the load path.

The strut-and-tie model is new to these Specifications. More detailed information on this method is given by Schlaich et al. (1987) and Collins and Mitchell (1991).

Traditional section-by-section design is based on the assumption that the reinforcement required at a particular section depends only on the separated values of the factored section force effects V_u, M_u, and T_u and does not consider the mechanical interaction among these force effects as the strut-and-tie model does. The traditional method further assumes that shear distribution will vary linearly over the depth of the beam.

For members such as the deep beam shown in Figure C5.6.3.2-1, these assumptions are not valid. The behavior of a component, such as a deep beam, can be predicted more accurately if the flow of forces through the complete structure is studied. Instead of determining V_u and M_u at different sections along the span, the flow of compressive stresses going from the loads, P, to the supports and the required tension force to be developed between the supports should be established.

The angle between the axes of a strut and tie should be limited between 25 to 65 degrees in order to mitigate wide crack openings and excessive strain in the

reinforcement at failure.

For additional applications of the strut-and-tie model, see Articles 5.10.9.4, 5.13.2.3, and 5.13.2.4.1.

5.6.3.2 Structural Modeling

The structure and a component or region, thereof, may be modeled as an assembly of steel tension ties and concrete compressive struts interconnected at nodes to form a truss capable of carrying all applied loads to the supports. The determination of a truss is dependent on the geometry of the CCC and CCT nodal regions as defined in Figure 1. The geometry of these singular nodal regions shall be detailed as shown in Figures 1 and 2. Proportions of nodal regions are dependent on the bearing dimensions, reinforcement location, and depth of the compression zone as illustrated in Figure 2.

Interior nodes that are not bounded by a bearing plate are referred to as smeared nodes. Since D-regions contain both smeared and singular nodes, the latter will be critical and a check of concrete stresses in smeared nodes is unnecessary (Schlaich et al. 1987)

The nominal resistance of each face of a nodal region and of a tie, ϕP_n , shall be proportioned to be greater than the factored force acting on the node face or in the tie, P_u :

$$\phi P_n \geq P_u \qquad \text{(A-1)}$$

where:

P_n = nominal resistance of **a node face** or tie (kip)

P_u = factored force acting on the face of a node or in a tie (kip)

ϕ = resistance factor for tension or compression specified in Article 5.5.4.2, as appropriate

C5.6.3.2

Cracked reinforced concrete carries load principally by compressive stresses in the concrete and tensile stresses in the reinforcement. The principle compressive stress trajectories in the concrete can be approximated by compressive struts. Tension ties are used to model the principal reinforcement.

A strut-and-tie model is shown in **Figure 1 for a simply supported deep beam**. The zone of high unidirectional compressive stress in the concrete is represented by a compressive strut. The regions of the concrete subjected to multidirectional stresses, where the struts and ties meet the joints of the truss, are represented by nodal zones.

Research has shown that a direct strut is the primary mechanism for transferring shear within a D-region. Therefore, a single-panel truss model is illustrated in Figure 1 and may be used in common D-regions such as: transfer girders, bents, pile caps, or corbels.

Stresses in a strut-and-tie model concentrate at the nodal zones. Failure of the structure may be attributed to the crushing of concrete in these critical nodal regions. For this reason, the capacity of a truss model may be directly related to the geometry of the nodal regions. Conventional techniques to be used for proportioning nodes are illustrated in Figure 2.

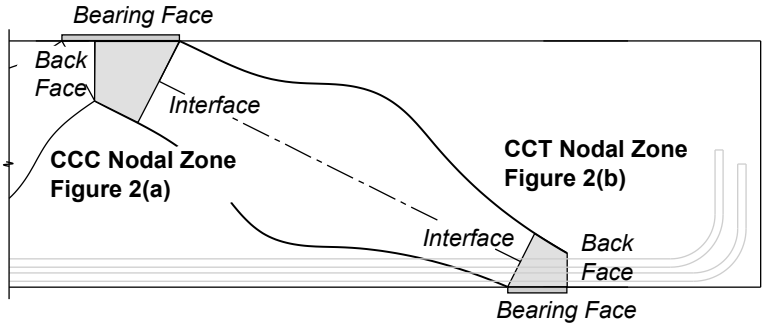

Figure 5.6.3.2-1 Strut-and-Tie Model for a Deep Beam

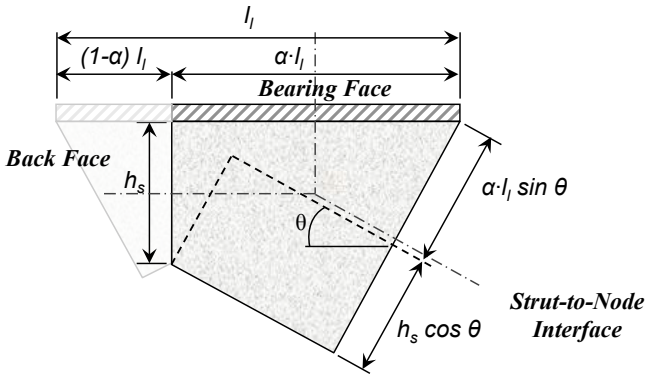

α = portion of the applied load that is resisted by near support

(a) CCC Node

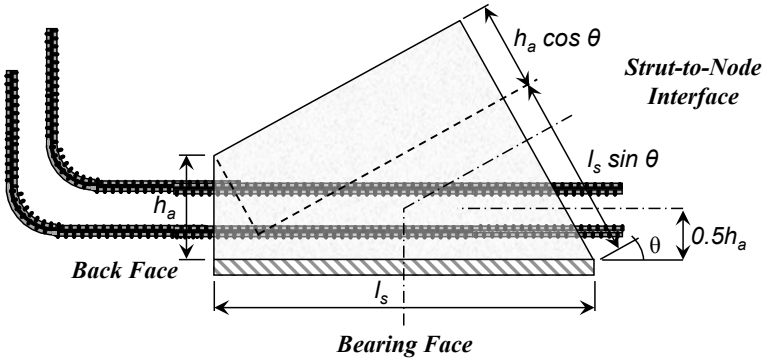

(b) CCT Node

Figure 5.6.3.2-2. Nodal Geometries.

5.6.3.3 Proportioning of Nodal Regions

5.6.3.3.1 Strength of ***the Face of a Node***

The nominal resistance of **the face of a node** shall be taken as:

$$P_n = f_{cu} \cdot \mathbf{A_{cn}} \qquad \text{(A-2)}$$

where:

P_n = nominal resistance of a **the face of a node** (kip)

f_{cu} = limiting compressive stress as specified in Article 5.6.3.3.3 (ksi)

$\mathbf{A_{cn}}$ = effective cross-sectional area of **the face of a node** as specified in Article 5.6.3.3.2 (in^2)

5.6.3.3.2 Effective Cross-Sectional Area of the Face of a Node

The value of $\mathbf{A_{cn}}$ shall be determined by considering the **details of the nodal region as illustrated in Figure 2**.

When a strut is anchored by reinforcement, **the back face of the CCT node, h_a,** may be considered to extend **twice the** distance **from the exterior surface of the beam to the centroid of the longitudinal tensile reinforcement**, as shown in **Figure 2(b).**

The depth of the back face of the CCC node, h_s , as shown in Figure 2(a), may be taken as the effective depth of the compression stress block determined from a conventional flexural analysis.

C5.6.3.3.2

A direct strut is the primary shear carrying mechanism for a deep beam. Therefore, previous reference to CTT nodal regions has been removed from the Specifications in order to place the emphasis of a deep beam design on the more critical CCC and CCT nodal regions.

Research has shown that the shear behavior of conventionally reinforced deep beams, as wide as 36 inches, are not significantly influenced by the distribution of stirrups across the section. Beams wider than 36 inches, or beams with a width to height aspect ratio greater than one may benefit from the addition of distributed stirrup legs.

5.6.3.3.3 Limiting Compressive Stress at the Face of a Node

Unless confining reinforcement is provided and its effect is supported by analysis or experimentation, the limiting compressive stress at the face of a node, f_{cu}, shall be taken as:

$$f_{cu} = m \cdot \nu \cdot f_c' \qquad \text{(A-3)}$$

where:

f_c' = specified compressive strength of concrete (psi)

m = confinement modification factor, taken as $\sqrt{A_2/A_1}$ but not more than 2 as defined in Article 5.7.5

v = concrete efficiency factor:

0.85, bearing and back face of CCC node

0.70, bearing and back face of CCT node

The stress applied to the back face of CCT node may be reduced as permitted in 5.6.3.3.3-1.

$0.85 - f_c'/20ksi$, CCC and CCT strut-to-node interface

Not to exceed 0.65 nor less than 0.45

0.45, CCC and CCT strut-to-node interface:

Structures that do not contain crack control reinforcement (Article 5.6.3.5)

In addition to satisfying strength criteria, the node regions shall be designed to comply with the stress and anchorage limits specified in Article 5.6.3.4.1 and 5.6.3.4.2.

5.6.3.3.3-1 Back Face of CCT Node

Bond stresses resulting from the force in a developed tension tie need not be applied to the back face of the CCT node.

C5.6.3.3.3

Concrete efficiency factors have been selected based on simplicity in application, compatibility with other sections of the Specifications, compatibility with tests of D-regions, and compatibility with other provisions.

C5.6.3.3.3-1

The stress that must be resisted by the back face of a CCT node can be attributed to the anchorage of the tie, bearing from an anchor plate or headed bar, or an external indeterminacy such as that which occurs at a node over a continuous support (Figure C1).

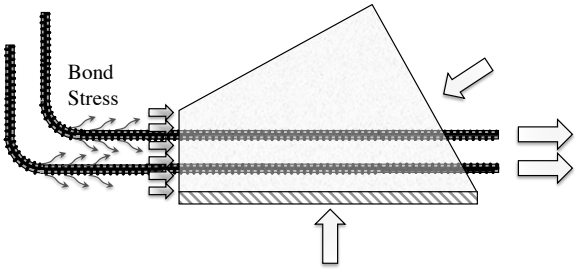

(a) Bond stress resulting from the anchorage of a developed tie.

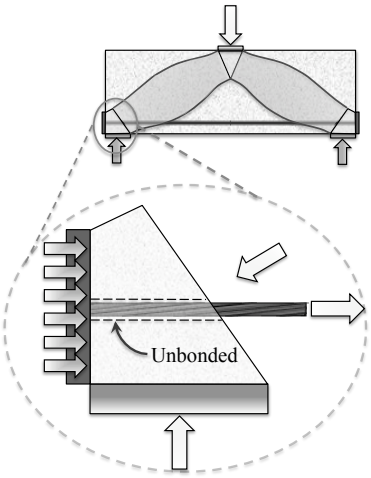

(b) Bearing stress applied from an anchor plate or headed bar.

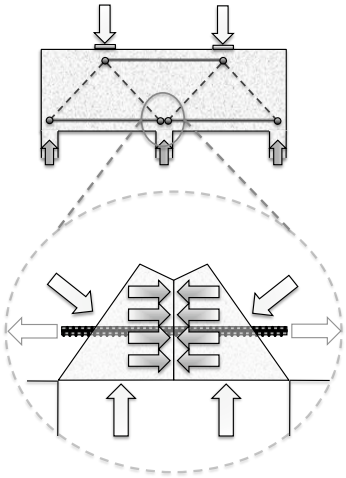

(c) Interior node over a continuous support.

Figure C5.6.3.3.3-1. Stress condition at the back face of a CCT node

If the tie is adequately developed, the bonding stresses are not critical and need not be applied as a direct force to the back face of a CCT node.

If the stress applied to the back face of a CCT node is the result of a combination of both anchorage and a discrete force from another strut, it is only necessary to proportion the node to resist the direct compression stresses. It is not necessary to apply the bonding stresses to the back face, provided the tie is adequately anchored.

5.6.3.4 Proportioning of Tension Ties

5.6.3.4.1 Strength of Tie

Tension tie reinforcement shall be anchored to the nodal zones by specified embedment lengths, hooks, or mechanical anchorages. The tension tie force shall be developed at the inner face of the nodal zone.

The nominal resistance of a tension tie in kips shall be taken as:

$$P_n = f_y A_{st} + A_{ps}[f_{pe} + f_y] \qquad \text{(A-4)}$$

where:

A_{st} = total area of longitudinal mild steel reinforcement in the tie (in^2)

A_{ps} = area of prestressing steel (in^2)

f_y = yield strength of mild steel longitudinal reinforcement (ksi)

f_{pe} = stress in prestressing steel due to prestress after losses (ksi)

5.6.3.4.2 Anchorage of Tie

The tension tie reinforcement shall be anchored to transfer the tension force therein to the node regions of the truss in accordance with the requirements for development of reinforcement as specified in Article 5.11

5.6.3.5 Crack Control Reinforcement

[Refer to Birrcher (2008) for proposed changes.]

C.5.6.3.4.1

The second term of the equation for P_n is intended to ensure that the prestressing steel does not reach its yield point, thus a measure of control over unlimited cracking is maintained. It does, however, acknowledge that the stress in the prestressing elements will be increased due to the strain that will cause the concrete to crack. The increase in stress corresponding to this action is arbitrarily limited to the same increase in stress that the mild steel will undergo. If there is no mild steel, f_y may be taken as 60.0 ksi for the second term of the equation.

A.3 EXPLANATION FOR PROPOSED CHANGES

Currently, AASHTO LRFD (2008) is organized such that a STM is separated into its primary elements: struts, ties, and nodes and designed accordingly. The philosophy of the proposed method is slightly different in that the design of a strut and node-to-strut interface is not distinguished from one another. Stresses concentrate within the nodal region, so the design of the node-to-strut interface indirectly accounts for the design of a strut. As a result, the proposed changes to AASHTO LRFD (2008) reorganize the design of a strut-and-tie model into the design of the nodal regions, and the design of the ties. Reference to the *design of a strut* and *design of a reinforced strut* has been removed to place the emphasis of a deep beam design on the critical nodal regions. The design of a strut is accounted for with the design of the node to strut interface.

A detailed explanation of the proposed limiting compressive stress (Equation A-3) is presented in Chapter 6.

In addition, the truss model used to derive the newly proposed efficiency factors is presented in Figures 1 and 2. The purpose for including this model in the code is to provide some explicit guidance for designers and to provide consistency between an AASHTO LRFD (2008) truss model and the model used to derive the new efficiency factors.

It is proposed that reference to CTT nodal regions be removed from the AASHTO LRFD deep beam provisions. A CTT node is typically a smeared node and is not as critical as a singular node. The purpose for removing the provision is to place the emphasis of a deep beam design on the critical stresses in the singular, CCC and CCT nodal regions**.**

The experimental program investigated the effectiveness of distributing reinforcement across the beam web; a discussion is provided in Chapter 4. Based on the findings of the program, it was concluded that the use of a multiple-panel

model was not appropriate for test specimens with an a/d ratio less than two. For the reasons discussed in Chapter 6, a single-panel model was selected to represent the shear transfer mechanism for deep beams with an a/d ratio less than two.

A.4 SUMMARY

Proposed changes to the AASHTO LRFD Bridge Design Specifications are summarized in this Appendix. These changes are based on the proposed STM design methodology presented in Chapter 6. The primary changes to AASHTO LRFD are: (i) the new efficiency factors; and (ii) the reorganization of the provisions to focus the design of a truss model on the nodal regions rather than the struts. As a result, the design of a strut is indirectly accounted for with the design of the strut-to-node interface.

A design example of a multiple column bent is presented in Appendix C in order to illustrate the differences between the proposed provisions and the current AASHTO LRFD (2008) Bridge Design Specifications.

APPENDIX B

Proposed Changes to ACI 318-08 Appendix A, Strut-and-Tie Models

B.1 INTRODUCTION

The STM design methodology presented in Chapter 6 can be incorporated into the ACI 318-08 STM provisions. The advantage of the proposed methodology is that the procedure removes some of the ambiguity associated with the loosely defined truss model and the redundant stress checks contained in the ACI 318-08 provisions. Also, the proposed procedure is significantly more accurate than the current ACI 318-08 method, as illustrated in Chapter 6.

Proposed changes to the ACI 318-08 provisions are presented as follows. An explanation of the changes is presented in Section B.3.

B.2 CHANGES TO ACI 318-08 APPENDIX A, STRUT-AND-TIE MODELS

A.2 Strut-and-tie model design procedure

A.2.1 – It shall be permitted to design structural concrete members, or D-Regions in such members, by modeling the member or region as an idealized truss. The truss model shall contain struts, ties, and nodes as defined in A.1. The truss model shall be capable of transferring all factored loads to the supports or adjacent B-regions.

A.2.2 – The strut-and-tie model shall be in equilibrium with the applied loads and the reactions.

A.2.3 – In determining the geometry of the truss, the dimensions of the struts, ties, and nodal zones shall be taken into account.

A.2.4 – Ties shall be permitted to cross struts. Struts shall cross or overlap only at nodes.

A.2.5 – The angle, θ, between the axes of any strut and any tie entering a single node shall not be taken as less than 25 degrees.

A.2.6 - The determination of a truss is dependent on the geometry of the CCC and CCT nodal regions as defined in Figure 1. The geometry of these singular nodal regions shall be detailed as shown in Figures A-1 and A-2. Proportions of nodal regions are dependent on the bearing dimensions, reinforcement

RA.2 – Strut-and-tie model procedure

RA.2.1 – The truss model described in A.2.1 is referred to as a strut-and-tie model. Details of the use of strut-and-tie models are given in Reference A.1 through A.7.

Strut-and-tie models represent strength limit states and designers should comply with the requirements for serviceability in the code. Deflections of deep beams or similar members can be estimated using an elastic analysis to analyze the strut-and-tie model. In addition, the crack widths in a tie can be checked using 10.6.4, assuming the tie is encased in a prism of concrete corresponding to the area **illustrated in Figure A-2(b).**

RA.2.5 – The angle between the axes of the struts and ties acting on a node should be large enough to mitigate cracking and to avoid incompatibilities due to shortening of the struts and lengthening of the ties occurring in almost the same directions. This limitation on the angle prevents modeling the shear spans in slender beams using struts inclined at less than 25 degrees from the longitudinal steel. See Reference A.6

RA.2.6 - Research has shown that a direct strut is the primary mechanism for transferring shear within a D-region. Therefore, a single-panel truss model is illustrated in Figure 1 and may be used in common D-regions such as: transfer girders, bents, pile caps, or corbels.

location, and depth of the compression zone as illustrated in Figure A-2.

A.2.7 - Interior nodes that are not bounded by a bearing plate are referred to as smeared nodes. Since D-regions contain both smeared and singular nodes, the latter will be critical and a check of concrete stresses in smeared nodes is unnecessary (Schlaich et al. 1987)

Stresses in a strut-and-tie model concentrate at the nodal zones. Failure of the structure may be attributed to the crushing of concrete in these critical nodal regions. For this reason, the capacity of a truss model may be directly related to the geometry of the nodal regions. Conventional techniques to be used for proportioning nodes are illustrated in Figure A-2.

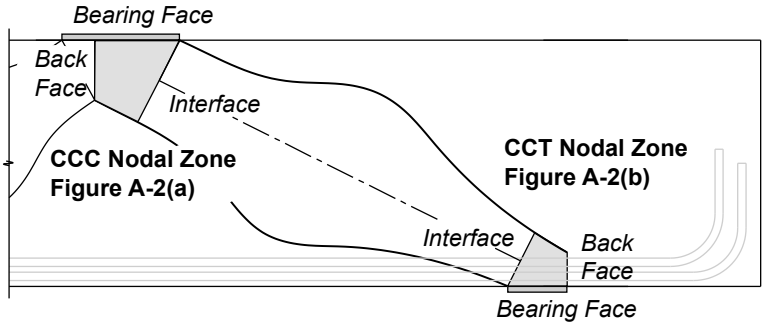

Figure A-1 Strut-and-Tie Model for a Deep Beam

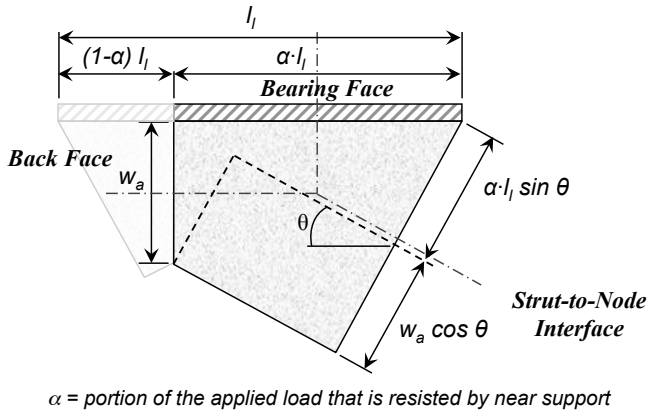

(a) CCC Node

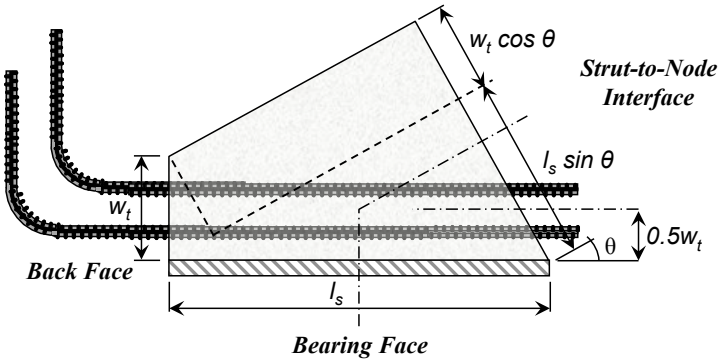

(b) CCT Node

Figure A-2. Nodal Geometries.

A.2.7 – Design of struts, ties, and nodal zones shall be based on

$$\varphi F_n \geq F_u \qquad \text{(A-1)}$$

where $\mathbf{F_u}$ is the factored force acting in a strut, in a tie, or on one face of a nodal zone; $\mathbf{F_n}$ is the nominal strength of the strut, tie, or nodal zone; and $\boldsymbol{\phi}$ is specified in 9.3.2.6.

RA.2.7 – Factored loads are applied to the strut-and-tie model, and the forces in all the struts, ties, and nodal zones are computed. If several loading cases exist, each should be investigated. The strut-and-tie model, or models, are analyzed for the loading cases and, for a given strut, tie, or nodal zone, $\boldsymbol{F_u}$ is the largest force in that element for all loading cases

A.3 Strength of struts

A.3.1 – The nominal compressive strength of a strut without longitudinal reinforcement, F_{ns}, shall be taken as the smaller value of

RA.3 – Strength of struts

RA.3.1 – The width of strut, $\boldsymbol{w_s}$ used to compute $\boldsymbol{A_{cs}}$ is the smaller dimension perpendicular to the axis of the strut at the ends of the strut. This strut

$$F_{ns} = f_{ce}A_{cs} \quad \text{(A-2)}$$

at the two ends of the strut, where $\mathbf{A_{cs}}$ is the cross-sectional area at one end of the strut, and $\mathbf{f_{ce}}$ is

the effective compressive strength of the concrete **at the node-to-strut interface** given in A.**6**.2.

A.4 Minimum Reinforcement

A.4.1 – Except for slabs or footings, a minimum amount of shear reinforcement shall be provided according to A.4.2 and A.4.3.

A.4.2 – The area of shear reinforcement perpendicular to the flexural tension reinforcement, A_v, shall not be less than $0.002b_ws_1$, and s_1 shall not exceed the smaller of d/5 and 12 in.

A.4.3 – The area of shear reinforcement parallel to the flexural tension reinforcement, A_{vh}, shall not be less than $.002b_ws_2$, and s_2 shall not exceed the smaller of d/5 and 12 in.

A.4.4 – [Serviceability requirement per Birrcher (2008)]

A.5 – Strength of Ties

A.5.1 – The nominal strength of a tie, Fnt , shall be taken as

$$F_{nt} = A_{ts}f_y + A_{tp}(f_{se} + \Delta f_p) \quad \text{(A-3)}$$

where $\mathbf{(f_{se} + \Delta f_p)}$ shall not exceed $\mathbf{f_{py}}$, and $\mathbf{A_{tp}}$ is zero for nonprestressed members.

In Eq. (A-3), it shall be permitted to take $\mathbf{\Delta f_p}$ equal to 80,000 psi for bonded prestressed reinforcement or 10,000 psi for unbonded reinforcement. Other values of $\mathbf{\Delta f_p}$ shall be permitted when justified by analysis.

A.5.2 – The axis of the tie reinforcement in a tie shall coincide with the tie in the strut-and-tie model

width is illustrated in **Figure A-2(a) and A-2(b)**.

Stresses in a strut-and-tie model concentrate at the nodal regions. Design of a strut at the strut-to-node interface is accounted for with the design of the nodal regions in A.6.

RA.4 – Transverse reinforcement in the vertical and horizontal direction provides deformation capacity for a structural member and reduces the risk of a premature failure after cracking has occurred.

RA.5.2 – The effective tie width assumed in design, $\mathbf{w_t}$, **may be considered to extend twice the distance from the exterior surface of the beam to the centroid of the longitudinal tensile reinforcement, as shown in Figure A-2(b)**

A.5.3 – Tie reinforcement shall be anchored by mechanical devices, post-tensioning anchorage devices, standard hooks, or straight bar development as required by A.5.3.1 through A.5.3.4.

A.5.3.1 – Nodal zones shall develop the difference between the tie force on one side of the node and the tie force on the other side.

A.5.3.2 – At nodal zones anchoring one tie, the tie forces shall be developed at the point where the centroid of the reinforcement in a tie leaves the extended nodal zone and enters the span.

A.5.3.3 – At nodal zones anchoring two or more ties, the tie force in each direction shall be developed at the point where the centroid of the reinforcement in the tie leaves the extended nodal zone.

A.5.3.4 – The transverse reinforcement required by A.4 shall be anchored in accordance with 12.13.

RA.5.3 – Figure RA-1 shows two ties anchored at the nodal zone. Development is required where the centroid of the tie crosses the outline of the extended nodal zone.

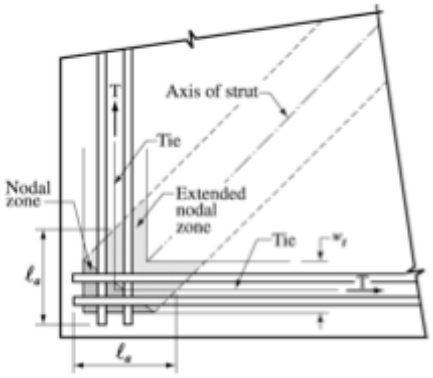

Figure RA-1 – Extended Nodal Zone Anchoring Two Ties (ACI 318-08)

The development length of the tie reinforcement can be reduced through hooks, mechanical devices, additional confinement, or by splicing it with several layers of smaller bars.

A.6 – Strength of nodal zones

A.6.1 – The nominal compression strength of a nodal zone, $\mathbf{F_{nn}}$, shall be

$$\mathbf{F_{nn} = f_{ce}A_{nz}} \qquad \text{(A-4)}$$

where $\mathbf{f_{ce}}$ is the effective compressive strength of the concrete in the nodal zone as given in A.**6**.2, and $\mathbf{A_{nz}}$ is the smaller of (a) and (b):

(a) The area of the face of the nodal zone on which $\mathbf{F_u}$ acts, taken perpendicular to the line of action of $\mathbf{F_u}$

(b) The area of a section through the nodal zone, taken perpendicular to the line of action of the resultant force on the section.

RA.6 – Strength of Nodal Zones

RA.6.1 – The value of A_{nz} shall be determined by considering the details of the nodal region as illustrated in Figure A-2.

When a strut is anchored by reinforcement, the back face of the CCT node, h_a, may be considered to extend twice the distance from the exterior surface of the beam to the centroid of the longitudinal tensile reinforcement, as shown in Figure 2(b).

The depth of the back face of the CCC node, h_s , as shown in Figure 2(a), may be taken as the effective depth of the compression stress block determined from a conventional flexural analysis.

A.**6**.2 – Unless confining reinforcement is provided within the nodal zone and its effect is supported by tests and analysis, the calculated effective compressive stress, $\mathbf{f_{ce}}$, on a face of a nodal zone due to the strut-and-tie forces shall not exceed the value given by

$$f_{ce} = 0.85 \cdot \beta_n \cdot m \cdot f_c' \qquad \text{(A-5)}$$

where the confinement modification factor, m, is taken as $\sqrt{A_2/A_1}$ **but not more than 2 as defined in 10.14. The** value of β_n is given in A.**6**.2.1 through A.**6**.2.**4**.

A.6.2.1 **–At the bearing and back face of a CCC node***:* $\beta_n = 1.0$***;***

A.6.2.2 **– At the bearing and back face of a CCT node:** $\beta_n = 0.85$***;***

The stress applied to the back face of a CCT node may be reduced as permitted in A.6.2.3

A.6.2.3 - Bond stresses resulting from the force in a developed tension tie need not be applied to the back face of the CCT node.

RA.6.2 – The nodes in two-dimensional members, such as deep beams, can be classified as **CCC** if all the members intersecting at the node are in compression; as **CCT** if on of the members acting on the node is in tension, and so on. The effective compressive strength of the nodal zone is given by Eq. (A-5), as modified by A.6.2.1 through A.6.2.3

The β_n values reflect the increasing degree of disruption of the nodal zones due to the incompatibility of tension strains in the ties and compression strains in the struts. The stress on any face of the nodal zone or on any section through the nodal zone should not exceed the value given by Eq. (A-5), as modified by A.6.2.1 through A.6.2.3.

The β_n values have been selected based on simplicity in application, compatibility with other sections of the Code, compatibility with tests of D-regions, and compatibility with other provisions

RA.6.2.3 - The stress that must be resisted by the back face of a CCT node can be attributed to the anchorage of the tie, bearing from an anchor plate or headed bar, or an external indeterminacy such as that which occurs at a node over a continuous support (Figure RA-2).

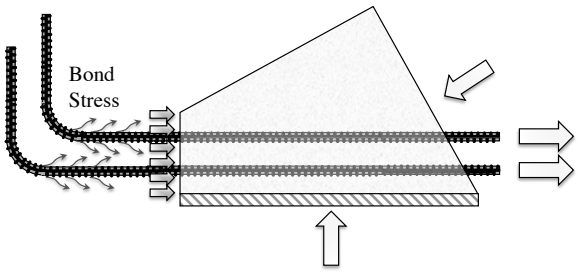

(a) Bond stress resulting from the anchorage of a developed tie.

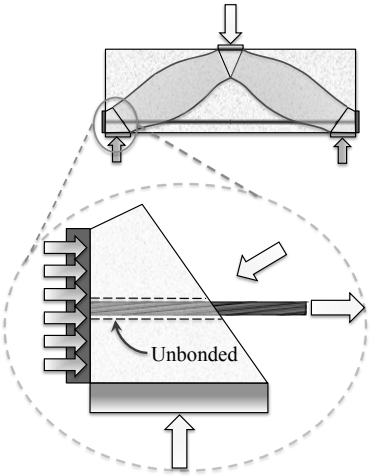

(b) Bearing stress applied from an anchor plate or headed bar.

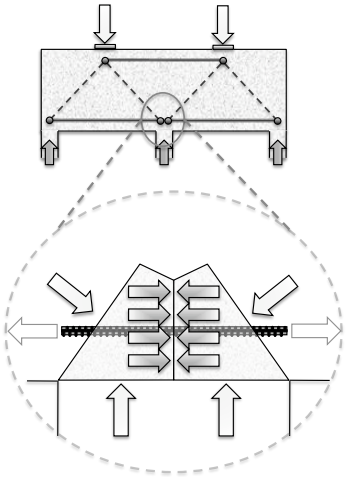

(c) Interior node over a continuous support.

Figure RA-2. Stress condition at the back face of a CCT node

If the tie is adequately developed, the bonding stresses are not critical and need not be applied as a direct force to the back face of a CCT node.

If the stress applied to the back face of a CCT node is the result of a combination of both anchorage and a discrete force from another strut, it is only necessary to proportion the node to resist the direct compression stresses. It is not necessary to apply the bonding stresses to the back face, provided the tie is adequately anchored.

A.6.2.4 **–At the CCC and CCT strut-to-node interface:**

(a) Structures meeting the minimum reinforcement requirements of A.4.2 and A.4.3:

$$\beta_n = 1 - \frac{f_c'}{17ksi} \qquad \textbf{(A-6)}$$

not less than 0.50 nor more than 0.75.

(b) Structures not meeting the minimum reinforcement requirements of A.4.2 and A.4.3: $\beta_n = 0.50$

(c) For struts in tension members, or the tension flanges of members: $\beta_n = 0.40$

A.6.2.5 – For all other cases: $\beta_n = 0.60$

A.**6**.3 – In a three-dimensional strut-and-tie model, the area of each face of a nodal zone shall not be less than that given in A.**6**.1, and the shape of each face of the nodal zones shall be similar to the shape of the projection of the end of the struts onto the corresponding faces of the nodal zones.

RA.6.3 – This description of the shape and orientation of the faces of the nodal zone is introduced to simplify the calculations of the geometry of a three-dimensional strut-and-tie model.

B.3 EXPLANATION FOR PROPOSED CHANGES

Currently, ACI 318-08 is organized such that a STM is separated into its primary elements: struts, ties, and nodes; and designed accordingly. The philosophy of the proposed method is slightly different. The geometry of a truss model is completely dependent on the geometry of the nodal regions. The design of a strut and node-to-strut interface is not distinguished from one another. Stresses concentrate within the nodal region, so the design of the node-to-strut interface indirectly accounts for the design of a strut.

The intent of the minimum reinforcement requirement when using a STM is to provide sufficient deformation capacity to the structure so that it may deform into the assumed truss model upon the application of load. However, the intent of the current reinforcement requirement in ACI 318-08 (Section A.3.3) is to provide integrity to a single element (i.e. a bottle-shaped strut) rather than the overall

structure. Therefore, it is proposed that the minimum reinforcement requirement be changed in order to provide deformation capacity globally rather than locally. The proposed minimum reinforcement requirement is similar to the empirical limit specified in Chapter 11 of the ACI 318 provisions. In addition, the proposed requirement is simpler, more straightforward, and does not allow the designer to provide reinforcement in an improper manner.

Reference to the use of compression reinforcement to increase the strength of a strut has been removed because, regardless of the strength of a strut, the capacity of a STM model is determined by the strength of the nodal boundaries.

A detailed explanation of the proposed limiting compressive stress (Equation A-8) is presented in Chapter 6.

Finally, it is proposed that a substantial amount of the discussion contained in the Commentary be removed from Appendix A. Currently, it appears that the information contained in the Commentary is aimed at educating engineers on the use of strut-and-tie models. However, the quantity of information can be considered overwhelming. The responsibility of the ACI 318-08 Building Code is not to educate its users. Therefore, it is recommended that the discussion contained in the Commentary be limited to information that provides additional insight or background information with regard to the design provisions.

B.4 SUMMARY

Proposed changes to the ACI 318-08 STM provisions are summarized in this Appendix. These changes are based on the proposed STM design methodology presented in Chapter 6. The primary changes to ACI 318-08 are: (i) the new efficiency factors and; (ii) the reorganization of the provisions to focus the design of a truss model on the nodal regions rather than the struts. The design of a strut is indirectly accounted for with the design of the strut-to-node interface.

A design example of a multiple column bent is presented in Appendix C in order to illustrate the differences between the proposed provisions and the current ACI 318-08 STM provisions.

APPENDIX C

Design Example: Multiple Column Bent Cap

C.1 OVERVIEW

The purpose of this example problem is to compare the AASHTO LRFD (2007) and ACI 318-08 deep beam shear design provisions with the newly proposed STM methodology presented in Chapter 6. This example problem examines an actual multiple-column bent cap that has experienced shear cracking problems. The structure contains several shear regions of interest, including: a D-region with an a/d ratio of 0.85; and a region with an a/d ratio of 2.05. As a result, the structure allows for an opportunity to compare design provisions for D-regions with relatively low and high a/d ratios. In addition, the capacity of the portion with an a/d ratio of 2.05 can be analyzed according to sectional shear or strut-and-tie modeling provisions. Thus, the example problem also provides an opportunity to examine the discontinuity between sectional shear and STM provisions. Finally, this example represents an actual structure that has experienced extensive diagonal shear cracking; so extensive, in fact, that a costly retrofit project was undertaken in order to strengthen the structure (Figure C-1). As such, this example provides for an opportunity to evaluate potential design deficiencies; both from a strength and serviceability standpoint.

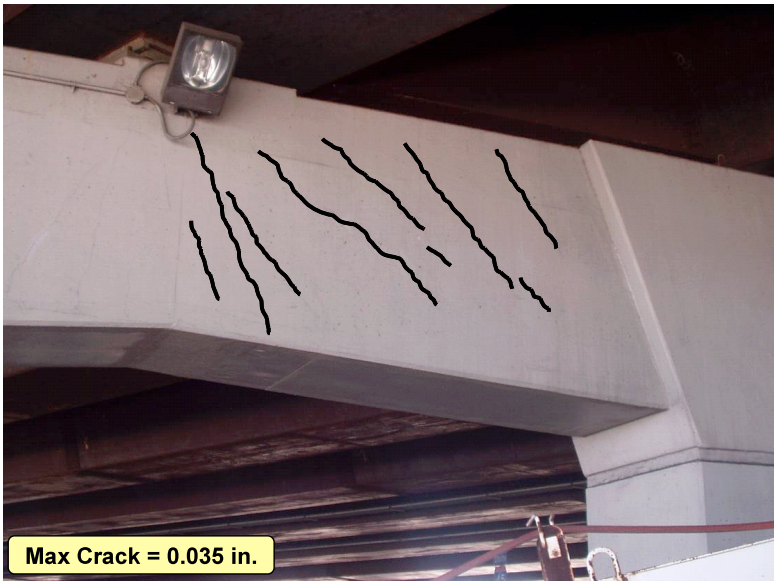

Figure C-1. I-45 over Greens Road Bent Cap

The multiple-column bent cap to be investigated is used to support an 86-foot wide portion of a 180-foot wide roadway; comprised of nine 12-foot wide traffic lanes and one 25-foot wide *high occupancy vehicle* (HOV) lane. This particular cap is considered to be the most critical of all the structures supporting the roadway. A layout of the bent cap is illustrated in Figure C-2; cross-sectional details are presented for the two critical regions under investigation (a/d equal to 0.85 and 2.05).

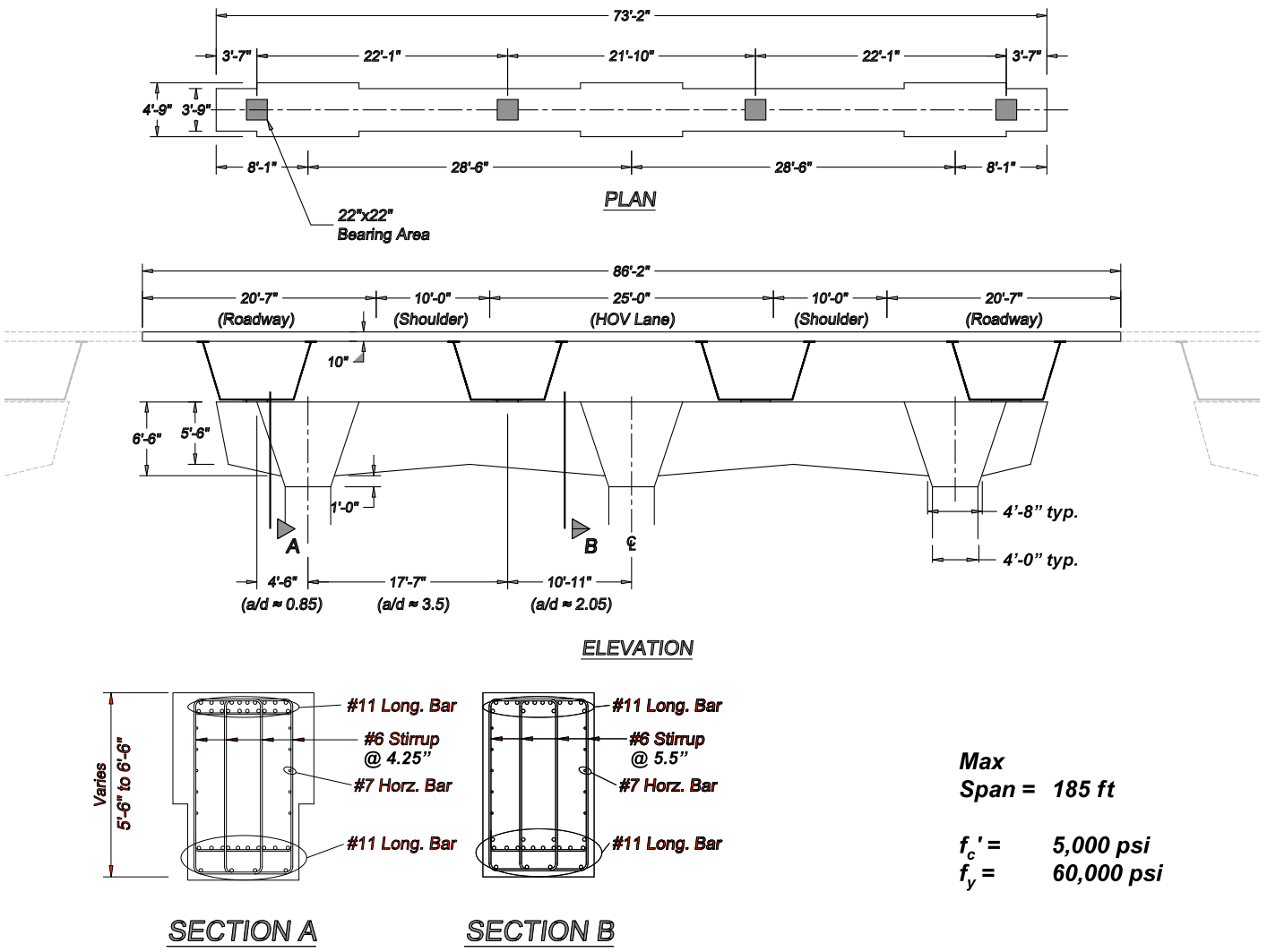

Figure C-2. Preliminary plan; elevation; and cross-sectional details at critical shear regions.

As mentioned, this cap has experienced diagonal cracking problems in the field. For that reason, the details presented in Figure C-2 are considered to be a preliminarily model of the structure. The capacity of each shear region is either verified to be adequate, or is modified as necessary in order to meet the requirements of AASHTO LRFD (2008), ACI 318-08, and the proposed provisions. Afterwards, comparisons are presented between the three design provisions for the two shear regions.

The design dead and live loadings are presented as follows. The self weight of the bent is distributed to the four girder locations in order to easily apply it to a truss model.

Dead Loads

Steel Box Girder:	$(1{,}252\ plf)\cdot(185\ ft)$	= 232 kip
Concrete Deck:	$\frac{(10in.)\cdot(86.2\,ft)\cdot(185\,ft)\cdot(0.15kcf)}{4\ girders}$	= 498 kip
Self Weight:	$\frac{(3.75\,ft)\cdot(73.2\,ft)\cdot(6\,ft)(0.15kcf)}{4\ girders}$	= 62 kip
	Σ Dead	***= 792 kip***

Live Loads

Potential Lanes:	$86.2\,ft \big/ 12\,ft$	= 7 lanes
Lane Load:	$\frac{(0.64klf)\cdot(185\,ft)\cdot(7\ lanes)}{4\ girders}$	= 207 kip
Axle Load:	$(1.3)\cdot\frac{(2\ wheels)\cdot(16kip)\cdot(7\ lanes)}{4\ girders}$	= 73 kip
	Σ Live	***= 280 kip***

Service Load

The load case that is used to examine the amount of service load applied to the structure is the SERVICE I load case specified in AASHTO LRFD (2008).

$P_s = 792\ kip + 280\ kip$ $\quad$ $\boldsymbol{P_s = 1072\ kip}$

Factored Load

Load factors specified by AASHTO LRFD (2008) and ACI 318-08 are slightly different from one another. For the purpose of comparison, the proposed methodology will use the same load factors as AASHTO LRFD (2008).

AASHTO LRFD: STRENGTH I

$P_u = 1.25 \cdot (792\ kip) + 1.75 \cdot (280\ kip)$ $\quad$ $\boldsymbol{P_{u\_AASHTO} = 1480\ kip}$

ACI 318-08

$P_u = 1.2 \cdot (792\ kip) + 1.6 \cdot (280\ kip)$ $\quad$ $\boldsymbol{P_{u\_ACI} = 1398\ kip}$

Resistance Factors

Resistance factors specified by AASHTO LRFD (2007) and ACI 318-08 are slightly different from one another. For the purpose of comparison, the proposed methodology will use the same resistance factors as AASHTO LRFD:

AASHTO LRFD

Struts and Nodal Regions, $\quad$ $\boldsymbol{\phi = 0.70}$

Steel Tie, $\quad$ $\boldsymbol{\phi = 0.90}$

ACI 318-08

Struts and Nodal Regions, $\quad$ $\boldsymbol{\phi = 0.75}$

Steel Tie, $\quad$ $\boldsymbol{\phi = 0.90}$

C.2 DEEP BEAM DESIGN

This bent example problem has three distinct shear regions. The first D-region has an a/d ratio of 0.85; this portion is designed using strut-and-tie provisions; as presented in Section C.2.2. The next shear region has an a/d ratio greater than 3.5 and would be designed using typical sectional shear provisions. Finally, the third region has an a/d ratio of approximately 2.05 (the a/d ratio varies between 1.9 and 2.1 depending where the depth is measured). This portion of the beam is considered to be in the transition zone where the shear behavior of a beam converts from sectional to deep beam shear. Therefore, this portion of the structure could be designed using either a strut-and-tie model or typical sectional

shear provisions. The STM design for this region is presented in Section C.2.3 and the sectional shear design for this region is presented in Section C.3.

When designing a D-region using a strut-and-tie model, the first step is to determine the configuration of the truss model and resulting forces in the truss elements. A preliminary truss model is determined as follows.

C.2.1 Determination of Preliminary Truss Model

The structure illustrated in Figure C-2 is modeled as a truss with compressive struts and tensile ties and presented in Figure C-3. The AASHTO LRFD (2007) factored load, P_{u_AASHTO}, is applied to the structure at each girder support. Only one half of the structure is presented; the bent is symmetric about its centerline, therefore, the loading and proportions of the other half are identical.

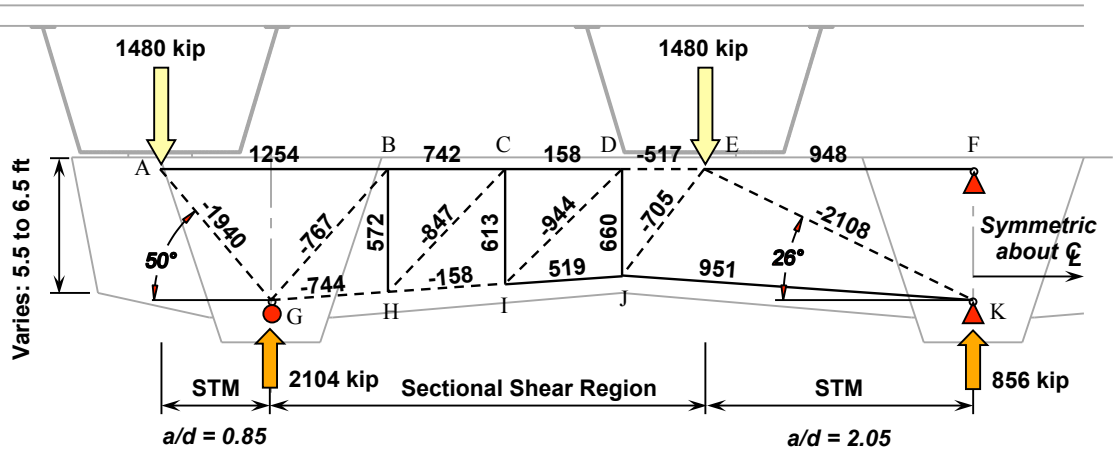

Figure C-3. Strut-and-tie model with AASHTO LRFD (2008) factored loads.

According to the proposed provisions, a deep beam region can be modeled with a single panel strut provided the a/d ratio is less than 2.5. Similarly, according to ACI 318-08, a single-panel strut may be used provided the angle of inclination is greater than 25-degrees; AASHTO LRFD (2008) does not limit a strut's angle of inclination. As a result, both D-regions are shown in Figure C-3 as single compression struts. Also, it is necessary to model the sectional shear portion of the bent as part of the overall truss in order to adequately represent the entire structure. Even though this portion of the structure is designed using

sectional shear provisions, it is necessary to model the entire bent so that the correct quantity of shear is transferred to Strut EK.

Typically, the top and bottom chord of a STM is positioned based on the location of the centroid of the longitudinal reinforcement or the depth of compression zone depending on whether the chord resists tension or compression, respectively. In a continuous element, the top and bottom chord resist both tension and compression. For the sake of simplicity, both of their locations are based on the centroid of the longitudinal reinforcement. For this example problem, the centroid of the longitudinal reinforcement is, on average, taken to be 5.75-inches below the top surface and 8.5-inches above the bottom surface.

C.2.2 Shear Region with an a/d Ratio Equal to 0.85

A close-up of the critical Strut AG and respective nodal zones is presented to scale in Figure C-4.

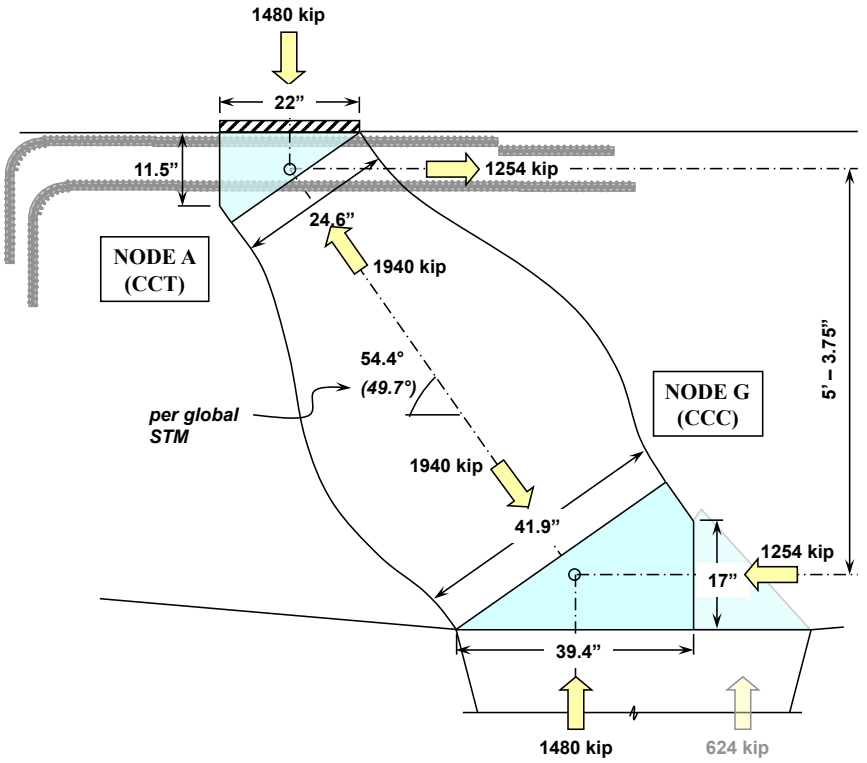

Figure C-4. Critical strut in region with a/d equal to 0.85 (AASHTO LRFD factored loads).

The length of Node G is proportioned based on the amount of force that is transferred to the near support. As a result, the angle of inclination of Strut AG shown in Figure C-4 is slightly different from the angle in the global model shown in Figure C-3 (54.4 versus 49.7-degrees, respectively). If the global truss model were to be updated with this new angle, then the forces in the elements would change slightly. However, it is common practice to ignore this slight discrepancy. Therefore, the truss elements shown in Figure C-4 are designed for the forces presented in Figure C-3.

In order to design Strut AG, the allowable capacity of each nodal face (i.e. bearing face, back face, and strut-to-node interface) must be greater than the force applied to the boundary. This procedure is presented for the proposed method, ACI 318-08 and AASHTO LRFD (2008) provisions in Sections C.2.2.1 through C.2.2.3.

C.2.2.1 Design of Region with a/d = 0.85: Proposed Method

For further information on the proposed STM procedure, details are presented in Chapter 6.

Node A (CCT Node)

The back face of node A must resist the bonding stresses developed by the anchorage of the tie. For this type of condition, stresses at the back face of a CCT node are not critical.

The first step of the proposed method is to determine the triaxial confinement factor, m, as illustrated in Figure C-5.

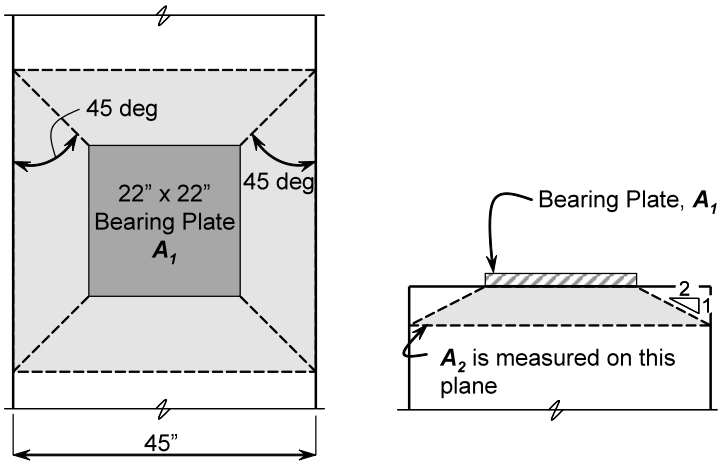

Figure C-5. Determination of Triaxial Confinement Factor

Triaxial Confinement Factor: $m = \sqrt{(45in)^2 / (22in)^2} = 2.04 \le 2$

BEARING FACE

Factored Load: $F_u = 1480\ kip$

Efficiency: $\nu = 0.70$

Concrete Capacity: $f_{cu} = m \cdot \nu \cdot f_c' = (2) \cdot (0.7) \cdot (5\ ksi) = 7.0\ ksi$

$\phi F_n = (0.7) \cdot (7.0\ ksi) \cdot (22\ in.) \cdot (22\ in.)$

$= 2372\ kip > 1480\ kip$ ***OK***

STRUT-TO-NODE INTERFACE

Factored Load: $F_u = 1940\ kip$

Efficiency: $0.65 \le \left(0.85 - 5ksi / 20ksi\right) \le 0.45 = 0.60$

Concrete Capacity: $f_{cu} = m \cdot \nu \cdot f_c' = (2) \cdot (0.60) \cdot (5\ ksi) = 6.0\ ksi$

$\phi F_n = (0.7) \cdot (6.0\ ksi) \cdot (24.6\ in.) \cdot (22\ in.)$

$= 2273\ kip > 1940\ kip$ ***OK***

Thus, according to the proposed procedure, the strength of Node A is sufficient to resist the applied forces. The capacity of Node G is determined as

follows. Node G is not triaxially confined, so the confinement factor, *m*, is equal to one.

Node G (CCC Node)

Triaxial Confinement Factor: $m = 1.0$

BEARING FACE

Factored Load: $F_u = 1480\ kip$

Efficiency: $\nu = 0.85$

Concrete Capacity: $f_{cu} = m \cdot \nu \cdot f_c' = (1) \cdot (0.85) \cdot (5\ ksi) = 4.3\ ksi$

$\phi F_n = (0.7) \cdot (4.3\ ksi)(39.4\ in.)(45\ \ in.)$

$= 5337\ kip > 1480\ kip$ ***OK***

BACK FACE

Factored Load: $F_u = 1254\ kip$

Efficiency: $\nu = 0.85$

Concrete Capacity: $f_{cu} = m\nu f_c' = (1)(0.85)(5\ ksi) = 4.3\ ksi$

$\phi F_n = \ (0.7)(4.3\ ksi)(17\ in.)(45\ \ in.)$

$= 2303\ kip > 1254\ kip$ ***OK***

STRUT-TO-NODE INTERFACE

Factored Load: $F_u = 1940\ kip$

Efficiency: $0.65 \le \left(0.85 - {}^{5ksi}\!/_{20ksi}\right) \le 0.45 = 0.60$

Concrete Capacity: $f_{cu} = m\nu f_c' = (1)(0.6)(5\ ksi) = 3.0\ ksi$

$\phi F_n = (0.7)(3.0\ ksi)(41.9\ in.)(45\ in.)$

$= 3960\ kip > 1940$ ***OK***

Thus, according to the proposed procedure, the strength of Node G is sufficient to resist the applied forces. The capacity of Tie AB must also be evaluated; its capacity is determined as follows.

Tie AB

Factored Load: $F_u = 1254\ kip$

Efficiency: $\nu = 1.0$

Tie Capacity: $(1.0)(60ksi)(20)(1.56\ in^2) = 1872\ kip$

$\phi F_n = (0.9)(1872\ kip)$

$= 1685\ kip > 1254\ kip$ ***OK***

Thus, the capacity of Tie AB is adequate. Verifying the tie capacity is essentially the same procedure for all three provisions. Therefore, this check is not repeated for other provisions.

Minimum Transverse Reinforcement

According to Birrcher (2008), the following minimum amount of transverse reinforcement is required to ensure adequate serviceability behavior.

$A_v = 0.003 \cdot b_w \cdot s_1 \quad = \quad 2(0.44\ in^2) = 0.003(45in)s_1$

$s_1 = 6.5in$

$A_{vh} = 0.003 \cdot b_w \cdot s_2 \quad = \quad 2(0.60\ in^2) = 0.003(45in)s_2$

$s_2 = 8.9in$

Provide #6 vertical stirrups at 6.5-inches and #7 horizontal bars at 8.5-inches on center. Distribute the horizontal reinforcement in the area defined in Figure 6-28.

A summary of the preceding design is presented in Section C.2.2.4 along with the other provisions. Next, Strut AG and respective nodal regions are designed according to ACI 318-08.

C.2.2.2 Design of Region with a/d = 0.85: ACI 318-08

Check the ACI 318-08, §A.3.3.1 requirement for an adequately reinforced strut (discussed in Chapter 2, Equation 2-4).

$$\sum \frac{A_{si}}{b_s \cdot s_i} \sin\alpha_i = \left(\frac{4 \cdot 0.44in^2}{45in \cdot 4.25in}\right)\sin 35.6° + \left(\frac{2 \cdot 0.60in^2}{45in \cdot 8.6in}\right)\sin 54.4°$$

$$= 0.008 > 0.003 \ \textbf{OK}$$

Thus, according to ACI 318-08 §A3.2.2, the strut is adequately reinforced. As a result, a higher strut efficiency factor of 0.75 may be used.

Refer to Figure C-4 for preliminary strut proportions and applied loads. The ACI 318-08 load factors are lower than those applied to the STM presented in Figure C-3; as a result, the loads shown are multiplied by a factor of 0.945 (i.e. $P_{u\_ACI}/P_{u\_AASHTO} = 1398/1480 = 0.945$).

Node A (CCT Node)

BEARING FACE

Factored Load: $F_u = 1398$ kip

Efficiency: $\beta = 0.80$

Concrete Capacity: $f_{cu} = 0.85\beta f_c' = (0.85)(0.8)(5\text{ ksi}) = 3.4$ ksi

$\phi F_n = (0.75)(3.4\text{ ksi})(22\text{ in.})(22\text{ in.})$

$= 1234$ kip < 1398 kip ***NG!***

BACK FACE

Factored Load: $F_u = 1185$ kip

Efficiency: $\beta = 0.80$

Concrete Capacity: $f_{cu} = 0.85\beta f_c' = (0.85)(0.8)(5\text{ ksi}) = 3.4$ ksi

$\phi F_n = (0.75)(3.4\text{ ksi})(11.5\text{ in.})(22\text{ in.})$

$= 645$ kip < 1185 kip ***NG!***

STRUT-TO-NODE INTERFACE

Factored Load: $F_u = 1833$ kip

Efficiency: $\beta = 0.75$

Concrete Capacity: $f_{cu}=0.85\beta f_c' = (0.85)(0.75)(5\text{ ksi}) = 3.2$ ksi

$\phi F_n = (0.75)(3.2\text{ ksi})(24.6\text{ in.})(22\text{ in.})$

$= 1299$ kip < 1833 kip ***NG!***

Thus, the capacity of Node A does not meet the requirements of ACI 318-08. By inspection, Node A is more critical than Node G. The most critical location of Node A is its back face. Therefore, the bearing plates and beam must be resized in order to provide the back face of Node A with sufficient capacity.

Typically, if a designer wishes to increase the capacity of a truss element, the simplest way is to increase the size of the bearing plate. However, there are realistic limits to the maximum size of a plate that can be provided. For this example, a 30”x30” bearing plate is considered to be a reasonable maximum size. It follows that increasing the size of the bearing plate to 30”x30” does not sufficiently increase the capacity of Strut AG in order for it to meet the requirements of ACI 318-08.

Based on the ACI 318-08 STM provisions, additional shear capacity can be attained by increasing the depth of the bent; increasing the compressive strength of concrete; providing supplementary longitudinal reinforcement in order to increase the assumed height of the back face of a CCT node; or by a combination of all three of these methods.

Increasing the compressive strength of concrete can sometimes be a simple way to increase the capacity of a structure. However, TxDOT has expressed concern about maximum curing temperature in regard to concrete durability. Thus, it is believed that concrete compressive strengths in excess of 5000-psi are impractical. In addition, for the purpose of comparison among different design provisions, the compressive strength of concrete is constantly maintained to be 5000-psi.

For the purpose of this example problem, additional capacity is acquired by increasing the depth of the bent and/or nodal region. Most likely, the solution determined for this example would vary from those selected in a design office given the many external factors involved. Nonetheless, the conclusions formed from comparing the provisions to one another will remain valid regardless of differences in preferences.

In order for Strut AG (Figure C-4) to meet the requirements of ACI 318-08, its overall depth must be increased by 18-inches and the depth of the back face of Node A must be increased by 2.5-inches. As a result, the depth of the global

model shown in Figure C-3 is increased by 16.75-inches (18" – $2.5"/2$ = 16.75") and the forces in the truss members are recalculated accordingly. The strut proportions and loads associated with these increases are illustrated in Figure C-6.

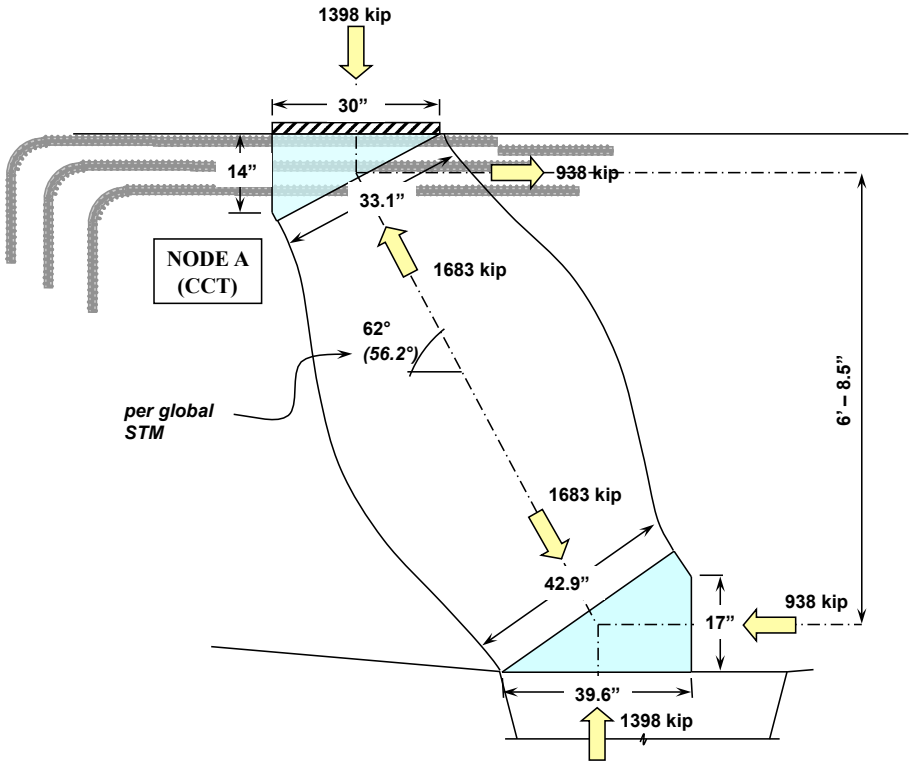

Figure C-6. Strut proportions associated with an increase in overall depth of 18-inches and increase in back face of Node A of 2.5-inches (ACI 318-08 load factors)

The capacity of the critical back face of Node A is calculated as follows according to ACI 318-08.

BACK FACE OF NODE A, PER FIGURE C-6

Factored Load: $F_u = 938\ kip$

Efficiency: $\beta = 0.80$

Concrete Capacity: $f_{cu} = 0.85\beta f_c' = (0.85)(0.8)(5\ ksi) = 3.4\ ksi$

$\phi F_n = (0.75)(3.4\ ksi)(14\ in.)(30\ in.)$

$= 1071\ kip > 938\ kip$ ***OK***

Thus, the capacity of the bent illustrated in Figure C-6 meets the requirements of ACI 318-08.

Minimum Transverse Reinforcement

ACI 318-08 does not require a minimum amount of transverse reinforcement. However, in order to use the higher strut efficiency factor, the following minimum amount of reinforcement must be provided:

$$\sum \frac{A_{si}}{b_s \cdot s_i} \sin\alpha_i > 0.003$$

If it is assumed the vertical and horizontal reinforcement ratios are identical,

$$\rho \cdot \sin 28° + \rho \cdot \sin 62° > 0.003$$

Thus,

$$\rho_v = \rho_{vh} > 0.0022$$

Provide #5 vertical stirrups at 6-inches and #6 horizontal bars at 8.5-inches on center.

A summary of the preceding ACI 318-08 design is presented in Section C.2.2.4 along with the other provisions. Next, Strut AG and respective nodal regions are designed according to AASHTO LRFD (2008).

C.2.2.3 Design of Region with a/d = 0.85: AASHTO LRFD

Refer to Figure C-4 for preliminary strut and nodal proportions, and respective applied loads.

Node A (CCT Node)

BEARING FACE

Factored Load: $F_u = 1480$ kip

Efficiency: $\nu = 0.75$

Concrete Capacity: $f_{cu} = \nu f_c' = (0.75)(5\text{ ksi}) = 3.8$ ksi

$\phi F_n = (0.7)(3.8\text{ ksi})(22\text{ in.})(22\text{ in.})$

$= 1287$ kip < 1480 kip ***NG!***

BACK FACE

Factored Load: $F_u = 1254\ kip$

Efficiency: $\nu = 0.75$

Concrete Capacity: $f_{cu} = \nu f_c' = (0.75)(5\ ksi) = 3.8\ ksi$

$\phi F_n = (0.7)(3.8\ ksi)(11.5\ in.)(22\ in.)$

$= 673\ kip < 1254\ kip$ ***NG!***

STRUT-TO-NODE INTERFACE

Factored Load: $F_u = 1940\ kip$

Solve set of four equations simultaneously:

Concrete Efficiency: $\nu = \dfrac{1}{0.8 - 170 \cdot \varepsilon_1} \le 0.85 \ = \ 0.76$

Tensile Strain Term: $\varepsilon_1 = \varepsilon_s + (\varepsilon_s + 0.002)\cot^2 54.4° \ = \ 0.0030$

Tie Tensile Strain: $\varepsilon_s = \dfrac{F_n \cdot \cos 54.4°}{\left(20 \cdot 1.56 in^2\right) \cdot \left(29{,}000 ksi\right)} \ = 0.0013$

Strength of Nodal Face: $F_n = \nu(5\ ksi)(24.6\ in.)(22\ in.) = 2058\ kip$

$\phi F_n = (0.7)(2058\ kip)$

$= 1441\ kip < 1940\ kip$ ***NG!***

By inspection, Node A is more critical than Node G. The most critical location of Node A is its back face. Therefore, the bearing plates and beam are proportioned such that Node A meets the requirements of AASHTO LRFD (2008). For the purpose of comparison, the nominal capacity of Node A is determined for the same strut proportions required by ACI 318-08 (Figure C-6).

BACK FACE OF NODE A, PER FIGURE C-6

Factored Load: $F_u = 993\ kip$

Efficiency: $\nu = 0.75$

Concrete Capacity: $f_{cu} = \nu f_c' = (0.75)(5\ ksi) = 3.8\ ksi$

$\phi F_n = (0.7)(3.8\ ksi)(14\ in.)(30\ in.)$

$= 1117\ kip > 993\ kip$ ***OK***

Thus, for an a/d ratio of 0.85, the requirements of AASHTO LRFD (2008) are similar to ACI 318-08.

Minimum Transverse Reinforcement

AASHTO LRFD requires a vertical and horizontal reinforcement ratio of 0.3% of the gross area for controlling crack widths. So, based on this requirement, provide #6 vertical stirrups at 6.5-inches and eighteen #7 horizontal bars distributed evenly across the height of the section (resulting spacing is 5.75-inches).

C.2.2.4 Comparison of Design Provisions for Shear Region with a/d = 0.85

A comparison between the results obtained from the three design methodologies for the D-region with an a/d ratio equal to 0.85 (Figure C-2, Cross-Section A) is presented in Figure C-7.

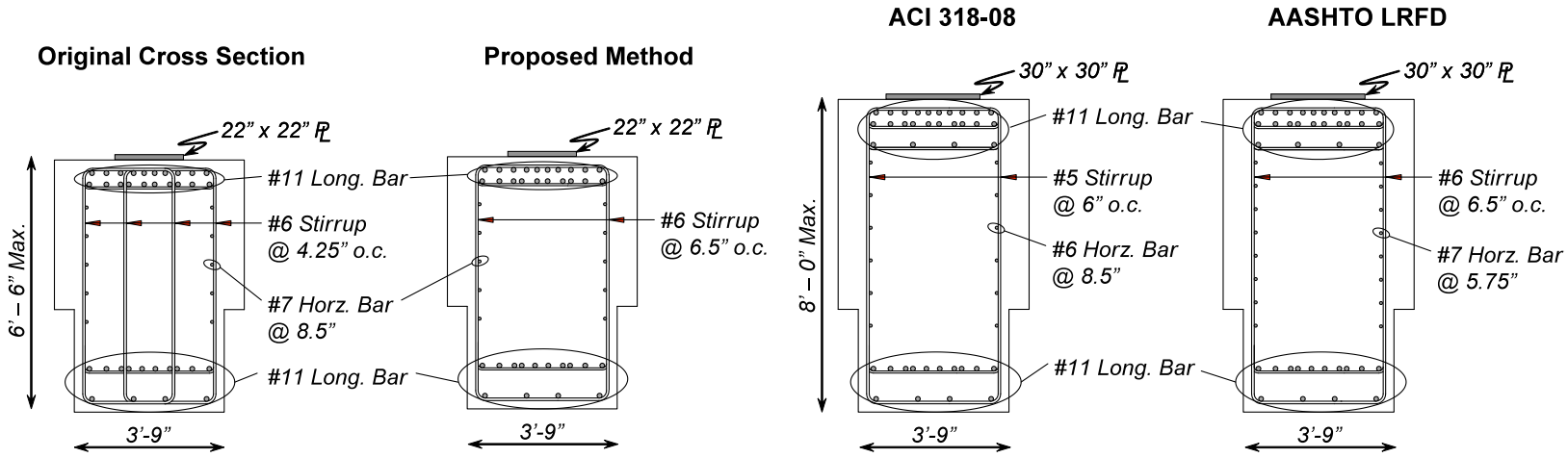

Increase Plate to 30"; Height by 18"; Depth of Node by 2.5"

Ratio of Capacity over Applied Load, $\varphi V_n / V_u$

Proposed = 1.17	**<u>Proposed = 1.17</u>**	**<u>ACI 318 = 1.14</u>**	**<u>AASHTO = 1.12</u>**
ACI 318 = 0.54	**ACI 318 = 0.54**	**Proposed = 1.86**	**Proposed = 1.86**
AASHTO = 0.54	**AASHTO = 0.54**	**AASHTO = 1.12**	**ACI 318 = 1.14**

Figure C-7. Comparison of required cross-section per the proposed method, ACI 318-08, and AASHTO LRFD: a/d ratio = 0.85.

Based on a comparison of the three provisions, the following observations can be made.

The proposed method results in a much higher nominal capacity than those obtained by using the ACI 318-08 and AASHTO LRFD (2008) provisions. As a result, the required cross-section is significantly smaller. This is primarily attributed to the fact that the proposed provisions recognize that the back face check is overly conservative when the applied stress is attributed to bond of the anchored reinforcement. The capacity of the structure as determined by the ACI 318-08 and AASHTO LRFD (2008) provisions is controlled by the capacity at the back face of the CCT node. According to the proposed provisions, provided the tie is properly anchored behind the node, the stress check at this nodal face is not critical.

Also, the smaller bearing plate (22”x22”) did not adversely affect the nominal capacity of the structure. The proposed method considers the increase in concrete compressive strength provided by triaxial confinement. Alternatively, the ACI 318-08 and AASHTO LRFD (2008) provisions do not consider the increase provided by triaxial confinement, so the bearing plate dimensions had to be increased to the maximum possible size (i.e. 30”x30”).

Finally, the minimum amount of transverse reinforcement required by the proposed method, ACI 318-08 and the AASHTO LRFD (2008) specifications is significantly less than the amount contained in the existing bent. However, the fact that the structure contains an amount in excess of the minimum is not a deficiency. On the contrary, additional transverse reinforcement will provide for narrower crack widths and better distribution of cracks upon diagonal cracking. Next, the bent proportions and reinforcement ratio are discussed with regard to its anticipated serviceability performance.

C.2.2.5 Serviceability Behavior for Region with a/d = 0.85

By comparing the amount of shear due to service loads to the cracking strength of concrete, it is possible to estimate the likelihood that the structure will crack under service loads. This topic is discussed in further detail by Birrcher (2008). The shear due to service loads for the portion of the bent with an a/d ratio of 0.85 is as follows:

$$V_{srv} = \textbf{1072 kip}$$

According to Birrcher (2008), for an a/d ratio of 0.85, the shear at which the first diagonal crack will form can conservatively be taken as the following:

$$V_{cr} = 5\sqrt{f_c'} \cdot b_w \cdot d = 5\sqrt{5000}(45in)(69.5in) = \textbf{1106 kip}$$

As a result, the first diagonal cracking load of this portion of the bent is very close to the expected service loading.

C.2.3 Shear Region with an a/d Ratio Equal to 2.05

Next, the nominal capacity determined by the provisions is investigated for the deep beam portion of the bent with an a/d ratio equal to 2.05. A close-up of the critical strut proportions and respective nodal zones is presented to scale in Figure C-8. Note, the vertical reactions are slightly different from one another due to the inclined tie at Node K.

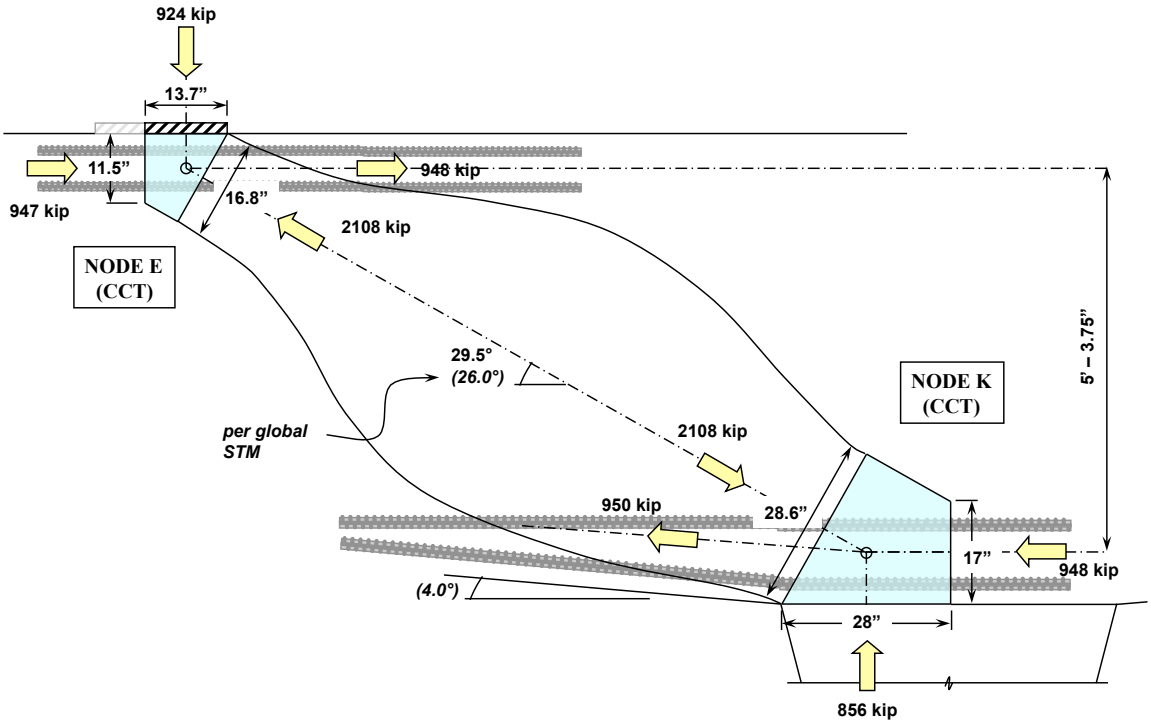

Figure C-8. Critical strut in region with a/d = 2.05.

The length of Nodes E and K are proportioned based on the amount of force that is transferred to the near support. As a result, the angle of inclination of the strut is slightly changed from the global model shown in Figure C-3. However, forces from the global model are not updated to account for the slight change in strut angle. This method is consistent with standard design practice.

Nodes E and K are classified as CCT nodes because of the presence of a tie. Tensile stresses in the tie must be developed in the nodal region to some degree. However, the stress condition at the back face of Nodes E and K is much more complicated because of the compressive force that is applied from an additional strut framing into each node. These compressive stresses are not attributed to the bonding stress of an anchored tie; therefore, they must be applied to the back face and the nodes must be designed accordingly. As a result, the allowable capacity of Nodes E and K are verified as follows.

In order to design this portion of the structure, the allowable capacity of each nodal face (i.e. bearing face, back face, and strut-to-node interface) must be greater than the applied force. This procedure is presented for the proposed method, ACI 318-08 and the AASHTO LRFD (2008) provisions in Sections C.2.3.1 through C.2.3.3.

C.2.3.1 Design of Region with a/d Ratio Equal to 2.05: Proposed Method

Refer to Chapter 6 for a detailed summary of the proposed STM methodology.

Node E (CCT Node)

Triaxial Confinement Factor: $m = \sqrt{(45in)^2 / (22in)^2} = 2.04 \leq 2$

BEARING FACE

Factored Load: 924 kip

Efficiency: $\nu = 0.70$

Concrete Capacity: $f_{cu} = m\nu f_c' = (2)(0.7)(5\ ksi) = 7.0\ ksi$

$\phi F_n = (0.7)(7.0\ ksi)(13.7\ in.)(22\ in.)$

$= 1477\ kip > 924\ kip$ ***OK***

STRUT-TO-NODE INTERFACE

Factored Load: 2108 kip

Efficiency: $0.65 \leq \left(0.85 - 5ksi/20ksi\right) \leq 0.45 = 0.60$

Concrete Capacity: $f_{cu} = m\nu f_c' = (2)(0.60)(5\ ksi) = 6.0\ ksi$

$\phi F_n = (0.7)(6.0\ ksi)(16.8\ in.)(22\ in.)$

$= 1552\ kip < 2108\ kip$ ***NG!***

BACK FACE

Factored Load: 947 kip

Efficiency: $\nu = 0.70$

Concrete Capacity: $f_{cu} = m\nu f_c' = (2)(0.70)(5\ ksi) = 6.0\ ksi$

$\phi F_n = (0.7)(6.0\ ksi)(11.5\ in.)(22\ in.)$

$= 1063\ kip > 1895\ kip$ **OK**

Node K (CCT Node)

Triaxial Confinement Factor: $m = 1.0$

BEARING FACE

Factored Load: 857 kip

Efficiency: $\nu = 0.70$

Concrete Capacity: $f_{cu} = mvf_c' = (1)(0.70)(5\ ksi) = 3.5\ ksi$

$\phi F_n = (0.7)(3.5\ ksi)(28\ in.)(45\ in.)$

$= 3087\ kip > 857\ kip$ **OK**

STRUT-TO-NODE INTERFACE

Factored Load: 2108 kip

Efficiency: $0.65 \le \left(0.85 - 5ksi/20ksi\right) \le 0.45 = 0.60$

Concrete Capacity: $f_{cu} = mvf_c' = (1)(0.6)(5\ ksi) = 3.0\ ksi$

$\phi F_n = (0.7)(3.0\ ksi)(28.6\ in.)(45\ in.)$

$= 2703\ kip > 2108$ **OK**

BACK FACE

Factored Load: 948 kip

Efficiency: $\nu = 0.70$

Concrete Capacity: $f_{cu} = mvf_c' = (1)(0.70)(5\ ksi) = 3.5\ ksi$

$\phi F_n = (0.7)(3.5\ ksi)(17\ in.)(45\ in.)$

$= 1874\ kip > 948\ kip$ **OK**

Tie EF

Factored Load: $F_u = 948\ kip$

Efficiency: $\nu = 1.0$

Tie Capacity: $(1.0)(60ksi)(14)(1.56\ in^2) = 1310\ kip$

$\phi F_n = (0.9)(1310\ kip)$

$= 1179\ kip > 948\ kip$ **OK**

Thus, according to the proposed procedure the Node E strut-to-node interface governs the capacity. Because the proposed method accounts for triaxial confinement of the nodal regions, the capacity of the truss model can be increased by increasing the width of the bent. Often times, due to clearance restrictions, it is desirable to gain capacity by increasing a beam's width rather than its depth. ACI 318-08 and AASHTO LRFD (2008) do not account for the increase in capacity gained from increasing the width of the web.

The strut-to-node interface of Node E is the most critical location. If a maximum size bearing plate is used (30"x30"), then the depth of the bent must be increased by 6-inches and the width would have to be increased by 6-inches in order for Node E to have an adequate capacity. The strut proportions and forces associated with a 6-inch increase in the depth of the bent are illustrated in Figure C-9. Notice that an increase in the depth of the truss decreases the force in the inclined strut.

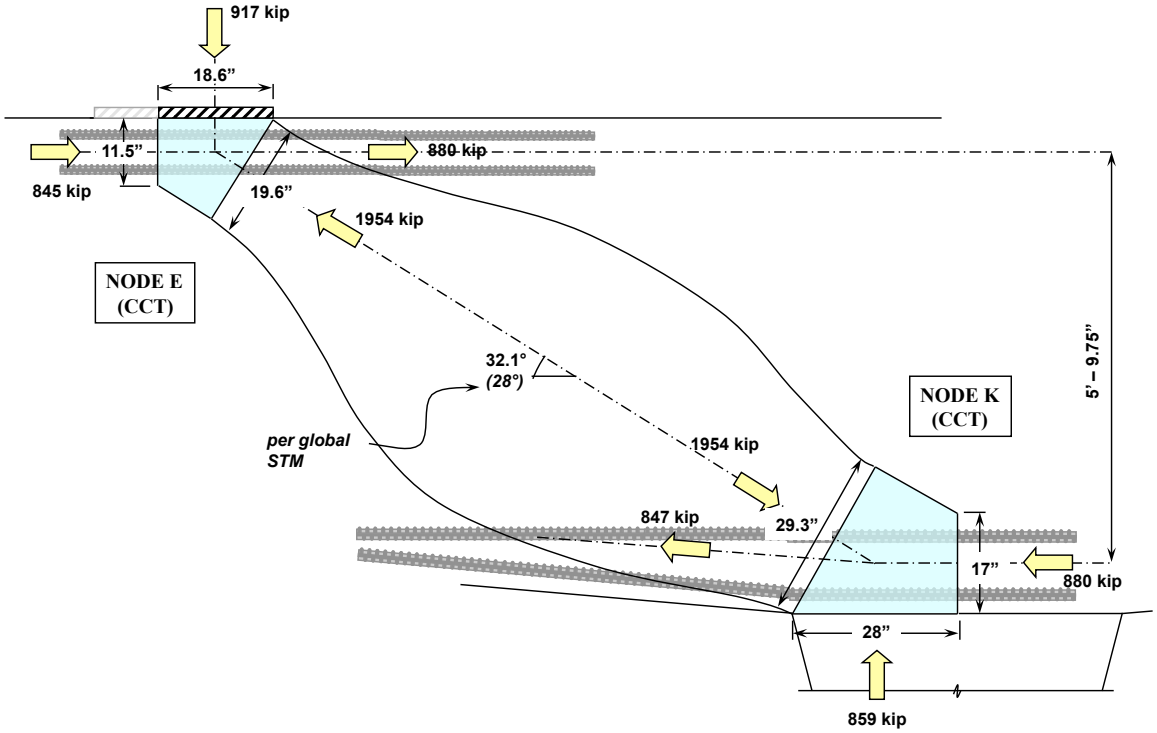

Figure C-9. Strut proportions and forces associated with a 6-inch increase in depth of bent.

NODE E STRUT-TO-NODE INTERFACE, PER FIGURE C-9

Factored Load: 1954 kip

Confinement Factor: $m = \sqrt{(51in)^2 / (30in)^2} = 1.7$

Efficiency: $0.65 \le \left(0.85 - 5ksi/20ksi\right) \le 0.45 = 0.60$

Concrete Capacity: $f_{cu} = mvf_c' = (1.7)(0.60)(5\ ksi) = 5.1\ ksi$

$\phi F_n = (0.7)(5.1\ ksi)(19.6\ in.)(30\ in.)$

$= 2099\ kip > 1954\ kip$ ***OK***

Thus, the capacity of strut illustrated in Figure C-9 meets the requirements of the proposed method.

Minimum Transverse Reinforcement

Based on the recommendations from Birrcher (2008), the following minimum amount of transverse reinforcement is required to ensure adequate serviceability behavior (Section 6.6).

$A_v = 0.003 \cdot b_w \cdot s_1$ $\quad 2(0.44\ in^2) = 0.003(51in)s_1$

$s_1 = 5.75in$

$A_{vh} = 0.003 \cdot b_w \cdot s_2$ $\quad 2(0.60\ in^2) = 0.003(51in)s_2$

$s_2 = 7.8in$

Provide #6 vertical stirrups at 5.5-inches and #7 horizontal bars at 7.5-inches on center. Distribute the horizontal reinforcement in the area defined in Figure 6-24.

A summary of the preceding design is presented in Section C.2.3.4 along with the other provisions. Next, Strut EK and respective nodal regions are designed according to ACI 318-08.

C.2.3.2 Design of Region with a/d Ratio Equal to 2.05: ACI 318-08

Refer to Figure C-8 for preliminary forces, strut, and nodal dimensions. By inspection, Node E is the most critical nodal zone. Therefore, the design of Strut EK is based on the design of Node E. Recall, that the ACI 318-08 load factors are less than those presented in Figure C-8. Therefore, all of the load values are multiplied by a factor of 0.945 (i.e. $P_{u\_ACI}/P_{u\_AASHTO} = 1398/1480 = 0.945$).

Node E (CCT Node)

BEARING FACE

Factored Load: $F_u = 873\ kip$

Efficiency: $\beta = 0.80$

Concrete Capacity: $f_{cu} = 0.85\beta f_c' = (0.85)(0.8)(5\ ksi) = 3.4\ ksi$

$\phi F_n = (0.75)(3.4\ ksi)(13.7\ in.)(22\ in.)$

$= 769\ kip < 739\ kip$ ***NG!***

BACK FACE

Factored Load: $F_u = 895\ kip + 896\ kip = 1791\ kip$

Efficiency: $\beta = 0.80$

Concrete Capacity: $f_{cu} = 0.85\beta f_c' = (0.85)(0.8)(5\ ksi) = 3.4\ ksi$

$\phi F_n = (0.75)(3.4\ ksi)(11.5\ in.)(22\ in.)$

$= 645\ kip < 1791\ kip$ ***NG!***

STRUT-TO-NODE INTERFACE

Factored Load: $F_u = 1992\ kip$

Efficiency: $\beta = 0.75$

Concrete Capacity: $f_{cu} = 0.85\beta f_c' = (0.85)(0.75)(5\ ksi) = 3.2\ ksi$

$\phi F_n = (0.75)(3.2\ ksi)(16.8\ in.)(22\ in.)$

$= 887\ kip < 1992\ kip$ ***NG!***

According to ACI 318-08, the back face of Node E is the most critical location. In order to properly design this region, the bent is proportioned such that the back face of Node E has adequate capacity. In addition to providing the maximum 30-inch bearing plate, the depth of the bent must be increased by 25-inches and the depth of the back face of Node E must be increased by 6-inches. Strut proportions and forces associated with these changes are illustrated in Figure C-10.

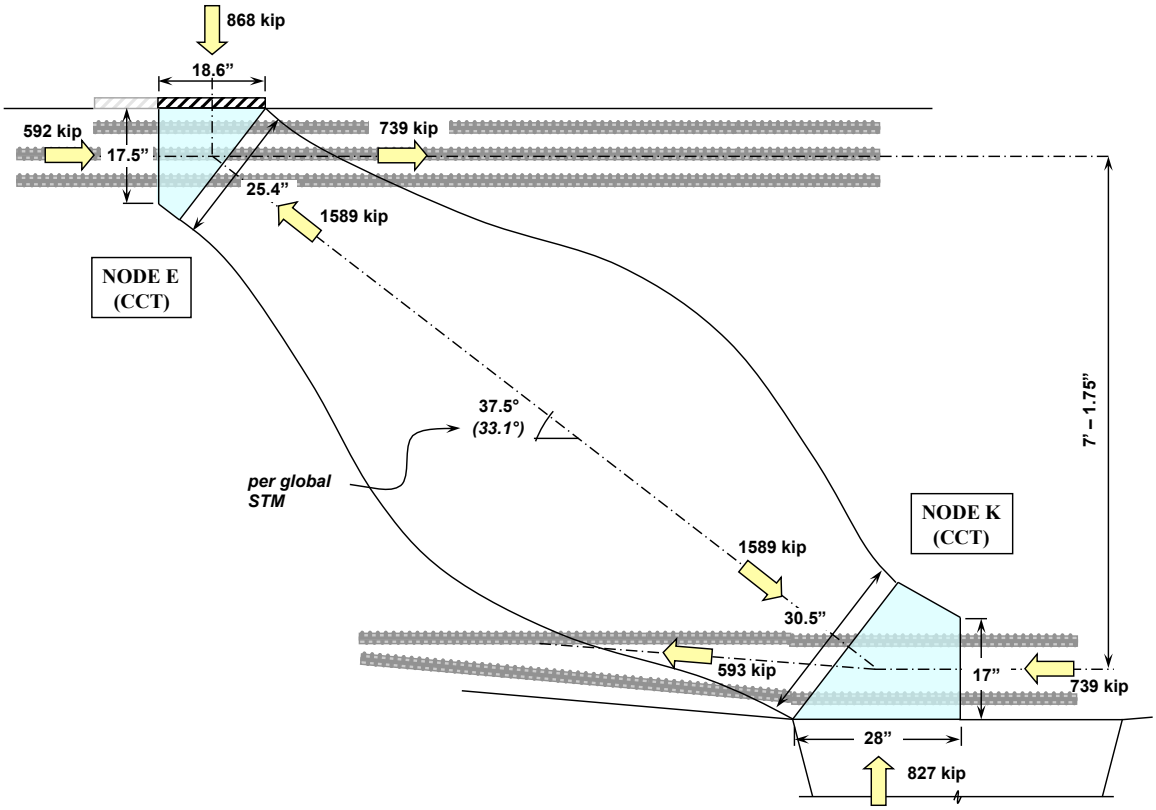

Figure C-10. Strut proportions and forces associated with a 25-inch increase in bent height and 6-inch increase in depth of Node E (ACI 318 factored loads)

BACK FACE OF NODE E: PER FIGURE C-10

Factored Load: $F_u = 739 \text{ kip} + 592 \text{ kip} = 1331 \text{ kip}$

Efficiency: $\beta = 0.80$

Concrete Capacity: $f_{cu} = 0.85\beta f_c' = (0.85)(0.8)(5 \text{ ksi}) = 3.4 \text{ ksi}$

$\phi F_n = (0.75)(3.4 \text{ ksi})(17.5 \text{ in.})(30 \text{ in.})$

$= 1339 \text{ kip} > 1331 \text{ kip}$ ***OK***

Thus, the capacity of the bent illustrated in Figure C-10 meets the requirements of ACI 318-08.

Minimum Transverse Reinforcement

ACI 318-08 does not stipulate a minimum amount of transverse reinforcement. However, in order to use the higher strut efficiency factor, the following minimum amount of reinforcement must be provided:

$$\sum \frac{A_{si}}{b_s \cdot s_i} \sin\alpha_i > 0.003$$

If it is assumed that the vertical and horizontal reinforcement ratios are identical,

$$\rho \cdot \sin 38° + \rho \cdot \sin 52° > 0.003$$

Thus,

$$\rho_v = \rho_{vh} > 0.0021$$

Provide #5 vertical stirrups at 6-inches and #6 horizontal bars at 8.5-inches on center.

A summary of the preceding ACI 318-08 results is presented in Section C.2.3.4 along with the other provisions. Next, Strut EK and respective nodal regions are designed according to AASHTO LRFD.

C.2.3.3 Design of Region with a/d Ratio Equal to 2.05: AASHTO LRFD

Refer to Figure C-8 for preliminary forces, strut and nodal proportions. By inspection, Node E is the most critical nodal zone. Therefore, design of Strut EK is based on the design of Node E.

Node E (CCT Node)

BEARING FACE

Factored Load: $F_u = 924$ *kip*

Efficiency: $\nu = 0.75$

Concrete Capacity: $f_{cu} = \nu f_c' = (0.75)\cdot(5\ ksi) = 3.8\ ksi$

$\phi \cdot F_n = (0.7)\cdot(3.8\ ksi)\cdot(13.7\ in.)\cdot(22\ in.)$

$= 802\ kip < 924\ kip$ ***NG!***

BACK FACE

Factored Load: $F_u = 947\ kip + 948\ kip = 1895\ kip$

Efficiency: $\nu = 0.75$

Concrete Capacity: $f_{cu} = \nu f_c' = (0.75)(5\ ksi) = 3.8\ ksi$

$\phi F_n = (0.7)(3.8\ ksi)(11.5\ in.)(22\ in.)$

$= 673\ kip < 1895\ kip$ ***NG!***

STRUT-TO-NODE INTERFACE

Factored Load: $F_u = 2108\ kip$

Solve set of four equations simultaneously:

Concrete Efficiency: $\nu = \frac{1}{0.8 - 170 \cdot \varepsilon_1} \le 0.85 = 0.39$

Tensile Strain Term: $\varepsilon_1 = \varepsilon_s + (\varepsilon_s + 0.002)\cot^2 29.5° = 0.0103$

Tie Tensile Strain: $\varepsilon_s = \frac{F_n \cdot \cos 29.5°}{\left(21.8 in^2\right) \cdot \left(29{,}000 ksi\right)} = 0.0010$

Strength of Nodal Face: $F_n = \nu(5\ ksi)(16.3\ in.)(22\ in.) = 705\ kip$

$\phi F_n = (0.7)(705\ kip)$

$= 722\ kip < 2108\ kip$ ***NG!***

The strut-to-node interface at Node E is the most critical location. Therefore, the size of the bent is increased in order to provide Node E with adequate capacity. As a preliminary check, evaluate whether or not the bent dimensions required per ACI 318-08 (Figure C-10) meet the requirements of AASHTO LRFD (2008). Recall, the loads illustrated in Figure C-10 are ACI 318-08 factored loads. AASHTO LRFD (2008) load factors are slightly higher, so the loads are multiplied by a factor of 1.059 (i.e. $P_{u\_AASHTO}/P_{u\_ACI} = 1480/1398 = 1.059$).

NODE E STRUT-TO-NODE INTERFACE, PER FIGURE C-10

Factored Load: $F_u = 1683\ kip$

Solve set of four equations simultaneously:

Concrete Efficiency: $\nu = \frac{1}{0.8 - 170 \cdot \varepsilon_1} \le 0.85 = 0.46$

Tensile Strain Term: $\varepsilon_1 = \varepsilon_s + (\varepsilon_s + 0.002)\cot^2 37.5° = 0.0080$

Tie Tensile Strain: $\varepsilon_s = \dfrac{F_n \cdot \cos 37.5°}{(28.1in^2)\cdot(29{,}000ksi)} = 0.0017$

Strength of Nodal Face: $F_n = \nu(5\ ksi)(25.4\ in.)(30\ in.) = 1761\ kip$

$\phi F_n = (0.7)(1761\ kip)$

$= 1233\ kip < 1683\ kip$ ***NG!***

In order for the bent to meet the requirements of AASHTO LRFD, the bent depth must be increased by 35-inches and the depth of Node E must be increased by 10.5-inches. Strut proportions associated with this increase and applied loads are illustrated in Figure C-11.

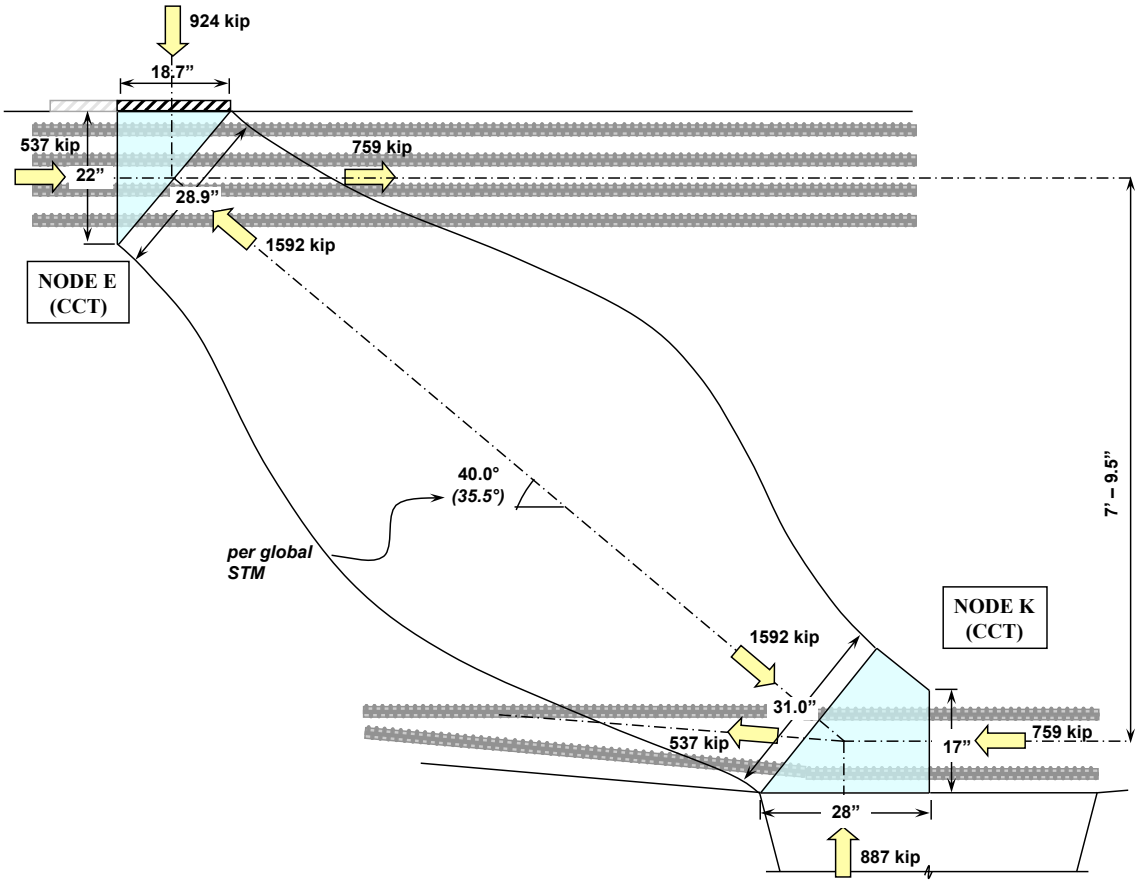

Figure C-11. Strut proportions and forces associated with a 35-inch increase in bent depth and 10.5-inch increase in depth of Node E (AASHTO LRFD factored loads).

NODE E STRUT-TO-NODE INTERFACE, PER FIGURE C-11

Factored Load: 1592 kip

Solve set of four equations simultaneously:

Concrete Efficiency: $\nu = \frac{1}{0.8 - 170 \cdot \varepsilon_1} \le 0.85 \;=\; 0.53$

Tensile Strain Term: $\varepsilon_1 = \varepsilon_s + (\varepsilon_s + 0.002)\cot^2 40.0° \;=\; 0.0064$

Tie Tensile Strain: $\varepsilon_s = \frac{F_n \cdot \cos 40.0°}{\left(40.6 in^2\right) \cdot \left(29{,}000 ksi\right)} \;= 0.0015$

Strength of Nodal Face: $F_n = \nu(5\ ksi)(28.9\ in.)(30\ in.) = \;2287\ kip$

$$\phi F_n = (0.7)(2287\ kip)$$

$$= 1601\ kip > 1592\ kip\ \textbf{OK}$$

Thus, the capacity of the bent illustrated in Figure C-11 meets the requirements of AASHTO LRFD (2007).

Minimum Transverse Reinforcement

AASHTO LRFD requires a vertical and horizontal reinforcement ratio of 0.3% of the gross area for the purpose of controlling cracking. So, based on this requirement, provide #6 vertical stirrups at 6.5-inches and twenty #8 horizontal bars distributed evenly across the height of the section (resulting in a spacing of 7-inches).

A summary of the preceding AASHTO LRFD results is presented along with the other provisions in the following section.

C.2.3.4 Comparison of Design Provisions for Shear Region with a/d = 2.05

A comparison between the results obtained from the three design methodologies (i.e. proposed method, ACI 318-08, and AASHTO LRFD) for the portion of the bent with an a/d ratio equal to 2.05 (Figure C-2, Cross-Section B) is presented in Figure C-12.

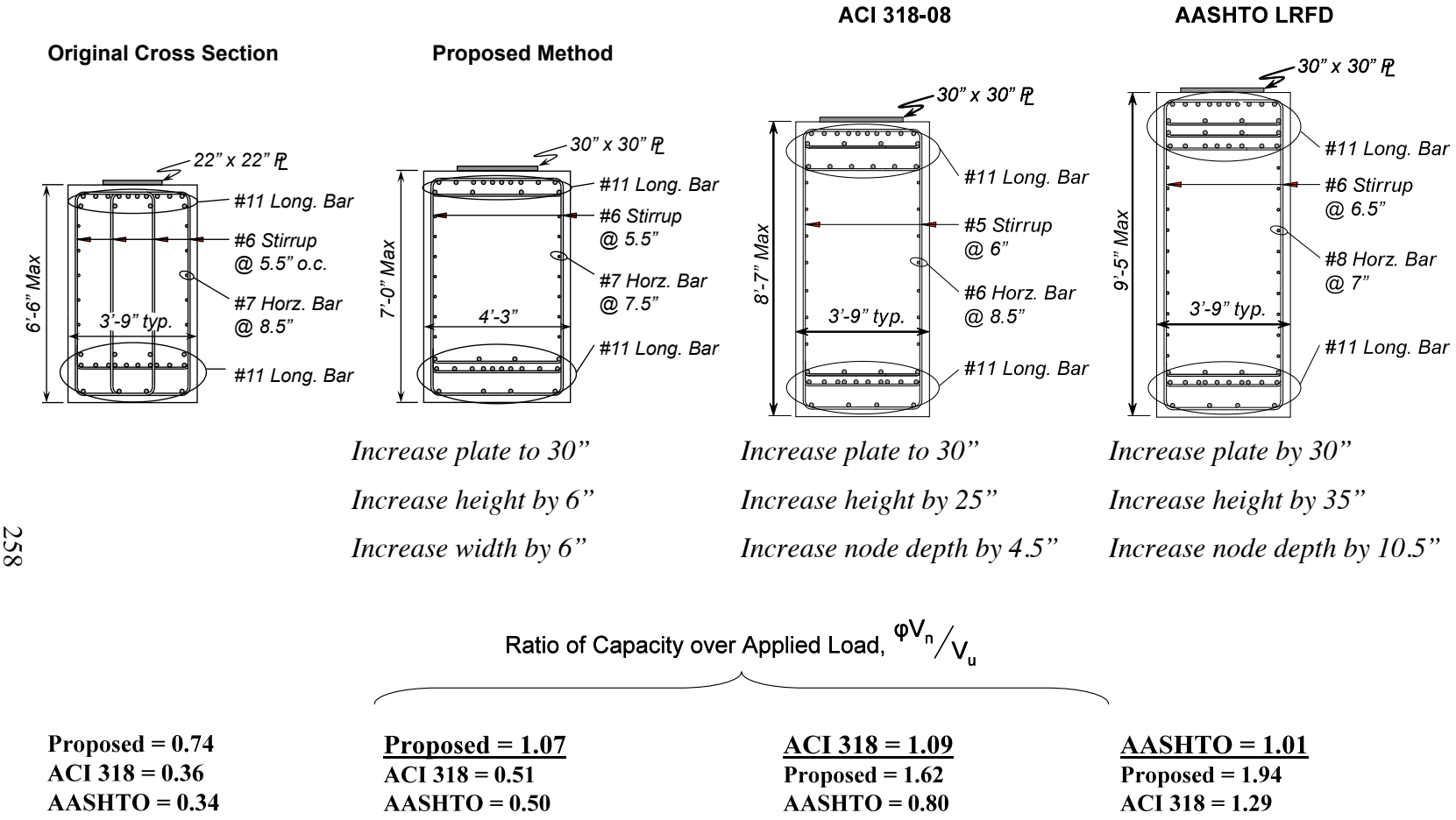

Figure C-12. Comparison of required cross-section per the proposed method, ACI 318-08, and AASHTO LRFD (2007): a/d ratio = 2.05.

Based on a comparison of the three provisions, the following observations can be made.

The proposed method results in a much higher capacity than the ACI 318-08 and AASHTO LRFD (2008) provisions. As a result, the cross-section required by the proposed procedure is significantly smaller. One reason for the difference can be attributed to the fact that the proposed procedure considers the increase in concrete compressive strength provided by triaxial confinement of the bearing plate. Neither the ACI 318-08 nor the AASHTO LRFD (2008) provisions consider the beneficial effects of triaxial confinement. In addition, according to the AASHTO LRFD (2008) provisions, the efficiency of the node-to-strut interface is decreased as the shear span-to-depth ratio increases. It follows that excessively conservative results can be expected when using AASHTO LRFD (2008) for D-regions with an a/d ratio in the range of two.

Despite the differences in the results of the three methods, they are similar in the fact that the results suggest that the dimensions of the original cross-section are inadequate to resist the application of the factored loads. However, this portion of the bent has an a/d ratio slightly greater than 2.0. Therefore, the capacity of this region may be determined according to sectional shear provisions. The sectional shear strength of this region is determined according to ACI 318-08 and AASHTO LRFD (2008). A discussion on the implications of using a sectional analysis rather than a deep beam analysis is presented in Section C.3.

In addition to the sectional shear strength, it is also of interest to examine the ratio of service load to cracking strength applied to this portion of the bent. The service loading is compared with the cracking strength of concrete in the following section.

C.2.3.5 Serviceability Behavior for Region with a/d = 2.05

By comparing the amount of service shear to the cracking strength of concrete, it is possible to estimate the likelihood that the structure will crack while

in service. The shear force due to service loads for the portion of the bent with an a/d ratio of 2.05 is as follows:

V_{srv} = *(856 kip)(1072kip/1480kip)* ***= 620 kip***

According to Birrcher (2008), for an a/d ratio of 2.05, the shear at which the first diagonal crack will form can conservatively be taken to be the following:

$$V_{cr} = 2\sqrt{f_c'} \cdot b_w \cdot d = 2\sqrt{5000}(45in)(63in) \qquad \textbf{= 401 kip}$$

Thus, the cracking capacity of this portion of the structure is less than the service level loading. As a result, it is expected that diagonal cracking will result for this structure. Diagonal cracks are expected to form under the application of 65% of the service-level loading (i.e. *401/620 = 0.65*). In order to prevent cracking from occurring under the application of service loads, bent dimensions much be increased such that $V_{cr} \geq V_{srv}$. If bent dimensions are increased while keeping the aspect ratio of the cross-section as similar, then the size of the bent must be increased to 56"x78" in order to comfortably reduce the likelihood of cracking under service loads:

$$V_{cr} = 2\sqrt{f_c'} \cdot b_w \cdot d = 2\sqrt{5000}\,\textbf{\textit{(56in)(78in)}} \qquad \textbf{= 618 kip}$$

C.3 SECTIONAL SHEAR DESIGN

The purpose of calculating the sectional shear capacity for the portion of the beam with an a/d ratio of 2.05 (Figure C-2, Section A) is to compare the results to those determined from a strut-and-tie model. The discontinuity in the shear capacity determined by either deep beam or sectional shear provisions is a topic of interest to the current project.

The ACI 318-08 and AASHTO LRFD (2008) provisions require that a designer use deep beam provisions for structures with a shear span-to-depth ratio less than or equal to two. For structures whose a/d ratio is near two, it is logical to expect that the capacity determined from a strut-and-tie model to be similar to that determined from a sectional model. In other words, the calculated capacity of a member should not significantly vary for an a/d ratio of 2.1 or 1.9. However, the

difference in the allowable shear capacity according to sectional shear or a STM is often quite drastic.

The purpose of determining the sectional shear capacity of Section A (Figure C-2) is to quantify the difference between the ACI 318-08 and AASHTO LRFD (2008) sectional shear provisions and the deep beam provisions previously presented. Additional discussion regarding the discontinuity between deep beam and sectional shear provisions is presented by Birrcher (2008).

C.3.1 Shear Region with a/d Ratio Equal to 2.05

Refer to Figure C-3 for the critical shear force in Section A. The AASHTO LRFD (2008) factored shear is 856-kip; the ACI 318-08 factored shear is 809-kip. The ACI 318-08 and AASHTO LRFD (2008) reduction factors for sectional shear are 0.75 and 0.9, respectively. The nominal shear capacity according to ACI 318-08 and AASHTO LRFD (2008) is presented in Sections C.3.1.1 and C.3.1.2.

C.3.1.1 ACI 318-08 §11.1, Shear Strength

Factored Load: $V_u = 809\ kip$

Sectional Capacity: $V_n = V_c + V_s$

Where,

$$V_c = 2\sqrt{f_c'} \cdot b_w \cdot d \quad = 2\sqrt{5000\,psi} \cdot (45in) \cdot (63in) \qquad = 401\ kip$$

$$V_s = A_v \cdot f_v \cdot d/s \quad = 4 \cdot (0.44in^2) \cdot (60ksi) \cdot (63in)/5.5in \qquad = 1210\ kip$$

$$\phi V_n = (0.75)\ (1611\ kip) \qquad = 1208\ kip > 809\ kip\ \textbf{OK}$$

According to ACI 318-08, the strength of the bent is adequate. However, recall that according to the STM design presented in Section C.2.3.2, the depth of the bent had to be considerably increased in order to meet the requirements of ACI 318-08. The degree of discontinuity between sectional shear and STM provisions is discussed in Section C.3.2. Next, the sectional shear capacity according to the AASHTO LRFD (2008) provisions is presented as follows.

C.3.1.2 AASHTO LRFD§5.8.3, Sectional Design Model

Factored Load: $V_u = 856\ kip$

Sectional Capacity: $V_n = V_c + V_s$

Where,

$$V_c = 0.0316\beta\sqrt{f_c'}\,b_v d_v$$

$$V_s = {A_v f_y d_v}\Big/{s \cdot \tan\theta}$$

and,

$\beta =$ factor indicating the ability of diagonally cracked concrete to transmit tension and shear.

According to AASHTO LRFD (2008), the factor, β, can conservatively be taken as two provided the depth of the member is less than 16-inches. For members with a greater depth, the factor is determined based on the longitudinal strain, shear stress, spacing and inclination of cracking across the web. For non-prestressed beams, sufficiently reinforced, the factor, β, may be determined according to Equation C-1:

$$\beta_s = \frac{4.8}{(1 + 750\varepsilon_s)} \qquad \text{Equation C-1}$$

And the angle of inclination of the cracking, θ, is determined according to Equation C-2:

$$\theta = 29 + 3500\varepsilon_s \qquad \text{Equation C-2}$$

Where the longitudinal strain, ε_s, in the web is determined according to Equation C-3.

$$\varepsilon_s = \frac{\left(\frac{|M_u|}{d_v} + 0.5N_u + 0.5|V_u|\cot\theta\right)}{2(E_s A_s)} \qquad \text{Equation C-3}$$

Where,

$M_u =$ Factored moment at critical section, kip-in.

$V_u =$ Factored shear at critical section, kip

N_u = Factor axial force at critical section, kip

θ = Angle of inclination of diagonal cracking, radian

d_v = distance between longitudinal top and bottom reinforcement, in.

E_s = Modulus of elasticity of steel reinforcement

A_s = Area of flexural tension reinforcement, in^2

Based on a linear analysis of the multiple-column bent, the factored moment at the critical section is 51,750-kip·inches and the factored shear force is 856-kip. The longitudinal strain and angle of inclination terms are simultaneously calculated as follows:

$$\varepsilon_s = \frac{\left(\frac{|51{,}750 kip \cdot in|}{57in} + 0.5(0kip) + 0.5|856kip|\cot 32.4°\right)}{2\left(29{,}000ksi \cdot 28.1in^2\right)} \qquad = 0.00097$$

$$\theta = 29 + 3500\,(0.00097) \qquad = 32.4^o$$

Thus,

$$\beta_s = \frac{4.8}{(1 + 750 \cdot 0.00097)} \qquad = 2.78$$

Therefore, the nominal shear capacity can be calculated as follows:

$$V_c = 0.0316 \cdot 2.7\sqrt{5ksi} \cdot (45in.)(57in.) \qquad = 489\ kip$$

$$V_s = \frac{4\left(0.44in^2\right) \cdot (60ksi) \cdot (57in)}{(5.5in.)\tan 32.4°} \qquad = 1724\ kip$$

ϕV_n = (0.90)(2214 kip)= 1992 kip > 856 kip **OK**

According to AASHTO LRFD (2008), the strength of the bent is adequate. Yet, recall that according to the STM design presented in Section C.2.3.3, the depth of the bent had to be considerably increased in order to meet the requirements of AASHTO LRFD (2008). The discontinuity between sectional shear and deep beam provisions is discussed in the following section.

C.3.2 Comparison of Deep Beam and Sectional Shear Provisions

The capacity of the bent at Section A (Figure C-2) has been determined according to the proposed, ACI 318-08, and AASHTO LRFD (2008) STM provisions; and the ACI 318-08 and AASHTO LRFD (2008) section-based provisions. A comparison between the results of these analyses is presented in Table C.1.

Table C.1. Shear Capacity of Original Cross-Section A (a/d = 2.05)

Design Procedure	Capacity / Factored Load		$\frac{\phi V_n \ Sectional}{\phi V_n \ STM}$
	STM, $\frac{\phi \cdot V_n}{V_u}$	Sectional, $\frac{\phi \cdot V_n}{V_u}$	
Proposed Method	0.74	1.42†	1.92
ACI 318	0.36	1.42	3.94
AASHTO LRFD	0.34	2.33	6.85

† ACI 318-08 sectional shear capacity (Section C.3.1.1)

The information presented in Table C.1 illustrates the relative discontinuity in nominal capacity as determined by sectional shear and deep beam provisions. This phenomenon is especially apparent for a structure with an a/d ratio equal to 2.05. As an example, according to the AASHTO LRFD (2008) sectional shear provisions, the capacity of the structure under investigation is estimated to be over five times greater than the capacity as determined per the deep beam provisions. The implication of such a discrepancy is that a bent over nine feet deep is required per AASHTO LRFD (2008) for an a/d ratio of 1.9 (Figure C-12), yet a 6.5-foot deep bent is sufficient if the a/d ratio is slightly greater than two.

The proposed strut-and-tie modeling procedure addresses this discontinuity to some degree. Granted, the estimated capacity of Section A according to sectional shear provisions is almost two times greater than that estimated using the new methodology. However, this discrepancy is significantly

less than that which results from using the ACI 318-08 or AASHTO LRFD (2008) provisions.

C.4 SUMMARY

The purpose of this example is to illustrate the benefits of the proposed strut-and-tie modeling provisions in comparison to the ACI 318-08 and AASHTO LRFD (2008) provisions. A deep beam region with an a/d ratio of 0.85 and 2.05 was designed using all three provisions. Based on a comparison of these design methods, it can be concluded that the capacity of a deep beam region, as determined by the proposed procedure, results in less unnecessary conservatism compared to the ACI 318-08 and AASHTO LRFD (2008) provisions. The reason that the proposed method has less unnecessary conservatism is that the procedure considers the beneficial effects of triaxial confinement, and disregards the bond stresses at the back face of a CCT node.

Additionally, as illustrated in Section C.3.2, the proposed STM provisions resulted in a smaller discrepancy between the deep beam and sectional shear designs for an a/d ratio near two. Thus, designers can expect consistent results when using the proposed STM provisions for the design of a beam with an a/d ratio close to two.

Finally, as presented in Section C.2.3.5, it is likely that the bent will experience diagonal cracking under the application of 64% of the service level loading. As illustrated in Figure C-1, cracks as wide as 0.035-inches formed in this portion of the structure. The reason that the section is at risk of cracking under service loads is because the sectional shear resistance provided by the concrete cross-section (V_c) is much less than the resistance provided by the transverse reinforcement (V_s). The transverse reinforcement does not provide any resistance until after the concrete cracks. Thus, a disproportionately high ratio of V_s to V_c results in a low cracking capacity. This configuration may result in substantial cracking under the application of service loads. Birrcher (2008)

provides additional discussion regarding the serviceability behavior of a shear region.

APPENDIX D

Collection Database

D.1 REFERENCES

1. Ahmad, S. H., and Lue, D. M., "Flexure-Shear Interaction of Reinforced High-Strength Concrete Beams," *ACI Journal*, No. 84, July-August 1987, pp. 330-341.

2. Alcocer, S. M., and Uribe, C. M., "Monolithic and Cyclic Behavior of Deep Beams Designed Using Strut-and-Tie Models," *ACI Journal*, No. 105, May-June 2008, pp. 327-337.

3. Angelakos, D., *The Influence of Concrete Strength and Longitudinal Reinforcement Ratio on the Shear Strength of Large-Size Reinforced Concrete Beams With, and Without, Transverse Reinforcement*, Master's Thesis, 1999, Department of Civil Engineering, University of Toronto, 195 pp.

4. Angelakos, D.; Bentz, E. C; and Collins, M. P., "Effect of Concrete Strength and Minimum Stirrups on Shear Strength of Large Members," *ACI Journal*, No. 98, May-June 2001, pp. 290-300.

5. Bažant, Z. P., and Kazemi, M. T., "Size Effect of Diagonal Shear Failure of Beams without Stirrups," *ACI Journal*, No. 88, May-June 1991, pp. 268-276.

6. Bresler, B., and Scordelis, A. C., "Shear Strength of Reinforced Concrete Beams," *ACI Journal*, No. 60, January 1963, pp. 51-74.

7. Brown, M. D.; Sankovich, C. L.; Bayrak, O.; Jirsa, J. O.; Breen, J. E.; and Wood, S. L., *Design for Shear in Reinforced Concrete Using Strut-and-Tie Models*, Report No. 0-4371-2, Center for Transportation Research, University of Texas at Austin, Austin, Texas, Apr. 2006.

8. Brown, M. D.; Sankovich, C. L.; Bayrak, O.; Jirsa, J. O., "Behavior and Efficiency of Bottle-Shaped Struts," *ACI Journal*, No. 103, May-June 2006, pp. 348-355.

9. Cao, S., *Size Effect and the Influence of Longitudinal Reinforcement on the Shear Response of Large Reinforced Concrete Members*, Master's Thesis, University of Toronto, Toronto, Ontario, Canada, 2001, 195 pp.

10. Chang, T. S., and Kesler, C. E., "Static and Fatigue Strength in Shear of Beams with Tensile Reinforcement," *ACI Journal*, No. 54, June 1958, pp. 1033-1057.

11. Clark, A. P., "Diagonal Tension in Reinforced Concrete Beams," *ACI Journal*, No. 48, October 1951, pp. 145-156.

12. de Cossio, R. D., and Siess, C. P., "Behavior and Strength in Shear of Beams and Frames without Web Reinforcement," *ACI Journal*, No. 56, February 1960, pp. 695-735.

13. de Paiva, H. A. R., and Siess, C. P., "Strength and Behavior of Deep Beams in Shear," Journal of the Structural Division, ASCE Proceedings, ST 5, October 1965, pp. 19-41.

14. Ferguson, P. M., "Some Implications of Recent Diagonal Tension Tests," *ACI Journal*, No. 53, August 1956, pp. 157-172.

15. Foster, S. J., and Gilbert, R. I., "Experimental Studies on High-Strength Concrete Deep Beams," *ACI Journal*, No. 95, July-August 1998, pp. 382-390.

16. Furuuchi, H.; Takahashi, Y.; Ueda, T.; and Kakuta, Y., "Effective Width for Shear Failure of RC Deep Slabs," *Transaction of the Japan Concrete Institute*, Vol. 20, 1998, pp. 209-216.

17. Ghoneim, M., "Shear Strength of High-Strength Concrete Deep Beams," *Journal of Engineering and Applied Science*, Vol. 48, No. 4, August 2001, pp. 675-693.

18. Hara, T., The Shear Strength of Reinforced Concrete Deep Beams, *Transaction of the Japan Concrete Institute*, Vol. 6, 1985, pp. 395-402.

19. Hassan, T. K.; Seliem, H. M; Dwairi, H.; Rizkalla, S. H.; Zia, P., "Shear Behavior of Large Concrete Beams Reinforced with High-Strength Steel," *ACI Journal*, No. 105, March-April 2008, pp. 173-179.

20. Hsuing, W. and Frantz, G. C., "Transverse Stirrup Spacing in R/C Beam," *ASCE Journal of Structural Engineering*, Vol. 11, No. 2, February 1985, pp. 353-362

21. Johnson, M. K., and Ramirez, J. A., "Minimum Shear Reinforcement in Beams with Higher Strength Concrete," *ACI Journal*, No. 86, July-August 1989, pp. 376-382.

22. edited by Kani, M. W.; Huggins, M. W.; and Wittkopp, R. R., *Kani on Shear in Reinforced Concrete*, University of Toronto Press, Toronto, 1979, 225 pp.

23. Kong, P. Y. L., and Rangan, B. V., "Shear Strength of High-Performance Concrete Beams," *ACI Journal*, No. 95, November-December 1998, pp. 677-688.

24. Kong, F.; Robins, P. J.; and Cole D. F., "Web Reinforcement Effects on Deep Beams," *ACI Journal*, No. 67, December 1970, pp. 1010-1018.

25. Krefeld, W. J., and Thurston, C. W., "Studies of the Shear and Diagonal Tension Strength of Simply Supported Reinforced Concrete Beams," *ACI Journal*, No. 63, April 1966, pp. 451-476.

26. Krefeld, W. J., and Thurston, C. W., "Contribution of Longitudinal Steel to Shear Resistance of Reinforced Concrete Beams," *ACI Journal*, No. 63, March 1966, pp. 325-344.

27. Leonhardt, F. and Walther, R., translation by Amerongen, C. V., "The Stuttgardt Shear Tests, 1961", from *Beton und Stahlbeton, Vol. 56, No. 12, 1961 and Vol. 57, No. 2, 3, 6, 7, and 8, 1962,* Translation No. 111, Cement and Concrete Association, London, 1964, 138 pp.

28. Manuel, R. F.; Slight, B. W.; and Suter, G. T., "Deep Beam Behavior Affected by Length and Shear Span Variables," *ACI Journal*, No. 68, December 1971, pp. 954-958.

29. Matsuo, M.; Lertsrisakulrat, T.; Yanagawa, A.; and Niwa, J., "Shear Behavior of RC Deep Beams with Stirrups," *Transaction of the Japan Concrete Institute*, Vol. 23, 2002, pp. 385-390.

30. Moody, K. G.; Viest, I. M.; Elstner, R. C.; and Hognestad, E., "Shear Strength of Reinforced Concrete Beams, Part 1 – Tests of Simple Beams," *ACI Journal*, No. 51, December 1954, pp. 317-332.

31. Morrow, J., and Viest, I. M., "Shear Strength of Reinforced Concrete Frame Members without Web Reinforcement," *ACI Journal*, No. 53, March 1957, pp. 833-869.

32. Oh, J., and Shin, S., "Shear Strength of Reinforced High-Strength Concrete Deep Beams," *ACI Journal*, No. 98, March-April 2001, pp. 164-173.

33. Ozcebe, G.; Ersoy, U.; and Tankut, T., "Evaluation of Minimum Shear Reinforcement Requirements for Higher Strength Concrete," *ACI Journal*, No. 95, May-June 1999, pp. 361-369.

34. Quintero-Febres, C. G.; Montesinos, G. P.; and Wight, J. K., "Strength of Struts in Deep Concrete Members Designed Using Strut-and-Tie Method," *ACI Journal*, No. 103, July-August 2006, pp. 577-586.

35. Rajagopalan, K. S., and Ferguson, P. M., "Exploratory Shear Tests Emphasizing Percentage of Longitudinal Steel," *ACI Journal*, No. 65, August 1968, pp. 634-638.

36. Ramakrishnan, V. and Ananthanarayana, Y., "Ultimate Strength of Deep Beams in Shear," *ACI Journal*, No. 65, February 1968, pp. 87-98.

37. Rigotti, M., *Diagonal Cracking in Reinforced Concrete Deep Beams – An Experimental Investigation*, PhD Dissertation, Concordia University, Montreal, Quebec, Canada, November 2002, 235 pp.

38. Rogowsky, D. M.; MacGregor, J. G.; and Ong, S. Y., "Tests of Reinforced Concrete Deep Beams," *ACI Journal*, No. 83, July-August 1986, pp. 614-623.

39. Roller, J. J., and Russell, H. G., "Shear Strength of High-Strength Concrete Beams with Web Reinforcement," *ACI Journal*, No. 87, March-April 1990, pp. 191-198.

40. Sarsam, K. F., and Al-Musawi, J. M. S., "Shear Design of High and Normal Strength Concrete Beams with Web Reinforcement," *ACI Journal*, No. 89, November-December 1992, pp. 658-664.

41. Shin, S.; Lee, K.; Moon, J.; and Ghosh, S. K., "Shear Strength of Reinforced High-Strength Concrete Beams with Shear Span-to-Depth Ratios between 1.5 and 2.5," *ACI Journal*, No. 96, July-August 1999, pp. 549-557.

42. Shioya, T. S., *Shear Properties of Large Reinforced Concrete Member*, Special Report of Institute of Technology, Shimizu Corporation, No. 25, February 1989, 213 pp.

43. Smith, K. N. and Vantsiotis, A. S., "Shear Strength of Deep Beams," *ACI Journal*, No. 79, May-June 1982, pp. 201-213.

44. Stanik, B. A. P., *The Influence of Concrete Strength, Distribution of Longitudinal Reinforcement, Amount of Transverse Reinforcement and Member Size on Shear Strength of Reinforced Concrete Members*, Master's Thesis, 1998, Department of Civil Engineering, University of Toronto, 369 pp.

45. Subedi, N. K.; Vardy, A. E.; and Kubota, N., "Reinforced Concrete Deep Beams – Some Test Results," *Magazine of Concrete Research*, Vol. 38, No. 137, December 1986, pp. 206-219.

46. Tan, K.; Kong, F.; Teng, S.; and Guan, L.,"High-Strength Concrete Deep Beams with Effective Span and Shear Span Variations," *ACI Journal*, No. 92, July-August 1995, pp. 1-11.

47. Tan, K.; Kong, F.; Teng, S.; and Weng, L., "Effect of Web Reinforcement on High-Strength Concrete Deep Beams," *ACI Journal*, No. 94, September-October 1997, pp. 572-582.

48. Tan, K. H., and Lu, H. Y., "Shear Behavior of Large Reinforced Concrete Deep Beams and Code Comparisons," *ACI Journal*, No. 96, September-October 1999, pp. 836-846.

49. Tan, K.; Teng, S.; Kong, F.; Lu, H., ”Main Tension Steel in High Strength Concrete Deep and Short Beams,” *ACI Journal*, No. 94, November-December 1997, pp. 752-768.

50. Tanimura, Y., and Sato, T., “Evaluation of Shear Strength of Deep Beams with Stirrups,” *Quarterly Report of the Railway Technical Research Institute*, Vol. 46, No. 1, February 2005, pp. 53-58.

51. Uzel, A., *Shear Design of Large Footings*, Ph. D. Dissertation, University of Toronto, Toronto, Ontario, Canada, 2003, 404 pp.

52. Van Den Berg, F. J., ”Shear Strength of Reinforced Concrete Beams without Web Reinforcement,” *ACI Journal*, No. 59, November 1962, pp. 1587-1600.

53. Vecchio, F. J., “Analysis of Shear-Critical Reinforced Concrete Beams,” *ACI Journal*, No. 97, January-February 2000, pp. 102-110.

54. Walraven, J., and Lehwalter, N., “Size Effects in Short Beams Loaded in Shear,” *ACI Journal*, No. 91, September-October 1994, pp. 585-593.

55. Watstein, D., and Mathey, R. G., “Strains in Beams having Diagonal Cracks,” *ACI Journal*, No. 55, December 1958, pp. 717-728.

56. Xie, Y.; Ahmad, S. H.; Yu, T.; Hino, S.; and Chung, W., “Shear Ductility of Reinforced Concrete Beams of Normal and High-Strength Concrete,” *ACI Journal*, No. 91, March-April 1954, pp. 140-149.

57. Yang, K.; Chung, H.; Lee, E.; and Eun, H., “Shear Characteristics of High-Strength Concrete Deep Beams without Shear Reinforcements,” *Engineering Structures*, No. 25, April 2003, pp. 1343-1352.

58. Yoon, Y.; Cool, W. D.; and Mitchell, D., “Minimum Shear Reinforcement in Normal, Medium, and High-Strength Concrete Beams,” *ACI Journal*, No. 93, September-October 1996, pp. 1-9.

59. Yoshida, Y., *Shear Reinforcement for large Lightly Reinforced Concrete Members*, Master’s Thesis, University of Toronto, Toronto, Ontario, Canada, 2000, 162 pp.

60. Zhang, N., and Tan, K., “Size Effect in RC Deep Beams: Experimental Investigation and STM Verification,” *Engineering Structures*, No. 29, October 2007, pp. 3241-3254.

APPENDIX E

Evaluation Database

E.1 OVERVIEW

For the convenience of the reader, a summary of the details for all 36 tests of the experimental program is presented in Table E.1. The following nomenclature is used to describe the details of the beams in the Evaluation Database.

b = beam width, in.

h = beam height, in.

d = distance form extreme compression fiber to centroid of tensile reinforcement, in.

$\mathbf{f_c'}$ = compressive strength of concrete at the time of testing, psi.

Note: if the compressive strength was measured based on the test of a standard 100 or 150-mm cube, then it was converted to the equivalent 6-inch cylinder strength according to fib (1999).

$\mathbf{f_{yl}}$ = yield strength of tensile reinforcement measured in accordance with ASTM A370, ksi.

$\mathbf{f_{yv}}$ = yield strength of transverse reinforcement measured in accordance with ASTM A370, ksi.

$\boldsymbol{\rho_l}$ = ratio of longitudinal tensile reinforcement to effective area, $A_s / b \cdot d$

$\boldsymbol{\rho_l'}$ = ratio of longitudinal compression reinforcement to effective area, $A_s' / b \cdot d$

$\boldsymbol{\rho_v}$ = ratio of vertical transverse reinforcement to effective area, $A_v / b \cdot s_1$

$\boldsymbol{\rho_h}$ = ratio of horizontal transverse reinforcement to effective area, $A_{vh} / b \cdot s_2$

s = spacing of vertical ties, in.

Load Plate = dimensions of the load bearing plate measured in the longitudinal and transverse direction (*l* x *w*), in.

Support Plate = dimensions of the support bearing plate measured in the longitudinal and transverse direction (*l* x *w*), in.

a/d ratio = shear span-to-depth ratio

$\mathbf{V_{test}}$ = maximum shear carried in test region, including the estimated self weight of the specimen and transfer girders, kip

Table E.1. Evaluation Database (1 of 8)

Beam I.D.	b in.	h in.	d in.	f'_c psi	f_{yl} ksi	f_{yv} ksi	ρ_l'	ρ_l	ρ_v	ρ_h	s in.	Load Plate l x w in.	Support Plate l x w in.	a/d ratio	V_{test} kip
Current Study (2008)															
M-03-4-CCC2436	36	48	40	4100	67	61	0.0043	0.0293	0.0031	0.0030	11	24x36	16x36	1.85	1128.3
M-09-4-CCC2436	36	48	40	4100	67	61	0.0043	0.0293	0.0086	0.0030	4	24x36	16x36	1.85	1426.0
M-02-4-CCC2436	36	48	40	2800	65	63	0.0043	0.0293	0.0022	0.0022	10	24x36	16x36	1.85	1102.0
M-03-4-CCC0812	36	48	40	3000	65	63	0.0043	0.0293	0.0031	0.0030	11	8x12	16x36	1.85	930.0
I-03-2	21	44	38.5	5240	73	67	0.0116	0.0229	0.0029	0.0033	6.5	20x21	16x21	1.84	569.2
I-03-4	21	44	38.5	5330	73	73	0.0116	0.0229	0.0030	0.0033	7	20x21	16x21	1.84	657.4
I-02-2	21	44	38.5	3950	73	67	0.0116	0.0229	0.0020	0.0020	9.5	20x21	16x21	1.84	453.7
I-02-4	21	44	38.5	4160	73	73	0.0116	0.0229	0.0021	0.0020	10	20x21	16x21	1.84	528.1
II-03-CCC2021	21	42	38.6	3290	64	65	0.0115	0.0231	0.0031	0.0045	9.5	20x21	10x21	1.84	499.5
II-03-CCC1007	21	42	38.6	3480	64	65	0.0115	0.0231	0.0031	0.0045	9.5	10x7	10x21	1.84	477.4
II-03-CCT1021	21	42	38.6	4410	66	71	0.0115	0.0231	0.0031	0.0045	9.5	36x21	10x21	1.84	635.4
II-03-CCT0507	21	42	38.6	4210	66	71	0.0115	0.0231	0.0031	0.0045	9.5	36x21	5x7	1.84	597.4
II-02-CCT0507	21	42	38.6	3120	69	64	0.0115	0.0231	0.0020	0.0019	15	36x21	5x7	1.84	401.4
II-02-CCC1007	21	42	38.6	3140	69	64	0.0115	0.0231	0.0020	0.0019	15	10x7	10x21	1.84	334.8
II-02-CCC1021	21	42	38.6	4620	69	67	0.0115	0.0231	0.0020	0.0019	15	10x21	10x21	1.84	329.0
II-02-CCT0521	21	42	38.6	4740	69	67	0.0115	0.0231	0.0020	0.0019	15	20x21	5x21	1.84	567.4
III-1.85-02	21	42	38.6	4100	66	64	0.0115	0.0231	0.0020	0.0019	14.5	20x21	16x21	1.84	487.8
III-1.85-025	21	42	38.6	4100	66	64	0.0115	0.0231	0.0024	0.0014	12	20x21	16x21	1.84	515.6
III-1.85-03	21	42	38.6	4990	69	64	0.0115	0.0231	0.0029	0.0029	10	20x21	16x21	1.84	412.3
III-1.85-01	21	42	38.6	5010	69	63	0.0115	0.0231	0.0010	0.0014	18	20x21	16x21	1.84	272.6
III-1.85-03b	21	42	38.6	3300	69	62	0.0115	0.0231	0.0031	0.0029	6	20x21	16x21	1.84	471.1
III-1.85-02b	21	42	38.6	3300	69	62	0.0115	0.0231	0.0020	0.0018	9.5	20x21	16x21	1.84	467.6
III-1.2-02	21	42	38.6	4100	66	60	0.0115	0.0231	0.0020	0.0018	9.5	20x21	16x21	1.84	846.5
III-1.2-03	21	42	38.6	4220	66	68	0.0115	0.0231	0.0031	0.0029	9.5	20x21	16x21	1.84	829.2
III-2.5-02	21	42	38.6	4630	66	62	0.0115	0.0231	0.0020	0.0018	9.5	20x21	16x21	1.84	298.3
III-2.5-03	21	42	38.6	5030	66	65	0.0115	0.0231	0.0031	0.0029	9.5	20x21	16x21	1.84	516.0

Table E.1. Evaluation Database (2 of 8)

Beam I.D.	b in.	h in.	d in.	f'_c psi	f_y ksi	f_{yv} ksi	ρ_l'	ρ_l	ρ_v	ρ_h	s in.	Load Plate l x w in.	Support Plate l x w in.	a/d ratio	V_{test} kip
Current Study (2008), continued…															
IV-2175-1.85-02	21	74.5	68.9	4930	68	66	0.0129	0.0237	0.0020	0.0018	9.5	29x21	16x21	1.85	762.7
IV-2175-1.85-03	21	74.5	68.9	4930	68	66	0.0129	0.0237	0.0031	0.0029	9.5	29x21	16x21	1.85	842.4
IV-2175-2.5-02	21	74.5	68.9	5010	68	64	0.0129	0.0237	0.0021	0.0021	14.3	24x21	16x21	2.50	509.9
IV-2175-1.2-02	21	74.5	68.9	5010	68	64	0.0129	0.0237	0.0021	0.0021	14.3	24x21	16x21	1.2	1222.8
IV-2123-1.85-03	21	22.5	19.5	4160	66	66	0.0232	0.0232	0.0030	0.0030	6.3	16.5x21	16x21	1.85	328.5
IV-2123-1.85-02	21	22.5	19.5	4220	66	81	0.0232	0.0232	0.0020	0.0017	5.3	16.5x21	16x21	1.85	347.0
IV-2123-2.5-02	21	22.5	19.5	4570	65	58	0.0232	0.0232	0.0020	0.0017	5.3	15.5x21	16x21	2.50	160.7
IV-2123-1.2-02	21	22.5	19.5	4630	65	58	0.0232	0.0232	0.0020	0.0017	5.3	18x21	16x21	1.20	591.6
Rogowsky, MacGregor, and Ong (1986)															
1/1.0N	7.9	39.4	37.4	3785	55	83	0.0000	0.0094	0.0015	0.0000	7.4	11.8x7.9	7.9x7.9	1.05	136.3
2/1.0N	7.9	39.4	37.4	3887	55	83	0.0003	0.0094	0.0015	0.0006	7.4	11.8x7.9	7.9x7.9	1.05	169.6
2/1.5N	7.9	23.6	21.1	6150	66	83	0.0005	0.0112	0.0019	0.0011	5.9	11.8x7.9	7.9x7.9	1.87	78.8
2/2.0N	7.9	19.7	17.9	6266	66	83	0.0006	0.0088	0.0014	0.0012	7.9	7.9x7.9	7.9x7.9	2.20	46.3
Brown, Sankovich, Bayrak, Jirsa, Breen, and Wood (2006)															
I-CL-8.5-0	6	30	27	2584	68	73	0.0195	0.0014	0.0043	0.0000	8.5	6x6	6x6	1.11	79.9
I-2C-8.5-0	6	30	27	3208	68	73	0.0195	0.0014	0.0043	0.0000	8.5	12x6	6x6	1.67	121.6
II-N-F-5.8-3	18	18	16	2880	68	73	0.0219	0.0008	0.0041	0.0000	3	10x18	6x18	1.69	180.8
Moody, Viest, Elstner, and Hognestad (1954)															
III-30	7	24	21	3680	44	47	0.0425	0.0213	0.0052	0.0000	6	8x7	8x7	1.52	108.1
III-31	7	24	21	3250	44	44	0.0425	0.0213	0.0095	0.0000	6	8x7	8x7	1.52	114.6

Table E.1. Evaluation Database (3 of 8)

Beam I.D.	b in.	h in.	d in.	f'_c psi	f_y ksi	f_{yv} ksi	ρ_l'	ρ_l	ρ_v	ρ_h	s in.	Load Plate l x w in.	Support Plate l x w in.	a/d ratio	V_{test} kip
Oh and Shin (2001)															
N42A2	5.1	22.1	19.7	3440	60	60	0.0156	0.0022	0.0012	0.0043	16	7.1x5.1	5.1x5.1	0.85	64.1
N42B2	5.1	22.1	19.7	3440	60	60	0.0156	0.0022	0.0022	0.0043	8.7	7.1x5.1	5.1x5.1	0.85	84.9
N42C2	5.1	22.1	19.7	3440	60	60	0.0156	0.0022	0.0034	0.0043	5.7	7.1x5.1	5.1x5.1	0.85	80.6
H41A2(1)	5.1	22.1	19.7	7121	60	60	0.0156	0.0022	0.0012	0.0043	16	7.1x5.1	5.1x5.1	0.50	160.3
H41B2	5.1	22.1	19.7	7121	60	60	0.0156	0.0022	0.0022	0.0043	8.7	7.1x5.1	5.1x5.1	0.50	158.7
H41C2	5.1	22.1	19.7	7121	60	60	0.0156	0.0022	0.0034	0.0043	5.7	7.1x5.1	5.1x5.1	0.50	159.3
H42A2(1)	5.1	22.1	19.7	7121	60	60	0.0156	0.0022	0.0012	0.0043	16	7.1x5.1	5.1x5.1	0.85	109.9
H42B2(1)	5.1	22.1	19.7	7121	60	60	0.0156	0.0022	0.0022	0.0043	8.7	7.1x5.1	5.1x5.1	0.85	102.7
H42C2(1)	5.1	22.1	19.7	7121	60	60	0.0156	0.0022	0.0034	0.0043	5.7	7.1x5.1	5.1x5.1	0.85	94.7
H43A2(1)	5.1	22.1	19.7	7121	60	60	0.0156	0.0022	0.0012	0.0043	16	7.1x5.1	5.1x5.1	1.25	78.2
H43B2	5.1	22.1	19.7	7121	60	60	0.0156	0.0022	0.0022	0.0043	8.7	7.1x5.1	5.1x5.1	1.25	85.8
H43C2	5.1	22.1	19.7	7121	60	60	0.0156	0.0022	0.0034	0.0043	5.7	7.1x5.1	5.1x5.1	1.25	90.6
H45A2	5.1	22.1	19.7	7121	60	60	0.0156	0.0022	0.0012	0.0043	16	7.1x5.1	5.1x5.1	2.00	47.6
H45B2	5.1	22.1	19.7	7121	60	60	0.0156	0.0022	0.0022	0.0043	8.7	7.1x5.1	5.1x5.1	2.00	53.6
H45C2	5.1	22.1	19.7	7121	60	60	0.0156	0.0022	0.0034	0.0043	5.7	7.1x5.1	5.1x5.1	2.00	53.1
N33A2	5.1	22.1	19.7	3440	60	60	0.0156	0.0022	0.0012	0.0043	16	7.1x5.1	5.1x5.1	1.25	51.5
N43A2	5.1	22.1	19.7	3440	60	60	0.0156	0.0022	0.0012	0.0043	16	7.1x5.1	5.1x5.1	1.25	57.5
N53A2	5.1	22.1	19.7	3440	60	60	0.0156	0.0022	0.0012	0.0043	16	7.1x5.1	5.1x5.1	1.25	46.9
H31A2	5.1	22.1	19.7	7121	60	60	0.0156	0.0022	0.0012	0.0043	16	7.1x5.1	5.1x5.1	0.50	167.6
H32A2	5.1	22.1	19.7	7121	60	60	0.0156	0.0022	0.0012	0.0043	16	7.1x5.1	5.1x5.1	0.85	119.1
H33A2	5.1	22.1	19.7	7121	60	60	0.0156	0.0022	0.0012	0.0043	16	7.1x5.1	5.1x5.1	1.25	85.0
H51A2	5.1	22.1	19.7	7121	60	60	0.0156	0.0022	0.0012	0.0043	16	7.1x5.1	5.1x5.1	0.50	157.9
H52A2	5.1	22.1	19.7	7121	60	60	0.0156	0.0022	0.0012	0.0043	16	7.1x5.1	5.1x5.1	0.85	127.8
H53A2	5.1	22.1	19.7	7121	60	60	0.0156	0.0022	0.0012	0.0043	16	7.1x5.1	5.1x5.1	1.25	81.8

Table E.1. Evaluation Database (4 of 8)

Beam I.D.	b in.	h in.	d in.	f'_c psi	f_y ksi	f_{yv} ksi	ρ_l'	ρ_l	ρ_v	ρ_h	s in.	Load Plate l x w in.	Support Plate l x w in.	a/d ratio	V_{test} kip
Foster and Gilbert (1998)															
B1.2-3	4.9	47.2	44.2	11603	58	62	0.0134	0.0017	0.0067	0.0028	3	9.8x4.9	9.8x4.9	0.76	292.9
B2.0-1	4.9	27.6	24.6	12038	58	62	0.0241	0.0030	0.0067	0.0037	3	9.8x4.9	9.8x4.9	1.32	179.0
B2.0-2	4.9	27.6	24.6	17404	58	62	0.0241	0.0030	0.0067	0.0037	3	9.8x4.9	9.8x4.9	1.32	185.8
B2.0-3	4.9	27.6	24.6	11313	58	62	0.0241	0.0030	0.0067	0.0037	3	9.8x4.9	9.8x4.9	1.32	157.7
B2.0A-4	4.9	27.6	24.6	12473	58	62	0.0241	0.0030	0.0067	0.0037	3	3.9x4.9	9.8x4.9	0.88	213.9
B2.0C-6	4.9	27.6	24.6	13489	58	62	0.0241	0.0030	0.0100	0.0000	2	9.8x4.9	9.8x4.9	1.32	164.4
B2.0D-7	4.9	27.6	24.6	15084	58	62	0.0241	0.0030	0.0067	0.0000	3	9.8x4.9	9.8x4.9	1.32	162.2
B3.0-1	4.9	27.6	24.6	11603	58	62	0.0241	0.0030	0.0067	0.0037	3	9.8x4.9	9.8x4.9	1.88	115.2
B3.0-2	4.9	27.6	24.6	17404	58	62	0.0241	0.0030	0.0067	0.0037	3	9.8x4.9	9.8x4.9	1.88	118.5
B3.0-3	4.9	27.6	24.6	11168	58	62	0.0241	0.0030	0.0067	0.0037	3	9.8x4.9	9.8x4.9	1.88	118.5
B3.0A-4	4.9	27.6	24.6	12763	58	62	0.0241	0.0030	0.0067	0.0037	3	3.9x4.9	9.8x4.9	1.28	174.7
Clark (1951)															
A1-1	8	18	15.3	3575	47	48	0.0310	0.0018	0.0038	0.0000	7.2	3.5x8	3.5x8	2.35	50.4
A1-2	8	18	15.3	3430	47	48	0.0310	0.0018	0.0038	0.0000	7.2	3.5x8	3.5x8	2.35	47.4
A1-3	8	18	15.3	3395	47	48	0.0310	0.0018	0.0038	0.0000	7.2	3.5x8	3.5x8	2.35	50.4
A1-4	8	18	15.3	3590	47	48	0.0310	0.0018	0.0038	0.0000	7.2	3.5x8	3.5x8	2.35	55.4
B1-1	8	18	15.3	3388	47	48	0.0310	0.0018	0.0037	0.0000	7.5	3.5x8	3.5x8	1.96	63.1
B1-2	8	18	15.3	3680	47	48	0.0310	0.0018	0.0037	0.0000	7.5	3.5x8	3.5x8	1.96	58.1
B1-3	8	18	15.3	3435	47	48	0.0310	0.0018	0.0037	0.0000	7.5	3.5x8	3.5x8	1.96	64.4
B1-4	8	18	15.3	3380	47	48	0.0310	0.0018	0.0037	0.0000	7.5	3.5x8	3.5x8	1.96	60.7
B1-5	8	18	15.3	3570	47	48	0.0310	0.0018	0.0037	0.0000	7.5	3.5x8	3.5x8	1.96	54.7
B2-1	8	18	15.3	3370	47	48	0.0310	0.0018	0.0073	0.0000	3.8	3.5x8	3.5x8	1.96	68.1
B2-2	8	18	15.3	3820	47	48	0.0310	0.0018	0.0073	0.0000	3.8	3.5x8	3.5x8	1.96	72.8
B2-3	8	18	15.3	3615	47	48	0.0310	0.0018	0.0073	0.0000	3.8	3.5x8	3.5x8	1.96	75.7
B6-1	8	18	15.3	6110	47	48	0.0310	0.0018	0.0037	0.0000	7.5	3.5x8	3.5x8	1.96	85.7

Table E.1. Evaluation Database (5 of 8)

Beam I.D.	b in.	h in.	d in.	f'_c psi	f_y ksi	f_{yv} ksi	ρ_l'	ρ_l	ρ_v	ρ_h	s in.	Load Plate *l* x *w* in.	Support Plate *l* x *w* in.	a/d ratio	V_{test} kip
Clark (1951) continued…															
C1-1	8	18	15.3	3720	47	48	0.0207	0.0018	0.0034	0.0000	8	3.5x8	3.5x8	1.57	62.8
C1-2	8	18	15.3	3820	47	48	0.0207	0.0018	0.0034	0.0000	8	3.5x8	3.5x8	1.57	70.3
C1-3	8	18	15.3	3475	47	48	0.0207	0.0018	0.0034	0.0000	8	3.5x8	3.5x8	1.57	55.7
C1-4	8	18	15.3	4210	47	48	0.0207	0.0018	0.0034	0.0000	8	3.5x8	3.5x8	1.57	64.7
C2-1	8	18	15.3	3430	47	48	0.0207	0.0018	0.0069	0.0000	4	3.5x8	3.5x8	1.57	65.6
C2-2	8	18	15.3	3625	47	48	0.0207	0.0018	0.0069	0.0000	4	3.5x8	3.5x8	1.57	68.1
C2-3	8	18	15.3	3500	47	48	0.0207	0.0018	0.0069	0.0000	4	3.5x8	3.5x8	1.57	73.2
C2-4	8	18	15.3	3910	47	48	0.0207	0.0018	0.0069	0.0000	4	3.5x8	3.5x8	1.57	65.2
C3-1	8	18	15.3	2040	47	48	0.0207	0.0018	0.0034	0.0000	8	3.5x8	3.5x8	1.57	50.7
C3-2	8	18	15.3	2000	47	48	0.0207	0.0018	0.0034	0.0000	8	3.5x8	3.5x8	1.57	45.4
C3-3	8	18	15.3	2020	47	48	0.0207	0.0018	0.0034	0.0000	8	3.5x8	3.5x8	1.57	42.7
C4-1	8	18	15.3	3550	47	48	0.0310	0.0018	0.0034	0.0000	8	3.5x8	3.5x8	1.57	69.9
C6-2	8	18	15.3	6560	47	48	0.0310	0.0018	0.0034	0.0000	8	3.5x8	3.5x8	1.57	95.7
C6-3	8	18	15.3	6480	47	48	0.0310	0.0018	0.0034	0.0000	8	3.5x8	3.5x8	1.57	98.2
C6-4	8	18	15.3	6900	47	48	0.0310	0.0018	0.0034	0.0000	8	3.5x8	3.5x8	1.57	96.7
D1-1	8	18	15.5	3800	49	48	0.0163	0.0018	0.0046	0.0000	6	3.5x8	3.5x8	1.16	68.1
D1-2	8	18	15.5	3790	49	48	0.0163	0.0018	0.0046	0.0000	6	3.5x8	3.5x8	1.16	80.6
D1-3	8	18	15.5	3560	49	48	0.0163	0.0018	0.0046	0.0000	6	3.5x8	3.5x8	1.16	58.1
D2-1	8	18	15.5	3480	49	48	0.0163	0.0018	0.0061	0.0000	4.5	3.5x8	3.5x8	1.16	65.6
D2-2	8	18	15.5	3755	49	48	0.0163	0.0018	0.0061	0.0000	4.5	3.5x8	3.5x8	1.16	70.6
D2-3	8	18	15.5	3595	49	48	0.0163	0.0018	0.0061	0.0000	4.5	3.5x8	3.5x8	1.16	75.6
D2-4	8	18	15.5	3550	49	48	0.0163	0.0018	0.0061	0.0000	4.5	3.5x8	3.5x8	1.16	75.7
D3-1	8	18	15.5	4090	49	48	0.0244	0.0018	0.0092	0.0000	3	3.5x8	3.5x8	1.16	89.2
D4-1	8	18	15.5	3350	49	48	0.0163	0.0018	0.0122	0.0000	2.3	3.5x8	3.5x8	1.16	70.6
Alcocer and Uribe (2008)															
MR	13.8	47	43.3	5134	65	62	0.0158	0.0079	0.0053	0.0029	6	15.8x13.8	15.8x13.8	1.27	363.4
MT	13.8	47	43.3	5076	65	62	0.0158	0.0079	0.0053	0.029	6	15.8x13.8	15.8x13.8	1.27	363.4

Table E.1. Evaluation Database (6 of 8)

Beam I.D.	**b** in.	**h** in.	**d** in.	**f'_c** psi	**f_y** ksi	**f_{yv}** ksi	**ρ_l'**	**ρ_l**	**ρ_v**	**ρ_h**	**s** in.	**Load Plate** *l* x *w* in.	**Support Plate** *l* x *w* in.	**a/d ratio**	**V_{test}** kip
Tanimura and Sato (2005)															
2A	11.8	17.7	15.8	3365	66	54	0.0214	0.0033	0.0021	0.0000	3.9	3.9x11.8	3.9x11.8	0.50	184.9
3A	11.8	17.7	15.8	3365	66	56	0.0214	0.0033	0.0048	0.0000	3.9	3.9x11.8	3.9x11.8	0.50	187.6
4A	11.8	17.7	15.8	3365	66	53	0.0214	0.0033	0.0084	0.0000	3.9	3.9x11.8	3.9x11.8	0.50	195.7
6A	11.8	17.7	15.8	4206	66	54	0.0214	0.0033	0.0021	0.0000	3.9	3.9x11.8	3.9x11.8	1.00	164.7
7A	11.8	17.7	15.8	4206	66	56	0.0214	0.0033	0.0048	0.0000	3.9	3.9x11.8	3.9x11.8	1.00	169.0
8A	11.8	17.7	15.8	4206	66	53	0.0214	0.0033	0.0084	0.0000	3.9	3.9x11.8	3.9x11.8	1.00	181.1
11A	11.8	17.7	15.8	3336	66	56	0.0214	0.0033	0.0048	0.0000	3.9	3.9x11.8	3.9x11.8	1.50	110.9
12A	11.8	17.7	15.8	3408	66	53	0.0214	0.0033	0.0084	0.0000	3.9	3.9x11.8	3.9x11.8	1.50	128.6
14B	11.8	17.7	15.8	4641	66	54	0.0214	0.0000	0.0021	0.0000	3.9	3.9x11.8	3.9x11.8	1.00	169.2
15B	11.8	17.7	15.8	4641	66	56	0.0214	0.0000	0.0048	0.0000	3.9	3.9x11.8	3.9x11.8	1.00	174.4
16B	11.8	17.7	15.8	4641	66	53	0.0214	0.0000	0.0084	0.0000	3.9	3.9x11.8	3.9x11.8	1.00	191.3
17C	11.8	17.7	15.8	4540	66	54	0.0214	0.0033	0.0021	0.0000	3.9	3.9x11.8	3.9x11.8	1.00	128.5
18C	11.8	17.7	15.8	4569	66	56	0.0214	0.0033	0.0048	0.0000	3.9	3.9x11.8	3.9x11.8	1.00	174.2
19C	11.8	17.7	15.8	4612	66	53	0.0214	0.0033	0.0084	0.0000	3.9	3.9x11.8	3.9x11.8	1.00	170.4
20D	11.8	17.7	15.8	3524	102	138	0.0214	0.0033	0.0048	0.0000	3.9	3.9x11.8	3.9x11.8	1.00	149.9
21D	11.8	17.7	15.8	3902	102	152	0.0214	0.0033	0.0084	0.0000	3.9	3.9x11.8	3.9x11.8	1.00	149.0
22D	11.8	17.7	15.8	3800	102	138	0.0214	0.0033	0.0048	0.0000	3.9	3.9x11.8	3.9x11.8	1.50	121.2
23D	11.8	17.7	15.8	3814	102	152	0.0214	0.0033	0.0084	0.0000	3.9	3.9x11.8	3.9x11.8	1.50	127.7
28A	11.8	17.7	15.8	3698	66	56	0.0214	0.0033	0.0048	0.0000	3.9	3.9x11.8	3.9x11.8	0.75	145.8
29A	11.8	17.7	15.8	3800	66	53	0.0214	0.0033	0.0084	0.0000	3.9	3.9x11.8	3.9x11.8	0.75	150.0
30A	11.8	17.7	15.8	3829	66	56	0.0214	0.0033	0.0088	0.0000	5.9	3.9x11.8	3.9x11.8	0.75	157.9
31A	11.8	17.7	15.8	3858	102	56	0.0214	0.0033	0.0048	0.0000	3.9	3.9x11.8	3.9x11.8	2.00	94.1
32A	11.8	17.7	15.8	3974	102	53	0.0214	0.0033	0.0084	0.0000	3.9	3.9x11.8	3.9x11.8	2.00	99.5
33A	11.8	17.7	15.8	3582	66	56	0.0214	0.0033	0.0095	0.0000	2.0	3.9x11.8	3.9x11.8	1.00	145.9
34A	11.8	17.7	15.8	3597	66	54	0.0214	0.0033	0.0095	0.0000	7.9	3.9x11.8	3.9x11.8	1.00	134.8
36E	11.8	17.7	15.8	3553	193	56	0.0042	0.0033	0.0048	0.0000	3.9	3.9x11.8	3.9x11.8	0.50	121.5
37E	11.8	17.7	15.8	3742	193	53	0.0042	0.0033	0.0084	0.0000	3.9	3.9x11.8	3.9x11.8	0.50	124.8
39E	11.8	17.7	15.8	3684	193	56	0.0042	0.0033	0.0048	0.0000	3.9	3.9x11.8	3.9x11.8	1.00	106.1

Table E.1. Evaluation Database (7 of 8)

Beam I.D.	b in.	h in.	d in.	f'_c psi	f_y ksi	f_{yv} ksi	ρ_l'	ρ_l	ρ_v	ρ_h	s in.	Load Plate l x w in.	Support Plate l x w in.	a/d ratio	V_{test} kip
Tanimura and Sato (2005), continued…															
40E	11.8	17.7	15.8	3756	193	53	0.0042	0.0033	0.0084	0.0000	3.9	3.9x11.8	3.9x11.8	1.00	106.1
41A	11.8	17.7	15.8	2988	109	56	0.0214	0.0033	0.0048	0.0000	3.9	3.9x11.8	3.9x11.8	2.50	73.5
42A	11.8	17.7	15.8	3104	109	53	0.0214	0.0033	0.0084	0.0000	3.9	3.9x11.8	3.9x11.8	2.50	85.2
46F	11.8	17.7	15.8	14141	109	139	0.0214	0.0033	0.0021	0.0000	3.9	3.9x11.8	3.9x11.8	1.00	279.8
47F	11.8	17.7	15.8	13967	109	138	0.0214	0.0033	0.0048	0.0000	3.9	3.9x11.8	3.9x11.8	1.00	292.7
48F	11.8	17.7	15.8	13706	109	139	0.0214	0.0033	0.0021	0.0000	3.9	3.9x11.8	3.9x11.8	1.50	210.0
49F	11.8	17.7	15.8	13663	109	138	0.0214	0.0033	0.0048	0.0000	3.9	3.9x11.8	3.9x11.8	1.50	220.8
L6	7.9	41.3	39.4	4525	147	56	0.002	0.004	0.0029	0.0000	9.8	5.9x7.9	5.9x7.9	1.00	150.7
L7	15.8	80.7	78.7	4424	147	54	0.0005	0.004	0.0029	0.0000	19.7	11.8x15.8	11.8x15.8	1.00	589.9
Matsuo, Lertsrisakulrat, Yanagawa, and Niwa (2002)															
D604	5.9	25.6	23.6	4960	146	48	0.0176	0.0006	0.0042	0.0000	3.9	5.9x5.9	5.9x5.9	1.00	132.1
D608	5.9	25.6	23.6	5120	146	48	0.0176	0.0006	0.0084	0.0000	2.0	5.9x5.9	5.9x5.9	1.00	149.5
Brown, Sankovich, Bayrak, and Jirsa (2006)															
G	6	36	36	4300	0	73	0.0005	0.0000	0.0031	0.0031	6	12x6	12x6	0.00	264.5
L	6	36	36	5290	0	73	0.0005	0.0000	0.0000	0.0031	0	12x6	12x6	0.00	366.8
M	6	36	36	4300	0	73	0.0005	0.0000	0.0000	0.0031	0	12x6	12x6	0.00	283.2
N	6	36	36	4300	0	73	0.0005	0.0000	0.0000	0.0031	0	6x6	6x6	0.00	202.1
O	6	36	36	5500	0	73	0.0002	0.0000	0.0000	0.0027	0	12x6	12x6	0.00	352.4
P	6	36	36	5500	0	73	0.0005	0.0000	0.0000	0.0061	0	12x6	12x6	0.00	377.0
Q	6	36	36	4200	0	73	0.0000	0.0000	0.0000	0.0010	0	12x6	12x6	0.00	224.0
T	6	36	36	5290	0	73	0.0000	0.0000	0.0000	0.0046	0	12x6	12x6	0.00	343.1
U	6	36	36	4350	0	73	0.0000	0.0000	0.0000	0.0023	0	6x6	6x6	0.00	189.0
V	6	36	36	4350	0	73	0.0000	0.0000	0.0046	0.0015	4	12x6	12x6	0.00	259.7
W	6	36	36	4350	0	73	0.0005	0.0000	0.0000	0.0031	0	16x6	16x6	0.00	370.1
X	6	36	36	4350	0	73	0.0005	0.0000	0.0000	0.0031	0	12x6	12x6	0.00	246.7
Y	10	36	36	4350	0	73	0.0010	0.0000	0.0000	0.0037	0	12x4	12x4	0.00	299.5
Z	10	36	36	4350	0	73	0.0010	0.0000	0.0000	0.0037	0	12x4	12x4	0.00	303.8

Table E.1. Evaluation Database (8 of 8)

Beam I.D.	b in.	h in.	d in.	f'_c psi	f_y ksi	f_{yv} ksi	ρ_l'	ρ_l	ρ_v	ρ_h	s in.	Load Plate l x w in.	Support Plate l x w in.	a/d ratio	V_{test} kip
Walraven and Lehwalter (1994)															
V411/4	9.8	31.5	29.9	3083	60	60	0.0107	0.0000	0.0017	0.0000	7.5	7.5x9.8	7.5x9.8	0.97	105.7
V022/3	9.8	15.8	14.2	3554	60	60	0.0113	0.0000	0.0035	0.0000	3.9	3.5x9.8	3.5x9.8	1.00	85.6
V511/3	9.8	23.6	22.1	3861	60	60	0.0112	0.0000	0.0033	0.0000	5.9	5.5x9.8	5.5x9.8	1.01	130.8
V411/3	9.8	31.5	29.9	3590	60	60	0.0107	0.0000	0.0033	0.0000	7.5	7.5x9.8	7.5x9.8	0.97	150.2
Zhang and Tan (2007)															
1DB70bw	6.3	27.6	25.3	4104	76	54	0.0111	0.0010	0.0021	0.0000	5.9	4.1x6.3	4.1x6.3	1.10	96.2
1DB100bw	9.1	39.4	35.6	4162	75	66	0.0123	0.0007	0.0021	0.0000	5.9	5.9x9.1	5.9x9.1	1.10	174.9
Deschenes and Bayrak (2009)															
VALID	21	42	36.1	5061	66	65	0.0310	0.0100	0.0030	0.0058	9.5	20x21	16x21	1.85	576.6
NR1	21	42	36.1	7250	66	65	0.0310	0.0100	0.0030	0.0058	9.5	20x21	16x21	1.85	560.8

APPENDIX F

Outline of Calculations used for STM Design Provisions

F.1 OVERVIEW

The overall capacity of all of the beams in the evaluation database was estimated according to the following deep beam design provisions: ACI 318-08; AASHTO LRFD (2008); *fib* (1999); ACI 318-99 Chapter 11; and the newly proposed STM method (Chapter 6). The purpose of this Appendix is to present the details for these calculations.

F.2 KNOWN STM TRUSS GEOMETRIES

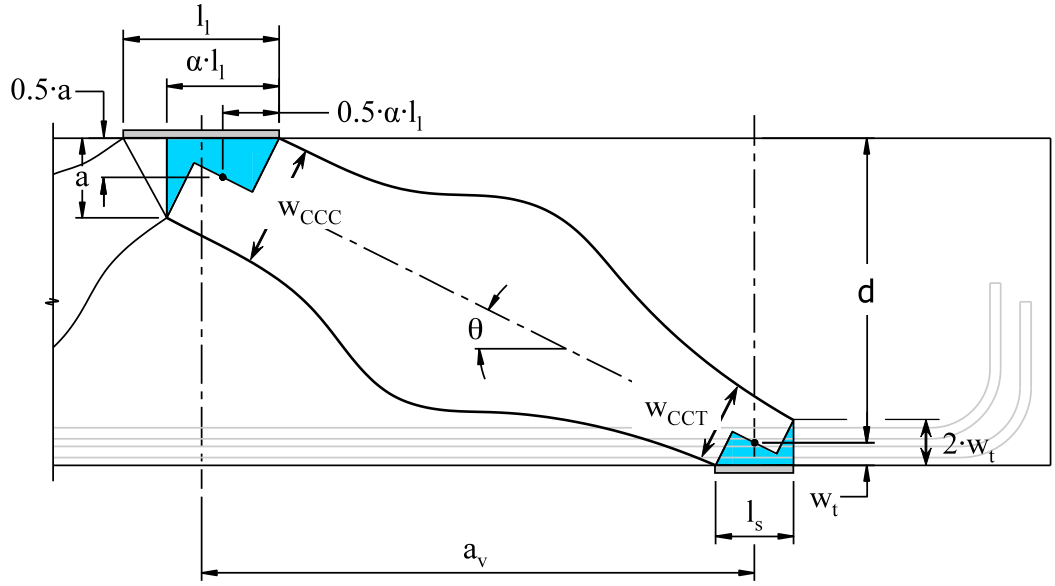

Figure F-1. Truss model.

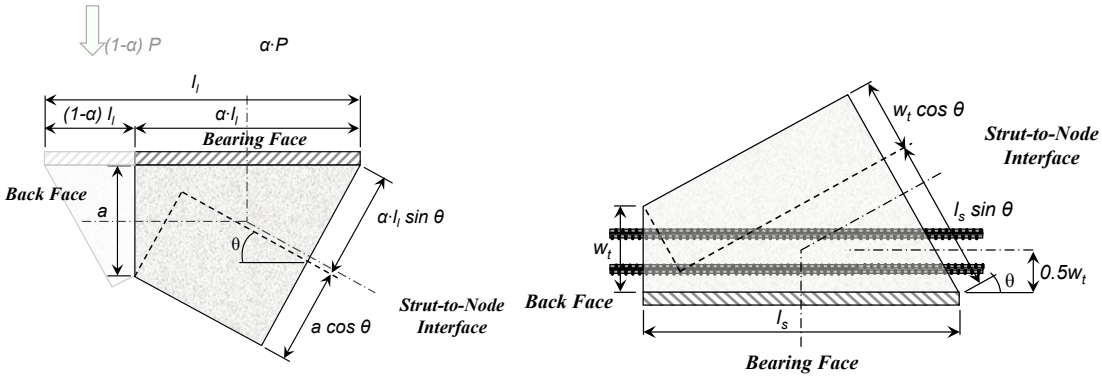

CCC Node **CCT Node**

Figure F-2 CCC and CCT nodes.

Where,

1) $\alpha =$ portion of load that is resisted by near support.

2) $\theta =$ tan^{-1}

3) $w_t =$ $2\cdot(h-d)$

4) $W_{CCC} =$ $\alpha\cdot l_l\cdot sin\theta + \alpha\cdot cos\theta$

5) $W_{CCT} =$ $l_s\cdot sin\theta + w_t\cdot cos\theta$

6) $a =$ $\dfrac{\left(A_s\cdot f_s - A_s^{'}\cdot f_s^{'}\right)}{0.85 f_c^{'}\cdot b_w}$

7) $\rho_{\perp} =$ $\rho_v \cos\theta + \rho_{vh}\sin\theta$

8) $b_l =$ width of the load plate (CCC)

9) $b_s =$ width of the support plate (CCT)

F.3 EXPERIMENTAL STRESS AT EACH NODE FACE AND IN THE TIE

Stresses at each nodal face and in the tie are determined based on the experimental measured capacity, V_{test}, for each beam in the database.

CCC NODE: Experimental Stress

10) Bearing Face; $f_{cb} =$ $V_{test}\big/\alpha\cdot l_l\cdot b_l$

11) Back Face; $f_{ck} = \left(V_{test} / \tan\theta\right) / a \cdot b_l$

12) Strut-Node Interface; $f_{cs} = \left(V_{test} / \sin\theta\right) / W_{CCC} \cdot b_l$

CCT NODE: Experimental Stress

13) Bearing Face; $f_{tb} = V_{test} / l_b \cdot b_b$

14) Back Face; $f_{tk} = \left(V_{test} / \tan\theta\right) / 2(h-d) \cdot b_s$

15) Strut-Node Interface; $f_{ts} = \left(V_{test} / \sin\theta\right) / W_{CCT} \cdot b_s$

TIE: Experimental Stress

16) $f_{tie} = \left(V_{test} / \tan\theta\right) / A_s$

F.4 ALLOWABLE CAPACITY OF EACH NODE FACE AND OF THE TIE

The capacity at each nodal face is determined according to the respective STM design provision. Once the capacity of each part of a STM is estimated (i.e. bearing face, back face, strut to node interface, and tie), the region that has the highest ratio of experimental to calculated capacity is the region that determines the overall STM design capacity.

F.4.1 ACI 318-08, Appendix A

CCC NODE: Design Strength

17) Bearing Face; $f_{n\_cb} = 0.85 \cdot 1 \cdot f_c' = 0.85 f_c'$

Experimental/Calculated = (10)/(17)

18) Back Face; $f_{n\_ck} = 0.85 \cdot 1 \cdot f_c' = 0.85 f_c'$

Experimental/Calculated = (11)/(18)

19) Strut-Node Interface; $f_{n\_cs} = \begin{cases} 0.85 \cdot 0.75 = 0.64 f_c' & if\ \rho_\perp \geq 0.003 \\ 0.85 \cdot 0.60 = 0.51 f_c' & if\ \rho_\perp < 0.003 \end{cases}$

Experimental/Calculated = (12)/(19)

CCT NODE: Design Strength

20) Bearing Face; $f_{n\_tb} = 0.85 \cdot 0.8 \cdot f_c' = 0.68 f_c'$

Experimental/Calculated = (13)/(20)

21) Back Face; $f_{n\_tk} = 0.85 \cdot 0.8 \cdot f_c' = 0.68 f_c'$

Experimental/Calculated = (14)/(21)

22) Strut-Node Interface; $f_{n\_ts} = \begin{cases} 0.85 \cdot 0.75 = 0.64 f_c' & if\ \rho_\perp \geq 0.003 \\ 0.85 \cdot 0.60 = 0.51 f_c' & if\ \rho_\perp < 0.003 \end{cases}$

Experimental/Calculated = (15)/(22)

TIE: Design Strength

23) $f_{n\_tie} = 1.0 f_y$

Experimental/Calculated = (16)/(23)

The maximum Experimental/Calculated ratio for each node face and tie [i.e. the maximum presented in (17) through (23)] is used to determine the Experimental/Calculated ratio for each beam in the database according to the ACI 318-08 design provisions.

F.4.2 AASHTO LRFD (2008)

CCC NODE: Design Strength

24) Bearing Face; $f_{n\_cb} = 0.85 f_c'$

Experimental/Calculated = (10)/(24)

25) Back Face; $f_{n\_ck} = 0.85 f_c'$

Experimental/Calculated = (11)/(25)

26) Strut-Node Interface; $f_{n\_cs} = 0.85 f_c'$

Experimental/Calculated = (12)/(26)

CCT NODE: Design Strength

27) Bearing Face; $f_{n\_tb} = 0.75 f_c'$

Experimental/Calculated = (13)/(27)

28) Back Face; $f_{n\_tk} = 0.75 f_c'$

Experimental/Calculated = (14)/(28)

29) Strut-Node Interface. Solve the following set of equations simultaneously:

$$\varepsilon_s = \frac{F_{strut}\cos\theta}{A_s E_s}$$

$$\varepsilon_1 = \varepsilon_s + (\varepsilon_s + 0.002)\cot^2\theta$$

$$f_{cu} = \min\begin{cases} \dfrac{f_c'}{0.8 + 170\varepsilon_1} \\ 0.85 f_c' \end{cases}$$

$$F_{strut} = \begin{cases} \dfrac{f_{n\_cb}\cdot\alpha\cdot l_l\cdot b_l}{\sin\theta} & \text{if (24) controls} \\ \dfrac{f_{n\_ck}\cdot a\cdot b_l}{\cos\theta} & \text{if (25) controls} \\ f_{n\_cs}\cdot W_{CCC}\cdot b_l & \text{if (26) controls} \\ \dfrac{f_{n\_tb}\cdot l_b\cdot b_s}{\sin\theta} & \text{if (27) controls} \\ \dfrac{f_{n\_tk}\cdot 2(h-d)\cdot b_s}{\cos\theta} & \text{if (28) controls} \\ f_{cu}\cdot W_{CCT}\cdot b_s & \text{if (29) controls} \\ \dfrac{A_s\cdot f_y}{\cos\theta} & \text{if (30) controls} \end{cases}$$

$f_{n\_ts} = f_{cu}$

Experimental/Calculated = (15)/(29)

TIE: Design Strength

30) $f_{n\_tie} =$ $1.0 f_y$

Experimental/Calculated = (16)/(30)

The maximum Experimental/Calculated ratio for each node face and tie [i.e. the maximum presented in (24) through (30)] is used to determine the Experimental/Calculated ratio for each beam in the database according to the AASHTO LRFD (2007) design provisions.

F.4.3 *fib* (1999)

CCC NODE: Design Strength

Triaxial Confinement Modification Factor, M_{CCC}

31) $M_{CCC} =$ $\min \begin{cases} b_w / b_l \\ 4 \end{cases}$

32) Bearing Face; $f_{n\_cb} =$ $0.85\left(1 - \frac{f_c'}{40ksi}\right) \cdot M_{CCC} \cdot f_c'$

Experimental/Calculated = (10)/(32)

33) Back Face; $f_{n\_ck} =$ $0.85\left(1 - \frac{f_c'}{40ksi}\right) \cdot M_{CCC} \cdot f_c'$

Experimental/Calculated = (11)/(33)

34) Strut-Node Interface; $f_{n\_cs} =$ $0.85\left(1 - \frac{f_c'}{40ksi}\right) \cdot M_{CCC} \cdot f_c'$

Experimental/Calculated = (12)/(34)

CCT NODE: Design Strength

Triaxial Confinement Modification Factor, M_{CCT}

35) $$M_{CCT} = \min \begin{cases} b_w / b_b \\ 4 \end{cases}$$

36) Bearing Face; $$f_{n\_tb} = 0.7\left(1 - \frac{f_c'}{40ksi}\right) \cdot M_{CCT} \cdot f_c'$$

Experimental/Calculated = (13)/(36)

37) Back Face; $f_{n\_tk} =$ [Not Applicable]

38) Strut-Node Interface; $$f_{n\_ts} = 0.7\left(1 - \frac{f_c'}{40ksi}\right) \cdot M_{CCT} \cdot f_c'$$

Experimental/Calculated = (15)/(38)

TIE: Design Strength

39) $$f_{n\_tie} = 1.0 f_y$$

Experimental/Calculated = (16)/(39)

The maximum Experimental/Calculated ratio for each node face and tie [i.e. the maximum presented in (32) through (34) and (36) through (39)] is used to determine the Experimental/Calculated ratio for each beam in the database according to the *fib* (1999) design provisions.

F.4.4 ACI 318-99, § 11.8

40) $$k = \min \begin{cases} 3.5 - 2.5\left(a / 2d\right) \\ 2.5 \end{cases}$$

41) $V_c =$ $\min \begin{cases} k\left(1.9\sqrt{f_c'} + 2500 \cdot \rho_l \cdot \left(2d/a\right)\right) \cdot b_w \cdot d \\ 6\sqrt{f_c'} \cdot b_w \cdot d \end{cases}$

42) $V_s =$ $\left[\rho_v \cdot b_w \left(\frac{1 + l_n/d}{12}\right) + \rho_{vh} \cdot b_w \left(\frac{11 - l_n/d}{12}\right)\right] \cdot f_y \cdot d$

43) $V_n =$ $\min \begin{cases} V_c + V_s \\ 10\sqrt{f_c'} \cdot b_w \cdot d \end{cases}$

Experimental/Calculated = V_{test}/(43)

F.4.5 Proposed STM Procedure

CCC NODE: Design Strength

Triaxial Confinement Modification Factor, M_{CCC}

44) $M_{CCC} =$ $\min \begin{cases} \sqrt{A_2/A_1} \\ 2 \end{cases}$

Strut-to-Node Interface Efficiency Factor, ν

45) $\nu =$ $0.45 \le 0.85 - \frac{f_c'}{20ksi} \le 0.65$

46) Bearing Face; $f_{n\_cb} =$ $0.85 \cdot M_{CCC} \cdot f_c'$

Experimental/Calculated = (10)/(46)

47) Back Face; $f_{n\_ck} =$ $0.85 \cdot M_{CCC} \cdot f_c'$

Experimental/Calculated = (11)/(47)

48) Strut-Node Interface; $f_{n\_cs} =$ $\nu \cdot M_{CCC} \cdot f_c'$

Experimental/Calculated = (12)/(48)

CCT NODE: Design Strength

Triaxial Confinement Modification Factor, M_{CCT}

49) $$M_{CCT} = \min \begin{cases} \sqrt{A_2 / A_1} \\ 2 \end{cases}$$

50) Bearing Face; $f_{n\_tb} =$ $0.70 \cdot M_{CCT} \cdot f_c'$

Experimental/Calculated = (13)/(50)

51) Back Face; $f_{n\_tk} =$ [Not Applicable]

52) Strut-Node Interface; $f_{n\_ts} =$ $\nu \cdot M_{CCT} \cdot f_c'$

Experimental/Calculated = (15)/(52)

TIE: Design Strength

53) $f_{n\_tie} =$ $1.0 f_y$

Experimental/Calculated = (16)/(53)

The maximum Experimental/Calculated ratio for each node face and tie [i.e. the maximum presented in (46) through (48) and (50) through (53)] is used to determine the Experimental/Calculated ratio for each beam in the database according to the Proposed design provisions.

References

1. AASHTO LRFD, *2008 Interim Revisions, Bridge Design Specifications, 4th Edition, 2007*, American Association of State Highway and Transportation Officials, Washington, D.C., 2008.

2. AASHTO, *Standard Specifications for Highway Bridges, 17th Edition*, American Association of State Highway and Transportation Officials, Washington, D. C., 2002.

3. ACI Committee 318-02, *Building Code Requirements for Reinforced Concrete (ACI 318-02)*, American Concrete Institute, Farmington Hills, MI, 2002.

4. ACI Committee 318-08, *Building Code Requirements for Reinforced Concrete (ACI 318-08)*, American Concrete Institute, Farmington Hills, MI, 2008.

5. ACI Committee 318-56, *Building Code Requirements for Reinforced Concrete (ACI 318-56)*, American Concrete Institute, Detroit, MI, 1956.

6. ACI Committee 318-63, *Building Code Requirements for Reinforced Concrete (ACI 318-63)*, American Concrete Institute, Detroit, MI, 1963.

7. ACI Committee 318-71, *Building Code Requirements for Reinforced Concrete (ACI 318-71)*, American Concrete Institute, Detroit, MI, 1971.

8. ACI-ASCE Joint Committee 426-73, *The Shear Strength of Reinforced Concrete Members (ACI-ASCE 426-72)*, American Concrete Institute, Detroit, MI, 1973.

9. ACI-ASCE Joint Committee 445, *Recent Approaches to Shear Design of Structural Concrete (ACI 445R-99)*, American Concrete Institute, Farmington Hills, MI, 1999.

10. Adebar, P. and Zhou, Z., "Bearing Strength of Compressive Struts Confined by Plain Concrete," *ACI Structural Journal*, Vol. 90, No. 5, September-October 1993, pp. 534-541.

11. Anderson, N. S. and Ramirez, J. A., "Detailing of Stirrup Reinforcement," *ACI Structural Journal*, Vol. 86, No. 5, September-October, 1989, pp. 507-515.

12. ASTM A 370 – 08a, *Standard Test Methods and Definitions for Mechanical Testing of Steel Products*, American Society for Testing and Materials, West Conshohocken, PA, May 2008.

13. ASTM A 615/A 615M – 08, *Standard Specification for Deformed and Plain Carbon-Steel Bars for Concrete Reinforcement*, American Society for Testing and Materials, West Conshohocken, PA, March 2008.

14. ASTM C 31/C 31M – 08a, *Standard Practice for Making and Curing Concrete Test Specimens in the Field*, American Society for Testing and Materials, West Conshohocken, PA, April 2008.

15. ASTM C 39/C 39M – 05, *Standard Test Method for Compressive Strength of Cylindrical Concrete Specimens*, American Society for Testing and Materials, West Conshohocken, PA, November 2005.

16. ASTM C 143/C 143M – 08, *Standard Test Method for the Slump of Hydraulic-Cement Concrete*, American Society for Testing and Materials, West Conshohocken, PA, March 2008.

17. EUROCODE 2, *Concrete Structures Euro-Design Handbook*, Ernst and Sohn, Berlin, 1995.

18. Barton, D. L.; Anderson, R. B.; Bouadi, A.; Jirsa, J. O.; and Breen, J. E., *An Investigation of Strut-and-Tie Models for Dapped Beam Details*, Report No. 1127-1, Center for Transportation Research, University of Texas at Austin, Austin, Texas, May 1991.

19. Bergmeister, K.; Breen, J. E.; Jirsa, J. O.; and Kreger, M. E., *Detailing for Structural Concrete*, Report No. 1127-3F, Center for Transportation Research, University of Texas at Austin, Austin, Texas, May 1993.

20. Birrcher, D., *Title*, Ph. D. Dissertation in Progress, University of Texas at Austin, December 2008.

21. Brown, M. D.; Sankovich, C. L.; Bayrak, O.; Jirsa, J. O.; Breen, J. E.; and Wood, S. L., *Design for Shear in Reinforced Concrete Using Strut-and-Tie Models*, Report No. 0-4371-2, Center for Transportation Research, University of Texas at Austin, Austin, Texas, Apr. 2006.

22. Chow, L.; Conway, H. D.; and Winter, G., "Stresses in Deep Beams," *ASCE Proceedings*, Paper No. 2557, May 1952, pp. 686-702.

23. FIB, *Structural Concrete, Textbook on Behaviour, Design, and Performance*, Volume 3, International Federation for Structural Concrete, Lausanne, Switzerland, 1999, 269 pp.

24. Furuuchi, H.; Takahashi, Y.; Ueda, T.; and Kakuta, Y., "Effective Width for Shear Failure of RC Deep Slabs," *Transaction of the Japan Concrete Institute*, Vol. 20, 1998, pp. 209-216.

25. Hawkins, N. M., "The Bearing Strength of Concrete Loaded through Rigid Plates," *Magazine of Concrete Research*, Vol. 20, No. 62, Cement and Concrete Association, March 1968.

26. Hsuing, W. and Frantz, G. C., "Transverse Stirrup Spacing in R/C Beam," *ASCE Journal of Structural Engineering*, Vol. 11, No. 2, February 1985, pp. 353-362.

27. Huizinga, M. R., *Strength and Serviceability Performance of Large-Scale Deep Beams: Effect of Transverse Reinforcement*, Master's Thesis, University of Texas at Austin, August 2007, 232 pp.

28. edited by Kani, M. W.; Huggins, M. W.; and Wittkopp, R. R., *Kani on Shear in Reinforced Concrete*, University of Toronto Press, Toronto, 1979, 225 pp.

29. Lampert, P. and Thürlimann, B., "Ultimate Strength and Design of Reinforced Concrete Beams in Torsion and Bending," *IABSE Publications*, No 31-1, Zurich, Switzerland, p. 107-131, 1971.

30. Leonhardt, F. and Walther, R., translation by Amerongen, C. V., "The Stuttgardt Shear Tests, 1961", from *Beton und Stahlbeton, Vol. 56, No. 12, 1961 and Vol. 57, No. 2, 3, 6, 7, and 8, 1962,* Translation No. 111, Cement and Concrete Association, London, 1964, 138 pp.

31. MacGregor, J. G. and Wight, J. K., *Reinforced Concrete, Mechanics and Design*, 4th Edition, Pearson Prentice Hall, New Jersey, 2005, 1132 pp.

32. MacGregor, J. G., "Derivation of Strut and Tie Models for the 2002 ACI Code," *ACI SP-208 Examples for the Design of Structural Concrete with Strut-and-Tie Models*, American Concrete Institute, Michigan, 2002, 242 pp.

33. Marti, P., "Basic Tools of Reinforced Concrete Beam Design," *ACI Journal*, Vol. 82, No. 1, January-February 1985, pp. 46-56.

34. Mitchell, D., and Collins, M.P., "Diagonal Compression Field Theory – A Rational Model for Structural Concrete in Pure Torsion," *ACI Journal*, Vol. 71, No. 8, August 1974, pp. 396-408.

35. Nielson, M. P.; Braestrup, M. W.; Jensen, B. C.; and Bach, F., *Concrete Plasticity, Beam Shear – Shear in Joints – Punching Shear*, Special Publication,

Danish Society for Structural Science and Engineering, Technical University of Denmark, Lyngby, 1978, 129 pp.

36. NACU Standard No. 4, "Standard Building Regulations for the Use of Reinforced Concrete," *National Association of Cement Users*, Philadelphia, Pennsylvania, 1920, 20 pp.

37. Ramirez, J.A., and Breen, J.E., *Proposed Design Procedures for Shear and Torsion in Reinforced and Prestressed Concrete*, Report No. 248-4F, Center for Transportation Research, University of Texas at Austin, Austin, Texas, 1983.

38. Ramirez, J.A., and Breen, J.E., "Evaluation of Modified Truss-Model Approach for Beams in Shear," *ACI Structural Journal*, Vol. 88, No. 5, September-October 1991, pp. 562-571.

39. Rogowsky, D. M. and MacGregor, J. G., "Design of Reinforced Concrete Deep Beams," *Concrete International*, Vol 8, August 1986, pp. 49-58.

40. Rogowsky, D. M.; MacGregor, J. G.; and Ong, S. Y., "Tests of Reinforced Concrete Deep Beams," *ACI Journal*, Vol. 83, No. 4, July-August 1986, pp. 614-623.

41. Schlaich, J., Schäfer, K. and Jennewein, M., "Toward a Consistent Design of Structural Concrete," *PCI Journal*, Vol. 32, No. 3, May-June 1987, pp.74-150.

42. Thompson, M. K.; Young, M. J.; Jirsa, J. O., Breen, J. E., and Klingner, R. E., *Anchorage of Headed Reinforcement in CCT Nodes*, Research Report 1855-2, Center for Transportation Research, University of Texas at Austin, Austin, Texas, 2003.

43. Vecchio, F. J. and Collins, M. J., "The Modified Compression Field Theory for Reinforced Concrete Element Subjected to Shear," *ACI Structural Journal*, Vol. 83, No. 2, March-April 1986, pp.219-231.

44. Wight, J.K., and Parra-Montesinos, G., "Use of Strut-and-Tie Model for Deep Beam Design as per ACI 318 Code," *ACI Concrete International,* Vol. 25, No. 5, May 2003, pp. 63-70.